



รายงานวิจัยฉบับสมบูรณ์

โครงการ พฤติกรรมการดักและออกซิเดชันของมลพิษอนุภาคจากเชื้อเพลิง หมุนเวียนชีวภาพออกซิเจนเนต

โดย ดร.ปรีชา การินทร์

รายงานวิจัยฉบับสมบูรณ์

โครงการ พฤติกรรมการดักและออกซิเดชันของมลพิษอนุภาคจากเชื้อเพลิง หมุนเวียนชีวภาพออกซิเจนเนต

ดร.ปรีชา การินทร์ สถาบันเทคโนโลยีพระจอมเกล้าเจ้าคุณทหารลาดกระบัง

บทคัดย่อ

รหัสโครงการ: MRG5580249

ชื่อโครงการ: พฤติกรรมการดักและออกซิเดชันของมลพิษอนุภาคจากเชื้อเพลิงหมุนเวียนชีวภาพ

ออกซิเจนเนต

ชื่อนักวิจัย: ดร.ปรีชา การินทร์

อีเมลล์: kkpreech@kmitl.ac.th, karintr@hotmail.com, aeautolab@gmail.com

ระยะเวลาโครงการ: 2 ปี (1 สิงหาคม 2555 - 30 กรกฎาคม 2557)

บทคัดย่อ:

มลพิษอนุภาคเขม่า (Particulate Matters: PMs) จำเป็นต้องถูกกำจัดจากไอเสียเครื่องยนต์ดีเซล เพื่อปกป้องสภาพแวดล้อมและสุขภาพของมนุษย์ โดยปัญหาของมลพิษอนุภาคเขม่าสามารถแก้ไขได้โดย การใช้อุปกรณ์กรองมลพิษอนุภาคเขม่าดีเซล (Diesel Particulate Filter: DPF) นอกจากนั้นการใช้ เชื้อเพลิงไบโอดีเซลยังสามารถลดปริมาณมลพิษอนุภาคเขม่าจากเครื่องยนต์ลงได้ประมาณร้อยละ 50

โครงสร้างในระดับนาโนของมลพิษอนุภาคเขม่าถูกศึกษาด้วยกล้องอิเลคตรอนแบบส่องกราดและ แบบส่องผ่าน ขนาดเฉลี่ยของกลุ่มมลพิษอนุภาคเขม่าอยู่ในช่วง 100-300 nm ส่วนขนาดเฉลี่ยก้อนเดี่ยวของ มลพิษอนุภาคเขม่าไบโอดีเซลและดีเซลประมาณ 30-40 nm และ 50-60 nm ตามลำดับ การวิเคราะห์ ภาพถ่ายจากกล้องอิเลคตรอนแบบส่องผ่านสามารถวิเคราะห์เกล็ดคาร์บอนในมลพิษอนุภาคเขม่าดีเซล และไบโอดีเซลซึ่งพบว่าความยาวเฉลี่ยของเกล็ดคาร์บอนอยู่ในช่วง 0.1-7.0 nm นอกจากนั้นยังสามารถ คำนวนปริมาณอะตอมคาร์บอนต่อหน่วยปริมาตรของมลพิษอนุภาคเขม่าซึ่งพบว่ามีค่าประมาณ 500-900 carbon-atom/nm³

ส่วนประกอบทางเคมีและจลศาสตร์เคมีของการออกซิเดชันมลพิษอนุภาคเขม่าถูกศึกษาด้วย เครื่องมือวิเคราะห์ทางความร้อน (Thermo-gravimetric Analysis: TGA) และเครื่องมือวิเคราะห์ ส่วนประกอบของก๊าซ (CHN analyzer) มลพิษอนุภาคเขม่าประกอบด้วยน้ำ เชื้อเพลิงที่เผาใหม้ไม่สมบูรณ์ ในรูปของไฮโรคาร์บอนและคาร์บอน พลังงานกระตุ้นของการทำปฏิกิริยาเคมีระหว่างออกซิเจนและมลพิษ อนุภาคไบโอดีเซลและดีเซลมีค่าต่ำกว่าคาร์บอนแบลคเพราะมลพิษอนุภาคเขม่ามีส่วนประกอบของ ไฮโดรคาร์บอน พลังงานกระตุ้นของการออกซิเดชันมลพิษอนุภาคเขม่าไบโอดีเซลและดีเซลมีค่าประมาณ 147–157 kJ/mole และ 153–165 kJ/mole ตามลำดับ

คำหลัก: เครื่องยนต์ดีเซล ไบโอดีเซล มลพิษอนุภาคเขม่า โครงสร้างนาโน อิเลคตรอนไมโครสโคป

Abstract

Project Code: MRG5580249

Project Title: Renewable Bio-oxygenated Fuels Particulate Matter Trapping and Oxidation

Behaviors

Investigator: Dr.Preechar Karin

E-mail Address: kkpreech@kmitl.ac.th, karintr@hotmail.com, aeautolab@gmail.com

Project Period: 2 years (August 1, 2012 – July 31, 2014)

Abstract:

Particulate matters (PMs) must be removed from the exhaust gas emitted from engines to protect the environment and human health. The problem of particulate emissions from diesel engine can be treated by Diesel Particulate Filter (DPF). In addition, biodiesel combustion produces PM about two times lower than that of diesel combustion.

Nanostructures of diesel and biodiesel engine Particulate Matters (PMs) were investigated by using a Scanning Electron Microscopy (SEM) and a Transmission Electron Microscopy (TEM). The average agglomerated particle sizes PMs are in the range of 100-300 nm. The average single particle sizes of biodiesel and diesel PMs are approximately 30-40 nm and 50-60 nm, respectively. Image processing process was used to estimate each carbon platelet length by using TEM image. The average carbon platelet length of biodiesel and diesel PMs are in the range of 0.1-7.0 nm. Moreover, carbon atoms per cubic volume of PMs are approximately 500-900 carbon-atom/nm³.

PM oxidation kinetics by Thermo-gravimetric analysis (TGA) was successfully studied. The chemical content percentage of PM can be divided by oxidation temperature zoning in three main regions which are moisture, unburned hydrocarbon and carbon. The estimated apparent activation energies (Ea) of biodiesel and diesel PM oxidation are lower than that of carbon black because of unburned oxygenated molecule. The estimated apparent activation energy of biodiesel and diesel PMs oxidize with air is in the range of 147–157 kJ/mole and 153–165 kJ/mole, respectively.

Keywords: Diesel Engine, Biodiesel, Particulate Matter, Nanostructure, Electron Microscopy

บทสรุปผู้บริหาร

รหัสโครงการ: MRG5580249

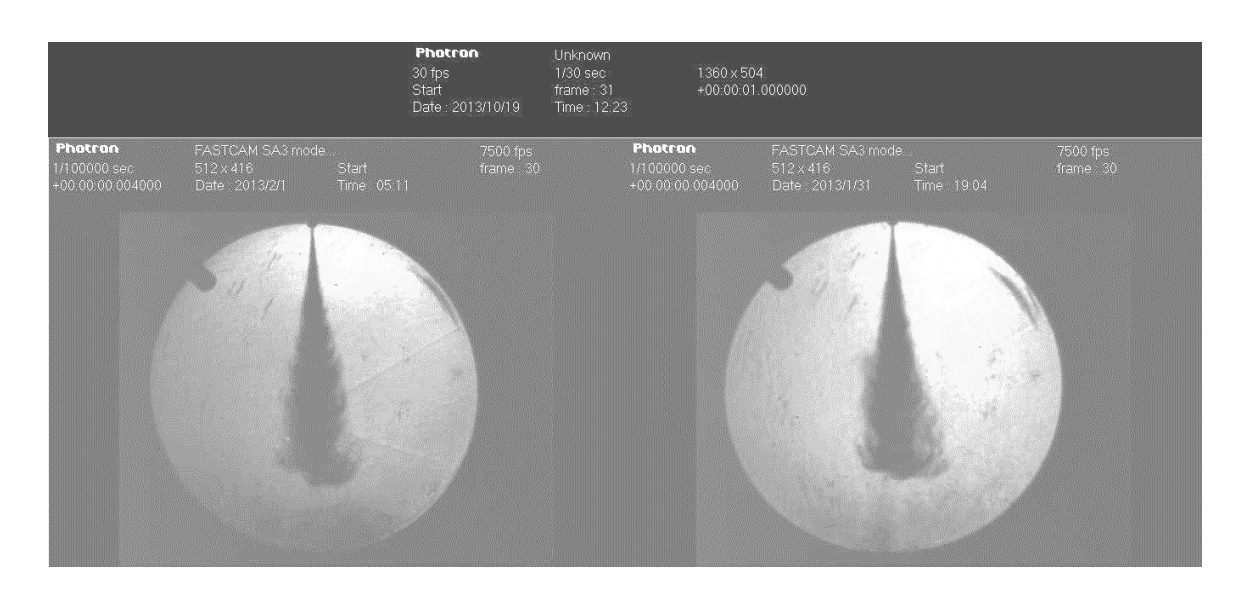
ชื่อโครงการ: พฤติกรรมการดักและออกซิเดชันของมลพิษอนุภาคจากเชื้อเพลิงหมุนเวียนชีวภาพ

ออกซิเจนเนต

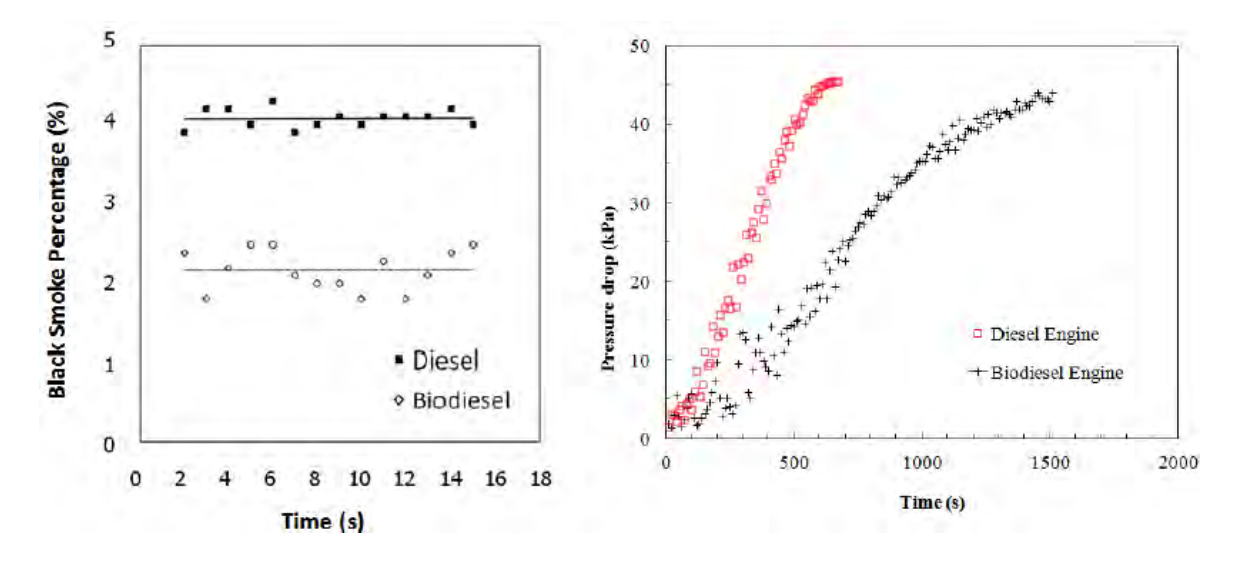
มลพิษอนุภาคเขม่า (Particulate Matters: PMs) จำเป็นต้องถูกกำจัดจากไอเสีย (Exhaust Gas) เครื่องยนต์ดีเซล (Diesel Engine) เพื่อปกป้องสภาพแวดล้อมและสุขภาพของมนุษย์ โดย ปั๊ญหาของมลพิษอนุภาคเขม่าสามารถแก้ไขได้โดยการใช้อุปกรณ์กรองมลพิษอนุภาคเขม่าดีเซล (Diesel Particulate Filter: DPF) ซึ่งเป็นอุปกรณ์ที่ทำหน้าที่กำจัดมลพิษอนุภาคที่ได้รับการออกแบบ พัฒนาจนสามารถนำมาใช้งานอย่างแพร่หลายในบริษัทผู้ผลิตรถยนต์ ในปัจจุบันเทคโนโลยีหลังการ เผาไหม้นี้ (After-treatment Technology) ถูกนำมาใช้กับประเทศที่มีกฎหมายมลพิษเข้มงวด เช่น สหภาพยุโรป ญี่ปุ่น และอเมริกา คาดว่าอุปกรณ์ดังกล่าวจะถูกนำมาใช้ในประเทศไทยในอนาคต อันใกล้นี้ โดยทั่วไปดีพีเอฟจะมีโครงสร้างเป็นวัสดุพรุน (Porous Media) ที่ผลิตจากเซรามิค (Ceramics) เช่น ซิลิคอนคาร์ไบด์ (SiC) และคอร์ดิไรท์ (Cordierite) ดีพีเอฟจะถูกติดตั้งไว้เป็นส่วน หนึ่งของท่อไอเสีย (Exhaust Pipe) ของไหลที่มีสถานะเป็นก๊าซในไอเสียจากเครื่องยนต์จะไหลผ่าน ผนังของวัสดุพรุนนี้ได้ ในขณะเดียวกันมลพิษอนุภาคซึ่งเป็นของแข็งจะถูกดักไว้ด้วยวัสดุพรุนซึ่ง ขบวนการนี้เรียกว่าขบวนการดัก (Trapping Process) และหลังจากมลพิษอนุภาคถูกดักจนสะสมกัน มากพอที่ความดันในท่อไอเสียสูงขึ้นจะมีผลกระทบกับเครื่องยนต์ มลพิษอนุภาคเหล่านั้นก็จำเป็นที่ จะต้องถูกกำจัดโดยสามารถทำได้ด้วยการเพิ่มอุณหภูมิไอเสียให้สูงขึ้นถึงจุดที่มลพิษอนุภาคเขม่า สามารถทำปฏิกิริยากับออกซิเจนได้ซึ่งมีค่าสูงถึงประมาณ 600 องศาเซลเซียส คาร์บอนในมลพิษ อนุภาคเขม่าจะสามารถทำปฏิกิริยากับออกซิเจนกลายเป็นก๊าซคาร์บอนไดออกไซด์ซึ่งเรียกว่า ขบวนการรีเจนเนอเรชั่นของดีพีเอฟ (DPF Regeneration Process) อย่างไรก็ตามขบวนการดักและ เผามลพิษอนุภาคเขม่าดังกล่าวมีพฤติกรรมที่ซับซ้อนมากจำเป็นอย่างยิ่งที่จะต้องศึกษาในเชิงลึกบน หลักการทางกลศาสตร์ของไหล (Fluid Mechanics) ควาบคู่ไปกับจลศาสตร์เคมี (Chemical Kinetics) ของการเกิดปฏิกิริยาเคมีระหว่างมลพิษอนุภาคเขม่ากับออกซิเจนในอากาศ

เชื้อเพลิงชีวภาพ (Bio Fuels) เป็นอีกทางเลือกหนึ่งที่สามารถนำมาใช้ได้จริงในเครื่องยนต์ สำหรับภาคขนส่งทั่วโลกเพราะมีคุณสมบัติทางกายภาพและเคมีของเชื้อเพลิงที่สามารถใช้แทน เชื้อเพลิงฟอสซิล (Fossil Fuels) ได้ ดังแสดงใน รูปที่ 1 สเปรย์ของเชื้อเพลิงดีเซลและไบโอดีเซลใน ห้องเผาไหม้ไม่ได้มีความแตกต่างทางด้านคุณสมบัติเชิงกล (Mechanical Properties) ในวิศวกรรม เครื่องยนต์สันดาปภายใน (Internal Combustion Engine Engineering) อย่างมีนัยสำคัญมากนัก ถึงแม้ว่าจะมีผลกระทบของความหนืด (Viscosity) ของเชื้อเพลิงไบโอดีเซลที่สูงกว่าดีเซลบ้างเล็กน้อย เพราะมีความหนาแน่น (Density) ที่สูงกว่า

ในมุมมองทางด้านวิศวกรรมการเผาไหม้ (Combustion Engineering) การใช้เชื้อเพลิงไบโอ ดีเซล (Biodiesel) ยังสามารถลดปริมาณมลพิษอนุภาคเขม่าจากเครื่องยนต์ลงได้ประมาณร้อยละ 50 ดังแสดงใน รูปที่ 2 เนื่องจากในโมเลกุลของเชื้อเพลิงไบโอดีเซลมีอะตอมของออกซิเจนที่จะช่วยให้ การออกซิเดชันเกิดได้รวดเร็วมากกว่าดีเซล อย่างไรก็ตามคุณลักษณะเฉพาะทางกายภาพและเคมี (Physical and Chemical Characteristics) ของมลพิษอนุภาคจากเครื่องยนต์ไบโอดีเซลจำเป็นต้อง ศึกษาวิจัยในเชิงลึกบนพื้นฐานทางวิทยาศาสตร์เพื่อทำความเข้าใจถึงโครงสร้างในระดับมาโคร ไมโคร นาโนและโมเลกุลของมลพิษ (Macro-, Micro-, Nano- and Molecular of PMs) ข้อมูลที่ได้จะสามารถ นำไปใช้ในการออกแบบและเลือกใช้ดีพีเอฟที่เหมาะสมและมีประสิทธิภาพสูงสุดได้



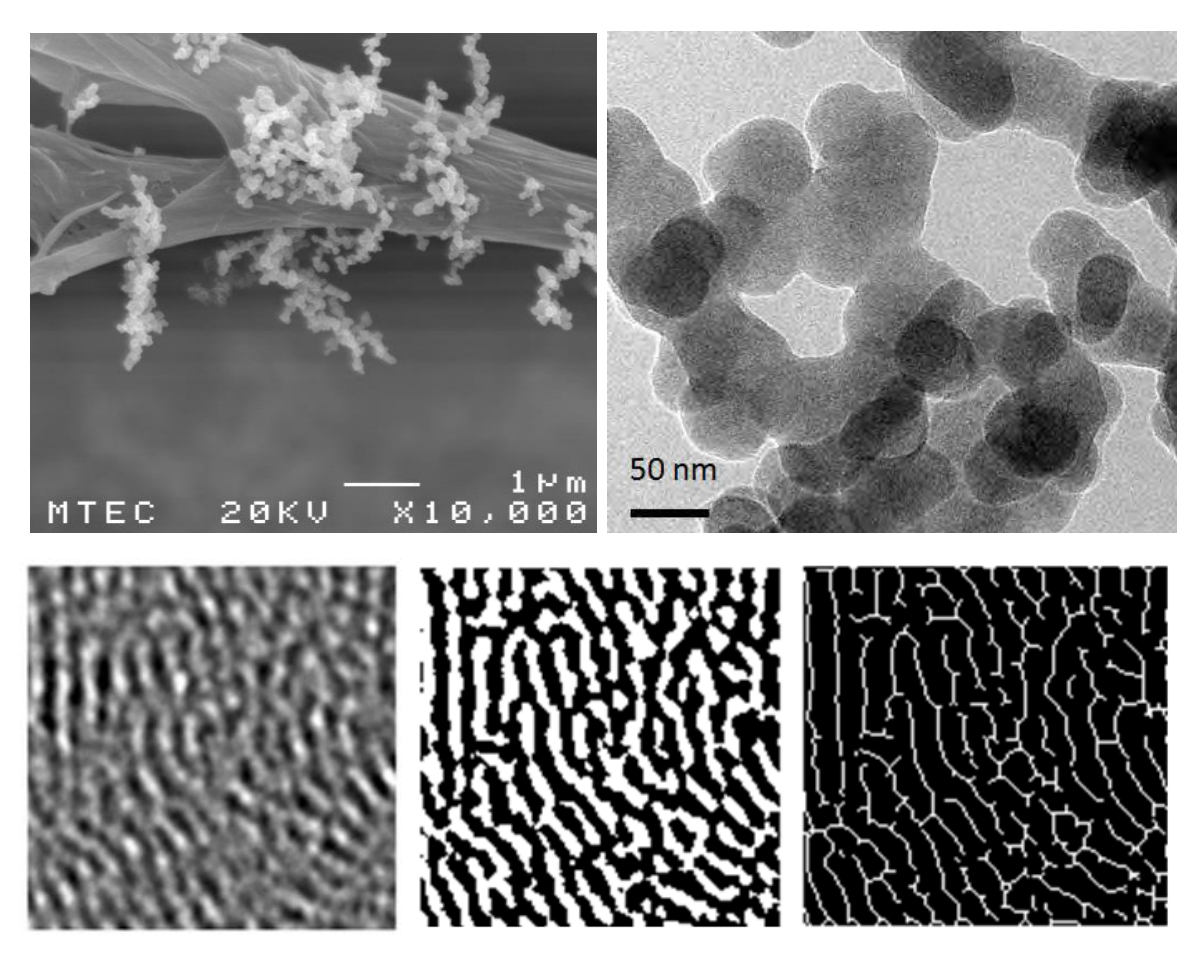
รูปที่ 1 สเปรย์ของเชื้อเพลิงดีเซล (Left) และไบโอดีเซล (Right) ในห้องเผาไหม้



รูปที่ 2 ปริมาณมลพิษอนุภาคจากการเผาใหม้เชื้อเพลิงดีเซลและไบโอดีเซลในเครื่องยนต์

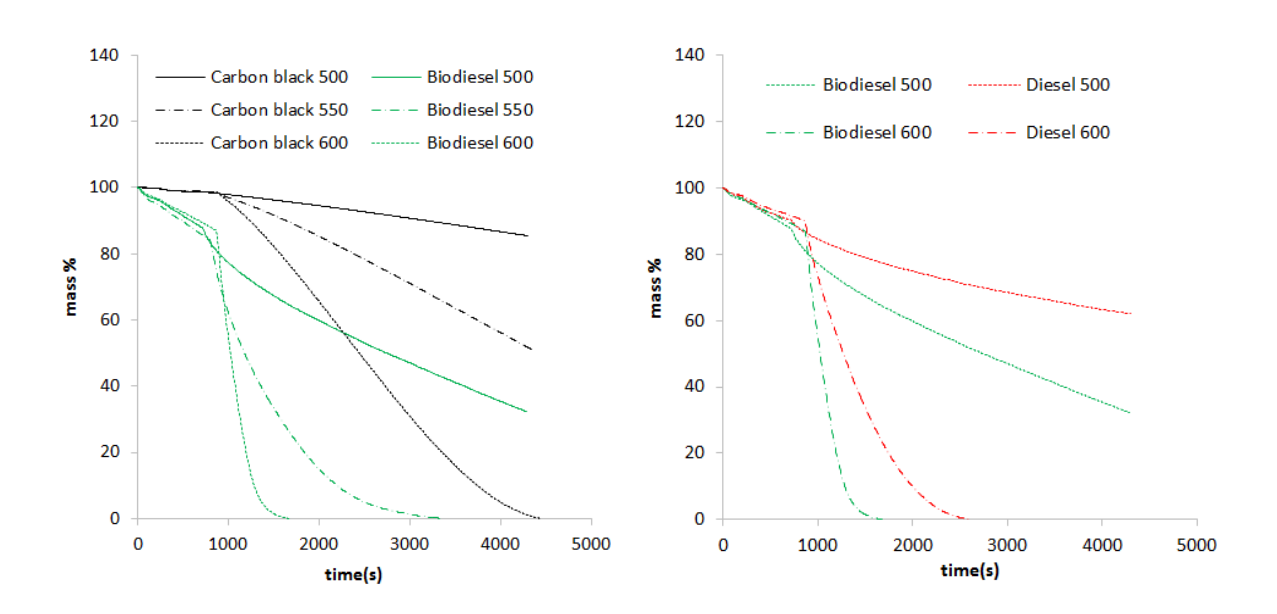
นอกจากนั้นการใช้เชื้อเพลิงไบโอดีเซลยังเป็นการลดปัญหาโลกร้อน (Global Warming) ที่ เกิดจากภาวะเรือนกระจก (Greenhouse Gas) ซึ่งมีสาเหตุหลักจากการปล่อยคาร์บอนไดออกไซด์ จากการเผาไหม้ของเชื้อเพลิง อย่างไรก็ตามพืชสามารถดูดก๊าซคาร์บอนไดออกไซด์กลับมาใช้ในการ สังเคราะห์แสงได้ดังนั้นการใช้เชื้อเพลิงไบโอดีเซลจากปาล์น้ำมันจึงเป็นที่ยอมรับกันว่าไม่ถือว่าเป็น การปล่อยก๊าซคาร์บอนไดออกไซด์ (Carbon Neutral)

โครงสร้างในระดับไมโครและนาโน (Micro-nanostructure) ของมลพิษอนุภาคเขม่าถูกศึกษา ด้วยกล้องอิเลคตรอนแบบส่องกราด (Scanning Electron Microscopy: SEM) และกล้องอิเลคตรอ นแบบส่องผ่าน (Transmission Electron Microscopy: TEM) ขนาดเฉลี่ยของกลุ่มมลพิษอนุภาค เขม่า (Agglomerated PM) อยู่ในช่วง 100-300 nm ส่วนขนาดเฉลี่ยก้อนเดี่ยวของมลพิษอนุภาค เขม่า (Single PM) ใบโอดีเซลและดีเซลประมาณ 30-40 nm และ 50-60 nm ตามลำดับ ดังแสดงใน รูปที่ 3 การวิเคราะห์ภาพถ่ายจากกล้องอิเลคตรอนด้วยคอมพิวเตอร์ (Image Processing) สามารถ วิเคราะห์ให้เห็นขนาดเกล็ดคาร์บอน (Carbon Platelets) ในมลพิษอนุภาคเขม่าดีเซลและไบโอดีเซล ซึ่งพบว่าความยาวเฉลี่ยของเกล็ดคาร์บอนอยู่ในช่วง 0.1-7.0 nm นอกจากนั้นยังสามารถคำนวน ปริมาณอะตอมคาร์บอนต่อหน่วยปริมาตรของมลพิษอนุภาคเขม่าซึ่งพบว่ามีค่าประมาณ 500-900 carbon-atom/nm³



รูปที่ 3 ภาพถ่ายมลพิษอนุภาคเขม่าและการวิเคราะห์หาความหนาแน่นด้วยคอมพิวเตอร์

ส่วนประกอบทางเคมี (Chemical Composition) และจลศาสตร์เคมี (Chemical Kinetics) ของ การออกซิเดชันมลพิษอนุภาคเขม่า (PM Oxidation) ถูกศึกษาด้วยเครื่องมือวิเคราะห์ทางความร้อน และเครื่องมือวิเคราะห์ส่วนประกอบของก๊าซ (CHN Analysis: TGA) (Thermo-gravimetric จากผลการวิเคราะห์แสดงให้เห็นว่ามลพิษอนุภาคเขม่าประกอบด้วยน้ำ (Moister) เชื้อเพลิงที่เผาใหม่ไม่สมบูรณ์ในรูปของไฮโรคาร์บอน (Unburned ประมาณไม่เกินร้อยละ 20 Hydrocarbon) ประมาณไม่เกินร้อยละ 60 และคาร์บอน (Carbon) ไม่เกินร้อยละ 70 ขึ้นอยู่กับ คุณสมบัติเชื้อเพลิงและภาระโหลดของเครื่องยนต์ มลพิษอนุภาคเขม่าไบโอดีเซลสามารถทำปฏิกิริยา กับออกซิเจนในอากาศได้รวดเร็วกว่ามลพิษอนุภาคดีเซลและคาร์บอนแบลค (Carbon ตามลำดับ ดังแสดงในรูปที่ 4 นอกจากนั้นยังพบว่าพลังงานกระตุ้น (Apparent Activation Energy: Ea) ของการทำปฏิกิริยาเคมีระหว่างออกซิเจนและมลพิษอนุภาคไบโอดีเซลมีค่าต่ำกว่าดีเซลและ คาร์บอนแบลค ตามลำดับ เพราะมลพิษอนุภาคเขม่ามีส่วนประกอบของไฮโดรคาร์บอนทำให้ทำ ปฏิกิริยาได้เร็วกว่าคาร์บอนโดยเฉพาะอย่างยิ่งไฮโดรคาร์บอนในเชื้อเพลิงไบโอดีเซลมีอะตอมของ ออกซิเจนในโมเลกุลด้วยจึงทำให้ทำปฏิกิริยาได้รวดเร็วมากยิ่งขึ้น โดยจากการทดลองพบว่าพลังงาน กระตุ้นของการออกซิเดชันมลพิษอนุภาคเขม่าไบโอดีเซลและดีเซลมีค่าประมาณ 147–157 kJ/mole และ 153–165 kJ/mole ตามลำดับ



รูปที่ 4 จลศาสตร์เคมีของการทำปฏิกิริยาระหว่างมลพิษอนุภาคเขม่ากับออกซิเจนในอากาศ

ผลงานวิจัยเกี่ยวกับคุณสมบัติเชิงกลและเคมีของเชื้อเพลิง คุณสมบัติทางกายภาพและเคมี ของมลพิษอนุภาคเขม่าและพฤติกรรมการดักและออกซิเดชันของมลพิษอนุภาคเขม่าในโครงสร้าง ระดับไมโครของผนังดีพีเอฟจะสามารถนำไปใช้ในการออกแบบและเลือกใช้อุปกรณ์กรองมลพิษ อนุภาคที่เหมาะสมกับเครื่องยนต์ดีเซล ไบโอดีเซลและเชื้อเพลิงผสมได้อย่างเหมาะสมและมี ประสิทธิภาพสูงสุดได้

เนื้อหางานวิจัย

รหัสโครงการ: MRG5580249

ชื่อโครงการ : พฤติกรรมการดักและออกซิเดชันของมลพิษอนุภาคจากเชื้อเพลิงหมุนเวียนชีวภาพ

ออกซิเจนเนต

บทน้ำ

มลพิษอนุภาคเขม่า (Particulate Matters: PMs) จำเป็นต้องถูกกำจัดจากไอเสียเครื่องยนต์ ู้ดีเซลเพื่อปกป้องสภาพแวดล้อมและสุขภาพของมนุษย์ โดยปั๊ญหาของมลพิษอนุภาคเขม่าสามารถ แก้ไขได้โดยการใช้อุปกรณ์กรองมลพิษอนุภาคเขม่าดีเซล (Diesel Particulate Filter: DPF) ซึ่งเป็น อุปกรณ์ที่ทำหน้าที่กำจัดมลพิษอนุภาคที่ได้รับการออกแบบพัฒนาจนสามารถนำมาใช้งานอย่าง แพร่หลายในบริษัทผู้ผลิตรถยนต์ ในปัจจุบัน เทคโนโลยีนี้ถูกนำมาใช้กับประเทศที่มีกฎหมายมลพิษ เข้มงวด เช่น สหภาพยุโรป ญี่ปุ่น และอเมริกา คาดว่าอุปกรณ์ดังกล่าวจะถูกนำมาใช้ในประเทศไทย ในอนาคตอันใกล้นี้ โดยทั่วไปดีพีเอฟจะมีโครงสร้างเป็นวัสดุพรุน (Porous Media) ที่ผลิตจากเซรามิค เช่น ซิลิคอนคาร์ใบด์ (SiC) และคอร์ดิไรท์ (Cordierite) ดีพีเอฟจะถูกติดตั้งไว้เป็นส่วนหนึ่งของท่อไอ เสีย ของใหลที่มีสถานะเป็นก๊าซในไอเสียจากเครื่องยนต์จะใหลผ่านผนังของวัสดุพรุนนี้ได้ ใน ขณะเดียวกันมลพิษอนุภาคซึ่งเป็นของแข็งจะถูกดักไว้ด้วยวัสดุพรุนซึ่งขบวนการนี้เรียกว่าขบวนการ ์ ดัก (Trapping Process) และหลังจากมลพิษอนุภาคถูกดักจนสะสมกันมากพอที่ความดันในท่อไอเสีย สูงขึ้นจะมีผลกระทบกับเครื่องยนต์ มลพิษอนุภาคเหล่านั้นก็จำเป็นที่จะต้องถูกกำจัดโดยการเพิ่ม อุณหภูมิใอเสียให้สูงขึ้นถึงจุดที่มลพิษอนุภาคสามารถทำปฏิกิริยากับออกซิเจนได้ประมาณ 600 องศาเซลเซียสและกลายเป็นก๊าซคาร์บอนไดออกไซด์ซึ่งเรียกว่าขบวนการรีเจนเนอเรชั่นของดีพีเอฟ (DPF Regeneration Process) อย่างไรก็ตามขบวนการดักและเผามลพิษอนุภาคจากเครื่องยนต์ ดังกล่าวมีพฤติกรรมที่ซับซ้อนมากจำเป็นอย่างยิ่งที่จะต้องศึกษาบนหลักการทางกลศาสตร์ของไหลค วาบคู่ไปกับจลศาสตร์เคมีของการเกิดปฏิกิริยาเคมีระหว่างมลพิษอนุภาคเขม่ากับออกซิเจนในอากาศ

นอกจากนั้นการใช้เชื้อเพลิงใบโอดีเซลยังสามารถลดปริมาณมลพิษอนุภาคเขม่าจาก เครื่องยนต์ลงได้ประมาณร้อยละ 50 เนื่องจากในโมเลกุลของเชื้อเพลิงไบโอดีเซลมีอะตอมของ ออกซิเจนที่จะช่วยให้การออกซิเดชันเกิดได้รวดเร็วมากขึ้น อย่างไรก็ตามคุณลักษณะเฉพาะทาง กายภาพและเคมีของมลพิษอนุภาคจากเครื่องยนต์ดีเซลและไบโอดีเซลจำเป็นต้องศึกษาวิจัยในเชิง ลึกบนพื้นฐานทางวิทยาศาสตร์เพื่อทำความเข้าใจถึงโครงสร้างในระดับมาโคร ไมโคร นาโนและ โมเลกุลของมลพิษ ข้อมูลที่ได้จะสามารถนำไปใช้ในการออกแบบและเลือกใช้ดีพีเอฟ

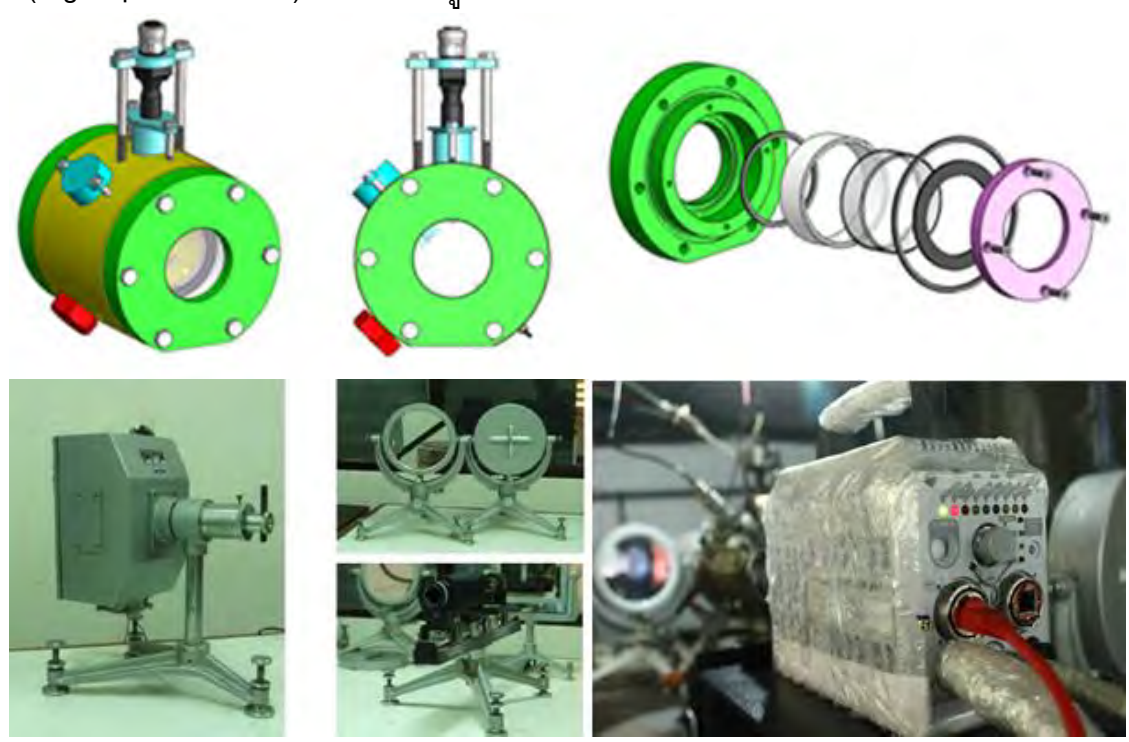
Particulate Filter: DPF) ที่เหมาะสมและมีประสิทธิภาพสูงสุดได้

วัตถุประสงค์

- ศึกษาพฤติกรรมการเกิดมลพิษอนุภาคเขม่า (Particulate Matter: PM) จาก
 การเผาใหม้เชื้อเพลิงดีเซลและใบโอดีเซล
- ศึกษาคุณลักษณะเฉพาะทางกายภาพและเคมี (Physical and Chemical Characterization) ของมลพิษอนุภาคเขม่าจากเครื่องยนต์ที่ใช้เชื้อเพลิงไบโอดีเซล
- ศึกษาพฤติกรรมการดักและออกซิเดชันของมลพิษอนุภาคเขม่า (Particulate Matter Trapping and Oxidation) จากเครื่องยนต์ที่ใช้เชื้อเพลิงไบโอดีเซลในอุปกรณ์กรอง มลพิษอนุภาคเขม่าดีเซล (Diesel Particulate Filter: DPF)
- สร้างองค์ความรู้เกี่ยวกับมลพิษอนุภาคเขม่าจากเครื่องยนต์ใบโอดีเซลเพื่อ เป็นข้อมมูลในการออกแบบและพัฒนาอุปกรณ์กรองมลพิษอนุภาคเขม่าดีเซล (Diesel Particulate Filter: DPF)

ระเบียบวิธีวิจัย

■ ศึกษาพฤติกรรมการเกิดมลพิษอนุภาคเขม่า (Particulate Matter) จากการ เผาไหม้เชื้อเพลิงดีเซลและไบโอดีเซลในเปลวไฟแบบแพร่และศึกษาการกระจายตัวของ สเปรย์เชื้อเพลิงห้องเผาไหม้ปริมาตรคงที่ (Constant Volume Combustion Chamber: CVCC) ด้วยเทคนิคการถ่ายภาพแบบชูรีเรน (Schlieren) และกล้องถ่ายภาพความเร็วสูง (High Speed Camera) ดังแสดงใน รูปที่ 1



รูปที่ 1 ห้องเผาใหม้ปริมาตรคงที่ (Constant Volume Combustion Chamber) และอุปกรณ์ การถ่ายภาพถ่ายภาพความเร็วสูง (High Speed Camera) แบบชูรีเรน (Schlieren)

■ ศึกษาคุณลักษณะเฉพาะทางกายภาพและเคมีของมลพิษอนุภาคเขม่าจาก เครื่องยนต์ที่ใช้เชื้อเพลิงไบโอดีเซล (Biodiesel Engine) ด้วยเครื่องมือวิเคราะห์ทาง วิทยาศาสตร์ เช่น Scanning Electron Microscopy (SEM), Transmission Electron Microscopy (TEM), Energy Dispersive Spectroscopy (EDS), Thermo-gravimetric Analysis (TGA) และ Carbon-hydrogen-nitrogen Analysis (CHN) เป็นตัน ดังแสดงใน รูป ที่ 2





(a) (b)

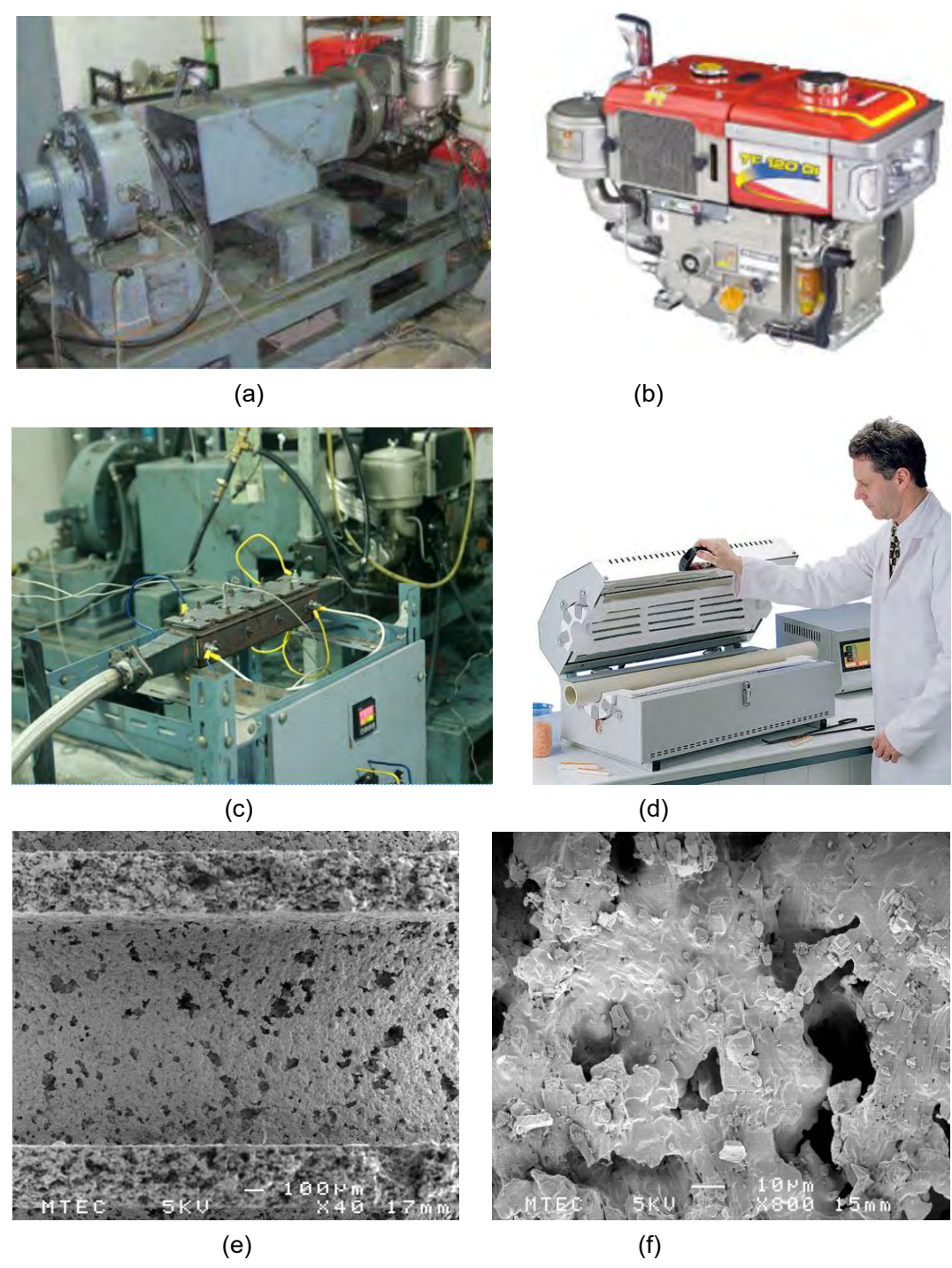




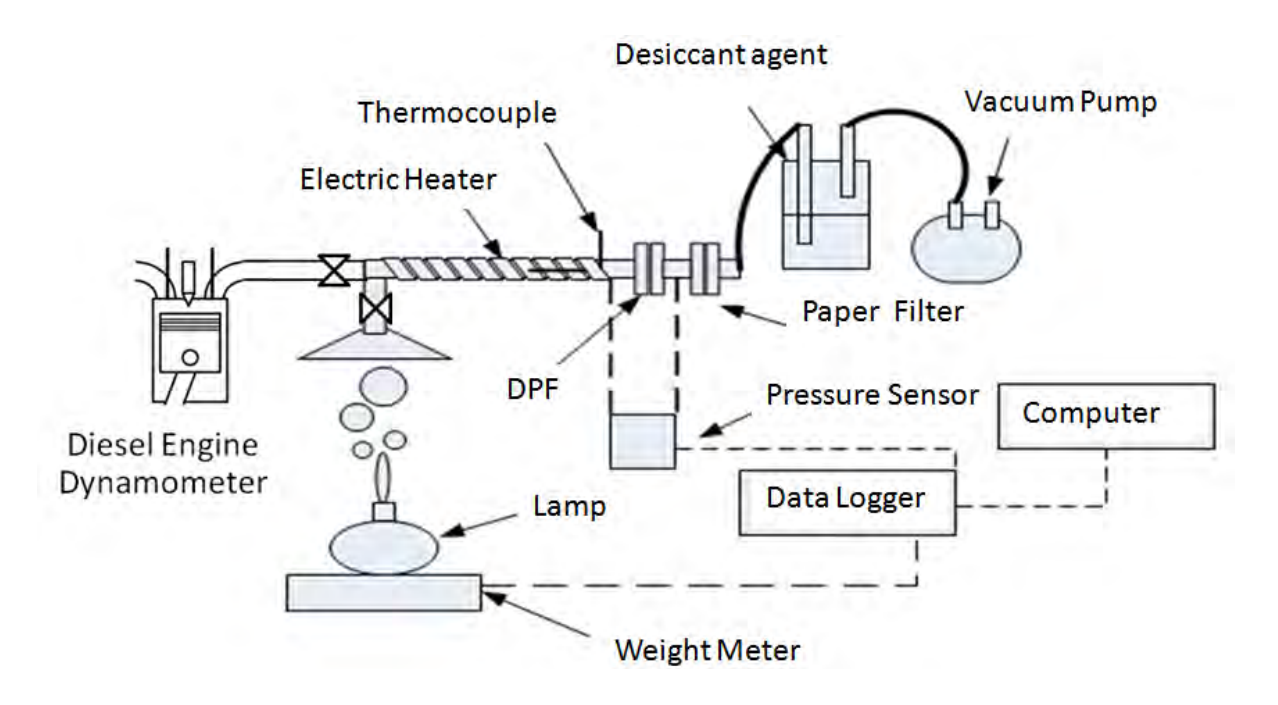
(c) (d)

รูปที่ 2 เครื่องมือวิเคราะห์ทางวิทยาศาสตร์ (a) Transmission Electron Microscopy (TEM), (b) Scanning Electron Microscopy (SEM) and Energy Dispersive Spectroscopy (EDS), (c) Thermo-gravimetric Analysis (TGA) และ (d) Carbon-hydrogen-nitrogen Analysis (CHN)

• ศึกษาพฤติกรรมการดักและออกซิเดชันของมลพิษอนุภาคเขม่าจาก เครื่องยนต์ที่ใช้เชื้อเพลิงใบโอดีเซลในอุปกรณ์กรองมลพิษอนุภาคดีเซล (Conventional Diesel Particulate Filter: DPF) ด้วยเครื่องมือวิเคราะห์อุปกรณ์กรองมลพิษอนุภาค (DPF Analyzer) โดยการใช้ชุดทดสอบเครื่องยนต์ไดนาโมมิเตอร์ (Engine Dynamometer) ดัง แสดงใน รูปที่ 3



รูปที่ 3 ชุดทดสอบเครื่องยนต์และชุดทดสอบอุปกรณ์กรองมลพิษอนุภาคเขม่า (a) Engine Dynamometer, (b) CI Diesel Engine, (c) DPF Analyzer, (d) Tube Furnace, (e) DPF Wall Surface และ (f) DPF Wall Surface's Pores



รูปที่ 4 ชุดทดสอบพฤติกรรมการดักและเผามลพิษอนุภาคเขม่าด้วยอุปกรณ์กรองมลพิษ อนุภาคเขม่าดีเซล

การศึกษาพฤติกรรมการดักและเผามลพิษอนุภาคสามารถทำได้ด้วยการทดสอบการดักและ เผามลพิษอนุภาคด้วยอุปกรณ์กรองมลพิษอนุภาคดีเซล (Diesel Particulate Filter: DPF) ด้วยชุด อุปกรณ์การทดสอบที่สามารถวัดค่าผลกระทบของความดันแตกต่าง (Pressure ประสิทธิภาพการกรอง (Filtration efficiency) ในขบวนการดักและสลายมลพิษอนุภาคได้ ดังแสดงใน เป็นอุปกรณ์ที่ทำหน้าที่กำจัดมลพิษอนุภาค ซึ่งได้รับการออกแบบพัฒนาจนสามารถ นำมาใช้งานอย่างแพร่หลายในบริษัทผู้ผลิตรถยนต์ ในปัจจุบัน เทคโนโลยีนี้ถูกนำมาใช้กับประเทศที่มี กฎหมายมลพิษเข้มงวด เช่น สหภาพยุโรป ญี่ปุ่น และอเมริกา คาดว่าอุปกรณ์ดังกล่าวจะถูกนำมาใช้ ในประเทศไทยในอนาคตอันใกล้นี้ โดยทั่วไป DPF จะมีโครงสร้างเป็นวัสดุพรุน (Porous Media) ที่ ผลิตจากเซรามิค เช่น ซิลิคอนคาร์ใบด์ (SiC) และคอร์ดิไรท์ (Cordierite) DPF จะถูกติดตั้งไว้เป็น ส่วนหนึ่งของท่อไอเสีย ของไหล (Fluid) ที่มีสถานะเป็นก๊าซในไอเสียของเครื่องยนต์จะไหลผ่านวัสดุ พรุนนี้ได้ ในขณะเดียวกันมลพิษอนุภาคจะถูกดักไว้ด้วยวัสดุพรุน ซึ่งขบวนการนี้เรียกว่า ขบวนการ ดัก (Trapping Process) และหลังจากมลพิษอนุภาคถูกดักจนสะสมกันมากพอที่ความดันในท่อไอเสีย ์ สูงขึ้นจะมีผลกระทบกับเครื่องยนต์ มลพิษอนุภาคเหล่านั้นก็จำเป็นที่จะต้องถูกกำจัดโดยการเพิ่ม อุณหภูมิใอเสียให้สูงขึ้นถึงจุดที่มลพิษอนุภาคสามารถทำปฏิกิริยากับออกซิเจนได้ประมาณ 600 องศาเซลเซียสและกลายเป็นก๊าซคาร์บอนไดออกไซด์ ซึ่งเรียกว่า ขบวนการรีเจนเนอเรชั่นของ อุปกรณ์กรองมลพิษอนุภาค (DPF Regeneration Process) อย่างไรก็ตามขบวนการดักและเผา มลพิษอนุภาคจากเครื่องยนต์ดังกล่าวมีพฤติกรรมที่ซับซ้อนมากจำเป็นอย่างยิ่งที่จะต้องศึกษาบน หลักการทางกลศาสตร์ของใหลควาบคู่ไปกับจลศาสตร์เคมีของการเกิดปฏิกิริยาเคมีระหว่างมลพิษ อนุภาคเขม่ากับออกซิเจนในอากาศ

INTRODUCTION TO THE RESEARCH PLOBLEM AND ITS SIGNIFICANTS

Energy Consumption

The use of all energy sources increases over time. The US Energy Information Administration (EIA) [1] reported the estimated world market for energy by fuel type, as shown in Fig. 1(a). In the short term, liquid fuels are expected to remain the largest source of energy. In the absence of significant technological advances, liquids continue to dominate in world transportation markets.

Because anthropogenic emissions of CO₂ result primarily from the combustion of fossil fuels, world energy use continues to be at the center of the climate change debate. The relative contributions of different fossil fuels to the total energy-related CO₂ emissions have changed over time, as shown in Fig. 1(b) [1]. The Kyoto Protocol, which requires the participating countries to reduce their greenhouse gas emissions to an annual average of about 5% below their 1990 level over the period from 2008–2012, came into force on February 16, 2005.

The transportation sector continues to rely heavily on liquid fuels to meet travel demand. Total world consumption of liquid fuel increased by 25% from 2006 to 2030, as shown in Fig. 1(b) [1]. In the non-Organization for Economic Co-operation and Development (OECD) nations, the transportation sector accounts for 69% of the projected increase in liquid fuel consumption, 87% of the total increases in transportation energy use.

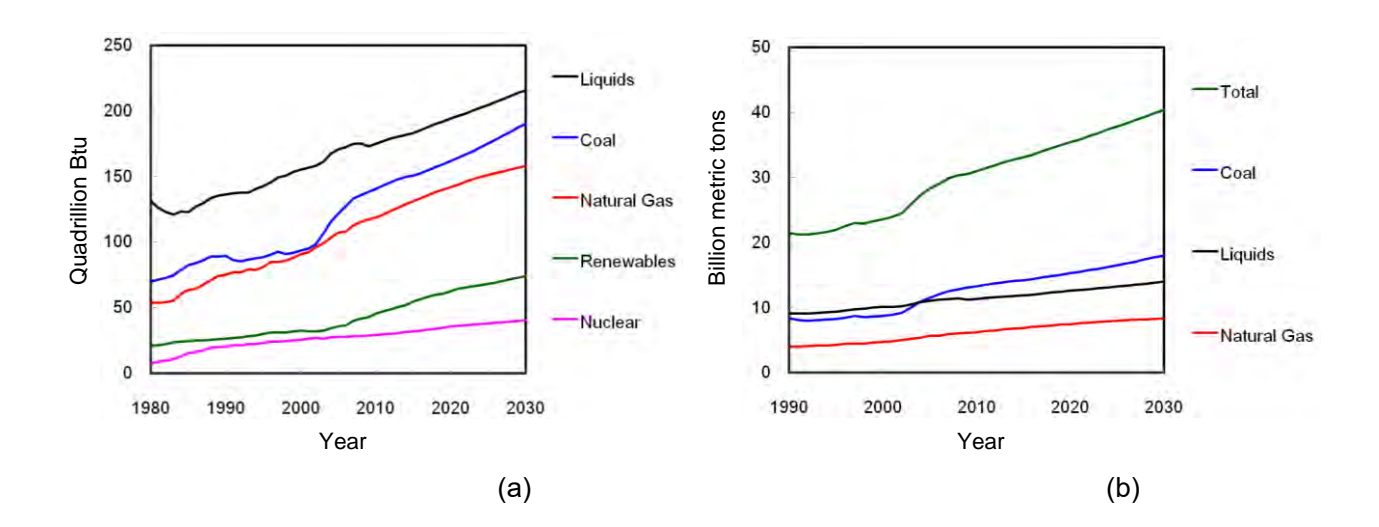


Figure 1 World market for (a) energy use and (b) energy-related CO₂ emissions by fuel type [1].

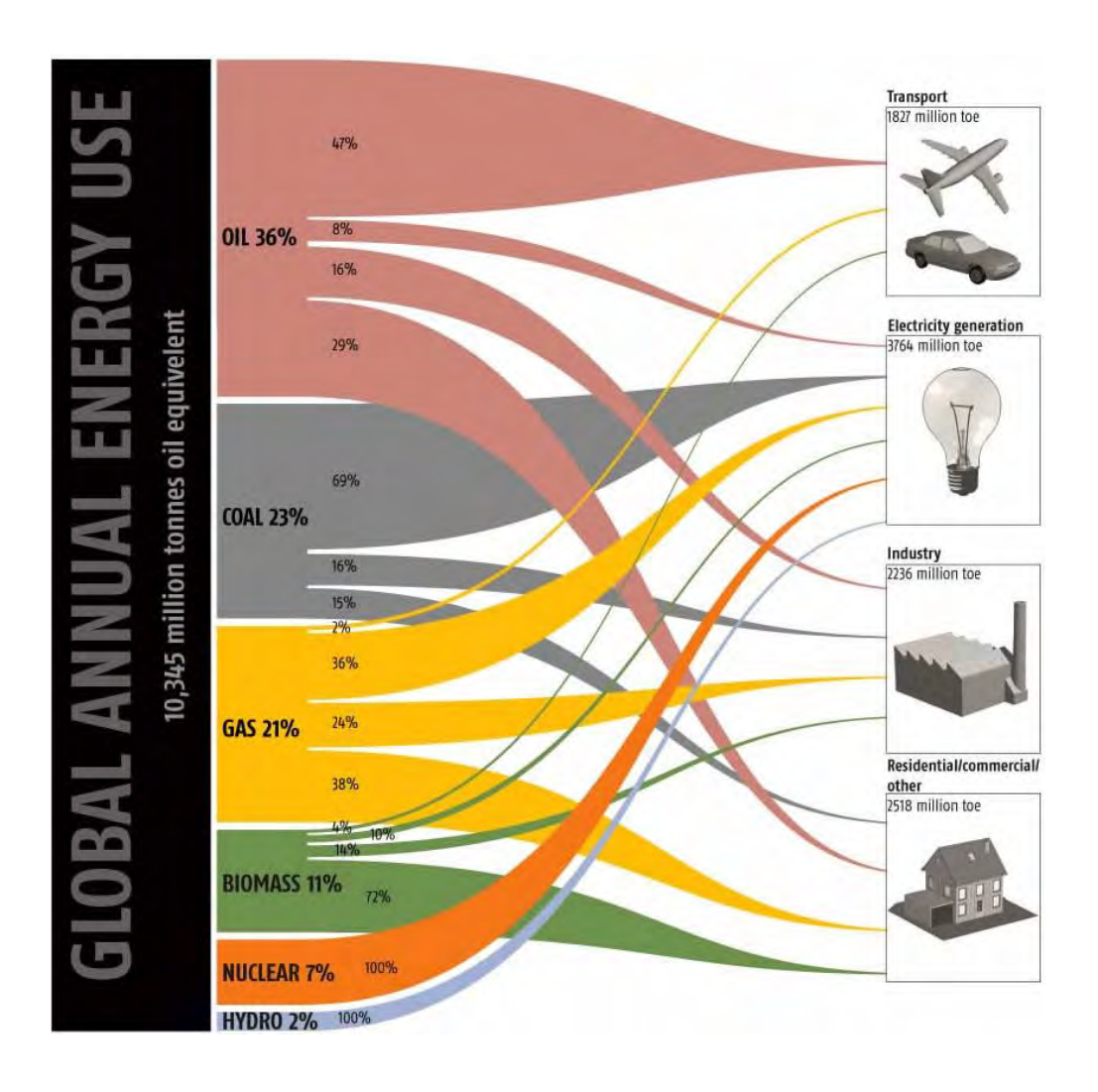


Figure 2 World energy use and the sectorial split of fuel use [2].

Figure 2 shows how the world use its fossil fuels, from which we see that we can separate use into four main sectors and that these sectors use a very different mix of fuels, with most oil being used in transport or heating and most cold being used for electricity production [2,3].

Emission Standards

Among internal combustion engines, diesel or compression-ignition (CI) engines have the highest thermal efficiency for a given output power. However, particulate matter (PMs) and NOx must be removed from the exhaust gas emitted from diesel engines to protect the environment and human health; therefore, regulation of vehicle emissions has become increasingly strict. The Euro regulations for PM and NOx emission levels are shown in Fig. 3 [3]. It is very difficult to develop combustion and after treatment systems for simultaneous removal of PM and NOx that will match these levels in the near future.

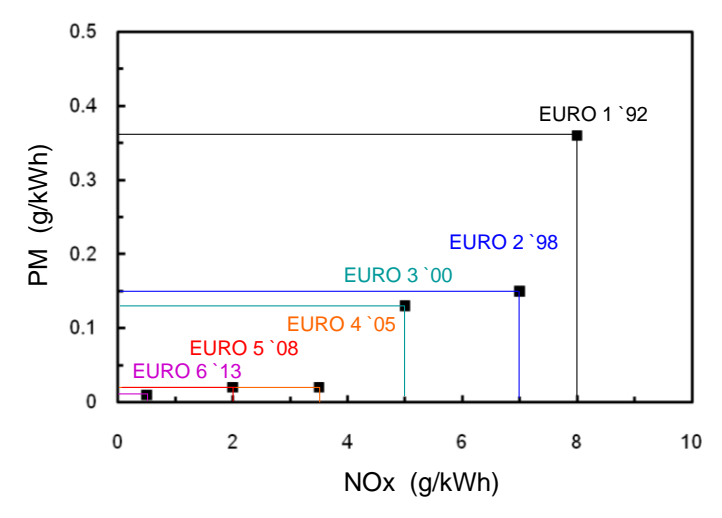


Figure 3 EU emission standards for PM and NOx emitted from diesel trucks and buses [3].

LITURATURE REVIEW

Diesel Emissions

J.B. Heywood [4] was clearly described the emissions from the internal combustion engines. Concentrations of NOx are comparable to those from gasoline or spark-ignition (SI) engines. Diesel hydrocarbon emissions are significant through exhaust concentrations are lower by about a factor of 5 than typical SI engine levels. The hydrocarbon in the exhaust may also condense to form white smoke during engine starting and warm-up. Specific hydrocarbon compounds in the exhaust gases are the source of diesel odor. Diesel engines are an important source of particulate emissions; between about 0.2 and 0.5 percent of the fuel mass in emitted as small (~0.1 µm diameter) particles which consist primary of soot with some additional absorbed hydrocarbon material. Diesel engines are not a significant source of carbon monoxide.

Diesel emission formation was summarized by J.B. Heywood [4]. In a diesel engine, the fuel is injected into the cylinder just prior to combustion, hence, throughout most of the critical parts of the cycle, the fuel distribution is nonuniform. Pollutant formation is strongly dependent on the fuel distribution and its variation with time due to mixing. Figure 4 illustrates how various parts of the fuel jet and flame affect the formation of NO, unburned HC, and soot (or particulates) during the premixed and mixing-controlled phases of diesel combustion in a direct injection engine with swirl injection. NO forms in the high-temperature burned gas regions as before, but the temperature and fuel/air ratio distributions within the burned gases are now nonuniform and the formation rates are highest in the nearly stoichiometric regions.

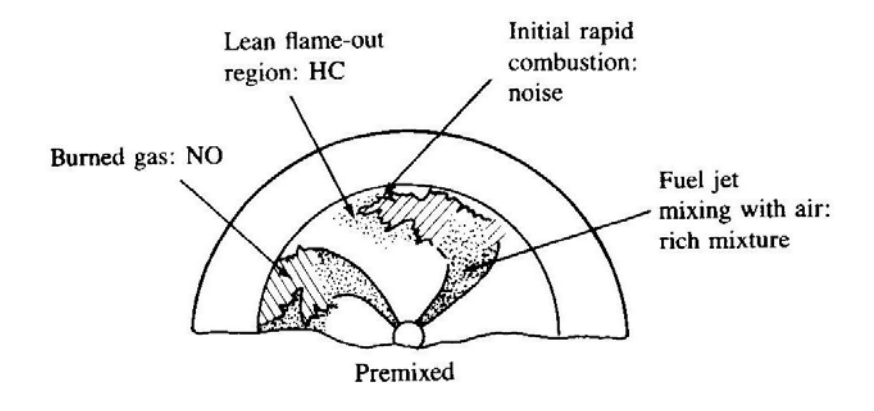
The formation of soot is through to take place via a number of elemental steps [5, 6]: pyrolysis, nucleation, surface growth and coagulation, aggregation and oxidation. These

processes take place on different time scales, ranging from a few microseconds to some milliseconds. Pyrolysis is the process in which gas-phase molecules form soot precursor molecules by free radical mechanism. This accelerating effect decreases with increasing temperature and with decreasing oxygen (air)-to-fuel ratio. Fuel molecules will first break down into olefins and then form acetylene (soot precursor). Nucleation is the process in which soot precursor molecules grow into small soot nuclei. The oxidation of pyrolysed diesel fuel molecules takes place at high temperatures and at high concentrations of reactive compounds such as ions and radical hydrocarbons, O and OH. Under these conditions, the decomposition rate of soot nuclei is lower than their rate of reaction other unsaturated, charged or radical hydrocarbons, resulting in a net growth of soot nuclei.

Surface growth is the process in which the precursor molecules grow from some 1-2 nm to 10-30 nm. Simultaneously, another process takes place: coagulation. Small soot particulates collide and coalesce, forming larger, still more or less spherical particles. Aggregation or chain-forming coagulation accounts for the formation of the well-known "fractal" structure of soot. During surface growth and coagulation, oxidation reactions do not seem to play an important role [5, 6].

Soot forms in the fuel spray cores containing rich unburned fuel, within the flame regions where the fuel vapor is heated by mixing with hot burned gases [4]. Soot then oxidizes in the flame zone when it contacts unburned oxygen, giving rise to a flame with yellow luminous character. HCs and aldehydes originate in regions where the flame quenches both on the walls and where excessive dilution with air prevents the combustion process from either starting or going to completion. Fuel vaporizing from the nozzle sac volume during the later stages of combustion is also a source of HCs. Combustion-generated noise is controlled by the early stage of the combustion process — the initial rapid heat release immediately following the ignition-delay period.

The substructure of primary soot particles was proposed by O.I smith [7]. The carbon atoms are bonded together in hexagonal face-centered arrays in planes commonly referred to as platelets. As illustrated in Fig. 5, the mean layer spacing is 0.355 nm, which is slightly larger than that of graphite. Platelets are arranged in layers to form crystallites. There are typically 2–5 platelets per crystallite, and on the order of 10³ crystallites per spherical soot particle. The crystallites are arranged with their planes more or less parallel to the particle surface. This structure of unordered layers is called turbostatic. Spherules, 10–50 nm in diameter, are fused together to form particles. A single spherule contains 10⁵ to 10⁶ carbon atoms.



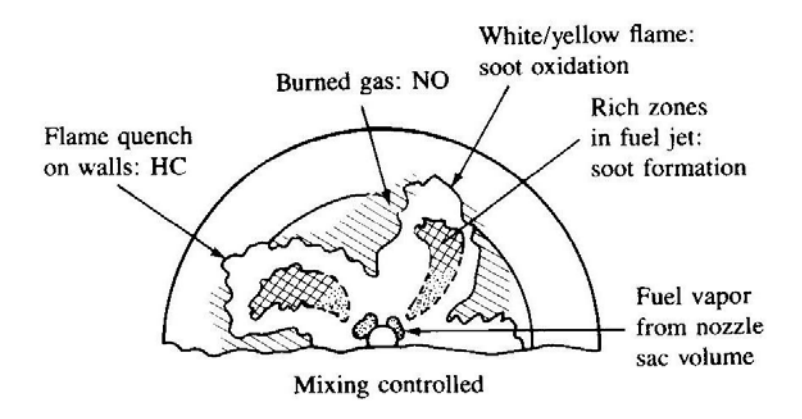


Figure 4 Summary of the pollutant formation mechanism in a direct-injection CI engine during premixed and mixing-controlled combustion phases [4].

Figure 6 shows the concept of diluted and cooled diesel PM reported by M.M. Maricq [8]. It consists of two particles: (a) fractal-like agglomerates of primary particles 15–30 nm in diameter, consisting of carbon and traces of metallic ash, and coated with condensed heavier and organic compounds and sulfate, and (b) nucleation particles composed of condensed HCs and sulfate.

The mean diameter of the agglomerated particles (accumulation mode) is almost always within the range of 60–100 nm. The composition of particles from diesel engines may vary widely, depending on the operating conditions and fuel composition. D.B. Kittelson [9] reported that the composition of soot emitted by a heavy-duty diesel engine consisted of 41% carbon, 25% unburned oil, 14% sulfate and water, 13% ash, and 7% unburned fuel.

The composition of diesel PM was also summarized by W.A. Majewski and M.K. Khair [10]. Based on analysis performance with a combination of physical and chemical methods, PM is traditionally divided into three main fractions: i) solid fraction (SOL) that consists of elemental carbon and ash, ii) soluble organic fraction (SOF) that consists of organic material derived from engine lubricating oil and fuel, and iii) sulfate particulates (SO₄) that consist of sulfuric acid and water.

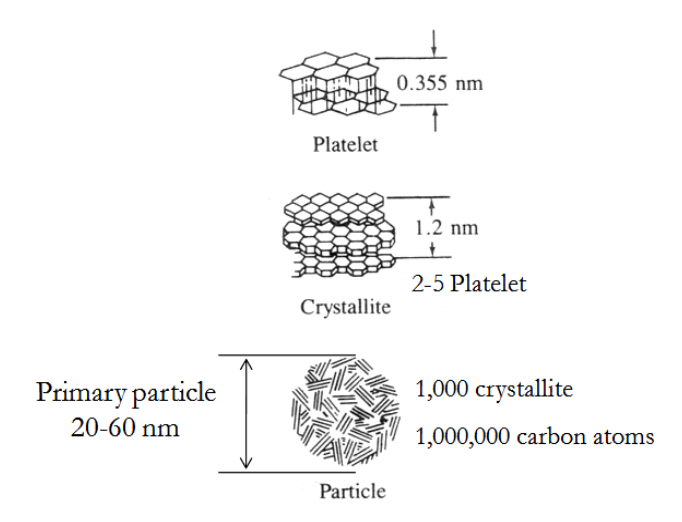


Figure 5 Substructure of a carbon particle [7].

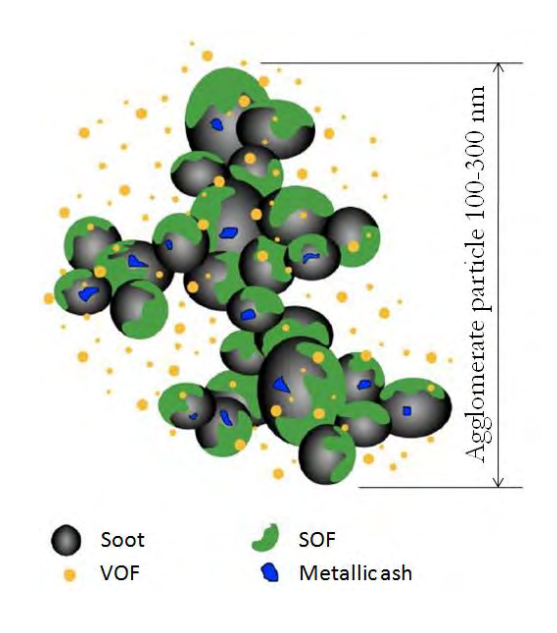


Figure 6 Artist's conception of diesel PM [8].

The SOL of diesel particulates is composed primarily of elemental carbon, sometimes referred to as inorganic carbon. This carbon, not chemically bound with other elements, is the finely dispersed carbon black or soot substance responsible for black smoke emission. Another important component of the solid fraction of PM is metallic ash. G.A. Merkel et al. [11] reported, in general, diesel exhaust ash consists of a mixture of: i) sulfates, phosphates, or oxides of calcium, zinc, magnesium, and other metals that are formed in the combustion chamber from burning additives in the engine lubricating oil, ii) metal oxide (iron, copper, chromium, and aluminum) impurities resulting from engine wear, which are carried into the combustion chamber by the lube oil, and iii) iron oxides resulting from corrosion of the engine exhaust manifold and exhaust system components.

HCs adsorbed on the surface of the carbon particles are present in the form of fine droplets from the SOF of diesel particulates. At times, this fraction is also referred to as the volatile organic fraction (VOF). The SOF fraction becomes liquid only after cooling to below 52 °C. The SOF fraction contains most of the polycyclic aromatic HCs (PAHs) and nitro-PAHs emitted with diesel exhaust gases. PAHs are aromatic HCs with two or more (up to five or six) benzene rings joined in various forms that are more or less clustered. These require special attention because of their mutagenic and, in some cases, carcinogenic character.

Transmission electron microscopic (TEM) observations of soot particles have been conducted by several researchers. The internal structure of primary soot particles was proposed by T. Ishiguro et al. [12]. A primary soot particle has two distinct parts: an inner core and an outer shell. The inner core, with a diameter of 10 nm, exists at the center of the primary particle and consists of several fine particles, 3-4 nm in diameter. The outer shell is composed of microcrystallites with periodic orientation of carbon sheets, also called a graphitic structure. Almost all the crystallites are planar, 1 nm thick and 3-5 nm wide, and are oriented perpendicular to the radius of the primary particle.

R.L. Vander wal et al. [13] reported the same structure of soot emitted by diesel engines. Figure 7 shows high-resolution transmission electron microscopic (HRTEM) images, obtained at NASA-Glenn, of soot from a diesel engine. Some primary particles were found to have a hollow interior and the outer shell exhibiting evidence of graphitization, with a higher crystalline than the non-hollowed particles. The percentage of such particles varied among soot samples, and tentatively appeared to be related to the oxidation history of the sample.

The size is relatively insensitive to the engine operating conditions— only a few extreme conditions lead to significantly different size distributions. There is also no strong dependence of the size on the engine type. The accumulation mode can be accompanied by a nucleation mode consisting of much smaller particles. Figure 8 shows idealized diesel exhaust particle number and mass-weighted size distributions reported by D.B. Kittelson et al. [9]. Most of the particle mass exists in the accumulation mode in the diameter range of 100–300 nm. This is where the carbonaceous agglomerates and associated adsorbed materials reside. The nuclei mode typically consists of particles in the 5–50 nm diameter range. This mode usually consists of volatile organic and sulfur compounds that form during exhaust dilution and cooling, and may also contain solid carbon and metal compounds. The nuclei mode typically contains 1%–20% of the particle mass, and more than 90% of the particle number. The coarse mode contains 5%–20% of the particle mass; it consists of accumulation mode particles that deposit on cylinder and exhaust system surfaces, and are

later re-entrained. Also shown in Fig. 1.9 are some size definitions for atmospheric particles: PM10, diameter (D) < 10 μ m; fine particles, D < 2.5 μ m; ultrafine particles, D < 0.10 μ m; and nanoparticles, D < 0.05 μ m or 50 nm.

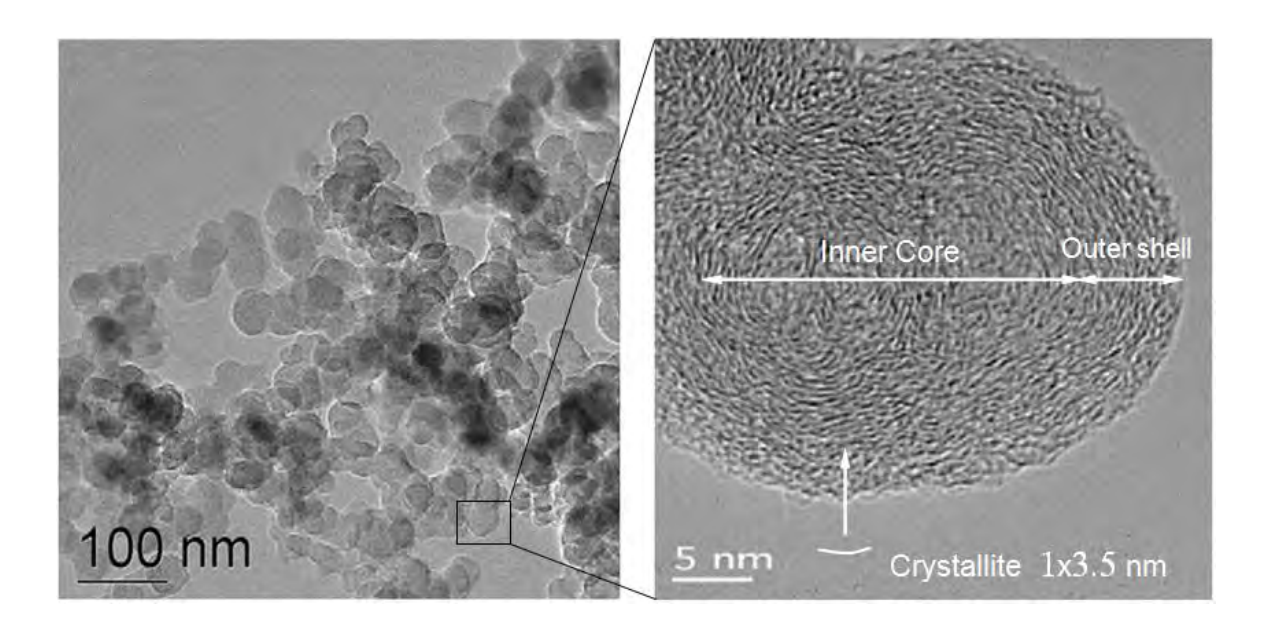


Figure 7 TEM images of soot particles from a diesel engine [13].

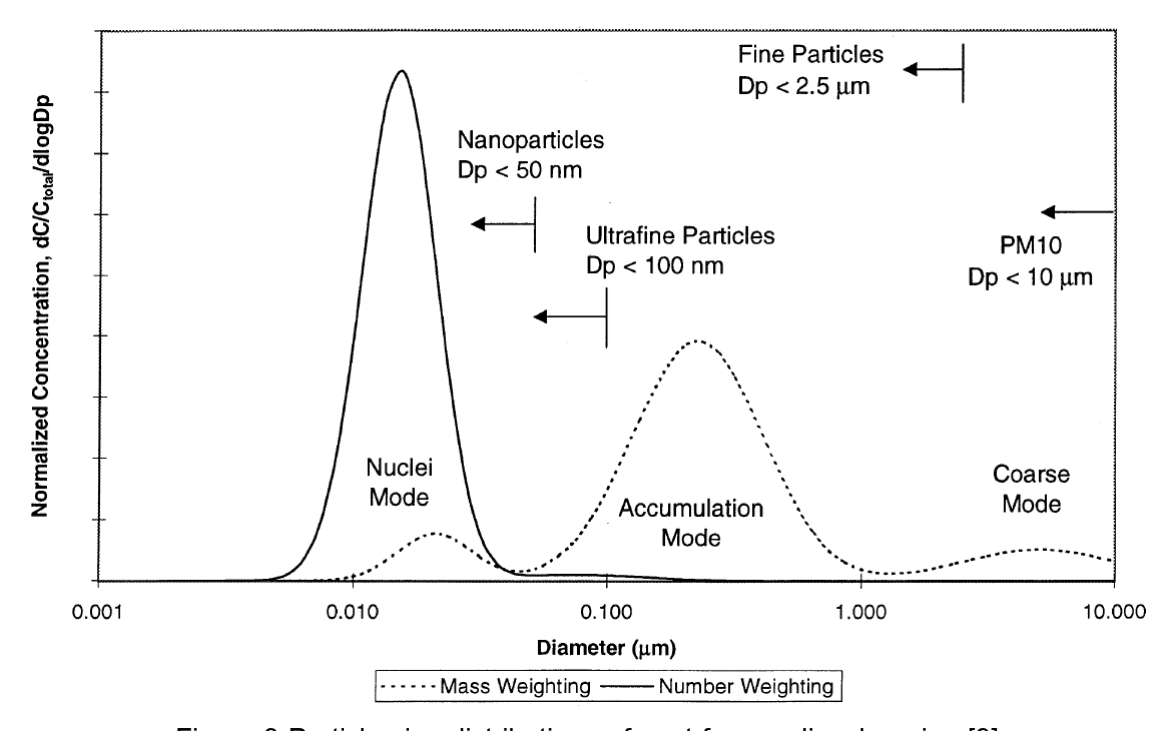


Figure 8 Particle size distributions of soot from a diesel engine [9].

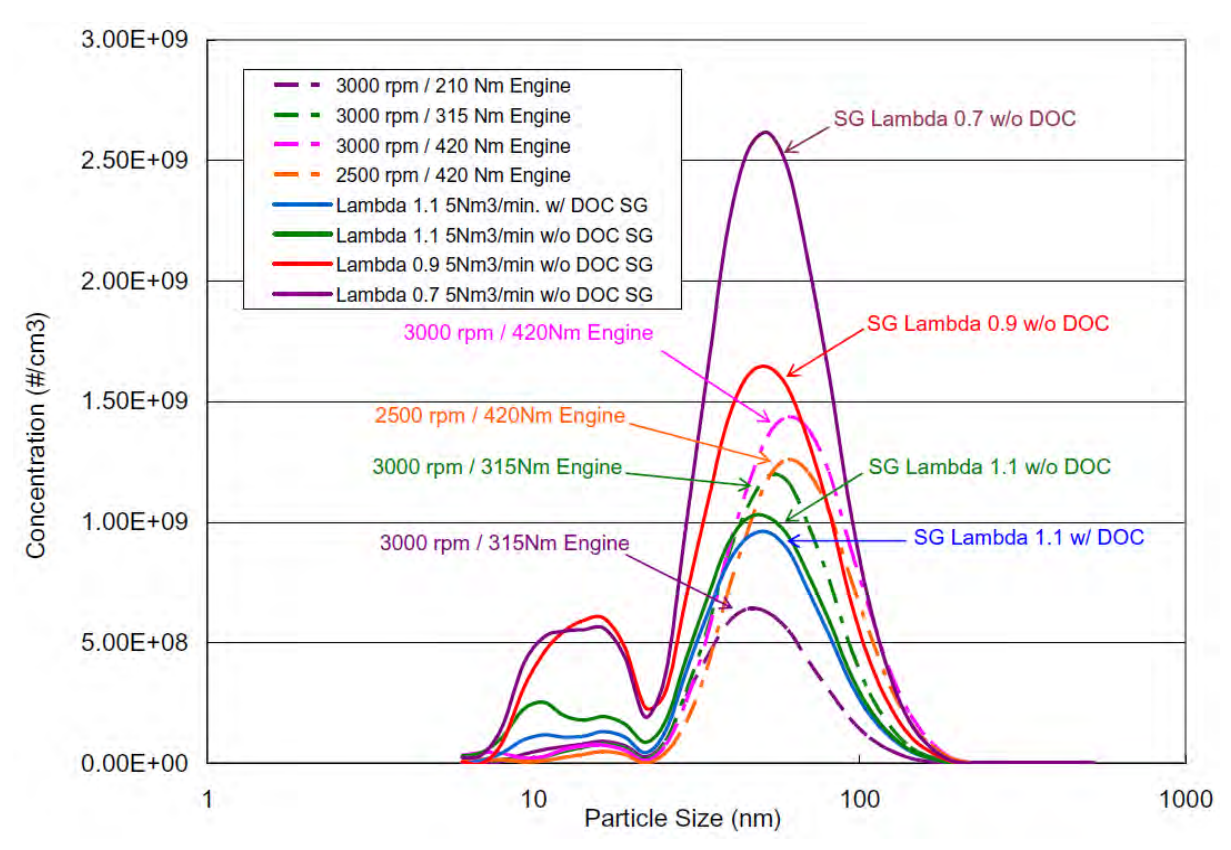


Figure 9 Particle size distributions of soot after the DOC [14].

The diesel oxidative catalyst (DOC) or catalytic oxidation of CO and HC, used in CI engines, consists of an active catalytic material in a specially designed metal casting that directs the exhaust gas flow through the catalyst bed. The active material employed for CO and HC oxidation (normally noble metals, although base metals oxides can be used) must be distributed over a large surface area. One system employs a ceramic honeycomb structure or monolith held in a metal can in the exhaust stream. During nucleation mode of soot, the SOF and VOF could be oxidized by the catalytic activities of metal oxides inside the DOC.

Figure 9 shows the size distribution of diesel PM emitted by a diesel engine and soot generator (SG) as reported by S. Fujii et al. [14]. The solid lines are the particle size distributions of the SG and the dashed lines are those from the engine. Particle size distributions having two peaks: at around 10–20 and 40–60 nm, were observed for both the SG and the engine. The 10–20 nm peaks of the SG were higher than those of the engine. The introduction of the DOC reduced the peak; thus, the 10–20 nm peaks might be due to the SOF, because DOC helps to reduce the SOF. The 40–60 nm peaks of the SG increased with a decrease in the combustion lambda, and lambda 0.7 showed a 40–60 nm higher peak than lambda 0.9 and 1.1. The major component of the 40–60 nm peaks is considered to be coagulated carbon (soot) particles, and richer combustion is considered to generate more

soot than leaner combustion. The particle size distributions of PM from the engine showed 10–20 nm lower peaks, which are due to the SOF treatment effect of the DOC.

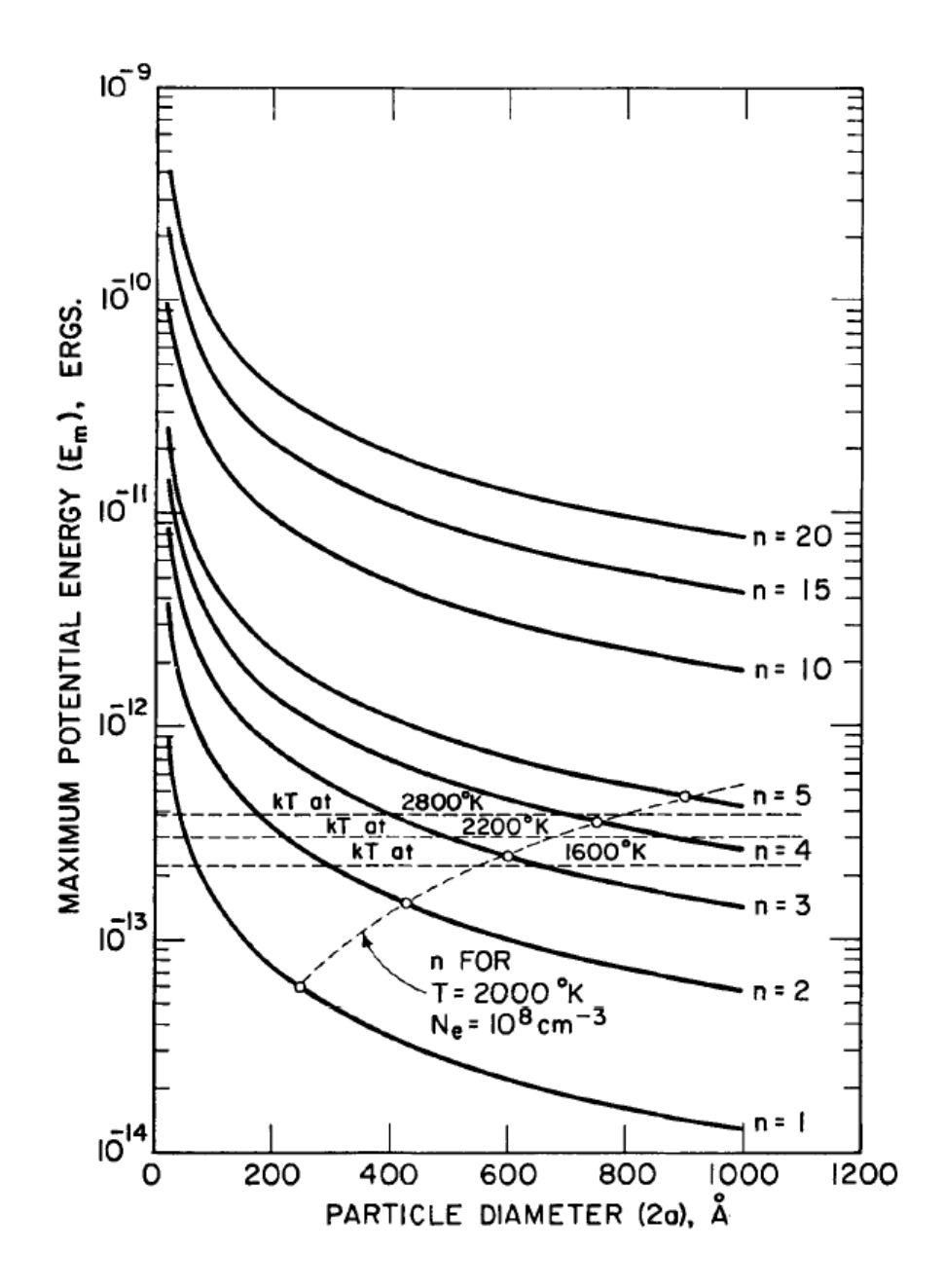


Figure 10 Variation of the maximum potential energy of two sphere graphite particles with diameter and charge [15].

The electric charge of carbon particles sampled downstream from the reaction zone in a premixed flame was reported by R. T. Ball and J. B. Howard [15]. The number of charges/particle ranged from 1 to 40, with an average of 2. The charge/particle ratio and average particle size decrease with the number of particles/agglomerate. Carbon particles in the later stage of growth are assumed to be charged by thermionic emission (thermal

electron emission) and electron capture. A given particle approaches equilibrium with the free electrons of the frame by assuming a net charge, which adjusts the effective work function and electron collision cross section to such values that the rate of electron emission equals the rate of electron capture. The energy barrier to the collision of charged carbon particles has been calculated by considering both the electrostatic repulsive and attractive energies arising from dispersion forces. The energy barrier for the degree of charging observed here greatly exceeds the available kinetic energy, implying that agglomeration occurs prior to the attainment of observed charge. Agglomeration is believed to occur along with the growth of particles in the flame reaction zone. Figure 10 shows that the potential energy increases with an increasing radius for a constant number of charges.

The electrical characteristics of particles emitted in motor vehicle exhaust are examined via single and tandem differential mobility analysis (DMA) and reported by M.M. Mariq [16]. The measurements reveal large functions of the particles; approximately 60%–80% are electrically charged, but with near equal numbers of positively and negatively charged particles. The analysis reveals exhaust particles with up to ±4 units of electrical charge, as shown in Fig. 11.

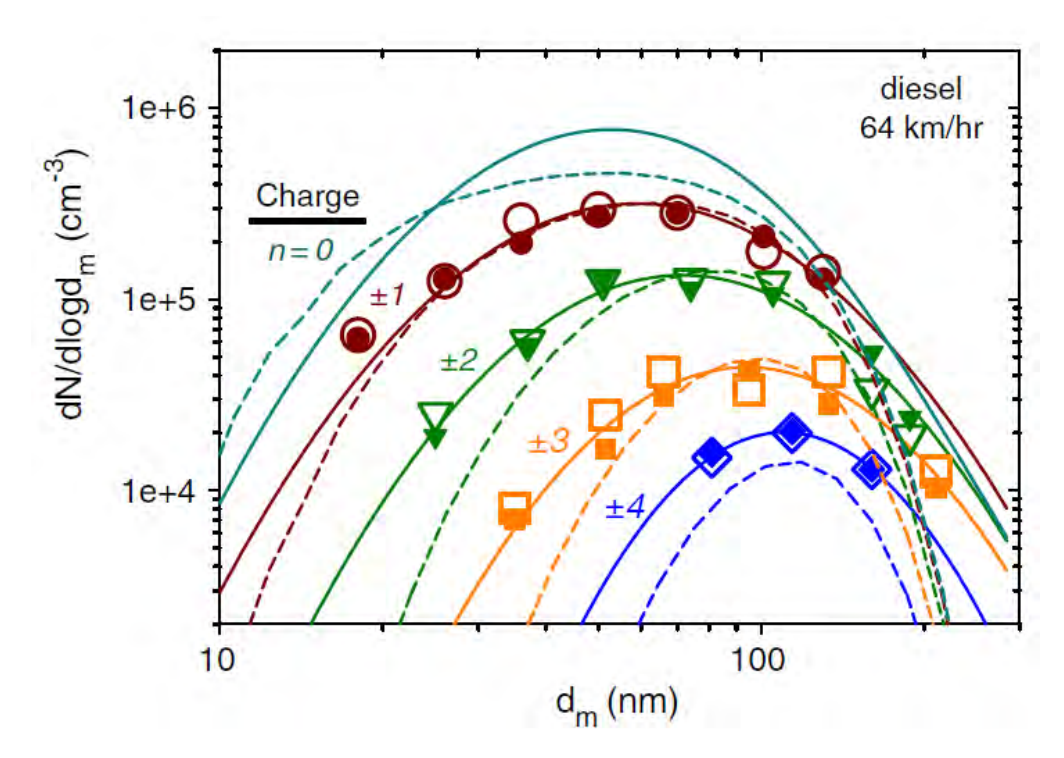


Figure 11 Charge selected particle size distributions in diesel exhaust at 64 km/h [16].

Diesel Particulate Filters (DPFs)

A diesel after-treatment technology that substantially reduces diesel engine particulate emissions is a diesel particulate filter (DPF), as shown in Fig. 12. The DPF plays an important role in particulate trapping and oxidation. Although these processes involve the most complex behavior of particulates and reaction phenomena, not much information is available for understanding them.

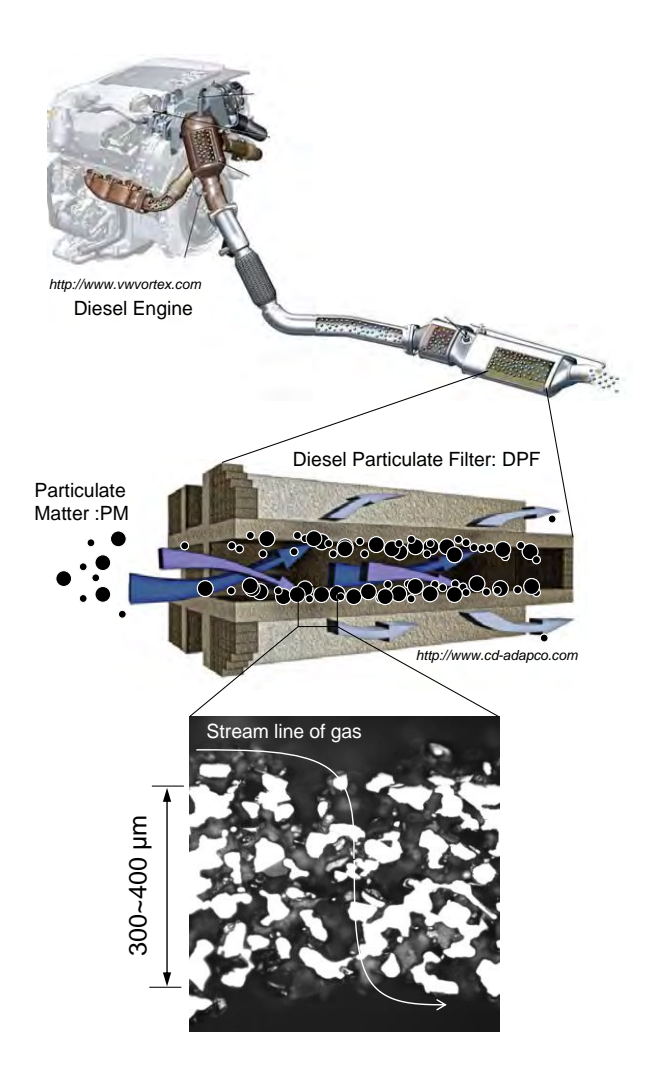


Figure 12 Schematic diagram of Diesel Particulate Filter (DPF).

A DPF is generally made of ceramic materials, such as cordierite or silicon carbide (SiC), and consists of several rectangular channels with alternate channels blocked with cement at each end. The exhaust gas is forced to flow through a channel wall having numerous micron-scale pores that trap the diesel PM. Further, the collected PM must be oxidized to regenerate the DPF and reduce the back pressure on the diesel engine.

There are two methods of DPF regeneration. One of them is an active system (periodic regeneration) that ignites particles trapped in the filter with burners or electric

heaters. In this system, the temperature of the DPF must be controlled between the DPF destruction point and the soot cake oxidation temperature, which is higher than 600 °C. The other is a passive system (continuous regeneration), in which catalytic additives reduce the overall activation energy required for particulate oxidation; oxidation occurs at a lower temperature than with active regeneration.

Simulation of Particulate Trapping

A number of studies have been performed to simulate particulate trapping and chemical reactions inside DPFs provide valuable information in designing them. A.G. Konstandopoulos et al. [17] reported many papers on the simulation of diesel PM trapping and oxidation processes. In the trapping process, at the filter wall scale, the flow resistance is determined by the Darcy permeability k and the Forchheimer coefficient β of the wall as:

$$\Delta P_{wall} = \frac{\mu}{k} u_w w_s + \beta \rho u_w^2 w_s \tag{1}$$

where ΔP_{wall} is the pressure drop across the filter, μ is the exhaust dynamic viscosity, u_w is the filtration velocity, w_s is the filter wall thickness, and ρ is the exhaust gas density. The permeability has the dimension of the length squared, and $k^{1/2}$ represents a pore-level length scale, which is a characteristic of porous medium. The Forchheimer coefficient has the dimension of inverse length, and β^{-1} represents a length scale, which is a characteristic of pore roughness. Both parameters depend on the pore size and porosity (\mathcal{E}) of the medium and are interrelated, according to Eq. 2.

$$\beta = \frac{const.}{\varepsilon^{1.5} \sqrt{k}} \tag{2}$$

The value of the constant in Eq. 2 can be 0.143, based on the original Ergun correlation, or 0.134 for smooth, and 0.298 for rough particles of packed beds, based on newer compilations. An additional pressure drop occurs in a wall-flow filter due to the frictional losses of the flow along the square channels of the filter. This pressure loss has a linear dependence on the channel velocity of the laminar flow in the inlet and outlet channels.

A.G. Konstandopoulos et al. [17] determined the permeability and the Forchheimer coefficient of each DPF structure using the experimental data of the pressure drop and filtration velocity, as shown in Fig. 13. Figure 14 compares experimental and simulation results of particulate trapping in a DPF sample. Depth filtration occurs at a soot load of about

 0.5 g/m^2 . In the phase, the pressure drop increases rapidly, and then surface filtration occurs, the pressure drop increases linearly, but more slowly than in the initial stage.

Diesel particulate transport and capture behavior in a DPF made of cordierite, observed with a Microfocus 3D X-ray technique, were simulated and reported by S. Tsushima et al. [19]. It was shown that particle diameter and inlet velocity strongly affect the deposition behavior in the DPF, because the Brownian motion of particles is highly influenced by the particle diameter. The particles penetrate the substrate in the early stage of particle loading. It was also shown that less than 40% of the pore channels were used in particle loading.

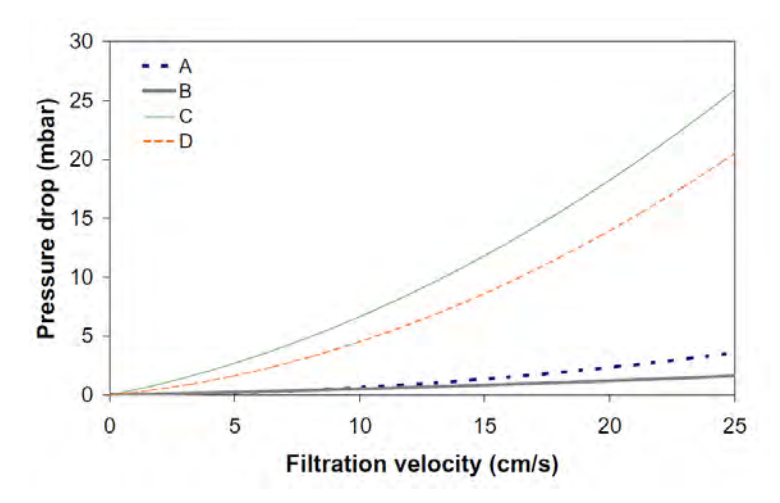


Figure 13 Pressure drop versus filtration velocity for samples A (metal fibrous with porosity of 85% and 1.36 mm thickness), B (SiC with porosity of 48% and 1 mm thickness), C (sintered metal with porosity of 50% and 0.57 mm thickness), and D (sintered metal with porosity of 50% and 0.88 mm thickness) [17].

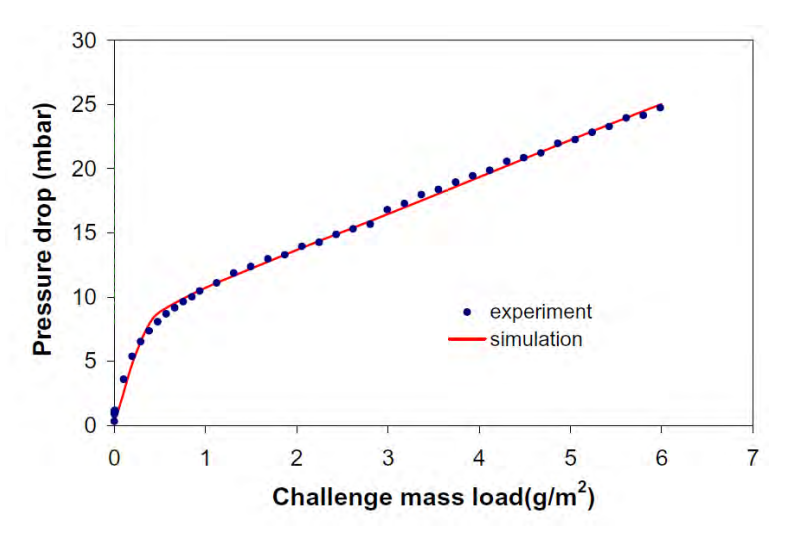


Figure 14 Experiment versus simulation of soot loading on the DPF sample [18].

Real-time Characterization of Particulate Trapping

E. Wirojsakunchai et al. [20] proposed the concept of diesel particulate trapping on the pore structure of a conventional DPF, as shown in Fig. 15. Stage 1 shows a clean DPF; stage 2 illustrates PM being collected on the inside walls of the substrate pores; in stage 3, the PM accumulates to cause pore bridging; finally, stage 4 is reached when a thin cake layer of PM begins to develop on the inlet channel wall.

A conceptual model of the pressure drop was described by G.A. Merkel et al. [21], as shown in Fig.16. The pressure drop rises quickly as the pores become plugged in stages 1 to 3 of Fig. 15. As seen in Fig. 16, transitioning from stage 1 to 2 has less effect on the pressure drop than the transition from stage 2 to 3. The figure also shows that the pressure drop during stages 1 to 3 increases non-linearly, but, once stage 4 is reached, there is a linear and slower rise in the pressure drop curve as the cake layer thickens.

However, from the visualization results, Hanamura laboratory (Tokyo Institute of Technology), the process generally called depth filtration is strongly influenced by the surface pores, because the mean pore-scale channels that are connected with the surface pores are blocked by particulates trapped during the initial stage. The particulates trapped inside the deeper pores (stages 1 to 2, according to G.A. Merkel et al. [21]) and on the top surface of porous particles, are very small compared to those on the surface pores. Therefore, the pressure drop must increase rapidly from stages 1 to 3 in the conceptual model.

Real-time DPF filtration efficiency measurements during trapping were compared using a scanning mobility particle sizer (SMPS) and a motor exhaust gas analyzer (MEXA) for particle number analysis and mass analysis, respectively. A plot of mass-based and number-based filtration efficiencies is shown in Fig. 17. These two measuring devices give very similar results.

R.A. Yapaulo et al. [22] reported the effect of filtration velocities on the pressure drop and penetration depth of soot during diesel particulate trapping. As shown in Fig. 18, a higher filtration velocity results in higher wall loading with approximately the same penetration depth into the wall. Results from ultraviolet (UV) microscopy and variable-pressure scanning electron microscopy (VP-SEM) imaging analysis indicate that the soot penetration depth (red regions) into the wall is affected more by the PM characteristics (which change with the engine operating conditions) than by filtration velocity.

The filtration velocity does not have a significant impact on the permeability of the soot cake layer; however, different filtration velocities showed distinct effects on wafer filtration performance during the wall loading stage (depth filtration). At a lower velocity, the

transition between wall filling and soot cake build-up occurs at a lower pressure drop across the filter than for a higher velocity.

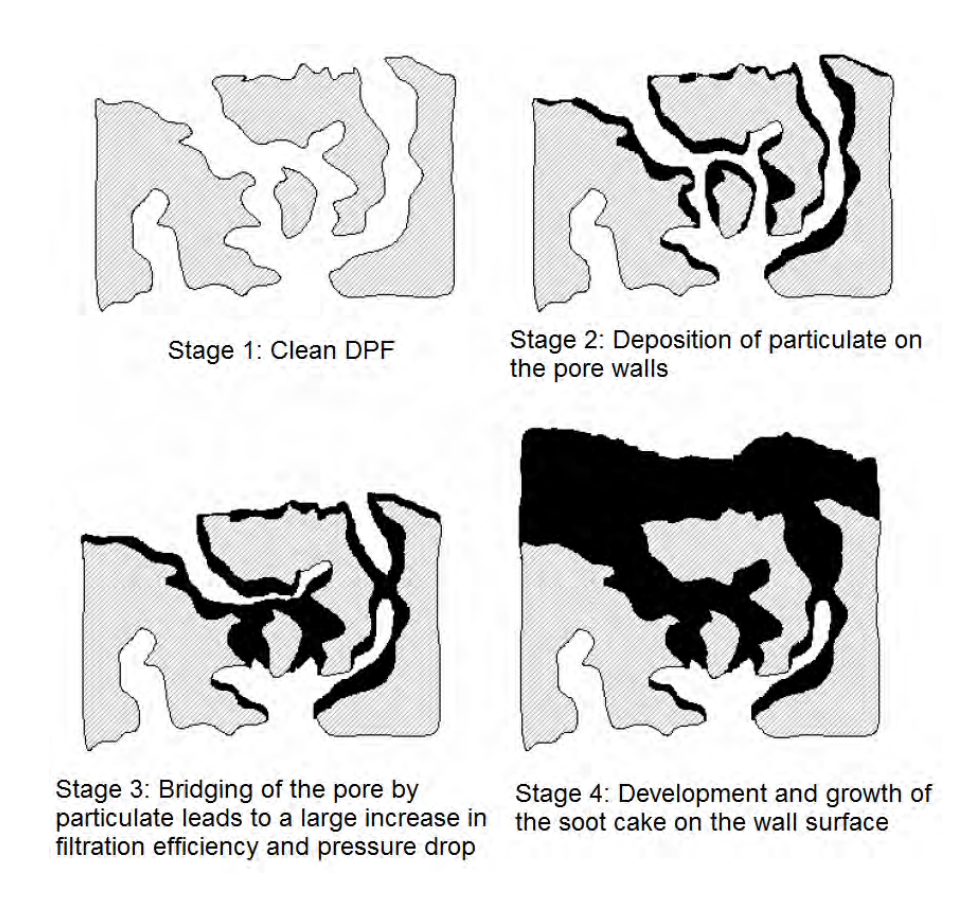


Figure 15 Conceptual model of PM trapping on the DPF wall [20].

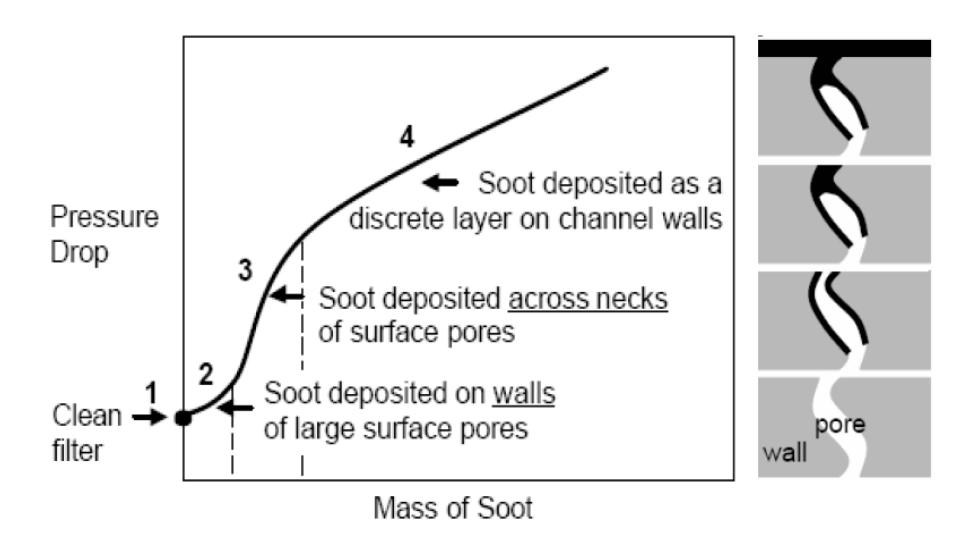


Figure 16 Conceptual model of pressure drop during particulate trapping [21].

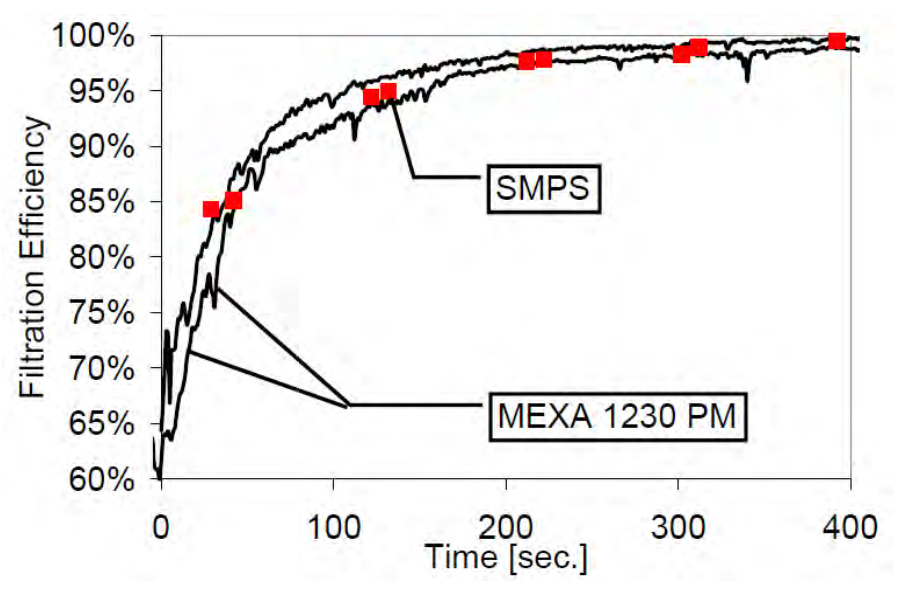


Figure 17 Comparison of filtration efficiencies of PM trapping [20].

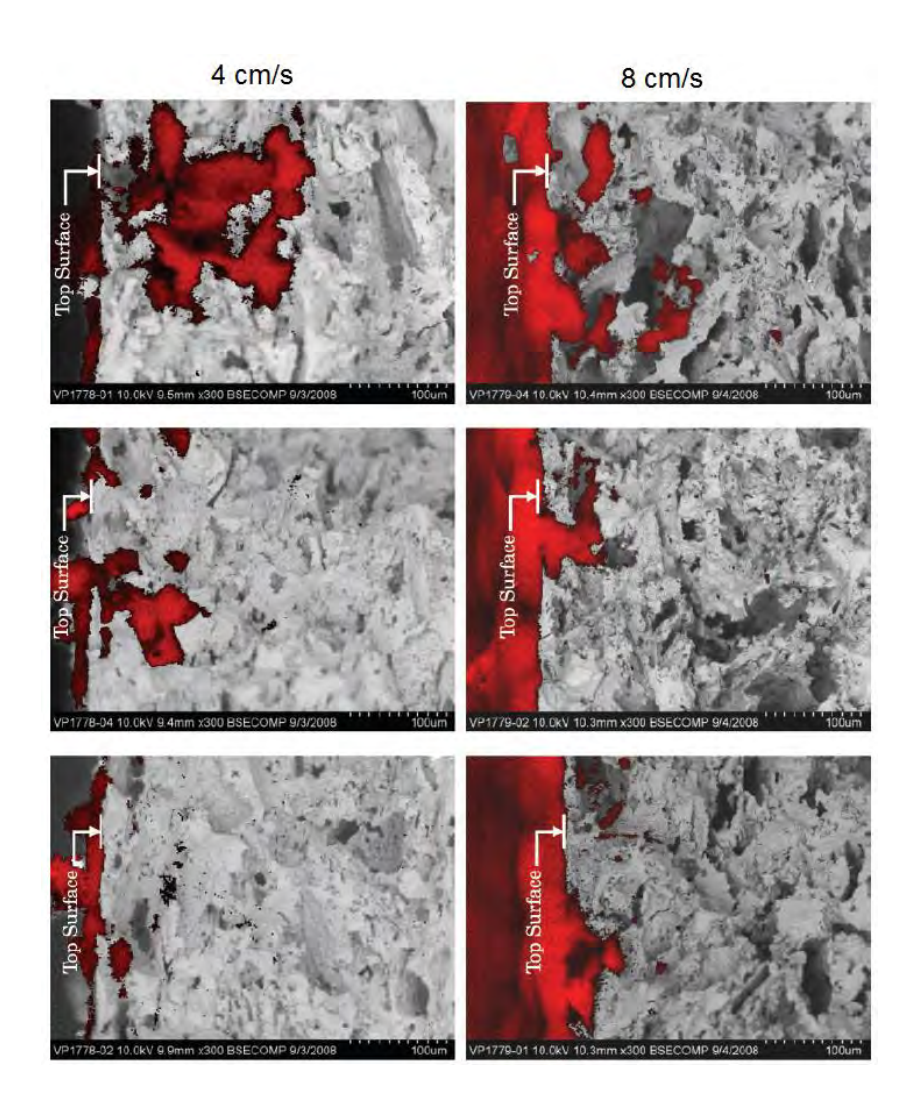


Figure 18 Carbon maps taken from VP-SEM showing soot distribution and penetration depth within the wall of wafer for 4 cm/s (left) and 8 cm/s (right) [22].

Kinetics of Diesel Soot Oxidation

The oxidation reaction of soot has been investigated using thermogravimetric analysis (TGA) and temperature program oxidation (TPO) to evaluate reaction activity. The kinetics of the uncatalyzed oxidation of flame and diesel soot were studied and reported by J.P.A. Neeft et al. [23]. Kinetic models often used to describe the reaction rates of carbonaceous materials have the general form:

$$r = N_t \cdot k(T) \cdot f(p_{O2}, p_{H2O}, \cdots)$$
(3)

where r is the reaction rate, N_t is the total number of active sites, k(T) is a temperature-dependent reaction rate constant, and $f(p_{O2}, p_{H2O}, ...)$ is a function that describes the dependence of the reaction rate on the partial pressure of the various reactants and gasphase components. The total number of active sites N_t is often described by:

$$N_t = \lambda \cdot S_a \tag{4}$$

where λ is the surface concentration of active sites and S_a the specific surface area. As it is generally accepted that the specific surface area S_a is a function of conversion ξ (the fraction of carbon that is oxidized), kinetic models describe the dependence of N_t as a function of conversion. A simple approach is to use an n^{th} order of (1- ξ):

$$S_a = S_{a,0} \cdot (1 - \xi)^{n_{\xi}} \tag{5}$$

where $S_{a,0}$ is the initial surface area (at $\zeta = 0$) and n_{ζ} is the reaction order in carbon. With increasing conversion, the model predicts a decrease in N_t and therefore, in the reaction rate. However, for highly porous carbons, such as soot and activated carbons, S_a can actually increase as a function of conversion, due to pore growth and opening of concluded pore space. Several models have been proposed to account for these phenomena.

The temperature dependence of the reaction rate is usually described by the Arrhenius equation:

$$k(T) = k_0 \cdot \exp(-\frac{E_a}{RT}) \tag{6}$$

where T is the absolute temperature, k_0 the pre-exponential factor, R the molar gas constant, and E_a the activation energy.

The function that describes the influence of the partial pressures of the gas-phase components on the reaction rate is usually limited to the influence of the oxygen partial pressure, described by the n^{th} order expression:

$$f(p_{O2}, p_{H2O}, \cdots) = p_{O2}^{n_{O2}}$$
(7)

where $p_{\rm O2}$ is the partial pressure of oxygen and $n_{\rm O2}$ is the order in the oxygen partial pressure.

The fit curve results of reaction order for both oxygen and carbon, and the activation energies, were defined. The order in carbon is ~0.73, which is close to the order of 2/3 (0.67), making it applicable for the shrinking-core model. The order of reaction rate in oxygen is close to 1. The activation energy of carbon oxidation (reaction rates in the same conversion level of different isothermal temperature conditions (Fig. 19 (a)) is 168 kJ/mol, as shown by the Arrhenius plots in Fig. 19 (b).

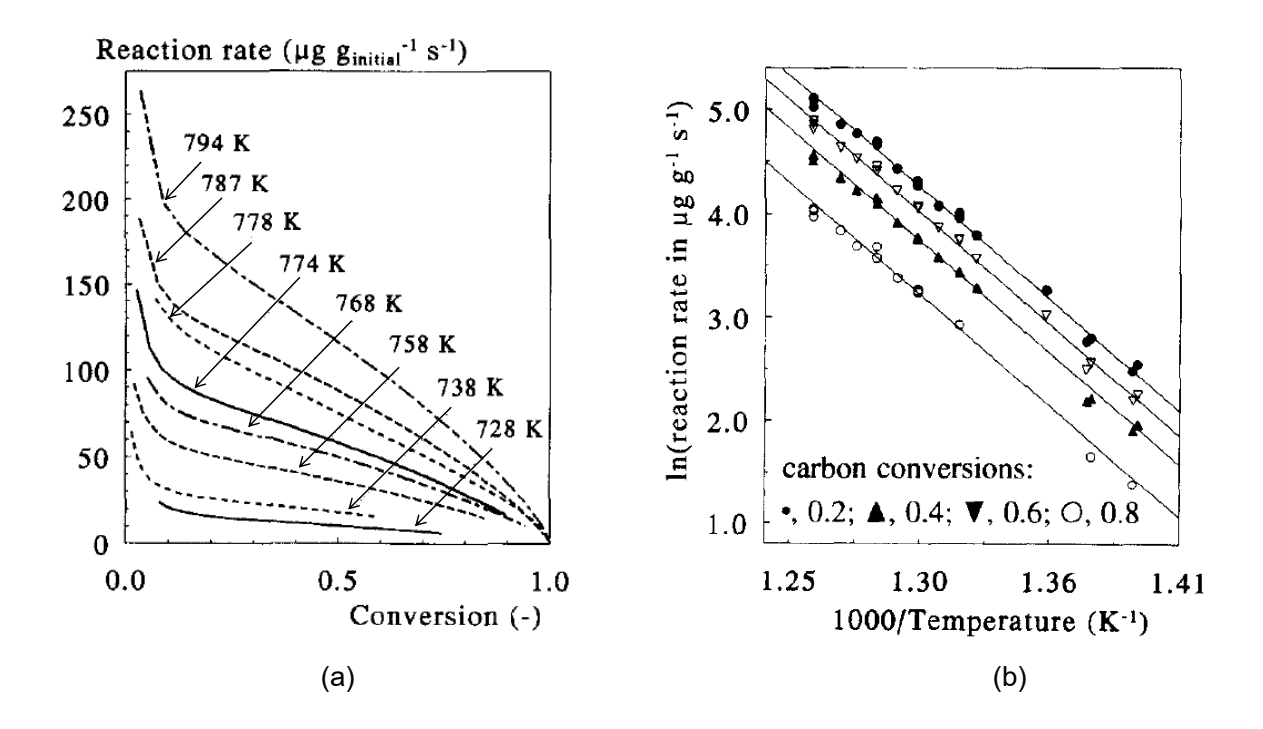


Figure 19 (a) carbon reaction rate with respect to carbon conversion and (b) Arrhenius plots for uncatalyzed oxidation of carbon [23].

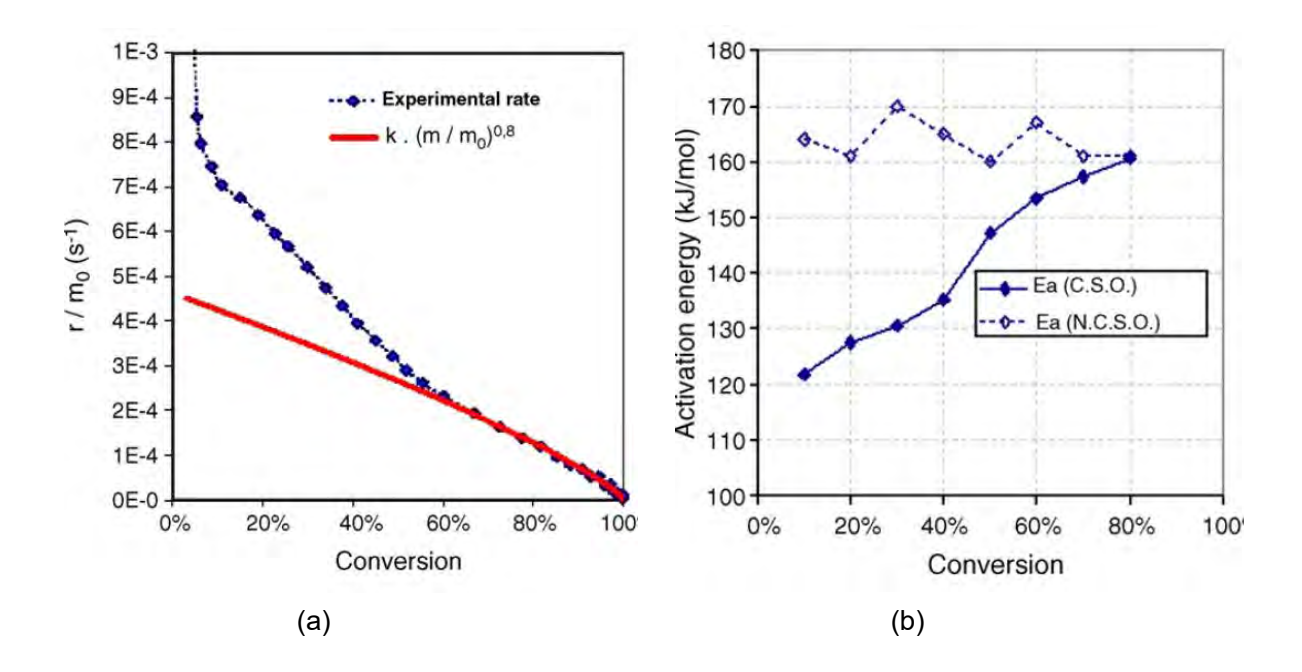


Figure 20 (a) reaction rate with respect to soot conversion for uncatalyzed oxidation of soot and (b) apparent activation energies with respect to soot conversion for catalyzed and uncatalyzed oxidation of soot [24].

Using a similar method, P. Da Costa et al. [24] reported the kinetics of catalyzed and non-catalyzed oxidation of soot emitted from a conventional diesel engine. Soot was produced from a diesel common rail engine on a bench test. Particulates were collected on a SiC DPF, and then were flushed out with air. Figure 20 shows the reaction rate of soot and apparent activation energies with respect to soot conversion by isothermal condition. The presence of the catalyst induces the existence of two distinct soot oxidation processes: a fast-catalyzed oxidation occurs at low conversion levels, when catalyst and soot are still in close contact, while at high conversion levels, only a slow-non-catalyzed oxidation remains, due to a loss of contact between soot and catalyst. The apparent activation energy of non-catalyzed oxidation of soot was about 164 kJ/mol, whereas, the apparent activation energies of catalyzed soot oxidation were about 114 kJ/mol for fast oxidation and 161 kJ/mol for slow oxidation, which looks like a non-catalytic oxidation.

Evaluation of Soot Oxidation in DPFs

To evaluate the regeneration behavior of different DPF technologies, the soot oxidation rate has to be calculated as a function of temperature. The normalized soot oxidation rate (s^{-1}) is defined as:

$$r_{soot} = \frac{1}{m_0} \frac{dm}{dt} \tag{8}$$

where m_o is the initial amount of soot mass collected. The soot consumption rate dm/dt is computed by summing the CO and CO₂ produced during oxidation. The evaluation of normalized soot oxidation rate as a function of temperature provides a means to compare and evaluate different DPF technologies with respect to their catalytic activity.

Catalytic fuel additives and catalyst DPFs have been proven to reduce the overall activation energy required for particulate oxidation, resulting in lower-temperature oxidation compared to non-catalyst DPFs. A number of studies have reported high catalytic activity of the soot oxidative catalyst. D. Fino et al. [25] reviewed a catalyst for the possible simultaneous removal of soot and NO_x . S.

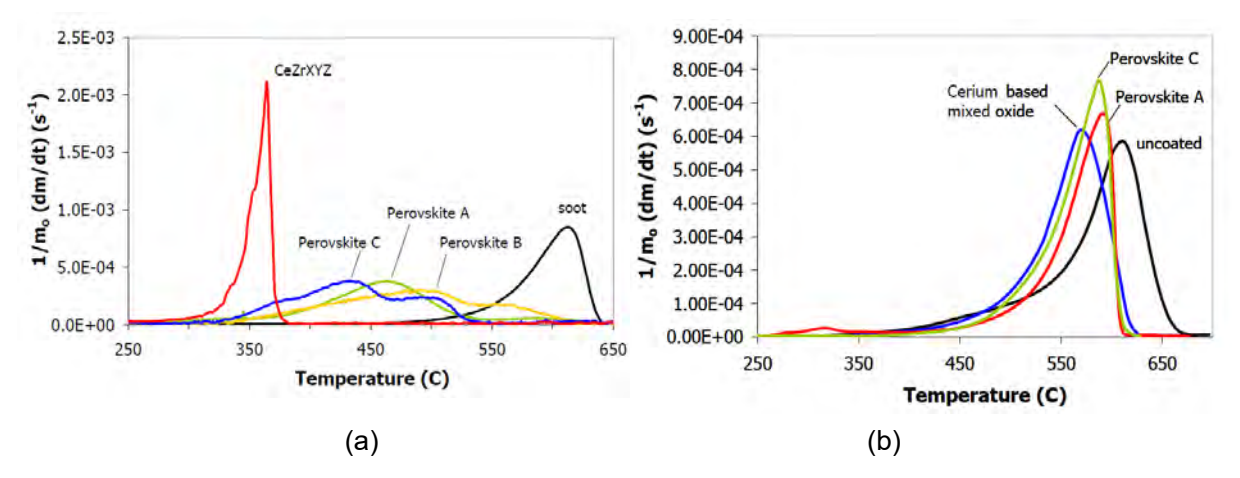


Figure 21 (a) Effect of catalyst formulation on the oxidation of soot (homogeneously mixed with catalyst particles) using thermo-gravimetric analysis (TGA) and (b) Soot oxidation rate on the catalytic coated monoliths [26].

Lorentzou et al. [26] reported the problem of a catalyzed DPF. The problem of catalyst-soot contact is well recognized as a drawback for the development of active catalyzed DPFs (CDPFs). It was observed that the chemistry of the catalyst may be masked when it is coated on the filter, due to the reduced contact with soot. Figure 21 (a) shows the high catalytic activities of soot oxidation with a uniform contact area of soot and catalyst particles.

However, low catalytic activities of soot oxidation were observed in practical use of DPF (catalytic coated monolith), as shown in Fig. 21 (b). As a result, the geometry of the DPF wall and catalyst nanostructures plays an important role in the efficient regeneration of the filter.

Macroscopic Visualization of Particulate Trapping and Oxidation in DPFs

Although the complexity of particulate behavior and reaction phenomena is well known, little information is available for understanding these phenomena. To observe the diesel particulate trapping and oxidation behavior inside conventional wall-flow DPFs, a macroscopic visualization system was developed by Hanamura et al. [27].

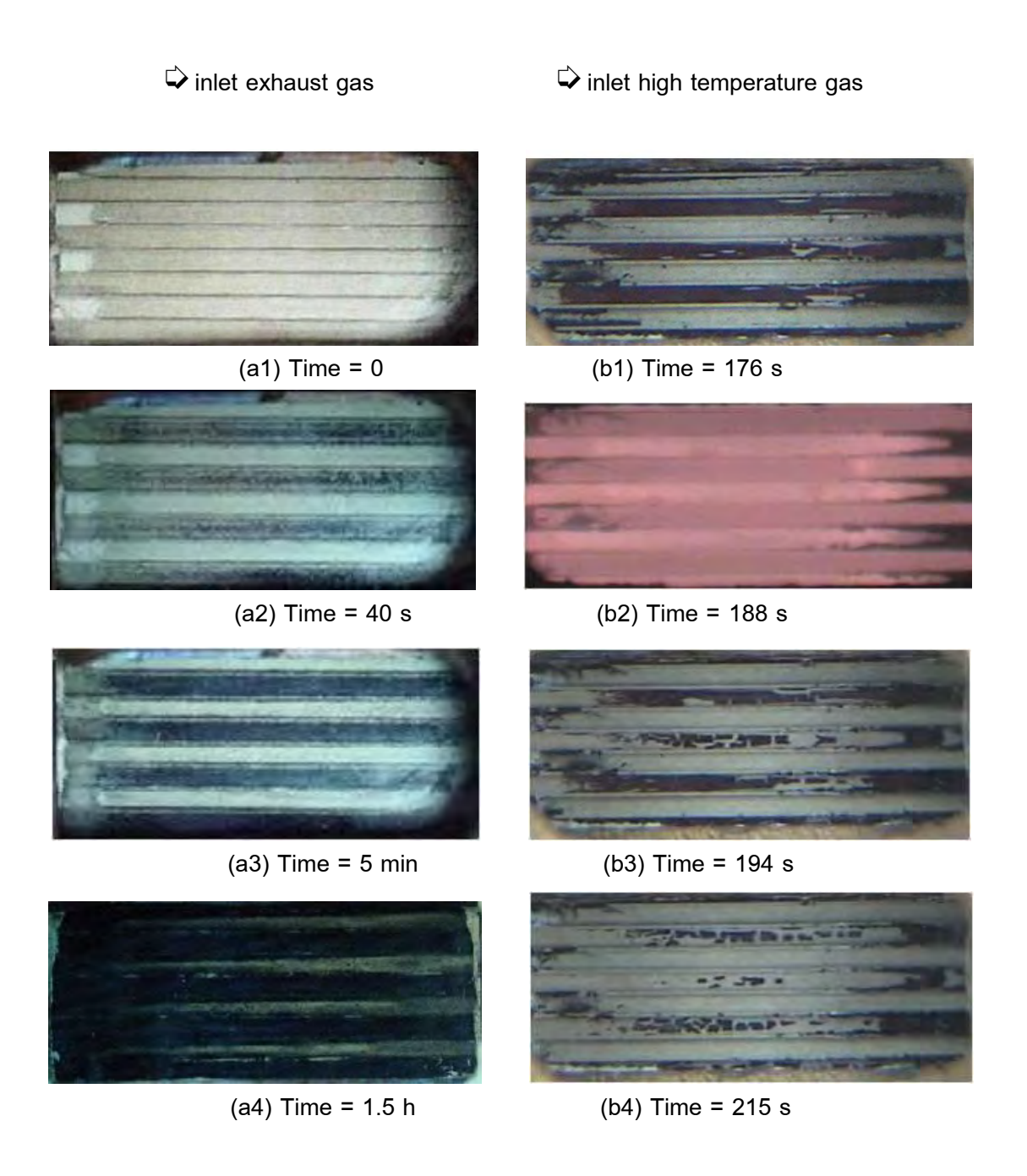


Figure 22 Surface views of a large-scale DPF made of cordierite in each time step during (a) trapping and (b) regeneration [27].

Figure 22 (a) shows the trapping process executed by a half-cylindrical DPF made of cordierite. Here, the exhaust gas flows from left to right. The alternate channels, where the exhaust gas is introduced, become darker with time. The particulates are almost uniformly trapped in all channels and over entire regions in the flow direction in each time interval, even in the case of a large-scale DPF. Very similar trapping behavior is observed in a large-scale DPF made of SiC.

In the regeneration process, the particulates are first ignited around the inlet, middle, and outlet in the flow direction (strongly dependent on the temperature), and the reaction zone propagates toward both the upstream and downstream sides. Many large soot cake islands remain, and they are uniformly distributed on the entire surface of the DPF wall, as shown in Fig. 22 (b). The low oxidation rate of the remaining soot cake is an important problem in practical application in actual vehicles.

Microscopic Visualization of Particulate Trapping and Oxidation in DPFs

According to visualization results [28], a major problem of conventional DPFs is the filtration performance at the beginning of the trapping process. During this phase, some diesel particulates pass through the DPF wall from the upstream to the downstream side. The amount of particulates trapped increases gradually with time along the shape of the surface pores after the mean pore-scale channels that are connected with the surface pores are blocked by particulates trapped during the initial stage. As a result, filtration performance increases with time, and most particulates are trapped by the soot cake layer after it develops. As shown in Fig. 23, the surface pores are filled with particulates and only a few particulates, which may have passed through at the beginning of the trapping process, are trapped in the deeper pores. However, the filtration performance decreases again after the DPF is regenerated. Consequently, the process generally called "depth filtration" is strongly related to the surface pores. The existence of the soot cake layer is also an important advantage for filtration performance because it can trap most particulates.

A nanoparticle membrane filter was proposed on the basis of the previous studies. It consists of a SiC-nanoparticle membrane filter sintered onto the conventional SiC-DPF. The filter was made of SiC nanoparticles with a mixed size of 80 nm and 500 nm and sintered onto the conventional SiC-DPF. The DPMF has a thickness of 20 μ m and a porosity of 60%, while the conventional DPF has 300 μ m thickness and 42% porosity.

Figure 24 shows SEM images of the DPMF sintered on the in-flow channel (top), microgrooves (middle), and the fine surface pores (bottom) on the surface of the DPMF. Because the nanoparticles were homogeneously distributed, the mean pore size of the

DPMF (0.5 μ m) was much smaller than that of the conventional filter (11 μ m). However, some microgrooves can be seen on the DPMF surface, as well as fine surface pores with a mean size of about 1 μ m. The PM trapping and oxidation in regeneration were investigated through microscopic visualization experiments and gas analysis during regeneration.

Figures 25 (a) and (b) show SEM images of ultrafine sizes dominant diesel particulates captured by glass fiber filters after passing through a conventional DPF with porosity of 42% and a DPMF, respectively, during five min of trapping. The SEM images show amount of particulate trapped after pass through the conventional DPF larger than that of the DPMF. This is because most of the ultrafine diesel particulates are likely to get trapped by the membrane, whereas they pass through the conventional DPF at the beginning of trapping.

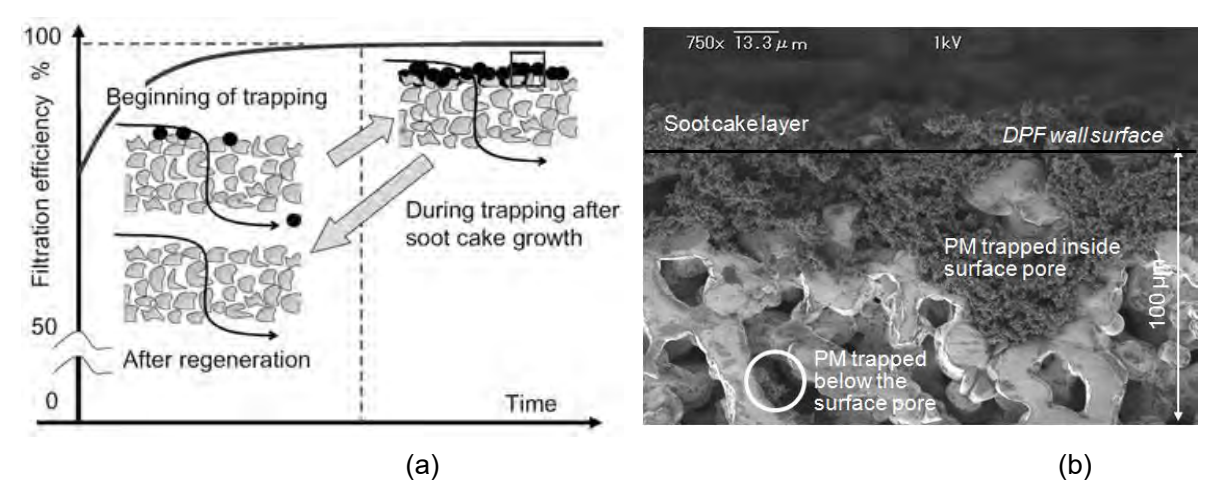


Figure 23 (a) Filtration efficiency of the conventional DPF and (b) SEM image of particulate trapped on the surface pore of DPF [28].

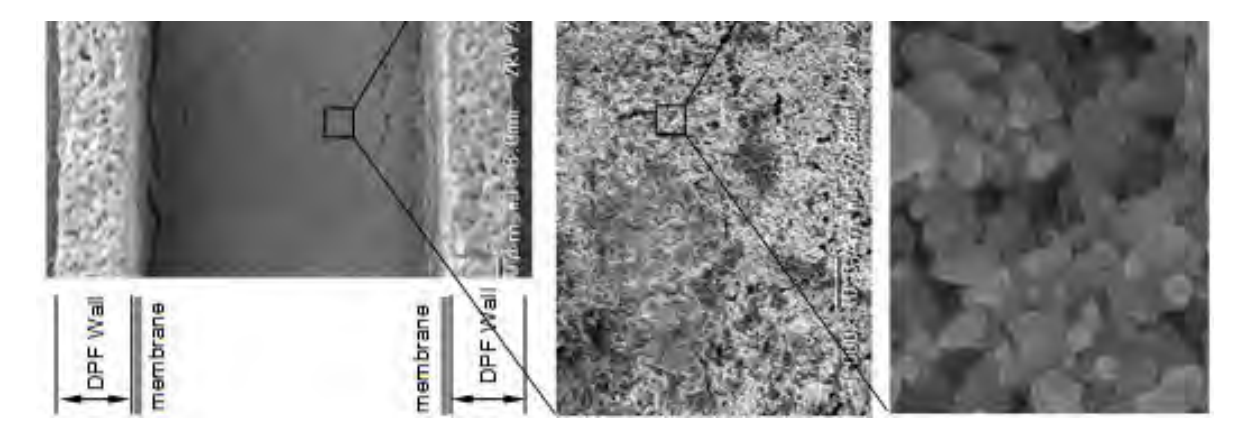


Figure 24 SEM images of DPMF sintered onto the conventional DPF wall (top), microgrooves on the DPMF surface (middle), and fine surface pores on the DPMF surface (bottom) [28].

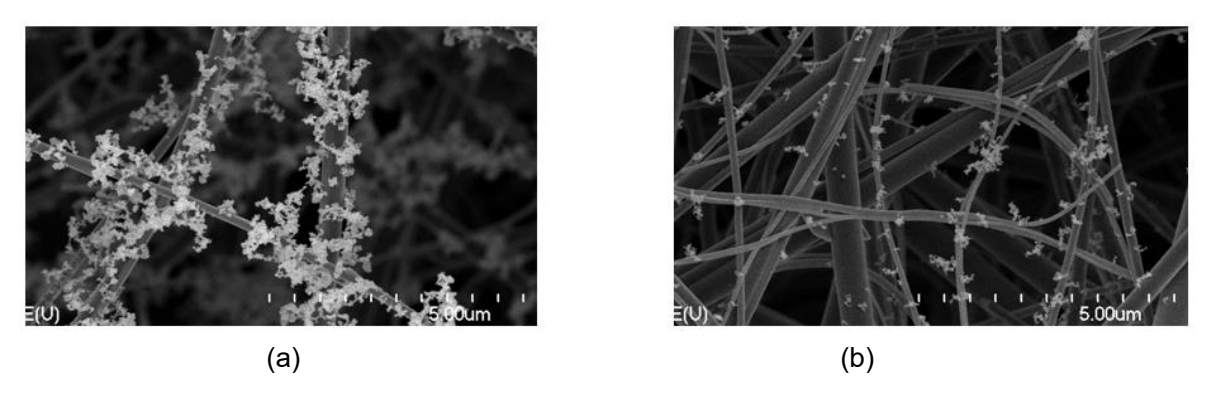


Figure 25 SEM images of soot captured by glass fiber filters after passing through (a) the conventional DPF and (b) DPMF [29].

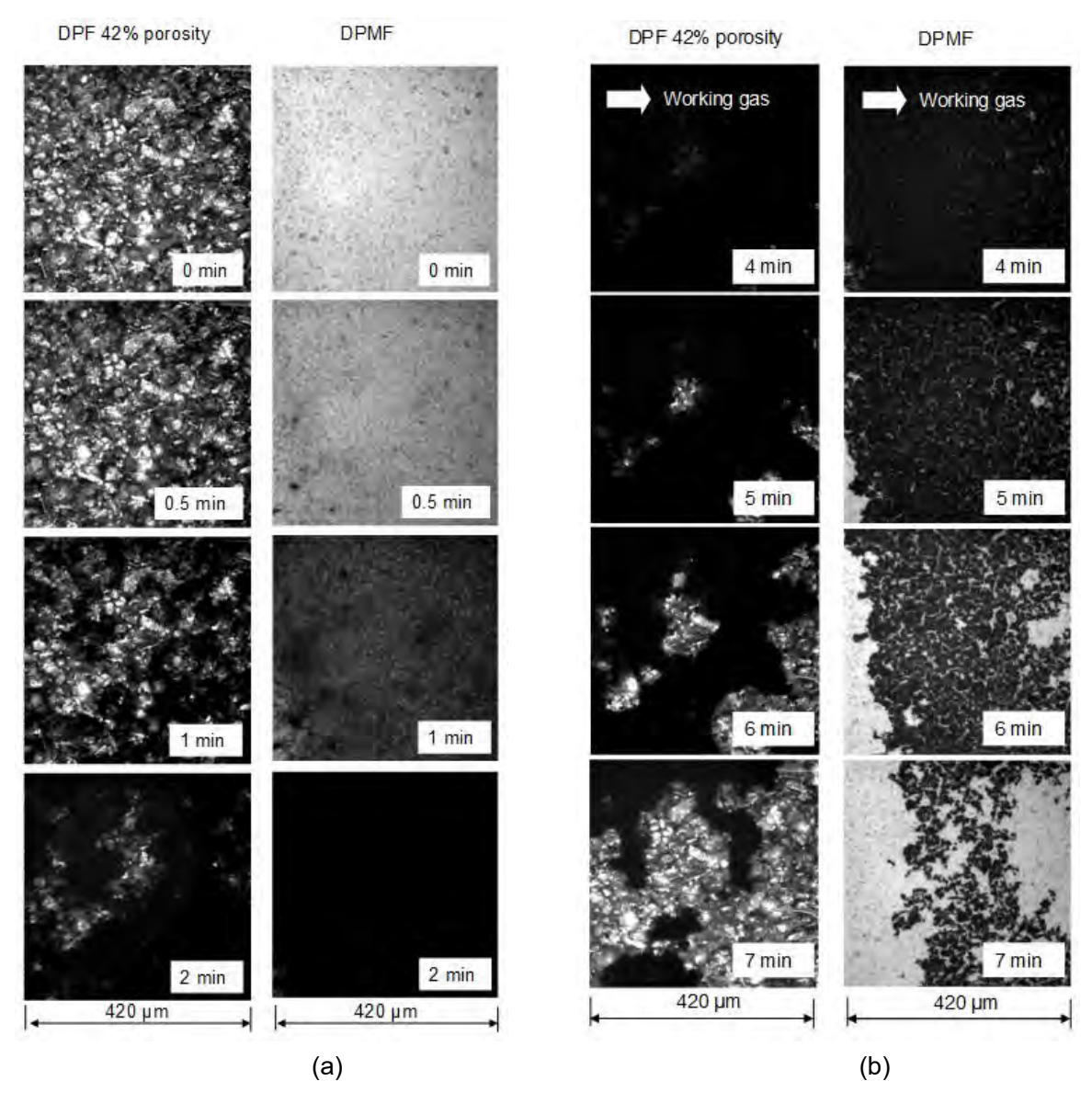


Figure 26 Optical surface views of the conventional DPF and DPMF for ultrafine sizes dominant particulate matters (a) trapping and (b) oxidation [29].

Figure 26 shows microscopic visualization trapping and oxidation on the conventional DPF and DPMF. In the trapping process, the nanoparticulates might contact the surface of SiCs near the bottom of the surface pores due to Brownian diffusion. After that, the particulates cannot be removed because the friction forces from the fluid dynamics of gas are less than the electrostatic forces of charged particulates, especially particulates smaller than 300 nm. This blocks the mean pore-scale channels that connect with the surface pores. The surface pores fill and a soot cake grows with time; thus, soot cake developed faster on the membrane filters than in the conventional DPFs.

In the regeneration process, the apparent activation energy for the oxidation of soot in the DPMFs becomes smaller than in the conventional non-catalyst DPFs. As a result, there might be some catalytic activity for the enhancement of oxidation of the soot layer on the SiC nanoparticles, which are elements of the DPMF. Some catalytic activity of oxide of silicon and silicon oxycarbide might support oxygen mobility around the soot oxidation territory.

Influents of Renewable Bio-oxygenated Fuel

Renewable bio-oxygenated fuels - liquid and gaseous fuels derived from organic matter - can play an important role in reducing CO2 emissions (greenhouse gas effect and global warming) because of bio-fuels is the carbon neutral, as shown in Fig. 27. To reduce dependency on oil and to contribute to growing efforts to decarbonizes the transport sector, bio-fuels provide away of shifting to low-carbon, non-petroleum fuels, often with minimal changes to vehicle stocks and distribution infrastructure. While improving vehicle efficiency is by far the most important low-cost way of reducing co emissions in the transport sector, biofuels will need to play a significant role in replacing liquid fossil fuels suitable for planes, marine vessels and other heavy transport modes that cannot be electrified. Production and use of bio-fuel can also provide benefits such as increased energy security, by reducing dependency on oil imports, and reducing oil price volatility. In addition, bio-fuels can support economic development by creating new sources of income in rural areas, as shown in Fig. 28. The cost of reducing greenhouse-gas emissions through the use of different fuel can be estimated by combining fuel costs with life-cycle greenhouse-gas emissions, compared to a common gasoline baseline. The same set of information can be used to evaluate the effect of carbon prices on the relative costs of different fuels. The incremental cost of a range of alternative fuels as a function of their CO2-equivalent saving potentials varies widely (Fig. 30). The rectangles in Fig. 29 indicate typical ranges of variation for both Co2-equivalent savings and cost [30].

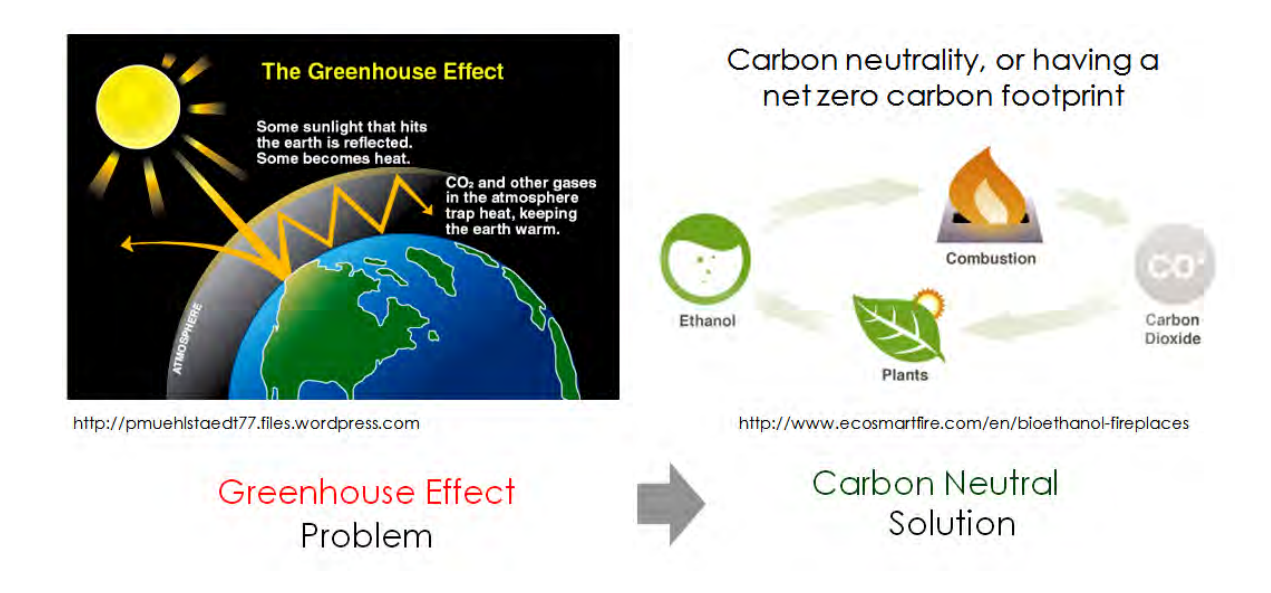


Figure 27 The green house effect (Carbon dioxide) and the concept of carbon neutral of renewable bio-oxygenated fuels.

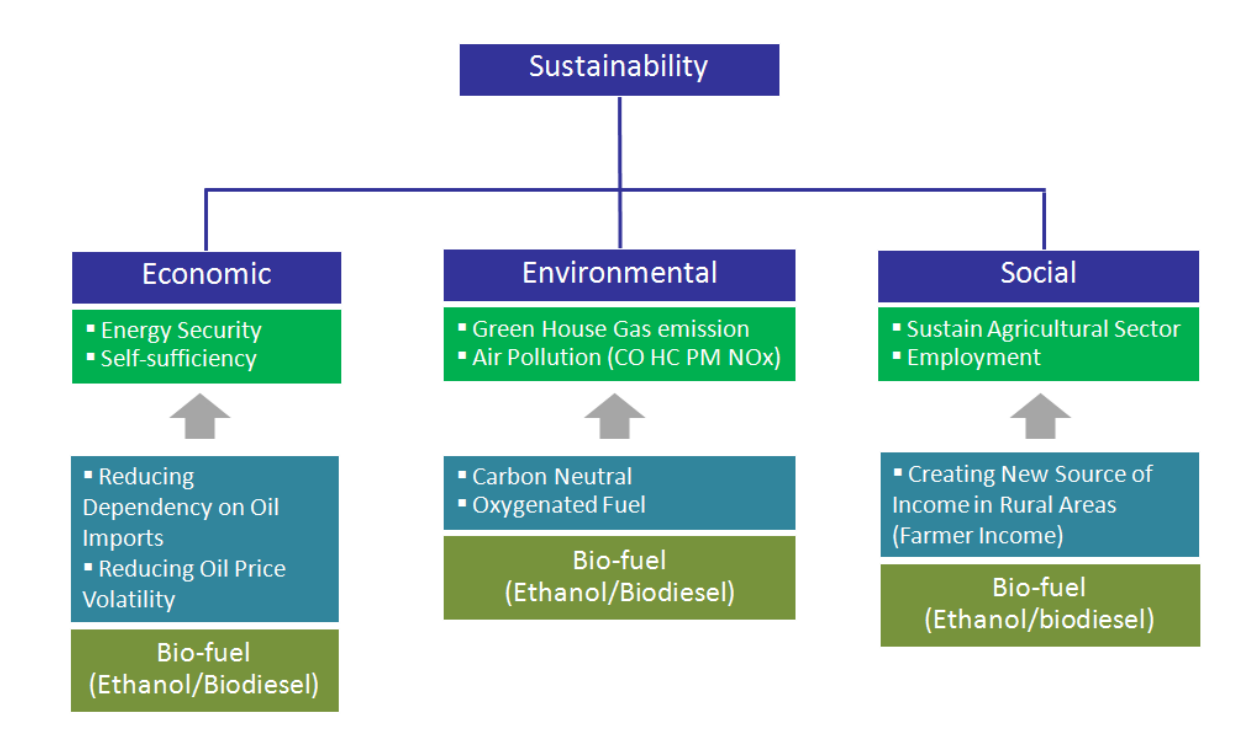


Figure 28 Summary of influent of renewable bio-oxygenated fuel (Ethanol and Biodiesel) for economic, environmental and social.

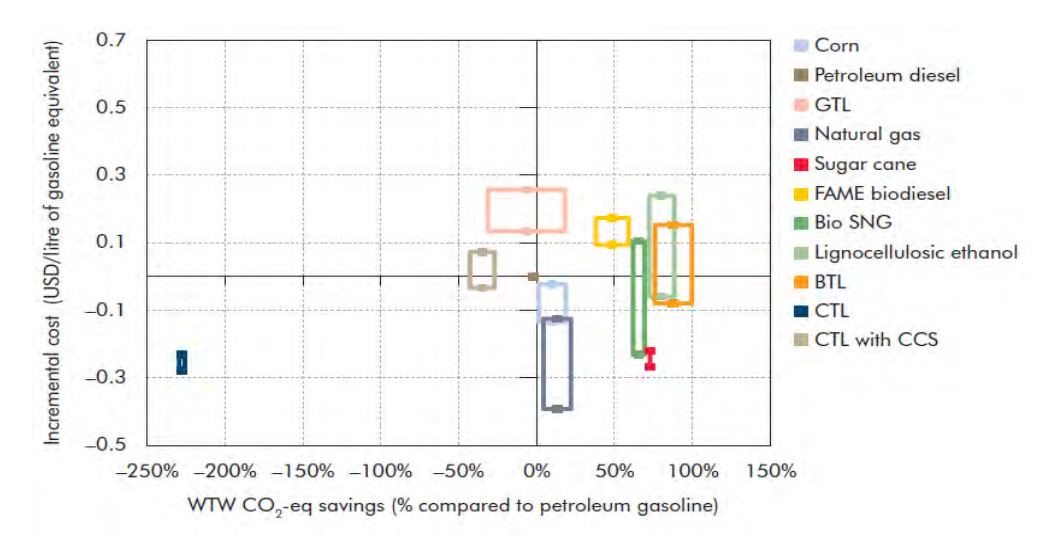


Figure 29 Incremental cost of alternative fuels as a function of their co2-equivalent saving potentials (at USD 120/bbl) [30].

References

- [1] Energy Information Administration (EIA), *International Energy Annual 2006,* www.eia.doe.gov, 2008.
- [2] D.A. Coley, Energy and Climate Change Creating a Sustainable Future, John Wiley & Sons, Ltd. 2008. (www.newscientist.com)
- [3] The European parliament and the council of the European, Regulation (EC) No. 715/2007, Official Journal of the European Union, http://eur-lex.europa.eu, 2007.
- [4] J.B. Heywood, Internal Combustion Engine Fundamental, *McGraw-Hill series in mechanical engineering*,1988.
- [5] J.P.A. Neeft, M. Makkee and J.A. Moulijn, Diesel particulate emission control, *Fuel Processing Technology*, Vol.47, pp.1-69, 1996.
- [6] P. Eastwood, Particulate Emissions from Vehicles, *SAE Order No.R-389*, SEA International, pp.64, 2008.
- [7] O.I. Smith, Fundamentals of soot formation in flames with application to diesel engine particulate emissions, *Progress in Energy and Combustion Science*, Vol. 7, pp.275-291, 1981.
- [8] M.M. Maricq, Review Chemical Characterization of particulate emissions from diesel engine: A review, *Journal of Aerosol Science*, Vol.38, pp.1079-1118, 2007.
- [9] D.B. Kittelson, Engines and nanoparticles: a review, *Journal of Aerosol Science*, Vol.29, pp.575-588, 1998.
- [10] W.A. Majewski and M.K. Khair, Diesel Emissions and Their Control, *SAE Order No.R-303*, SAE International, 2006.
- [11] G.A. Merkel, W.A. Cutler and C.J. Warren, Thermal Durability of Wall Flow Ceramic Diesel Particulate Filters, *SAE Technical paper*, 2001-01-0190, 2001.

- [12] T. Ishiguro, Y. Takatori and K. Akihama, Microstructure of Diesel Soot Particles Probed by Electron Microscopy: First Observation of Inner Core and Outer Shell, *Combustion and Flame*, 108, pp.231-234, 1997.
- [13] R.L. Vander Wal, A. Yezerets, N.W. Currier, D.H. Kim and C.H. Wang, HRTEM Study of diesel soot collected from diesel particulate filters, *Carbon*, 45, pp.70-77, 2007.
- [14] S.Fujii, T. Asako and K. Yuuki, Studies of diesel particulate filter performances by a diesel engine simulator, *SAE Technical paper*, 2010-01-0813, 2010.
- [15] R.T. Ball and J.B. Howard, Electric charge of carbon particles in flames, *Symposium* (International) on Combustion, Vol.13, Issue 1, pp.353-362, 1971.
- [16] M.M. Maricq, On the electrical charge of motor vehicle exhaust particles, *Journal of Aerosol Science*, Vol.37, pp.858-874, 2006.
- [17] A.G. Konstandopoulos, M. Kostoglou, N.Vlachos and E. Kladopoulos, Progress in Diesel Particulate Filter Simulation, *SAE Technical paper*, 2005-01-0946, 2005.
- [18] A.G. Konstandopoulos, D. Zarvalis, E. Kladopoulou and L. Dolios, A multi-reactor assembly for screening of diesel particulate filters, *SAE Technical paper*, 2006-01-0874, 2006.
- [19] S. Tushima, I. Nakamura, S.Sakashita, S. Hirai and D. Kitayama, Lattice Boltzmann simulation on particle transport and captured behaviors in a 3d-reconstructed micro porous DPF, *SAE Technical paper*, 2010-01-0534, 2010.
- [20] E. Wirojsakunchai, E. Schroeder, C. Kolodziej, D.E. Foster, N.Schmidt, T. Root, T. Kawai, T. Suga, T. Nevius and T. Kusaka, Detailed diesel exhaust particulate characterization and real-time DPF filtration efficiency measurements during PM filling process, *SAE Technical paper*, 2007-01-0320, 2007.
- [21] G.A. Merkel, W.A. cutler, T. Tao, A. chiffey, P. Phillips, M.V. Twigg and A. Walker, New cordierite diesel particulate filter for catalyzed and non-catalyzed applications, *Proceeding of the 9th diesel engine emissions reduction conference*, Newport Rhode Island, 2003.
- [22] R.A. Yapaulo, E. Wirojsakunchai, T. Orita, D.E. Foster, M. Akard, L.R. Walker and M.J. Lance, Impact of filtration velocities and particulate matter characteristics on diesel particulate filter wall loading, *International Journal of Engine research*, Professional Engineering Publishing, Vol.10, No.5/2009, pp.287-304, 2009.
- [23] J.P.A. Neeft, T.X. Nijhuis, E. Smakman, M. Makkee and J.A. Moulijn, Kinetics of the oxidation of diesel soot, *Fuel*, Vol.76, No.12, pp.1129-1136, 1997.
- [24] P. Darcy, P.D. Costa, H. Mellottee, J.M. Trichard and G.D. Mariadassou, Kinetics of catalyzed and non-catalyzed oxidation of soot form a diesel engine, *Catalysis Today*, Vol.119, pp.252-256, 2007.

- [25] D. Fino and V. Specchai, Review open issues in oxidative catalysis for diesel particulate abatement, *Powder technology*, Vol.180, pp.64-73, 2008.
- [26] S. Lorentzou, C.Pagkoura, A. Zygogianni, G. Kastrinaki and A.G. Konstandopoulos, Catalytic nano-structured materials for next generation diesel particulate filters, *SAE Technical paper*, 2008-01-0417, 2008.
- [27] K. Hanamura, T. Suzuki, T. Tanaka and Y. Miyari, Visualization of Combustion Phenomena in Regeneration of Diesel Particulate Filter, *SAE Technical paper*, 2003-01-0836, 2003.
- [28] P. Karin and K. Hanamura, "Particulate Matter Trapping and Oxidation on Catalyst-Membrane", SAE International Journal of Fuels and Lubricants, Vol.3 No.1, pp.368-379, 2010.
- [29] H. Oki, P. Karin and K. Hanamura, "Visualization of Oxidation of Soot Nanoparticles Trapped on a Diesel Particulate Membrane Filter", *SAE International Journal of Engines*, Vol. 4 no. 1, pp.515-526, 2011.
- [30] Energy International Agency (EIA), Technology Roadmap Biofuels for Transport, 2011.
- [31] M.M. Maricq, "Soot formation in ethanol/gasoline fuel blend diffusion flames", Combustion and Flame, www.elsevier.com/locate/combustflame, 2011.
- [32] S. Laosuwan, P. Karin and C. Charoenpornpanich, "Thermo-gravimetric Analysis of Biodiesel Diffusion Flame's Particulate Matter", *Second TSME International Conference on Mechanical Engineering (2nd TSME-ICoME)*, 19-21 October, Krabi-Thailand, 2011.
- [33] C. Charoenphonphanich, P. Ornman, P Karin, H. Kosaka and N. Chollacoop, "Experimental investigation in combustion characteristics of ethanol-gasoline blends for stratified charge engine", *The 17th Small Engine Technology Conference (SETC-2011)*, SAE No. 2011-32-0551, 8-10 November, Sapporo-Japan, 2011.
- [34] Y. Songsaengchan, C. Chareonphonphanich, P. Karin, N. Chollacoop, M. Thongroon, K. Hanamura, "Physical Characterization of Biodiesel Particulate Matter by STEM", Second TSME International Conference on Mechanical Engineering (2nd TSME-ICoME), 19-21 October, Krabi-Thailand, 2011.
- [35] K. Yamamoto, M. Nakamura, H. Yane and H. Yamashita, "Simulation on catalytic reaction in diesel particulate filter", *Catalysis Today* 153 (2010) 118-124.
- [36] J. Yang, M. Stewart, G. Maupin, D. Herling and A. Zelenyuk, "Single wall diesel particulate filter (DPF) filtration efficiency studies using laboratory generated particles", *Chemical Engineering Science* 64 (2009) 1625-1634.

คุณสมบัติเชื้อเพลิงไบโอดีเซล

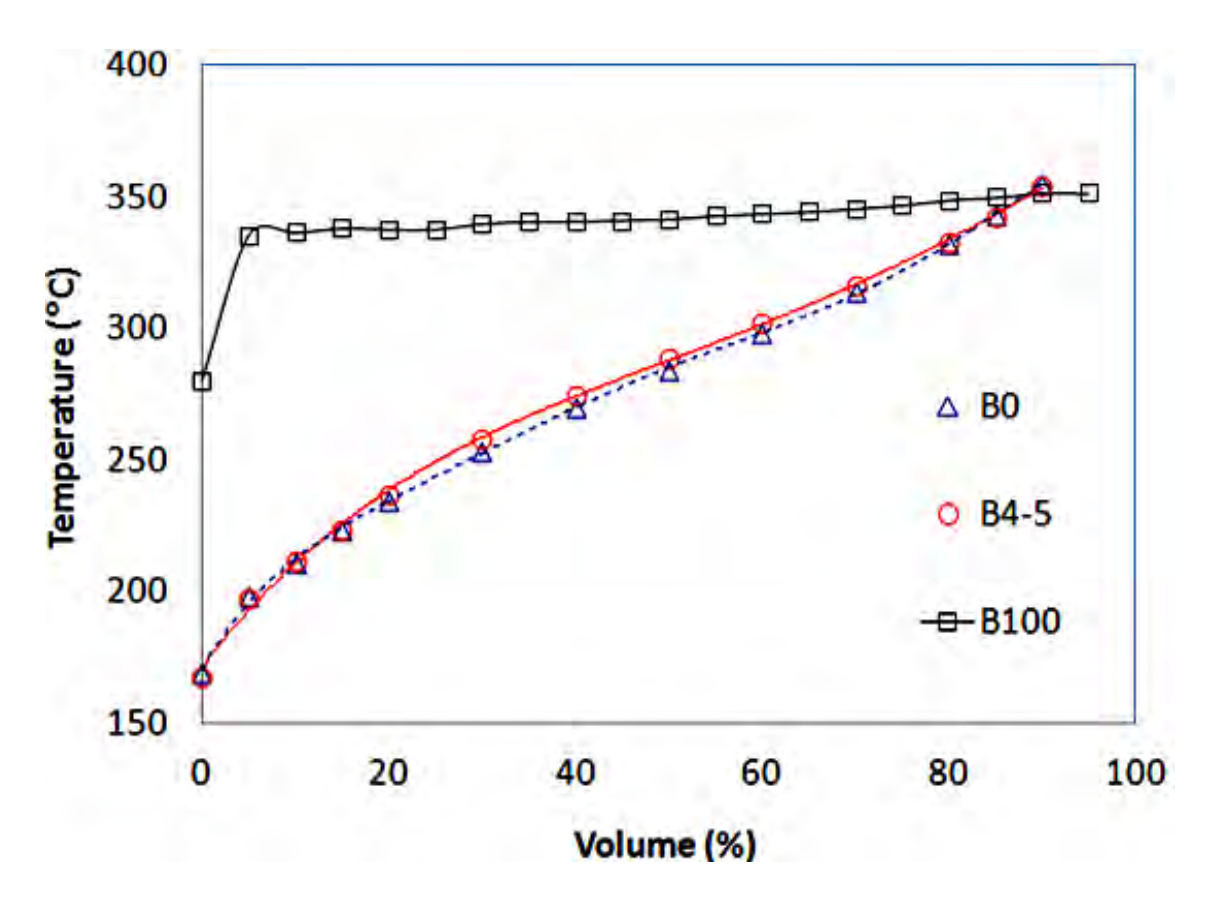
การใช้เชื้อเพลิงไบโอดีเซลเป็นอีกวิธีการหนึ่งที่สามารถลดปริมาณมลพิษจากการเผาไหม้ได้ เพราะออกซิเจนอะตอมในโมเลกุลของไบโอดีเซลจะช่วยในการเผาไหม้ให้มีประสิทธิภาพสูงกว่า เชื้อเพลิงจากฟอสซิลซึ่งไม่มีอะตอมของออกซิเจนในโมเลกุลเชื้อเพลิง ออกซิเจนอะตอมในเชื้อเพลิง ดังกล่าวมีผลทำให้ค่าอัตราส่วนผสมอากาศต่อเชื้อเพลิงที่พอดีตามทฤษฎีต่ำกว่าดีเซลที่มีค่าประมาณ 14.7:1 นอกเหนือจากส่วนผสมเชื้อเพลิงต่ออากาศที่เหมาะสมแล้ว ส่วนประกอบของธาตุในโมเลกุล ค่าความร้อน มวลโมเลกุลของเชื้อเพลิง ล้วนมีผลกระทบโดยตรงต่ออัตราส่วนผสมเชื้อเพลิงอากาศที่เหมาะสม ซึ่งคุณสมบัติดังกล่าวมีผลกระทบโดยตรงต่อการออกแบบเครื่องยนต์ให้มีประสิทธิภาพ สูงสุด กล่าวโดยสรุปการเติมส่วนผสมไบโอดีเซลในน้ำมันดีเซลมีผลทำให้ต้องการปริมาณน้ำมันผสม ที่มากขึ้นโดยมวลเมื่อเทียบกับดีเซลเมื่อพิจารณาที่ปริมาณพลังงานเท่ากัน ในขณะเดียวกันปริมาณ ของอากาศที่ใช้ทำปฏิกิริยากับเชื้อเพลิงก็มีค่าต่ำลงเมื่อเปรียบเทียบที่น้ำหนักของเชื้อเพลิงเท่ากัน ดังนั้นในกรณีที่เติมเชื้อเพลิงไบโอดีเซลในสัดส่วนที่มากเกินไปควรมีการปรับแต่งเครื่องยนต์ให้มี ส่วนผสมใกล้เคียงกับทฤษฎีเพราะเครื่องยนต์ที่ผลิตจากโรงงานโดยทั่วไปจะสามารถออกแบบให้ ทำงานได้ดีที่สุดที่ส่วนผสมอากาศต่อเชื้อเพลิงเพียงค่าเดียวหรือช่วงแคบๆ เท่านั้น

จากผลการทดลองพบว่าคุณสมบัติเบื้องต้นทางเคมีและทางกลของเชื้อเพลิงดีเซลและไบโอ ดีเซลไม่ได้แตกต่างกันมากนักดังแสดงใน ตารางที่ 1 จะเห็นว่าเชื้อเพลิงไบโอดีเซลจะมีอะตอมของ ออกซิเจนในโมเลกุลของเชื้อเพลิงซึ่งอะตอมของออกซิเจนดังกล่าวจะส่งผลดีโดยตรงต่อประสิทธิภาพ ในการเผาไหม้ อย่างไรก็ตามค่าความร้อนที่ได้จากการเผาไหม้เชื้อเพลิงต่อน้ำหนักเชื้อเพลิงดีเซลจะ สูงกว่าไบโอดีเซลเนื่องจากดีเซลมีจำนวนพันธะเคมีที่แข็งแรงมากกว่าไบโอดีเซล นอกจากนั้นความ หนืดและความหนาแน่นของเชื้อเพลิงไบโอดีเซลมีค่าสูงกว่าดีเซลเล็กน้อยซึ่งจะส่งผลโดยตรงต่อการ กระจายตัวของละอองเชื้อเพลิงและการระเหยระหว่างการฉีดเชื้อเพลิงด้วยหัวฉีดแรงดันสูงเข้าไปใน ห้องเผาไหม้

เชื้อเพลิงดีเซลที่ผลิตจากน้ำมันดิบมีส่วนประกอบของโมเลกุลไฮโดรคาร์บอนหลายชนิดเมื่อ เทียบกับเชื้อเพลิงไบโอดีเซลที่มีความบริสุทธิ์มาก รูปที่ 1 แสดงการทดสอบสัดส่วนโดยปริมาตรขณะ เกิดการระเหยตัวของเชื้อเพลิงดีเซล ไบโอดีเซล และ เชื้อเพลิงผสม จากกราฟแสดงให้เห็นอย่าง ชัดเจนถึงความเป็นโมเลกุลชนิดเดียวกันของเชื้อเพลิงไบโอดีเซลที่สามารถระเหยได้เกือบทั้งหมด ณ อุณหภูมิประมาณ 330 - 350 °C ในทางตรงกันเชื้อเพลิงดีเซลจากฟอสซิลมีความสามารถในการ ระเหยที่อุณหภูมิต่ำ ปานกลาง และ สูง ในสัดส่วนค่าหนึ่ง ซึ่งหมายถึงขนาดที่แตกต่างกันของโมเลกุล นั่นเอง จะเห็นว่าเชื้อเพลิงไบโอดีเซลมีโมเลกุลชนิดเดียวกัน สามารถระเหยตัวได้พร้อมกันที่อุณหภูมิ ค่าไดค่าหนึ่งนั้นสามารถเพิ่มประสิทธิภาพเชิงปริมาตรของเครื่องยนต์ได้ ในทางตรงกันข้ามเชื้อเพลิง จากฟอสซิลซึ่งมีความแตกต่างของชนิดโมเลกุลนั้นสามารถทำให้เกิดการติดไฟและเผาไหม้ได้ง่ายใน ช่วงแรกของการทำ ปฏิกิริยาเคมี

ตารางที่ 1 คุณสมบัติเบื้องต้นของเชื้อเพลิงดีเซลและไบโอดีเซล [1]

Fuel properties	Diesel	Biodiesel
Chemical formula	$C_{16.17}H_{32.01}$	C _{15.26} H _{29.48} O _{1.71}
Calorific value (MJ/kg)	45.80	39.90
Oxidation stability (hr)	158.21	22.86
Flash point (°C)	65.50	198.00
Viscosity (mm²/s)	3.205	4.452
Density (g/cm ³)	0.82649	0.87482

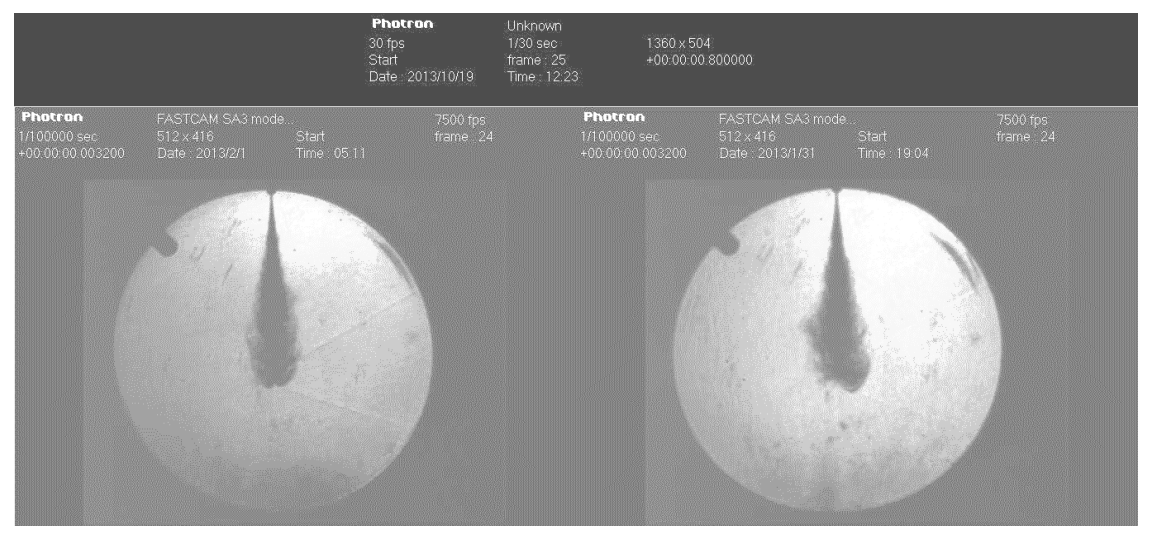


รูปที่ 1 ผลการเปรียบเทียบการระเหยตัวเมื่อเพิ่มอุณหภูมิ (Distillation Curve) ของเชื้อเพลิงดีเซล และไบโอดีเซล [2]

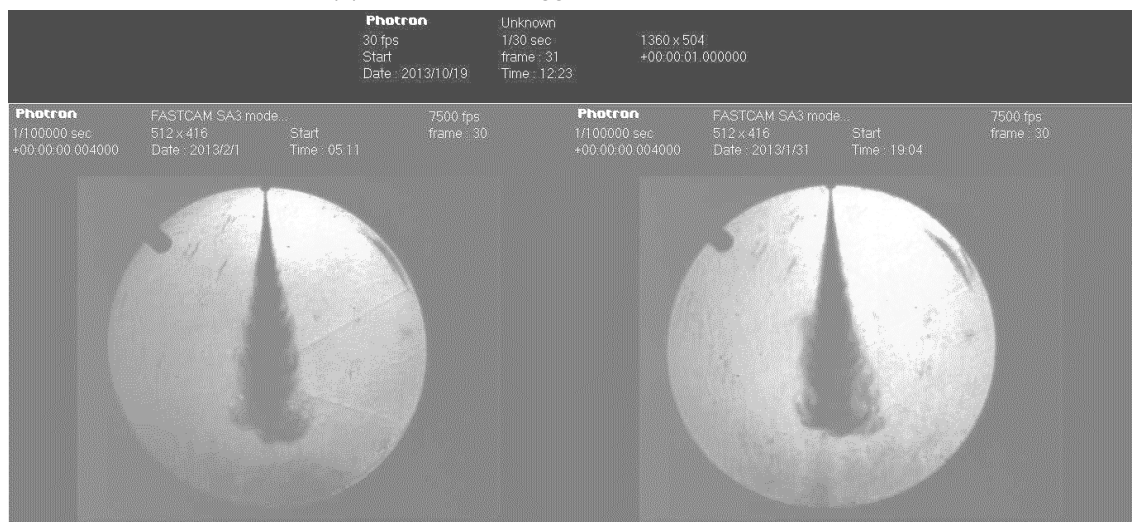
ผลการศึกษาการกระจายตัวของสเปรย์เชื้อเพลิงในห้องเผาไหม้ปริมาตรคงที่ (Constant Volume Combustion Chamber: CVCC) แสดงในรูปที่ 2 การเปรียบเทียบการฉีดน้ำมันเชื้อเพลิง ดีเซลและไบโอดีเซลด้วยหัวฉีดแรงดันสูงในห้องเผาไหม้จำลองเทียบเท่ากับสภาวะการทำงานจริงของ เครื่องยนต์ถูกทดสอบโดยกำหนดให้แรงดันในรางของระบบฉีดเชื้อเพลิงสูง 800 บาร์ (Rail Pressure of 800 bar, Nitrogen Chamber Pressure of 19 bar & Chamber Density of 21 kg/cm², Injection Duration of 2 ms, Injector Orifice Diameter of 140 micron) และถ่ายภาพด้วยกล้องถ่ายภาพ ความเร็วสูง (High Speed Camera, Photron SA-3 with z-type schlieren, Frame Rate of 7500 fps, Shutter Time of 1/100000 sec) จากภาพจะเห็นว่าองศาของสเปรย์ (Spray Angle) ระยะ สเปรย์ที่เชื้อเพลิงเคลื่อนที่พุ่งออกไปไกลสุด (Penetration Depth) นั้นไม่ได้มีความแตกต่างกันอย่างมี นัยสำคัญ จึงสามารถวิเคราะห์เบื้องต้นได้ว่ามีความเป็นไปได้สูงที่จะสามารถนำเชื้อเพลิงไบโอดีเซล มาใช้แทนเชื้อเพลิงดีเซลในเครื่องยนต์ได้ อย่างไรก็ตามจำเป็นต้องศึกษาผลกระทบระยะยาวที่อาจจะ เกิดขึ้นต่อเครื่องยนต์โดยเฉพาะอย่างยิ่งระบบลำเลียงและฉีดน้ำมันเชื้อเพลิง (Fuel Derivers and Injection System)

การศึกษาพฤติกรรมการเกิดมลพิษอนุภาคเขม่า (Particulate Matter: PM) จากการเผาไหม้ เชื้อเพลิงดีเซลและไบโอดีเซลในเปลวไฟแบบแพร่ (Diffusion Flame) ด้วยเทคนิคการถ่ายภาพแบบชู รีเรน (Schlieren) และกล้องถ่ายภาพความเร็วสูง (High Speed Camera) ดังแสดงใน รูปที่ 3 ทำให้ เห็นว่าเปลวไฟของเชื้อเพลิงดีเซลมีความหนาแน่น (Density) ของลำอนุภาคเขม่าสูงกว่าไบโอดีเซล อย่างชัดเจน สามารถกล่าวได้ว่าไบโอดีเซลปล่อยมลพิษอนุภาคเขม่าที่เกิดจากการเผาไหม้ไม่สมบูรณ์ (Incomplete Combustion) ในปริมาณที่ต่ำกว่าดีเซล การนำเชื้อเพลิงไบโอดีเซลจากปาล์มน้ำมันมี ผลกระทบทางบวกในการลดปริมาณมลพิษอนุภาคเขม่าที่เป็นตันเหตุของมะเร็งและมลภาวะเป็นพิษ ในเมืองได้ อย่างไรก็ตามเครื่องยนต์ควรถูกออกแบบให้เหมาะสมกับคุณสมบัติของเชื้อเพลิงหรือ ส่วนผสมของเชื้อเพลิงชนิดนั้นด้วย เพื่อเป็นการใช้พลังงานที่มีอยู่อย่างจำกัดให้เกิดประสิทธิภาพ สูงสุดได้ตามเป้าหมายที่วางไว้

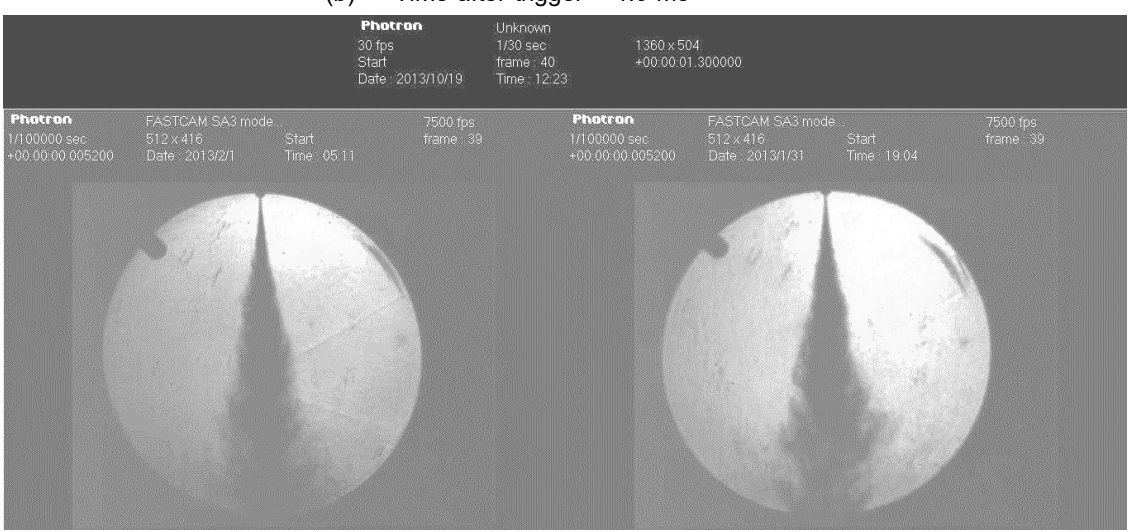
การวัดปริมาณมลพิษอนุภาคจากเครื่องยนต์ดีเซลอย่างง่ายสามารถวัดได้ด้วยเครื่องวัดควัน ดำ (Smoke Meter) ซึ่งเป็นที่นิยมอย่างมากเนื่องจากสามารถเห็นภาพได้ชัดเจนและง่ายต่อการใช้ งาน การทดสอบสามารถทำได้โดยเปรียบเทียบปริมาณควันดำที่สะสมบนกระดาษกรองเทียบกับสี ขาวของกระดาษกรองที่ไม่มีมลพิษอนุภาค ดังแสดงในรูปที่ 4 (a) จะเห็นได้ชัดเจนว่ามลพิษที่เกิดจาก เครื่องยนต์ใบโอดีเซลมีปริมาณที่ต่ำกว่าเครื่องยนต์ดีเซลประมาณ 50% ในทำนองเดียวกัน การวัด ปริมาณอนุภาคเขม่าด้วยความดันแตกต่าง (ความดันตกคร่อม, Pressure Drop) ระหว่างขาเข้าและ ขาออกตัวกรองมลพิษอนุภาคจะสามารถแสดงให้เห็นถึงปริมาณอนุภาคเขม่าที่ถูกดักไว้ได้ ดังแสดงในรูปที่ 4 (b) จากกราฟเห็นได้ชัดเจนว่าความดันแตกต่างระหว่างขาเข้าและขาออกตัวกรองมลพิษอนุภาคของเครื่องยนต์ดีเซลมีอัตราการเพิ่มขึ้นสูงกว่าไบโอดีเซลอย่างเห็นได้ชัด ซึ่งจากการวิเคราะห์ สามารถสรุปได้ว่าปริมาณมลพิษอนุภาคเขม่าจากเครื่องยนต์ดีเซลมีค่าสูงกว่าไบโอดีเซลประมาณ 50% เช่นเดียวกันกับผลการทดสอบด้วยเครื่องวัดควันดำ



(a) Time after trigger = 3.2 ms

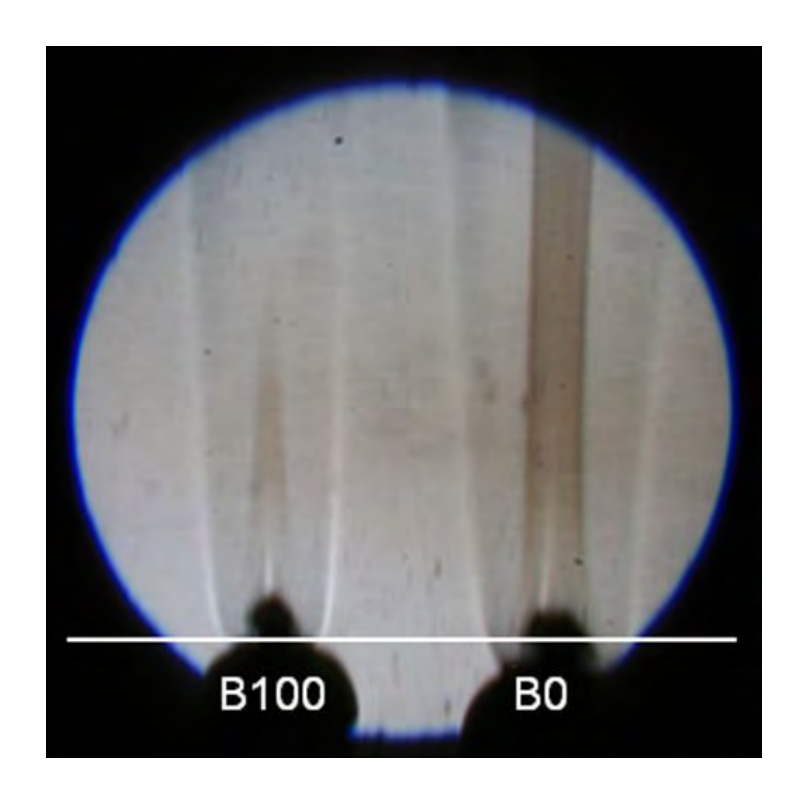


(b) Time after trigger = 4.0 ms

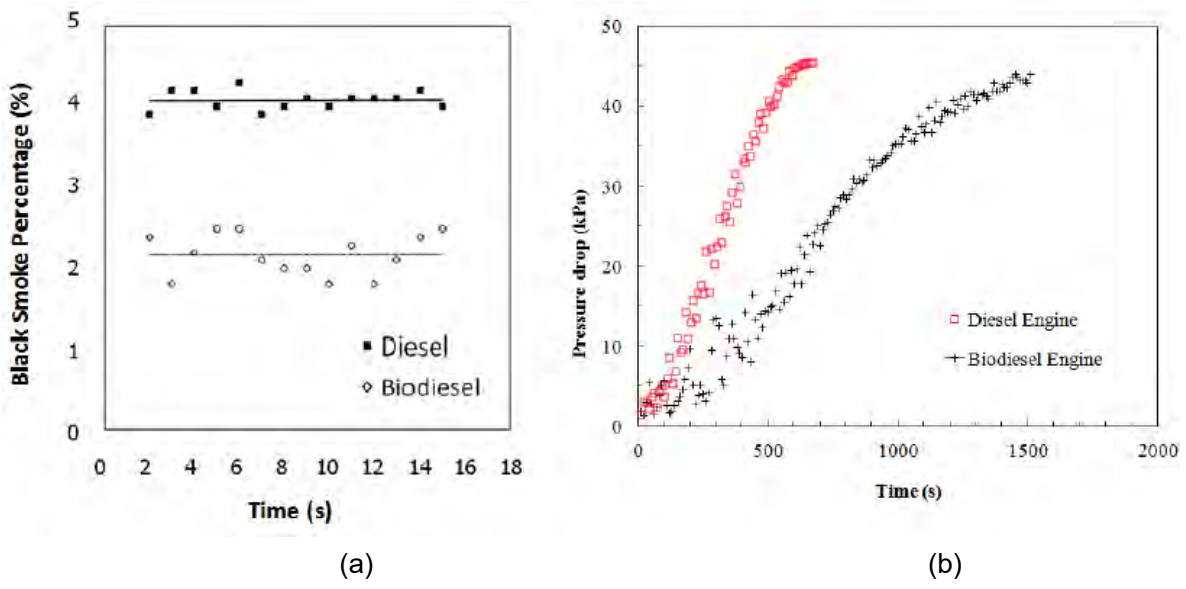


(c) Time after trigger = 5.20 ms

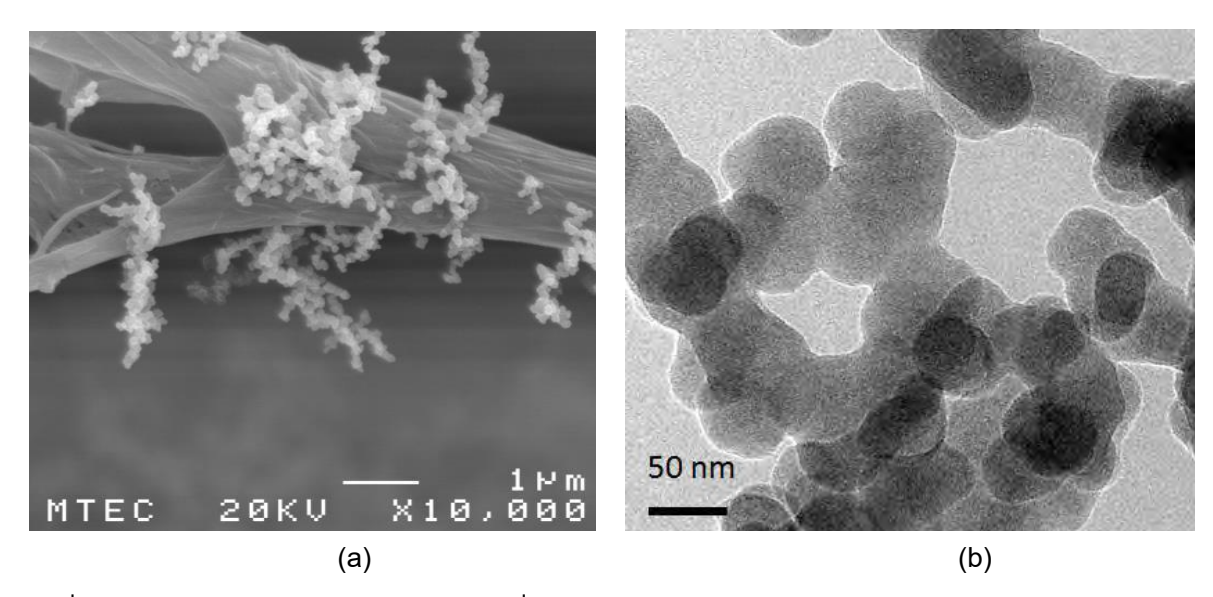
รูปที่ 2 ผลการเปรียบเทียบสเปรย์ของเชื้อเพลิงดีเซล (left) และไบโอดีเซล (right) ในห้องเผาใหม้ ปริมาตรคงที่ (Constant Volume Combustion Chamber) ด้วยกล้องถ่ายภาพถ่ายภาพความเร็วสูง (High Speed Camera) แบบชูรีเรน (Schlieren)



รูปที่ 3 ผลการเปรียบเทียบเปลวไฟแบบแพร่ของเชื้อเพลิงดีเซล (right) และไบโอดีเซล (left) ใน สภาวะบรรยากาศปกติ (Ambient pressure & temperature) ด้วยกล้องถ่ายภาพถ่ายภาพความเร็ว สูง (High Speed Camera) แบบชูรีเรน (Schlieren) [3]



รูปที่ 4 การวัดปริมาณมลพิษอนุภาคจากเครื่องยนต์ดีเซลและไบโอดีเซลด้วย (a) การวัดค่าควันดำ (Smoke Meter) และ (b) ความดันตกคร่อมระหว่างทางเข้าและออกของผนังอุปกรณ์กรองมลพิษ อนุภาค [4]

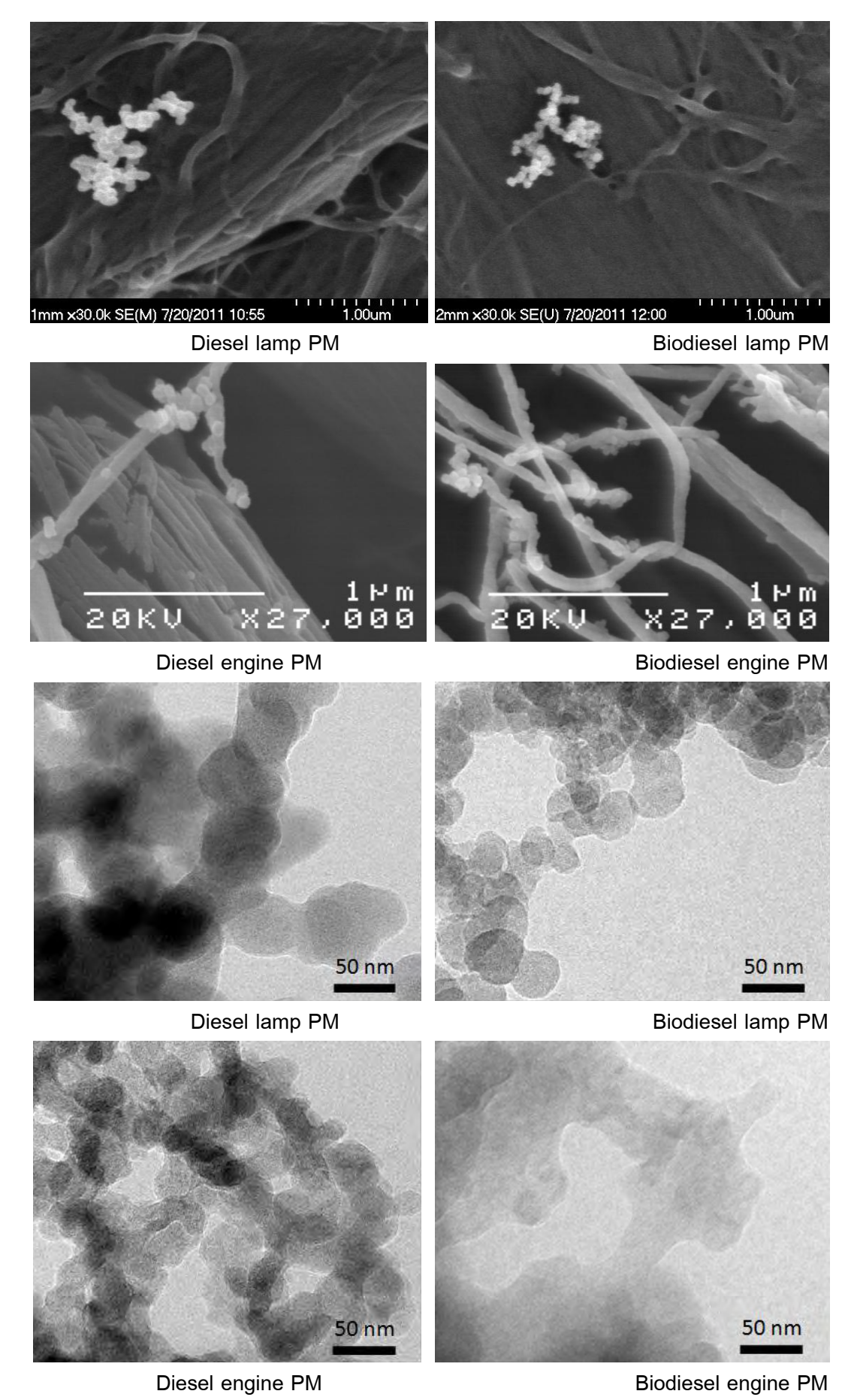


รูปที่ 5 ภาพถ่ายของมลพิษอนุภาคจากเครื่องยนต์ดีเซลโดยใช้กล้องอิเล็กตรอนแบบ (a) ส่องกราด และ (b) ส่องผ่าน [2]

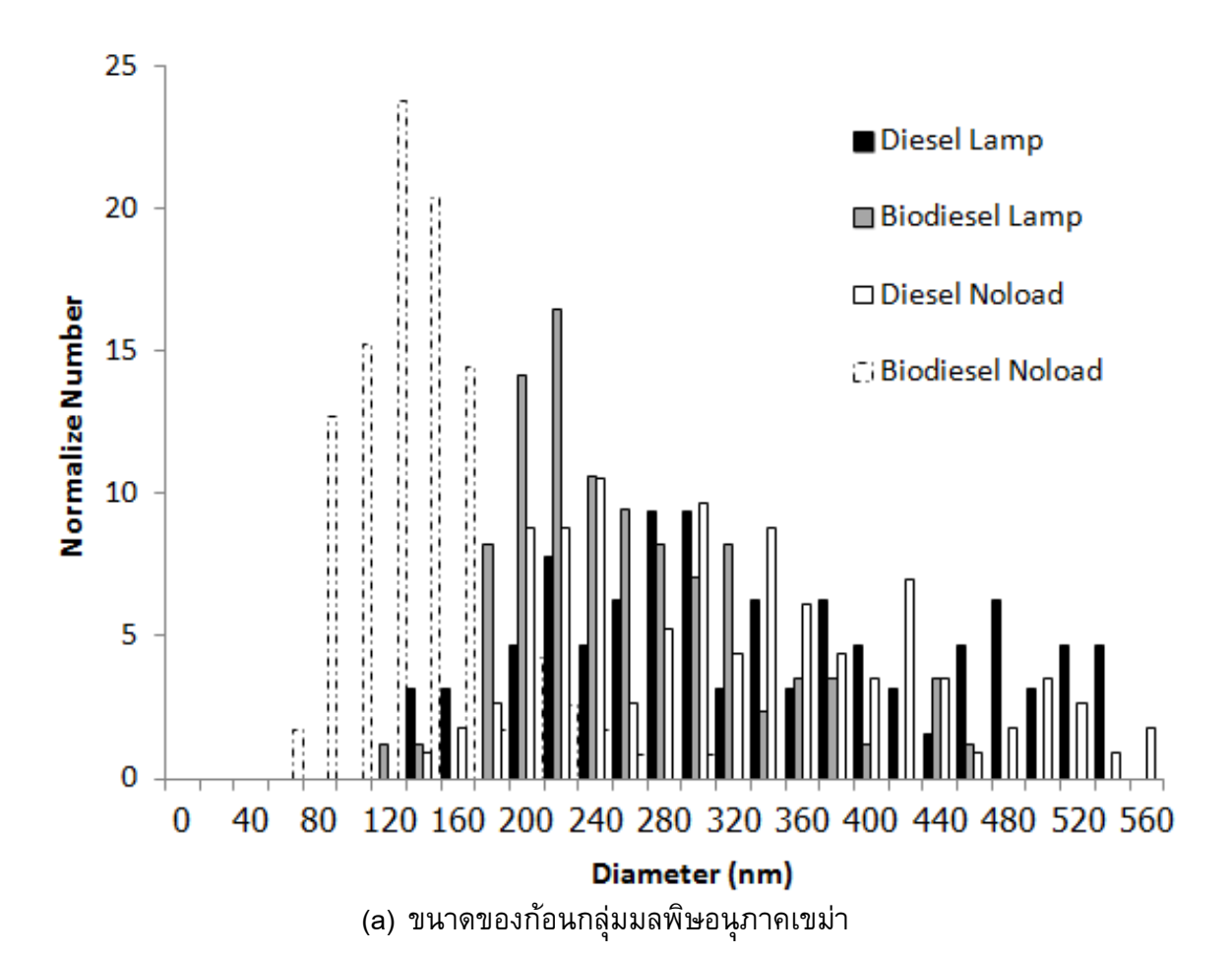
คุณลักษณะทางกายภาพของมลพิษอนุภาค (Physical Characteristics of PMs)

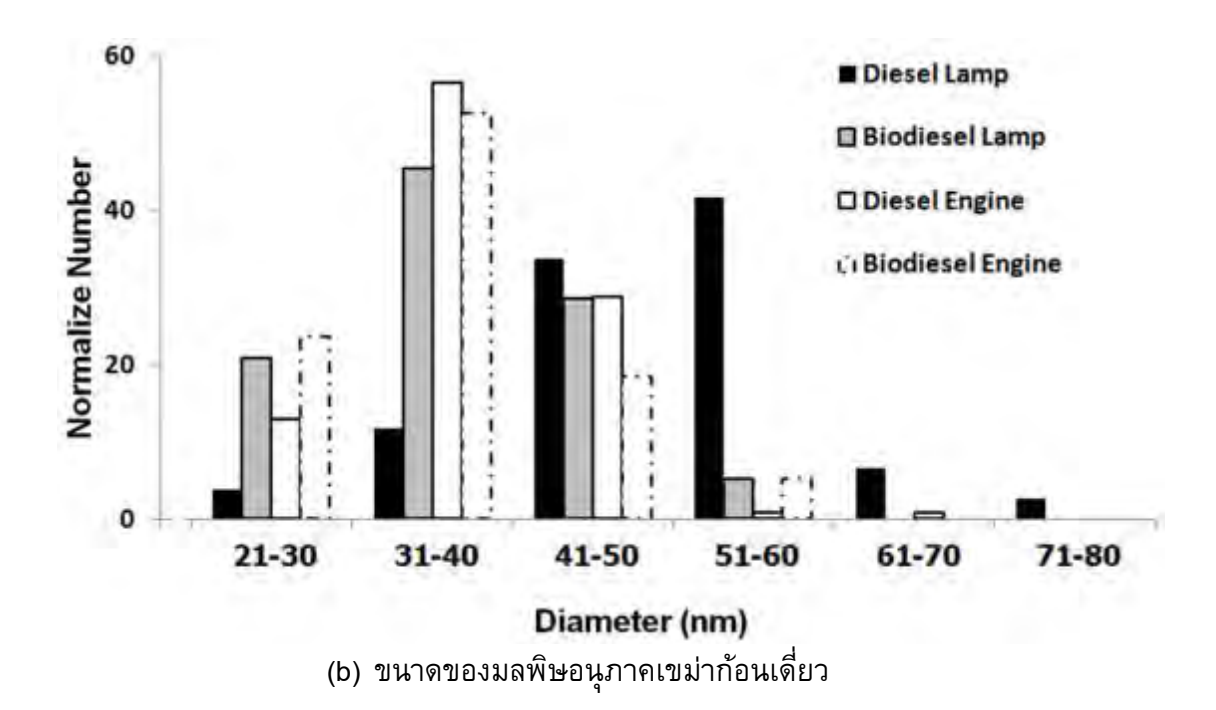
จากผลงานวิจัย พบว่ามลพิษอนุภาคจากเครื่องยนต์ดีเซลมีโครงสร้างทางกายภาพที่ ซับซ้อนมาก การนำกล้องจุลทรรศน์อิเล็กตรอนแบบส่องกราด (Scanning Electron Microscope; SEM) และกล้องจุลทรรศน์อิเล็กตรอนแบบส่องผ่าน (Transmission Electron Microscope; TEM) มา ใช้ในการวิเคราะห์โครงสร้างทางกายภาพของมลพิษอนุภาคทำให้สามารถเข้าใจถึงคุณลักษณะเฉพาะ ของมลพิษอนุภาคได้ดียิ่งขึ้น ดังแสดงในรูปที่ 6 ภาพถ่าย PM2.5/PM10 ด้วยกล้องอิเล็กตรอนแบบ ส่องกราด (SEM)) ภาพถ่ายมลพิษอนุภาคเดี่ยวด้วยกล้องอิเล็กตรอนแบบส่องผ่าน (TEM) เรา สามารถมองเห็นโครงสร้างทางกายภาพของมลพิษอนุภาคเดี่ยว การเกาะกลุ่มของมลพิษอนุภาคใน ระดับนาโนเมตรและไมครอนอย่างชัดเจน อย่างไรก็ตามจากการศึกษาพบว่าคุณสมบัติทางกายภาพ และเคมีเบื้องตันสามารถเปลี่ยนแปลงได้ในช่วงที่กว้างมากซึ่งขึ้นอยู่กับภาระการทำงานของ เครื่องยนต์และคุณสมบัติทางเคมีของเชื้อเพลิงชนิดนั้น นักวิจัยส่วนใหญ่ตระหนักว่ามีความจำเป็น อย่างยิ่งที่ต้องได้รับการวิจัยในเชิงลึกเพื่อแก้ไขปัญหาสุขภาพที่เกิดจากมลพิษที่มีขนาดเล็กมาก ๆ ดังกล่าวต่อไป

มลพิษอนุภาคเดี่ยว (Primary Particle) มีขนาดประมาณ 10-80 นาโนเมตร (Ultrafine Particle) และจะเกาะกันเป็นกลุ่ม (Accumulated Particle) มีขนาดโตขึ้นเป็นประมาณ 100-300 นาโนเมตร (Fine Particle) ดังแสดงในรูปที่ 7 จากการวิจัยพบว่าชนิดของเชื้อเพลิงและแหล่งกำเนิด มลพิษมีผลโดยตรงต่อพฤติกรรมการเผาไหม้ที่สามารถส่งผลกระทบต่อขนาดของมลพิษอนุภาคได้ การเผาไหม้ของเชื้อเพลิงไบโอดีเซลซึ่งมีอะตอมของออกซิเจนในเชื้อเพลิงนั้นจะปล่อยขนาดมลพิษอนุภาคที่มีขนาดเล็กกว่าดีเซลเล็กน้อย ซึ่งขนาดที่เล็กลงดังกล่าวอาจจะส่งผลโดยตรงต่อ ประสิทธิภาพการกรองมลพิษอนุภาคของอุปกรณ์กรองมลพิษ



รูปที่ 6 ภาพถ่ายจากกล้องอิเลคตรอนของมลพิษอนุภาคจากเครื่องยนต์ดีเซลและใบโอดีเซล [4]

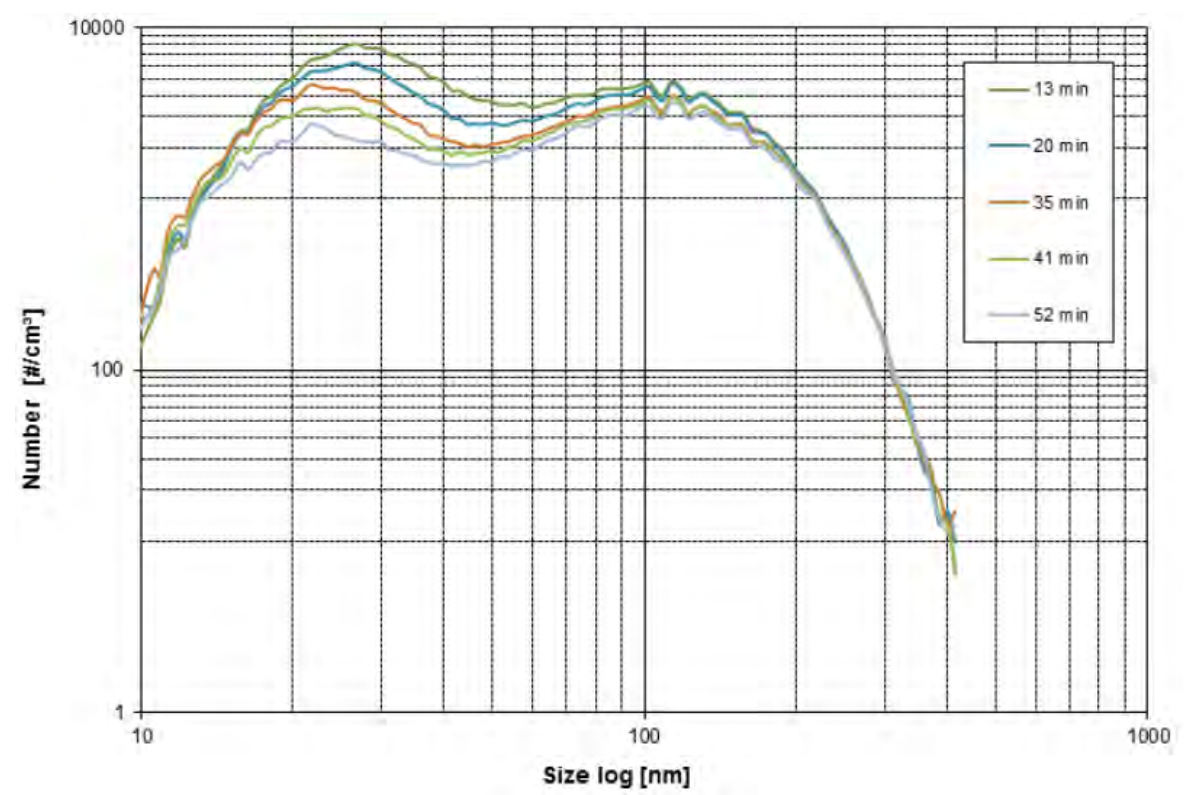




รูปที่ 7 ผลการวิเคราะห์ขนาดของ (a) มลพิษอนุภาคกลุ่ม (b) มลพิษอนุภาคเดี่ยวจากเครื่องยนต์ ดีเซลและไบโอดีเซลโดยใช้กล้องอิเล็กตรอนส่องผ่าน [4]



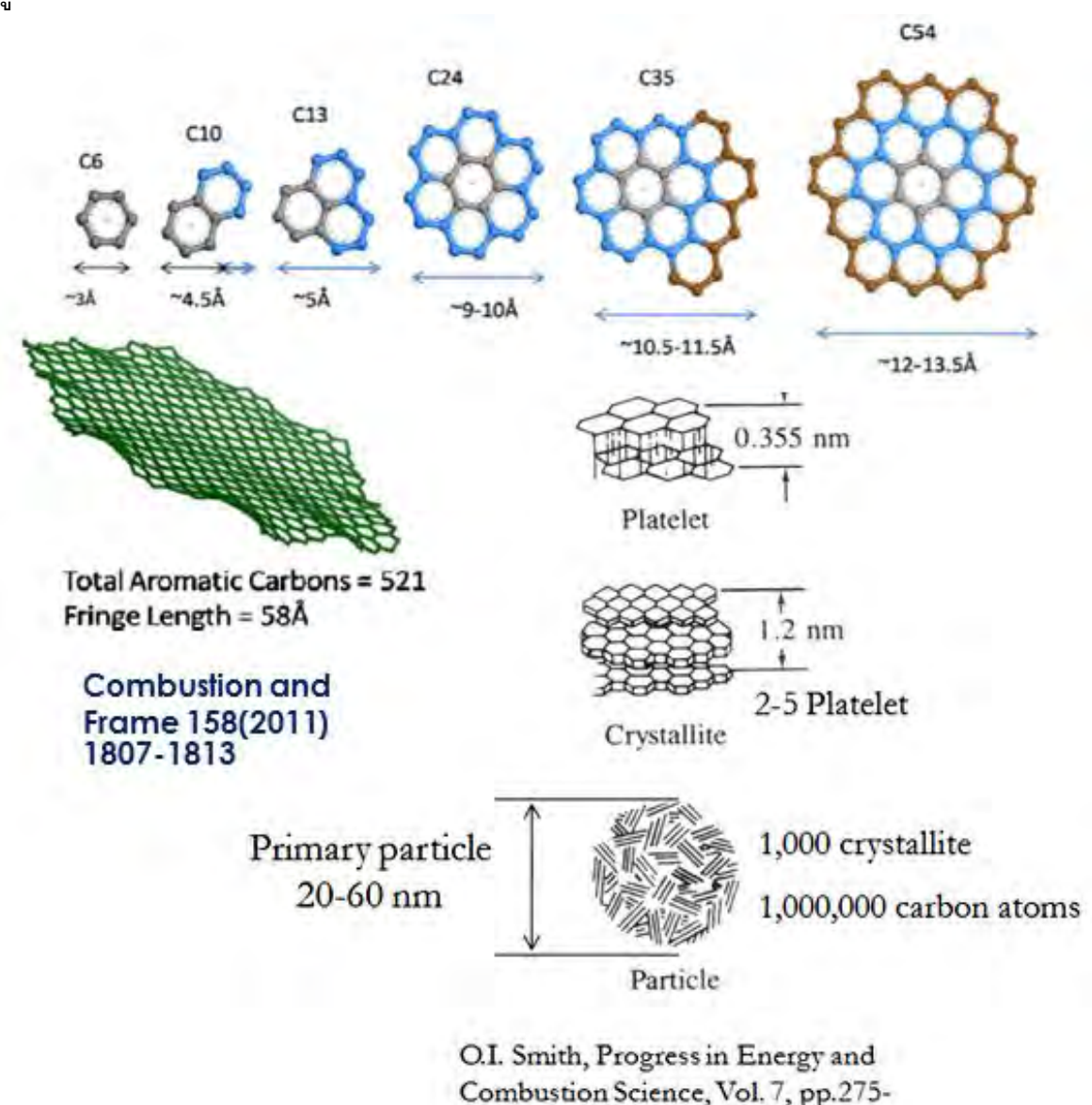




รูปที่ 8 ขนาดมลพิษอนุภาคจากเครื่องยนต์ดีเซลโดยการวัดด้วยไฟฟ้าสถิตย์ (Scanning Mobility Particle Sizer: SMPS) [5]

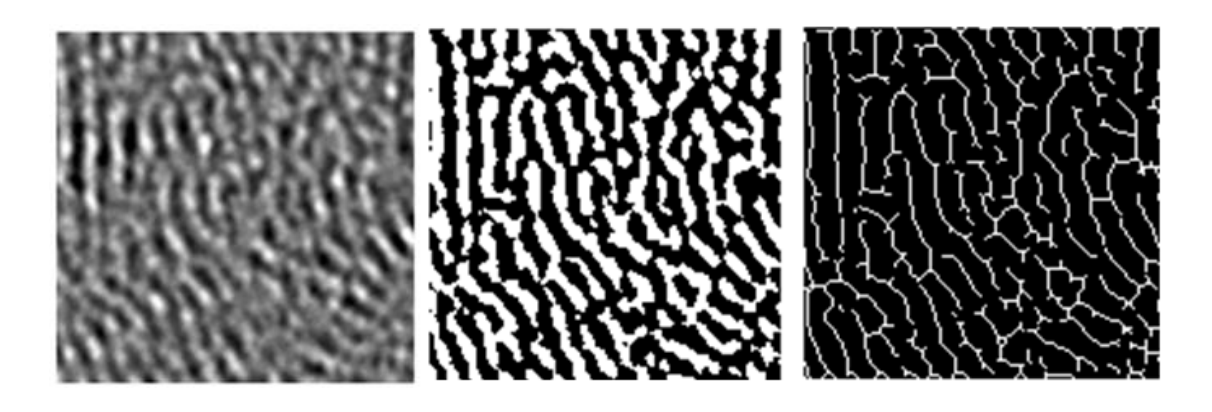
การวัดขนาดมลพิษอนุภาคจากเครื่องยนต์ดีเซลโดยการวัดด้วยไฟฟ้าสถิตย์ (Scanning Mobility Particle Sizer: SMPS) ดังแสดงในรูปที่ 8 ซึ่งเป็นอีกวิธีที่แม่นยำและนิยมใช้กันมากใน ประเทศที่มีเทคโนโลยีขั้นสูงแต่ในประเทศไทยยังไม่มีอุปกรณ์ดังกล่าวในสถาบันการศึกษาและ หน่วยงานวิจัยของรัฐ จะเห็นว่าผลการวัดขนาดของมลพิษอนุภาคด้วยวิธีดังกล่าวมีค่าใกล้เคียงกับ การวัดจากภาพถ่ายจากกล้องอิเลคตรอนมาก

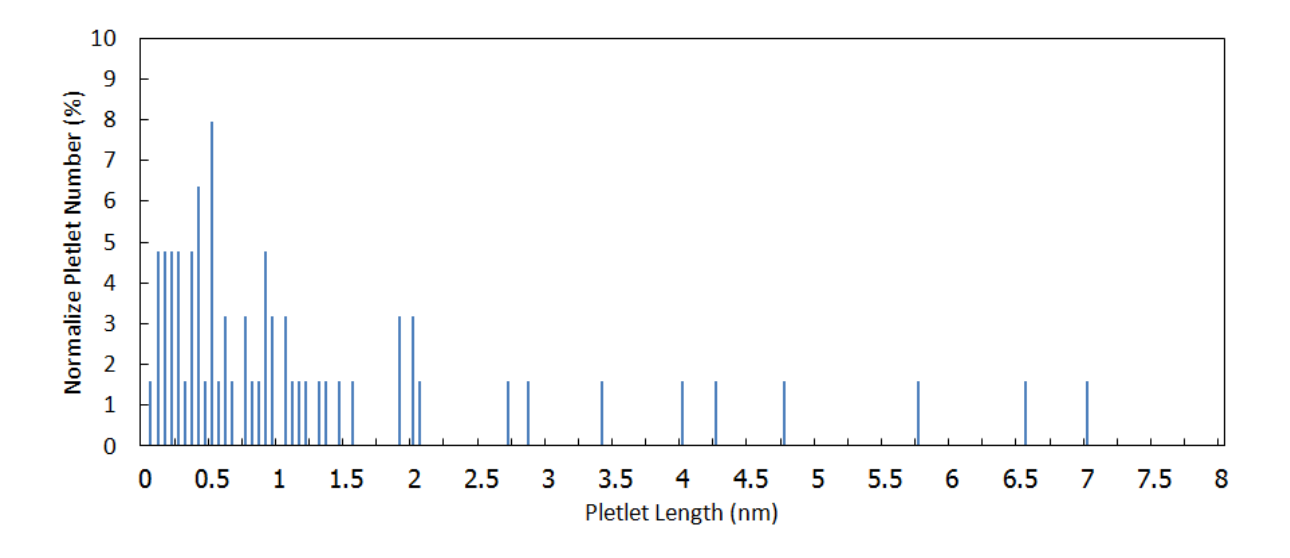
นอกเหนือจากนั้นการวิเคราะห์โครงสร้างในระดับนาโนจากภาพถ่ายอิเลคตรอนด้วย คอมพิวเตอร์ (TEM Image Processing Method) โดยอาศัยแนวคิดเรื่องคาร์บอนพื้นฐานหกอะตอม ซึ่งมีนักวิทยาศาสตร์ได้อธิบายโครงสร้างทางเคมีและกายภาพไว้อย่างชัดเจนแล้ว ดังแสดงในรูปที่ 9 ดังนั้นจึงสามารถทำให้คำนวนจำนวนอะตอมคาร์บอนและมวลของมลพิษอนุภาคต่อปริมาตรซึ่งเป็น พารามิเตอร์หลักที่จะสามารถนำไปเป็นข้อมูลพื้นฐานในการออกแบบโครงสร้างทางกายภาพของ อุปกรณ์กรองมลพิษให้มีประสิทธิภาพมากขึ้นได้ ดังแสดงในรูปที่ 10 โดยจากผลการคำนวนเบื้องต้น พบว่ามีความหนาแน่นของอะตอมคาร์บอนในมลพิษอนุภาคเขม่าประมาณ 800-900 อะตอมต่อ ลูกบาศก์นาโนเมตร



รูปที่ 9 โครงสร้างในระดับโมเลกุลและการรวมตัวเป็นผลึกและกลุ่มของมลพิษอนุภาคจากเครื่องยนต์ ดีเซล [6, 7]

291, 1981.

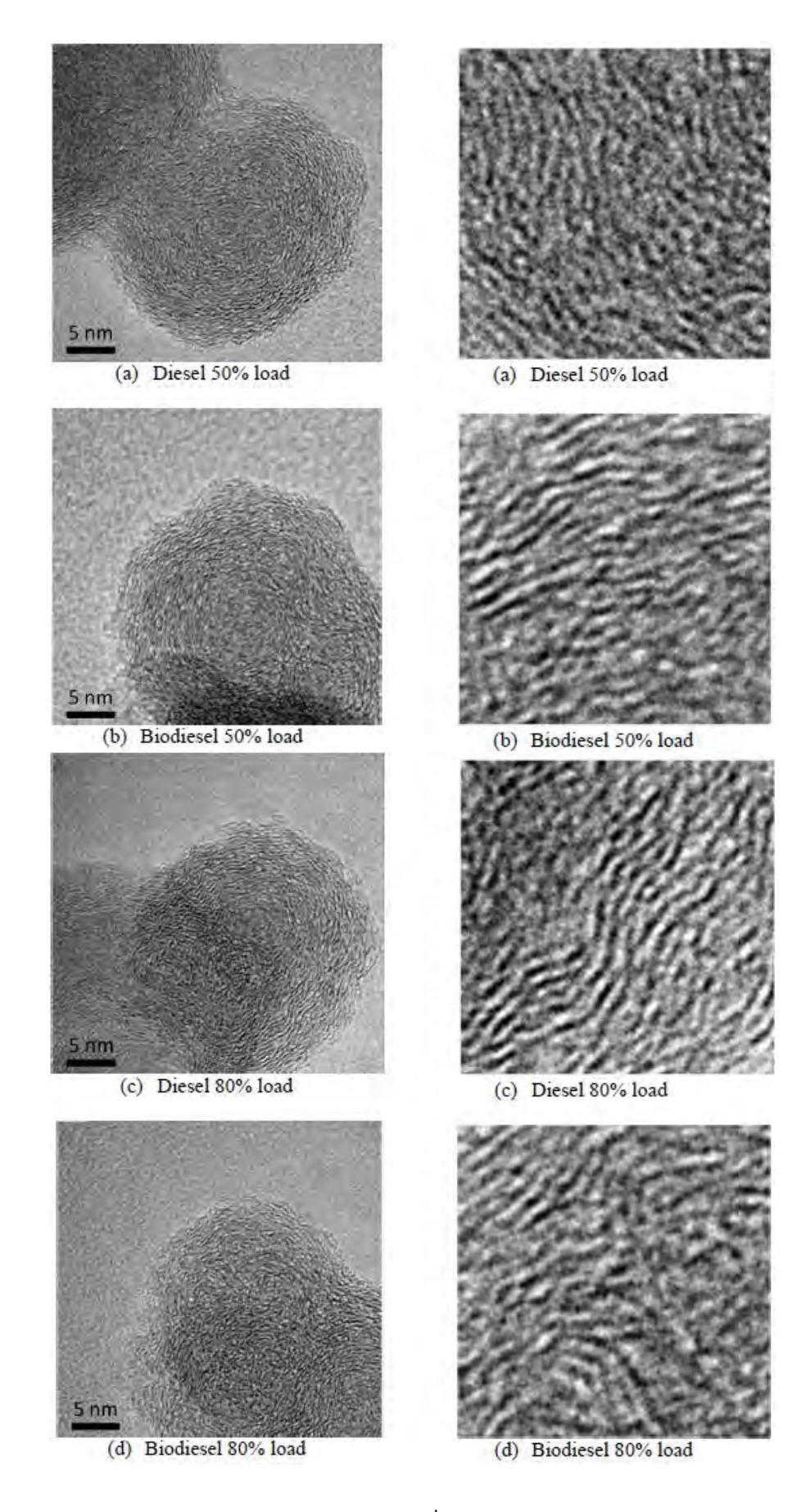




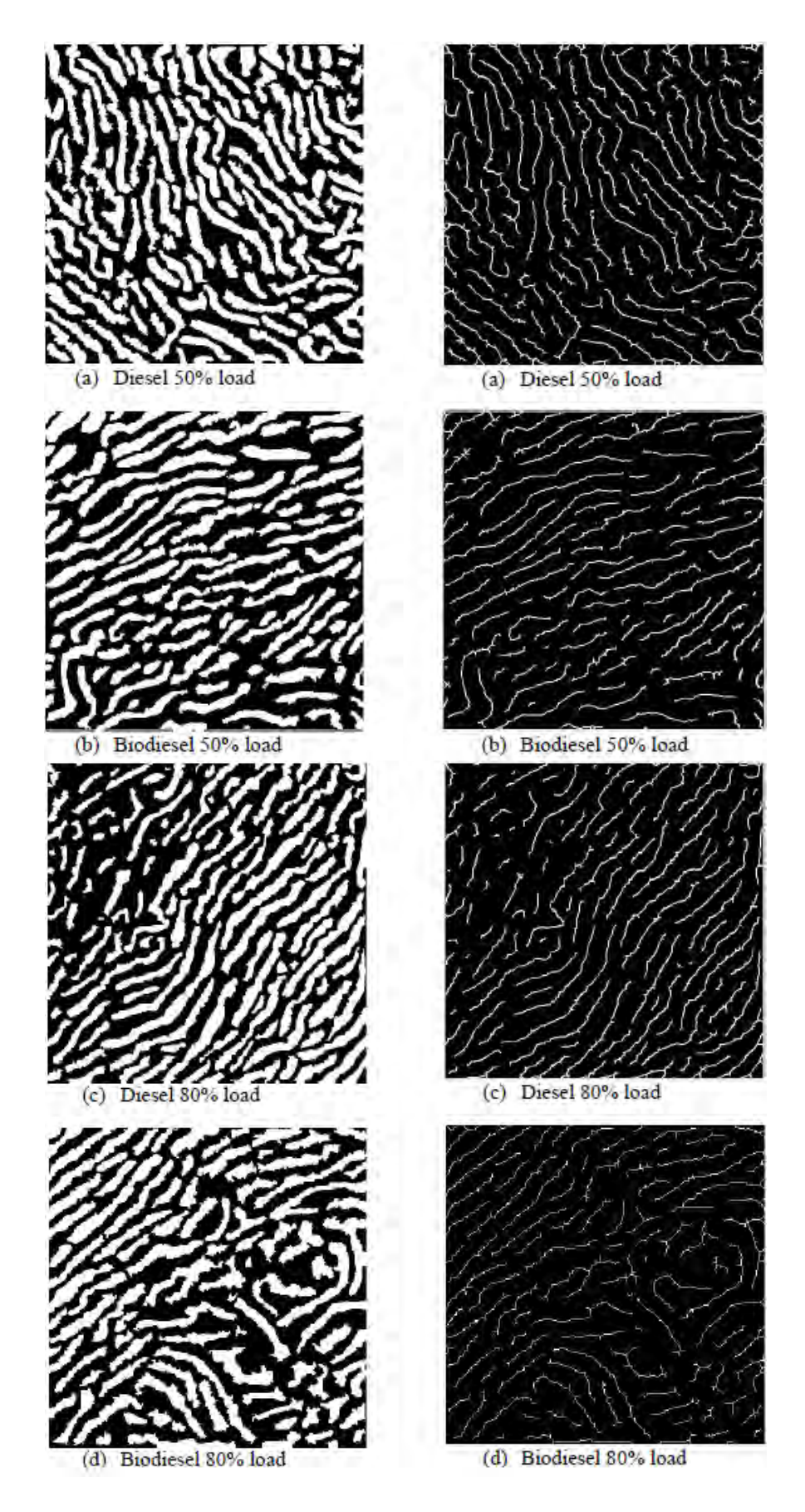
Carbon inside PM	Atom density	Mass
	(atoms)	(pg)
A cubic nanometer	829	1.65 E-8

รูปที่ 10 การคำนวณปริมาณอะตอมและมวลของมลพิษอนุภาคต่อปริมาตรด้วย TEM Image Processing Method [4]

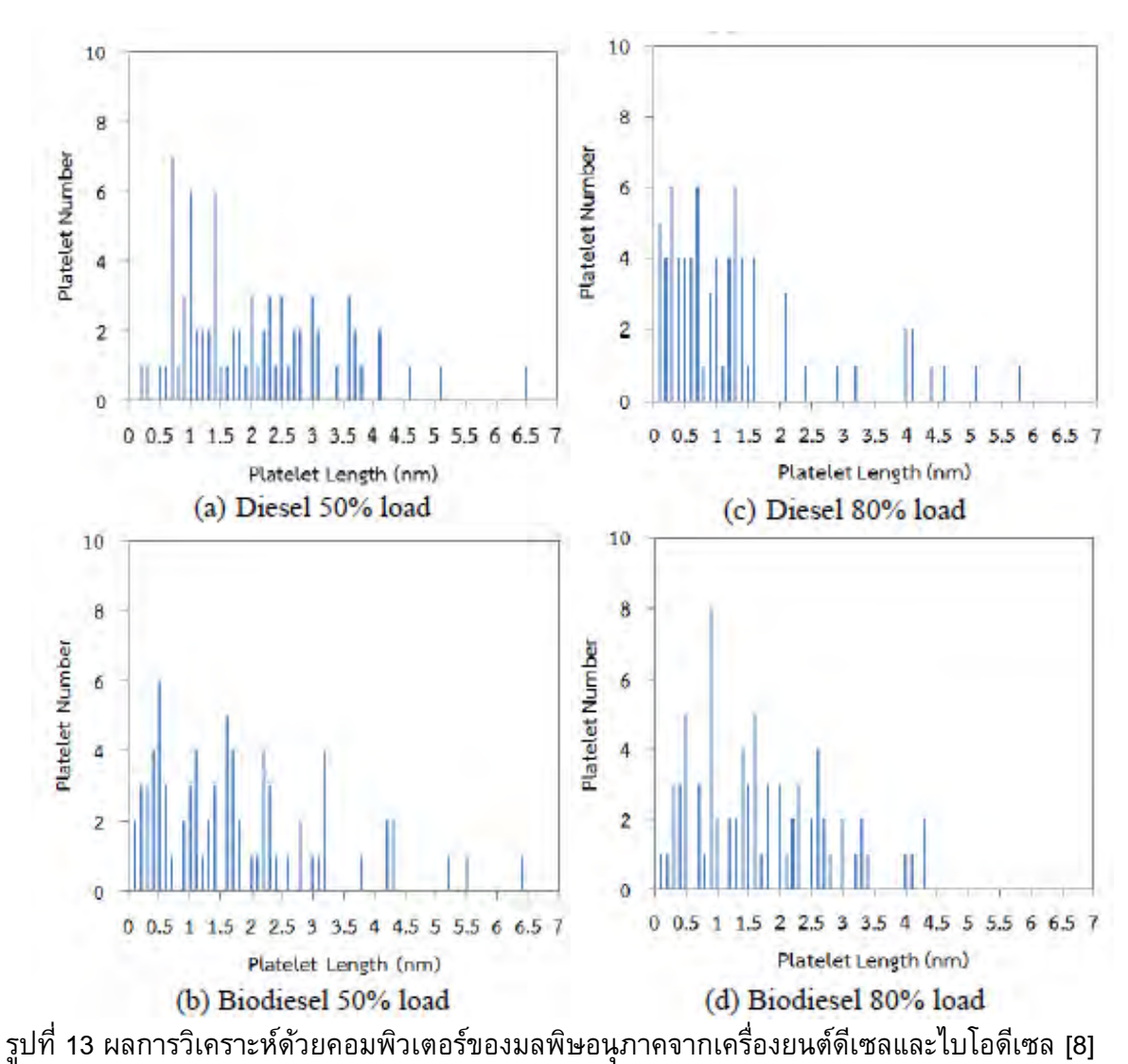
ในทำนองเดียวกัน จากการศึกษาเบื้องต้นพบว่าความหนาแน่นของอะตอมคาร์บอนใน มลพิษอนุภาคเขม่าขึ้นอยู่กับชนิดของเชื้อเพลิง แหล่งกำเนิดมลพิษอนุภาคเขม่าและภาระโหลดการ ทำงานของเครื่องยนต์ โดยมลพิษอนุภาคเขม่าจากไบโอดีเซลมีความหนาแน่นของคาร์บอนอะตอมต่ำ กว่าดีเซลประมาณ 100-300 อะตอมต่อลูกบาศก์นาโนเมตร ขึ้นอยู่กับสภาวะการใช้งานของ เครื่องยนต์ ดังแสดงในรูปที่ 10-13 และตารางที่ 2



รูปที่ 11 ภาพถ่ายจากกล้องอิเลคตรอนของมลพิษอนุภาคจากเครื่องยนต์ดีเซลและไบโอดีเซล [8]



รูปที่ 12 ภาพวิเคราะห์ด้วยคอมพิวเตอร์ของมลพิษอนุภาคจากเครื่องยนต์ดีเซลและไบโอดีเซล [8]



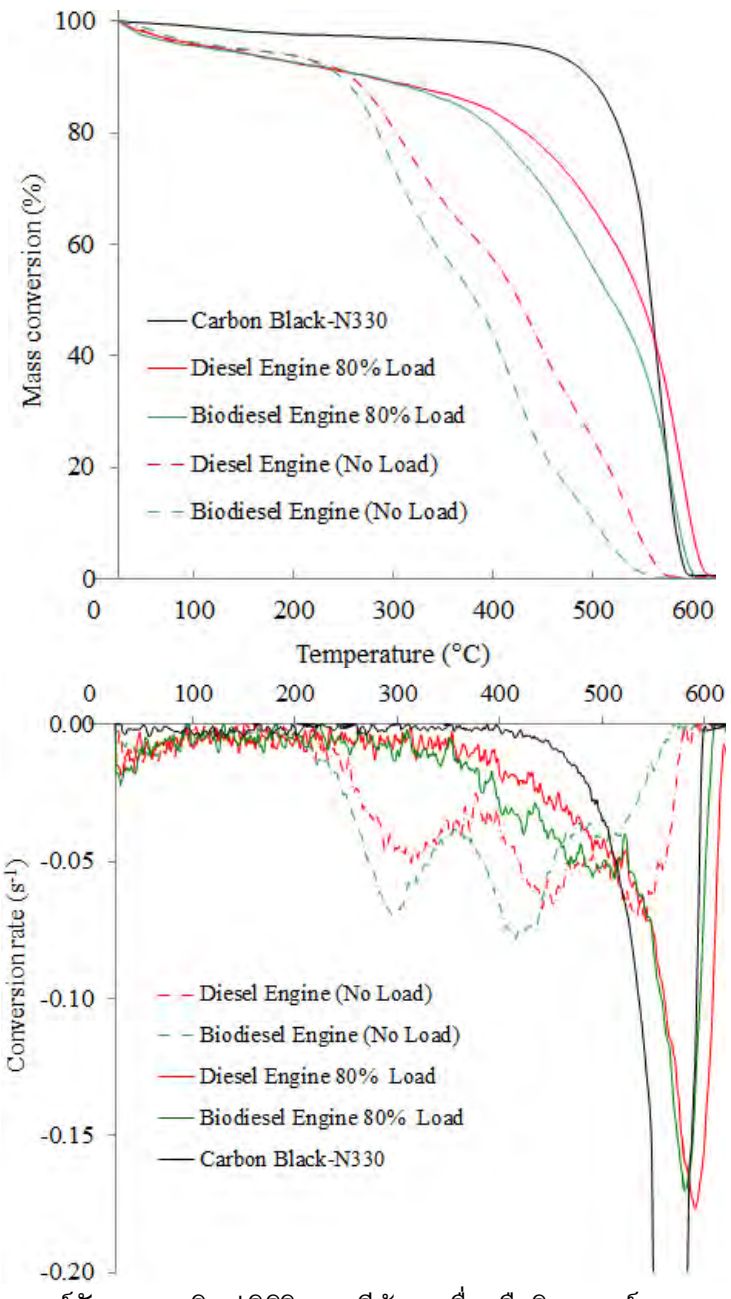
วีกม เว พยบ เวาเผว เรมผายผถาม เเผดวูกอาทยมาลดหึ่ง เผง เบเผวดวยหลุดเกษแนร เกาถดเกษ [g

ตารางที่ 2 คุณสมบัติเบื้องต้นทางกายภาพของมลพิษอนุภาคเขม่าดีเซลและไบโอดีเซล [8]

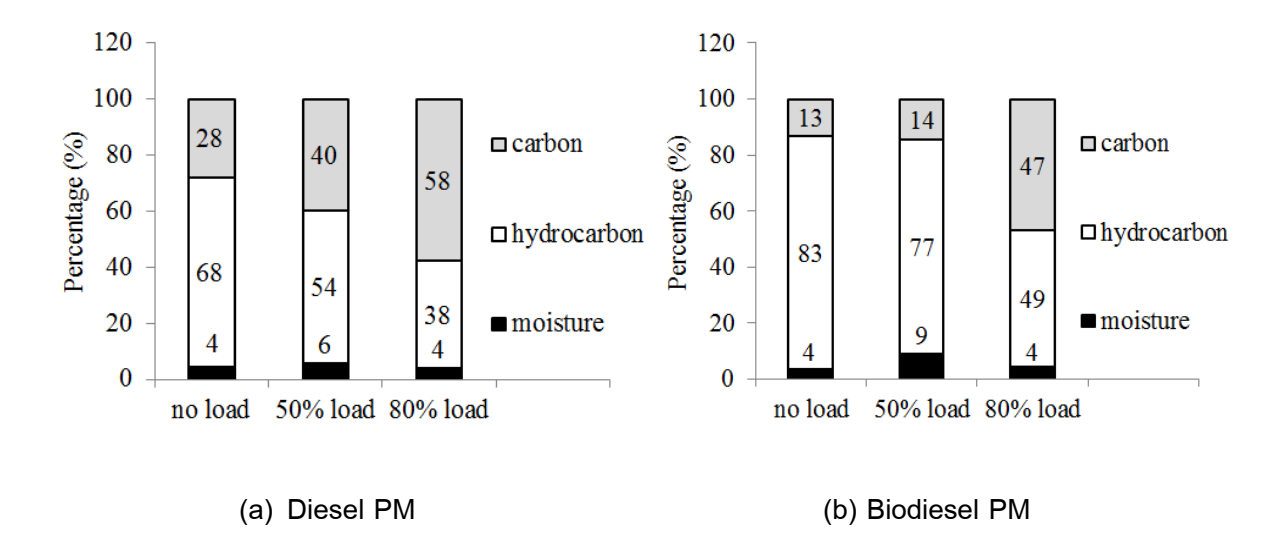
	PMs			
	Diesel		Biodiesel	
	50% load	80% load	50% load	80% load
Atom Density (atoms/nm3)	800	838	706	584
Mass per Volume (pg/nm3)	1.594 E-8	1.670 E-8	1.407 E-8	1.164 E-8
Average Single Diameter (nm)	32.13	30.90	31.59	30.31
Average Single Particle Mass (pg)	2.767 E-4	2.578 E-4	2.321 E-4	1.696 E-4
Average Single Particle Atom (Million atoms)	13.887	12.939	11.647	8.510

คุณลักษณะทางเคมีของมลพิษอนุภาค (Chemical Characteristics of PMs)

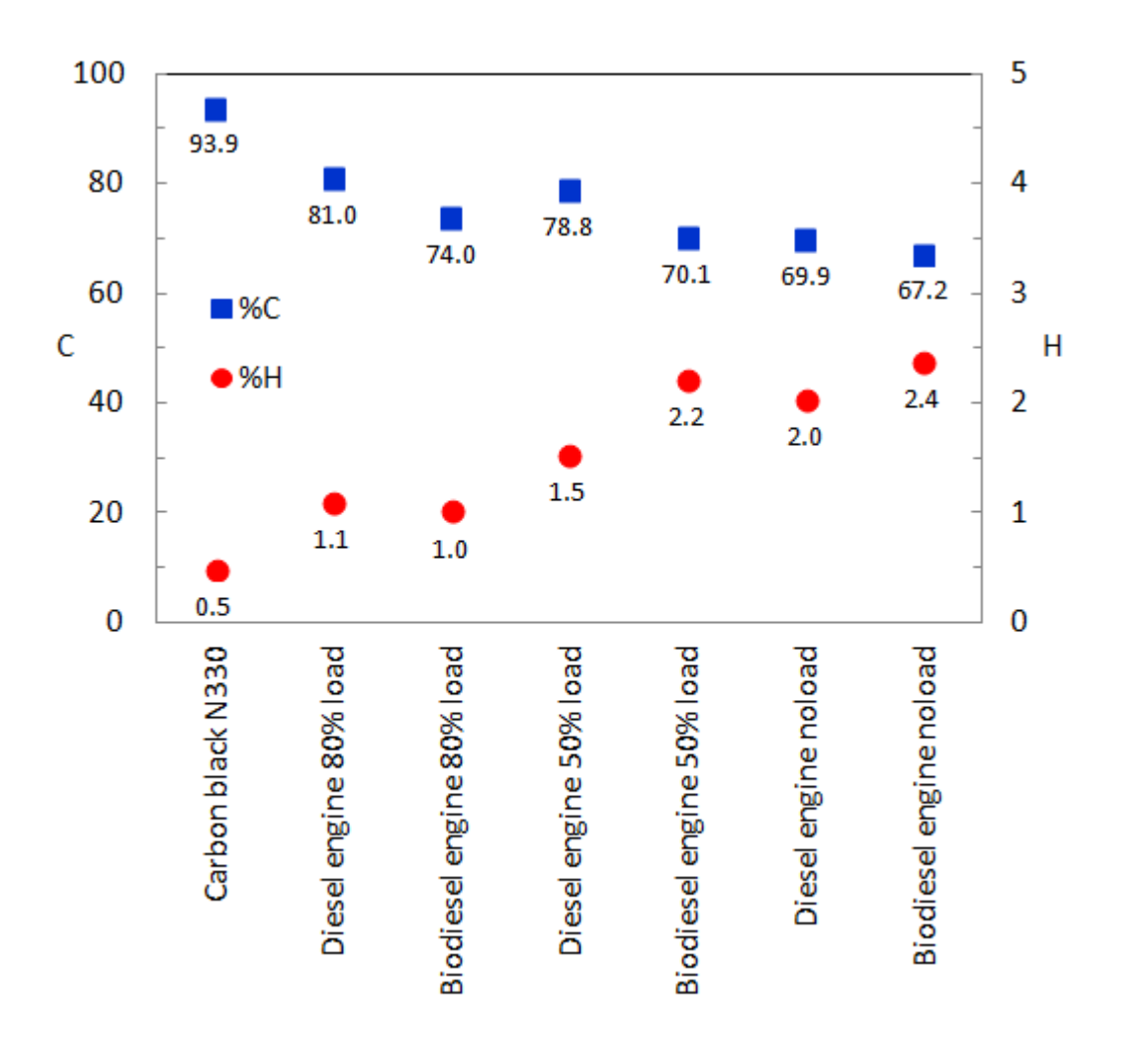
การศึกษาคุณสมบัติและส่วนประกอบทางเคมีของมลพิษอนุภาคก็เป็นอีกแขนงหนึ่งที่มี ความสำคัญอย่างยิ่งในการพัฒนาเทคโนโลยีหลังการเผาไหมัของยานยนต์ ผลการวิจัยพบว่า ส่วนประกอบทางเคมีและอัตราการเกิดปฏิกิริยาเคมีในการออกซิเดชันของมลพิษอนุภาคด้วยการ ทดสอบแบบอุณหภมิไม่คงที่ (Non Isothermal PMs Oxidation Kinetics) แสดงในรูปที่ 14-16 พบว่า มลพิษอนุภาคจากเครื่องยนต์ใบโอดีเซลสามารภทำปฏิกิริยากับออกซิเจนได้ดีกว่าดีเซลเนื่องจากมี อะตอมของออกซิเจนในเชื้อเพลิงที่เผาไหม้ไม่สมบูรณ์ในรูปของไฮโดรคาร์บอน ส่วนที่ภาระโหลดต่ำ จะมีส่วนผสมของเชื้อเพลิงที่เผาไหม้ไม่สมบูรณ์ในรูปของไฮโดรคาร์บอนสูงกว่าจึงทำให้สามารถ ออกซิใดซ์ได้ดีกว่ามลพิษอนุภาคเขม่าที่ภาระโหลดสูงมากซึ่งประกอบด้วยคาร์บอนเป็นหลัก



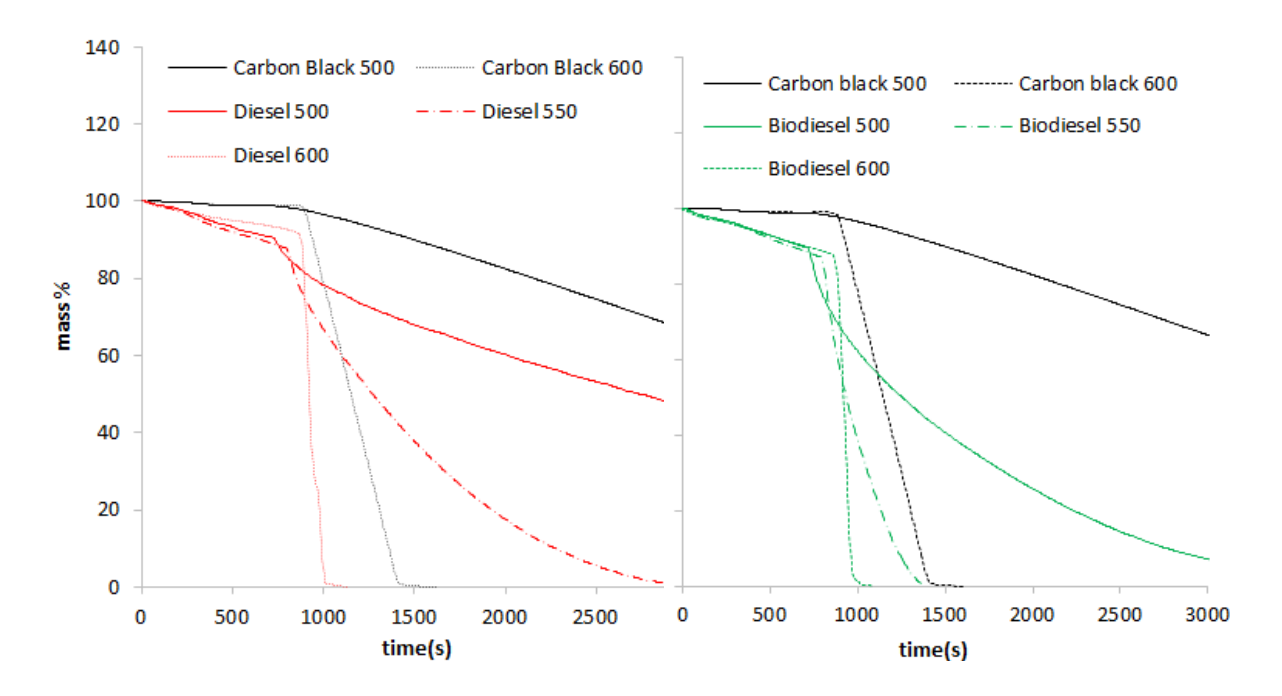
รูปที่ 14 ผลการวิเคราะห์อัตราการเกิดปฏิกิริยาเคมีด้วยเครื่องมือวิเคราะห์ TGA Nonisothermal [2]



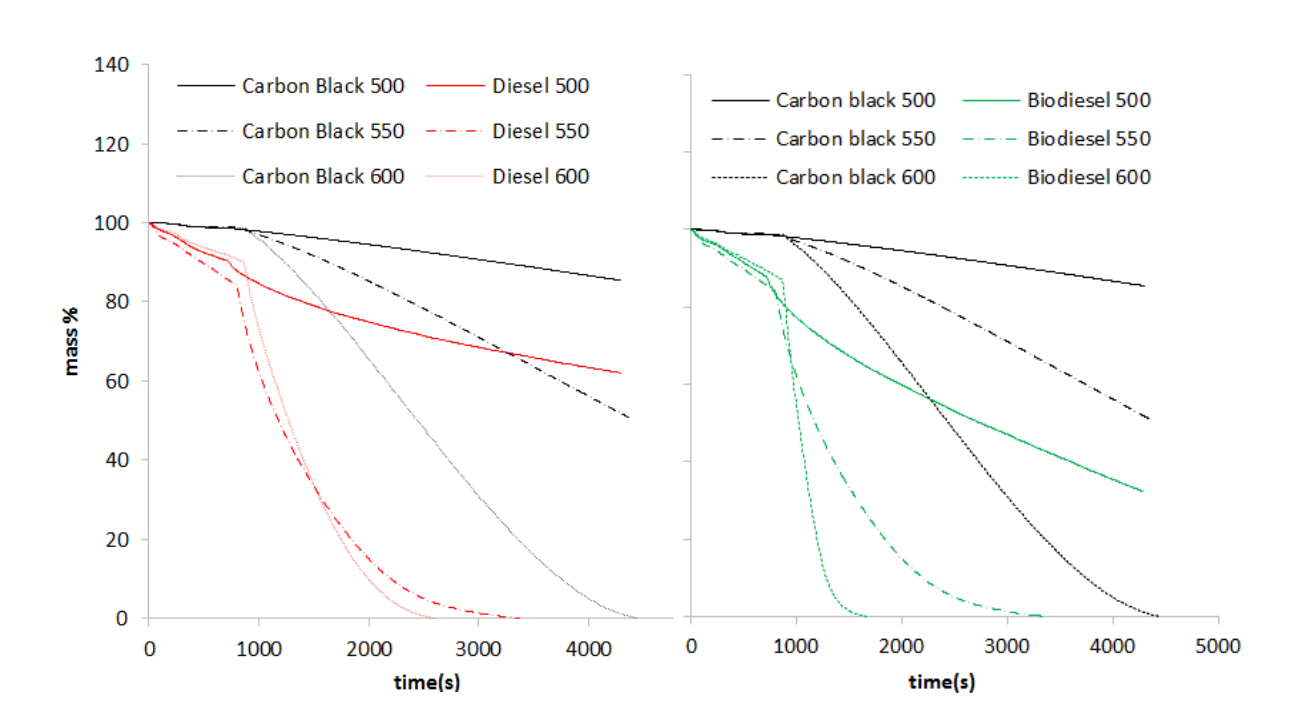
รูปที่ 15 ผลการวิเคราะห์ส่วนประกอบทางเคมีด้วยเครื่องมือวิเคราะห์ TGA Nonisothermal [2]



รูปที่ 16 คุณสมบัติทางเคมีและส่วนประกอบทางเคมีด้วยเครื่องมือวิเคราะห์ CHN Analyzer [2]

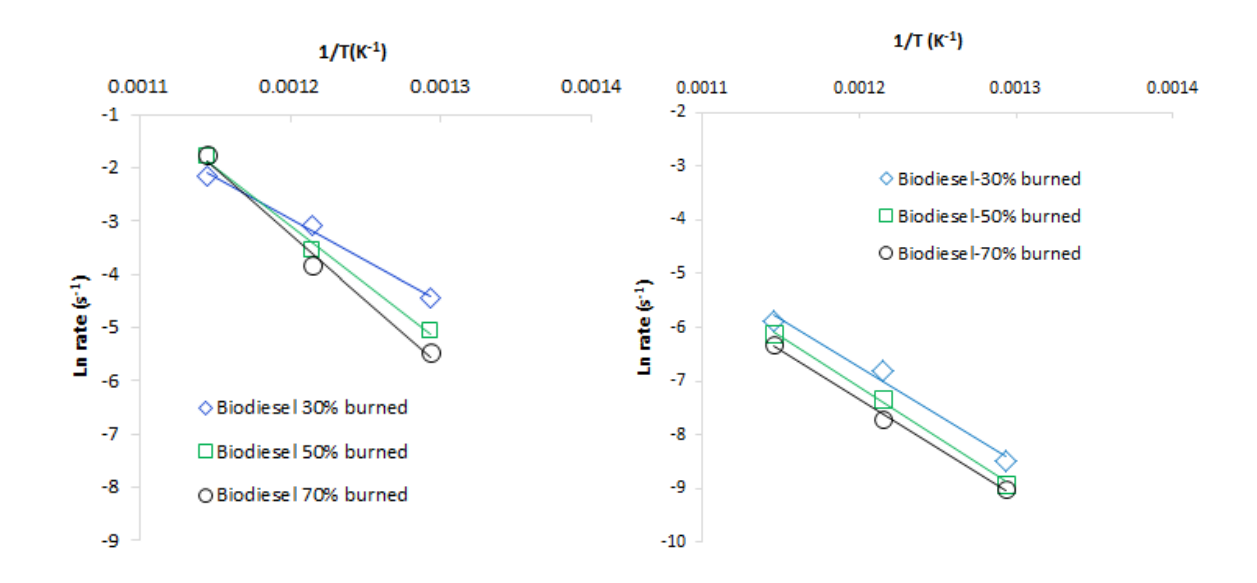


(a) การทำปฏิกิริยาระหว่างออกซิเจนกับมลพิษอนุภาคเขม่าด้วย TGA [2]



(b) การทำปฏิกิริยาระหว่างอากาศกับมลพิษอนุภาคเขม่าด้วย TGA [2]

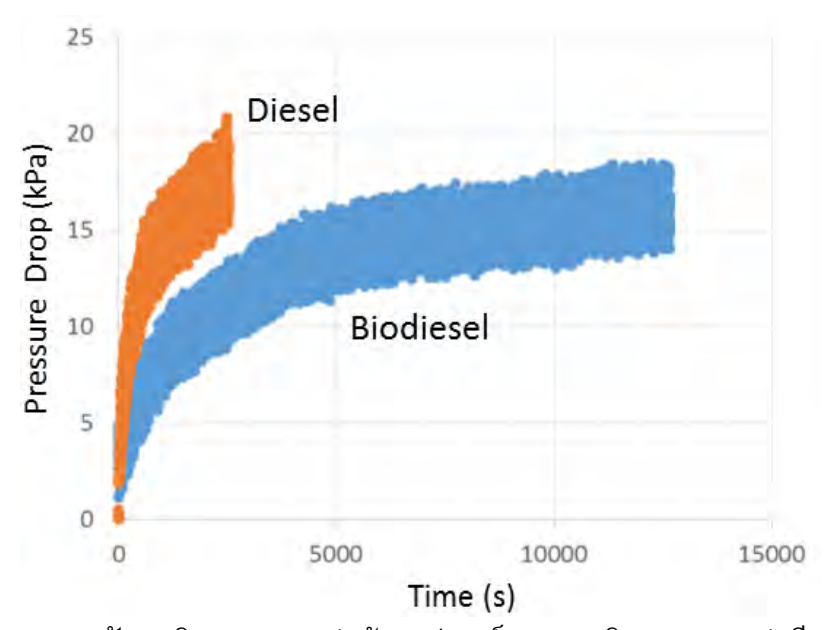
รูปที่ 17 ผลการวิเคราะห์อัตราการเกิดปฏิกิริยาเคมีด้วยเครื่องมือวิเคราะห์ TGA Isothermal [2]



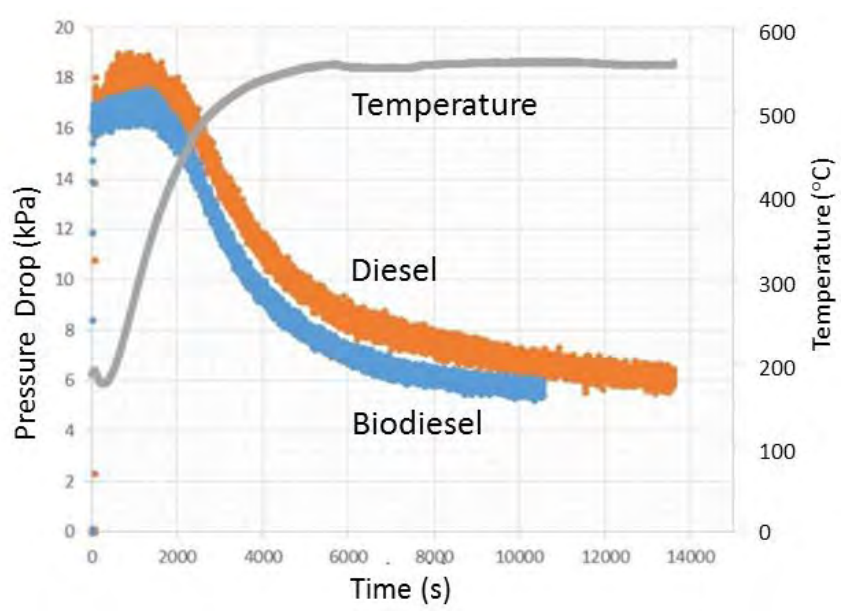
รูปที่ 18 ผลการวิเคราะห์พลังงานกระตุ้นการออกซิเดชันของมลพิษอนุภาคเขม่า [2] ตารางที่ 3 ผลการวิเคราะห์พลังงานกระตุ้นการออกซิเดชันของมลพิษอนุภาคเขม่า [2]

PM burned fraction	Apparent Ea (kJ/mole)	
	Pure oxygen	Air
Biodiesel	_	152±5
Biodiesel 30% burned	147	147
Biodiesel 50% burned	181	157
Biodiesel 70% burned	206	151
Diesel	•	159±6
Diesel 30% burned	182	153
Diesel 50% burned	245	165
Diesel 70% burned	236	159

จากผลการทดสอบอัตราการเกิดปฏิกิริยาเคมีในการออกซิเดชันของมลพิษอนุภาคด้วยการ ทดสอบแบบอุณหภมิคงที่ (Isothermal PMs Oxidation Kinetics) สามารถวิเคราะห์หาพลังงาน กระตุ้น (Apparent Activation Energy) ของการทำปฏิกิริยาระหว่างออกซิเจนกับมลพิษอนุภาคด้วย หลักการจลศาสตร์เคมีและสมการทางคณิตศาสตร์ (Arrhenius) ดังแสดงในรูปที่ 17-18 ซึ่งพบว่า พลังานกระตุ้นของการทำปฏิกิริยาระหว่างออกซิเจนกับมลพิษอนุภาคไบโอดีเซลต่ำกว่าดีเซล เล็กน้อยอาจจะเกิดจากอะตอมของออกซิเจนในไบโอดีเซลที่มาในรูปของไอโดรคาร์บอนที่เผาไหม้ไม่ สมบูรณ์สามารถทำปฏิกิริยาได้ง่ายกว่าเชื้อเพลิงดีเซล อย่างไรก็ตามค่าพลังงานกระตุ้นเฉลี่ยมี ค่าประมาณ 147-165 kJ/mole



(a) ผลทดสอบดักมลพิษอนุภาคเขม่าด้วยอุปกรณ์กรองมลพิษอนุภาคเขม่าดีเซล (DPF)



(b) ผลทดสอบออกซีไดซ์มลพิษอนุภาคเขม่าด้วยอุปกรณ์กรองมลพิษอนุภาคเขม่าดีเซล (DPF)

รูปที่ 19 ผลการทดสอบพฤติกรรมการดัก (Trapping) และการสลาย (Oxidation) มลพิษอนุภาคเขม่า ในผนัง DPF ด้วยชุดทดสอบอุปกรณ์กรองมลพิษอนุภาคเขม่า DPF Analyzer

รูปที่ 19 แสดงผลการทดสอบพฤติกรรมการดัก (Trapping) และการสลาย (Oxidation) มลพิษอนุภาค เขม่าในผนัง DPF ด้วยชุดทดสอบอุปกรณ์กรองมลพิษอนุภาคเขม่า DPF Analyzer ซึ่งแสดงผลอย่างชัดเจน ว่ามลพิษอนุภาคดีเซลมีปริมาณมากและเผาไหม้ยากกว่าไบโอดีเซล ซึ่งจากผลการทดลองจะสามารถนำไป เป็นข้อมูลในการออกแบบและเลือกใช้อุปกรณ์กำจัดมลพิษในเทคโนโลยีหลังการเผาไหม้อย่างเหมาะสม เพื่อให้เกิดการใช้พลังงานอย่างมีประสิทธิภาพได้

เอกสารอ้างอิง

- [1] M. Borhanipour, P. Karin, M. Tongroon, N. Chollacoop and H. Katsunori, "Comparison Study on Fuel Properties of Biodiesel from Jatropha, Palm and Petroleum Based Diesel Fuel," *SAE Technical Paper* No.2014-01-2017, SAE International, 2014.
- [2] P. Karin, M. Borhanipour, Y. Songsaengchana, S. Laosuwan, C. Charoenphonphanicha, N. Chollacoopb and H. Katsunori, "Oxidation Kinetics of Small CI Engine's Biodiesel Particulate Matter", *International Journal of Automotive Technology*, In Press (2014).
- [3] P. Karin, Y. Songsaengchan, S.Laosuwan, C. Charoenphonphanich, N.Chollacop and K.Hanamura, "Nanostructure of Renewable Oxygenated Fuels Particulate Matter", *ASEAN Engineering Journal*, AUN/SEED-Net, Vol.3 No.1, pp. 72-83, 2013.
- [4] P. Karin, Y. Songsaengchana, S. Laosuwan, C. Charoenphonphanicha, N. Chollacoopb and H. Katsunori, "Nanostructure Investigation of Particle Emission by Using TEM Image Processing Method", *Energy Procedia*, Elsevier, Vol.34 pp. 757 766, 2013.
- [5] P. Karin, C. Charoenphonphanicha, H. Katsunori, and T. Vuckovic, "Characterization of Engine Particle Emission Size Distribution by SMPS", *The 4th TSME International Conference on Mechanical Engineering*, 16-18 October 2013, Pattaya, Chonburi.
- [6] V. Fernandez-Alos, j. K. Waston, R. Vander Wal, and J. P. Mathews. Soot and Char Molecular Representations Generated Directly from HRTEM Lattice Fringe Images Using Fringe3D. *Combusting and Flame*, Vo., 158, pp. 1807-1813, 2011.
- [7] O.I. Smith, Fundamentals of soot formation in flames with application to diesel engine particulate emissions, *Progress in Energy and Combustion Science*, Vol. 7, pp.275-291, 1981.
- [8] P. Karin, Y. Songsaengchana, S. Laosuwan, C. Charoenphonphanicha, N. Chollacoopb and H. Katsunori, "Physical Characterization of Biodiesel Particle Emission by Electron Microscopy", *SAE Technical Paper* No. 2013-32-9150, SAE International, 2013.

สรุปผลและอภิปรายผล

Particulate matters (PMs) must be removed from the exhaust gas emitted from engines to protect the environment and human health. The problem of particulate emissions from diesel engine can be treated by Diesel Particulate Filter (DPF). In addition, biodiesel combustion produces PM about two times lower than that of diesel combustion. This means the energy consumption of engine for both the effect of pressure drop while driving and DPF regeneration process can be reduced approximately two times.

The first part of this research is study of PM micro-nanostructure by using Scanning Electron Microscopy (SEM) and Transmission Electron Microscopy (TEM) and Scanning Mobility Particle Sizer (SMPS). The single and agglomerated particle sizes of PMs are in the range of 10-60 nm and 60-130 nm, respectively. At the engine warm-up idle condition, the number of single particle is quite high and then gradually decreased with time. Finally, the single particle number is nearly constant after an hour of the engine operates in idle condition.

The average primary sizes of biodiesel and diesel fuels PMs are approximately 30-40 nm and 50-60 nm, respectively. The average carbon platelet sizes of both PMs are in the range of 0.1-7.0 nm. Moreover, approximately 800-900 carbon atoms per cubic nanometer of PMs also could be estimated in the present report. The results of this research would be used as basic information for design and develop removing process of PM emitted from engine combustion which using in diesel and biodiesel fuels.

Diesel and biodiesel PMs oxidation kinetics was clearly observed in the second part of this research. PM in high load condition of the engine has lower unburned hydrocarbons (HCs) fraction than that lower load condition. The amount of unburned HC in PM might effect in faster oxidation because oxidation temperature at lower than 500 °C of unburned HC can oxidization. Biodiesel PM is easier to oxidize than diesel PM and carbon black because of unburned oxygenated hydrocarbon.

The calculated apparent activation energy (non-isothermal method as practical use in the actual vehicle) of biodiesel PM oxidation is also lower than that of diesel PM and carbon black. The apparent activation energy of PMs emitted from the biodiesel and diesel high load engine is 152±5 kJ/mole and 159±6 kJ/mole, respectively. Because of oxygen atom included inside oxygenated fuel molecule promotes low PM oxidation activation energy. However, oxidation rate of PMs is strongly related to not only apparent activation energy but also physical impact of reaction order and frequency factor would be investigated.

ภาคผนวก

- [1] P. Karin, Y. Songsaengchan, S.Laosuwan, C. Charoenphonphanich, N.Chollacop and K.Hanamura, "Nanostructure of Renewable Oxygenated Fuels Particulate Matter", *ASEAN Engineering Journal*, AUN/SEED-Net, Vol.3 No.1, pp. 72-83, 2013.
- [2] P. Karin, Y. Songsaengchana, S. Laosuwan, C. Charoenphonphanicha, N. Chollacoopb and H. Katsunori, "Nanostructure Investigation of Particle Emission by Using TEM Image Processing Method", *Energy Procedia*, Elsevier, Vol.34 pp. 757 766, 2013.
- [3] P. Karin, C. Charoenphonphanicha, H. Katsunori, and T. Vuckovic, "Characterization of Engine Particle Emission Size Distribution by SMPS", *The 4th TSME International Conference on Mechanical Engineering*, 16-18 October 2013, Pattaya, Chonburi.
- [4] P. Karin, Y. Songsaengchana, S. Laosuwan, C. Charoenphonphanicha, N. Chollacoopb and H. Katsunori, "Physical Characterization of Biodiesel Particle Emission by Electron Microscopy", *SAE Technical Paper* No. 2013-32-9150, SAE International, 2013.
- [5] P. Karin, M. Borhanipour, Y. Songsaengchana, S. Laosuwan, C. Charoenphonphanicha, N. Chollacoopb and H. Katsunori, "Oxidation Kinetics of Small CI Engine's Biodiesel Particulate Matter", *International Journal of Automotive Technology*, In Press (2014).

Manufacturing Engineering Mechanical & Aeronautical Engineering

ASEAN Engineering Journal Part A Volume 3, Number 1 March 2013



ASEAN ENGINEERING JOURNAL

Contents	Volume 3, Number 1	March 2013
an Aircraft Using Unified N	ntification and Control System Design of Mathematical Model rastyo, Rianto Adhy Sasongko	f 5
÷	r Industrial Brush with Discrete Elemer Khanh, Nguyen Huu Hien, Nguyen Hong	
Overview of Coandă Jet Li Computational Studies Harijono Djojodihardjo, M	ft Enhancement and Two-Dimensional Solution of the state	39
Technology	nass to Electricity with Solid Oxide Fuel	l Cell 58
Preechar Karin, Yutthana S	le Oxygenated Fuels Particulate Matter Songsaengchan, Songtam Laosuwan, ich, Nuwong Chollacoop, Katsunori Ha	72 Inamura

NANOSTRUCTURE OF RENEWABLE OXYGENATED FUELS PARTICULATE MATTER

Preechar Karin¹, Yutthana Songsaengchan¹, Songtam Laosuwan², Chinda Charoenphonphanich², Nuwong Chollacoop³, Katsunori Hanamura⁴

¹International College, ²Faculty of Engineering, King Mongkut's Institute of Technology Ladkrabang, Ladkrabang, Bangkok, 10520 Thailand, Tel.+66-2-329-8261, Fax.+66-2-329-8262, Email:kkpreech@kmitl.ac.th

³National Metal and Materials Technology Center, National Science and Technology Development Agency, Klongluang, Pathumthani, Thailand 12120

⁴Department of Mechanical and Control Engineering, Tokyo Institute of Technology O-okayama, Meguro-ku, Tokyo, Japan, 152-8552

Received Date: November 5, 2012

Abstract

This paper describes a part of an ongoing research project in diesel Particulate Matter (PM) reduction by using renewable oxygenated fuel. In order to achieve the particulate matter reduction, physical structure and aggregation behavior should be investigated for better understanding of designs and configurations of Diesel Particulate Filter (DPF). The nanostructures of diesel and biodiesel PMs were investigated by using a Scanning Electron Microscopy (SEM) and a Transmission Electron Microscopy (TEM) for better understanding. The primary size distributions as well as particulate structures were presented by means of scanning images. The average primary sizes of diesel and biodiesel fuels PMs are approximately 50-60 nm and 30-40 nm, respectively. The average carbon platelet sizes of diesel and biodiesel PMs are in the range of 0.5-3.0 nm. In addition, Thermo-gravimetric Analysis (TGA) was used to investigate chemical kinetics of particulate matter oxidation. The apparent activation energies of oxygenated hydrocarbon, diesel hydrocarbon and carbon oxidation are approximately 91 kJ/mol, 130 kJ/mol and 155 kJ/mol, respectively.

Keywords: Diesel Engine, Particulate Matter, Diesel Particulate Filter, Oxygenated Fuel

Introduction

Among internal combustion engines, diesel engines have the highest thermal efficiency. However, particulate matters (PMs) must be removed from exhaust gases emitted from diesel engines to protect the environment and human health. Therefore, the regulation on the restriction of emission is increased.

Diesel particulate matters consist of a solid fraction (SOL) and a soluble organic fraction (SOF). Primary particles, composed of carbon and metallic ash, are coated with SOF and sulfate. The nanostructures of primary soot particles have been characterized using transmission electron microscopy (TEM) to understand them in details. The mean diameters of the primary and agglomerated particles are usually in the range of 20–80 nm and 80–300 nm, respectively. A primary soot particle has two distinct parts: an inner core and an outer shell. The inner core has a diameter of 10 nm and it is located at the central region of the primary particle. The composition of particles from a diesel engine may vary widely depending on the operating conditions and fuel composition [1–9].

Diesel particulate filters (DPFs) play an important role in particulate trapping and oxidation. A DPF is generally made of ceramic materials, such as cordierite or silicon carbide, consisting of many rectangular channels with alternate channels blocked using cement at each end. The exhaust gas is forced to flow through a channel wall having numerous micron-scale pores that trap the particle emissions. Furthermore, the collected

particulates must be oxidized to regenerate the DPF and reduce the back pressure on the diesel engine [10–17].

The problem of particle emissions from diesel engine should be reduced by development of high efficiency engine, after-treatment and pre-treatment technologies. The use of renewable oxygenated fuels is now a widespread means to reduce regulated pollutant emissions produced by internal combustion engines [9], as well as to reduce the greenhouse gas. However, particulate matter emitted from biodiesel must be investigated for better understanding to optimize the design of DPF configuration. The present research is to study the physical structure and oxidation behaviors of diesel and biodiesel particulate matters. The first objective is to investigate and compare the quantity, microstructure and nanostructure of diesel and biodiesel particulate matters by using DPF sample disc for particulate trapping, SEM and TEM for particulate structure investigation. The second objective is the study of diesel and biodiesel particulate matters oxidation kinetics by using Thermo-gravimetric analysis (TGA).

Experimental Setup

Particulate Matter Generator

Biodiesel which derived from palm-olein (biodiesel (B100) fuel of TIS 2313-2549) was used and compared with the results of commercial grade diesel (conventional diesel (B0) fuel of TIS 2155-2546). The carbon fraction of diesel and biodiesel are 82 and 78, respectively. Diesel and biodiesel diffusion flame particulate matters were generated by diesel and biodiesel lamps, as shown in Fig.1. The fuel consumption of each fuel was measured by weight loss respect to time for comparison in the view point of energy consumption. Particulate matters were introduced into the DPF samples by using the vacuum pump by controlling the constant gas flow rate and temperature base on the actual vehicle condition. The pressure drop between inlet and outlet of the DPF sample were measured in each trapping time by using manometer and in real time by pressure sensor.

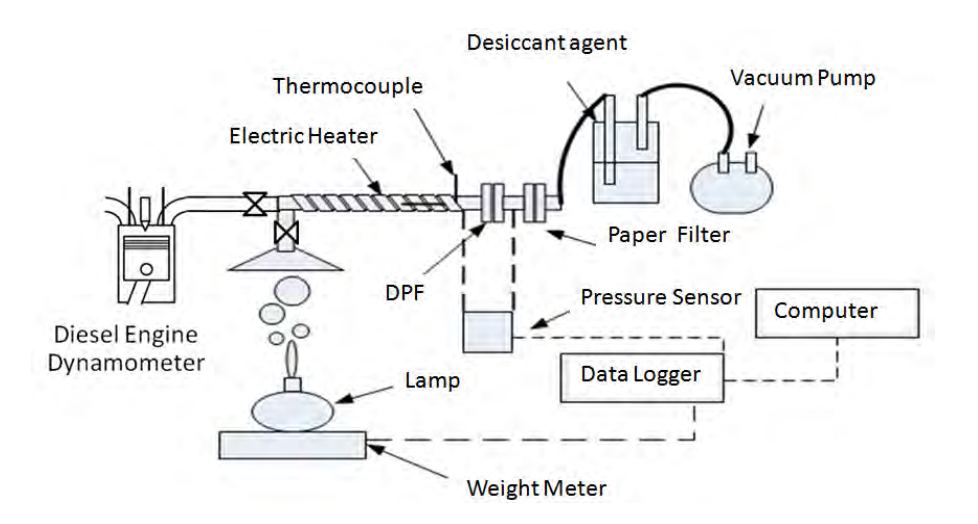


Figure 1. Experimental setup for particulate matter quantities investigation

On the other hand, a single cylinder, four strokes, direct injection diesel engine was also used in the soot generation process. The fuel injection pressure was 19.6 MPa and the engine speed was fixed at 2400 rpm without load on the engine dynamometer. The present research is focused on the effect of oxygenated fuel in particle emissions. Therefore, no

load condition is studied in this case for the first step even particulate matter size and unburned hydrocarbon content are strongly related to engine operating condition.

Particulate Matter Characterization Method

Nanostructures of single primary particle and carbon platelet structures were investigated by TEM image and post process by hand drawn images. Oxidation behaviors of isothermal and non-isothermal methods were investigated by TGA. Non-isothermal method was used to estimate apparent activation energy of each unburned hydrocarbon (oxygenated and fossil) under the condition of temperature increasing rate of 10°C per minute from 25°C to 800°C with 100% oxygen atmosphere. On the other hand, isothermal method was operated by temperature increasing rate of 10°C per minute from 25°C to 450°C to remove unburned hydrocarbon. Then, temperature was holding at 450°C for an hour. Similarity, each sample was tested under the condition of 500°C, 550°C and 600°C.

Chemical kinetics of particulate matter oxidation is studied by using Thermogravimetric analysis (TGA).

$$C + O_2 \to CO_2 \tag{1}$$

The chemical reaction rate in eq.1 can calculate from the TGA curve based on the chemical kinetic in eq.2

$$-\frac{d[C]}{dt} = -k[C]^n[O_2]^m \tag{2}$$

Where C is particulate matter mass, t is time, k is the rate constant of chemical reactions, m, n are the reaction orders. The dependence of the specific rate constant of chemical reactions k is expressed by eq.3

$$k = Ae^{-E_a/RI} (3)$$

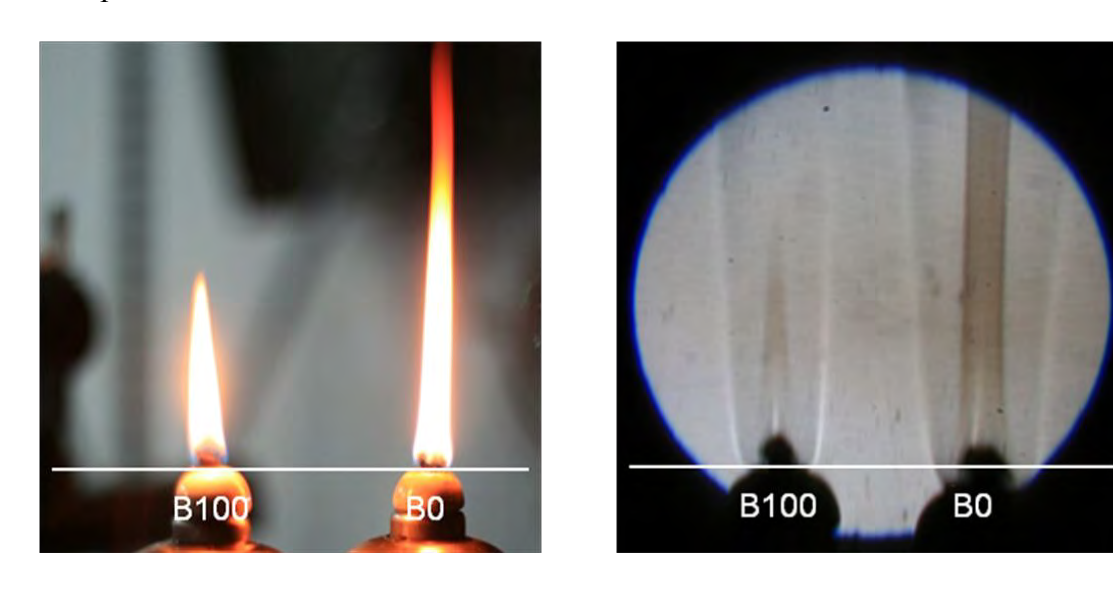
Where A is the frequency factor, E_a is the activation energy, R is the gas constant. The apparent activation energy can be calculated by eq.4.

$$\ln\left[\frac{-1}{[C]^n}\frac{d[C]}{dt}\right] = -\frac{E}{RT} + (\ln A + m\ln[O_2]) \tag{4}$$

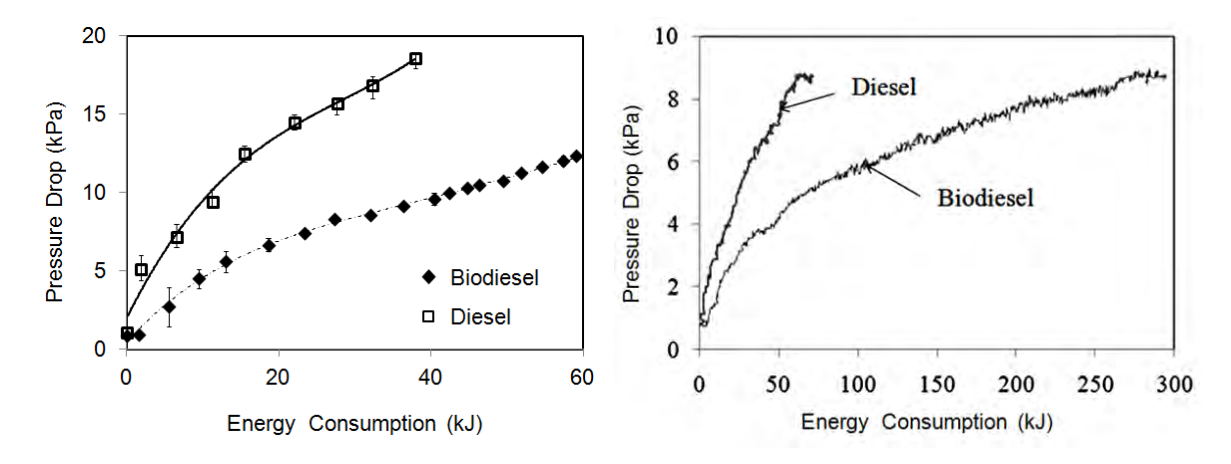
Results and Discussions

Particulate Matter Concentration

Figure 2 (a) shows diesel and biodiesel diffusion flames from optical image. The soot particle is formed in the fuel spray cores, in which the rich fuel is contained, whereas the fuel vapor is heated by mixing with hot burned gases in the flame regions. The particle is oxidized in the flame zone when it contacts with available oxygen, resulting in yellow luminous flame character. The length of biodiesel diffusion flame was shorter than that of diesel. Similarity, Fig. 2 (b) shows diesel and biodiesel diffusion flames produced by Schlieren method. The center of biodiesel diffusion flame was lighter than that of diesel because oxygen atoms inside an oxygenated fuel molecule can promote the conditions which approach to the complete combustion.



(a) Conventional digital camera (b) Schlieren method Figure 2. Biodiesel (B100) and diesel (B0) diffusion flame by (a) optical digital camera and (b) Schlieren method images [18,19]



(a) Pressure Drop by Manometer (b) Pressure Drop by Pressure Sensor Figure 3. Lamp's diesel and biodiesel particulate matters concentrations by (a) manometer and [19,20] and (b) pressure sensor

Figure 3 (a) shows the comparison of pressure drop between outlet and inlet of DPF disc sample with the size of 4.5 x 4.5 cm². Samples were taken during the trapping process at the same energy consumption rate of diffusion flame. As indicated in this graph which obtained from measurement of manometer, diesel particulates have a higher pressure drop than biodiesel particulates at a given energy input. Pressure drop of DPF wall during diesel particulate matters trapping was approximately 2 times higher than that of biodiesel particulate matter. Therefore, the apparent amount of diesel particulate matter could be also assumed to be 2 times higher than that of biodiesel. However, the actual concentrations should be measured by using higher precision device in the next step. Figure 3 (b) shows the same trend of particulate matter trapping inside the DPF disc sample size of 6 x 6 cm² and pressure drop was measured by pressure sensor.

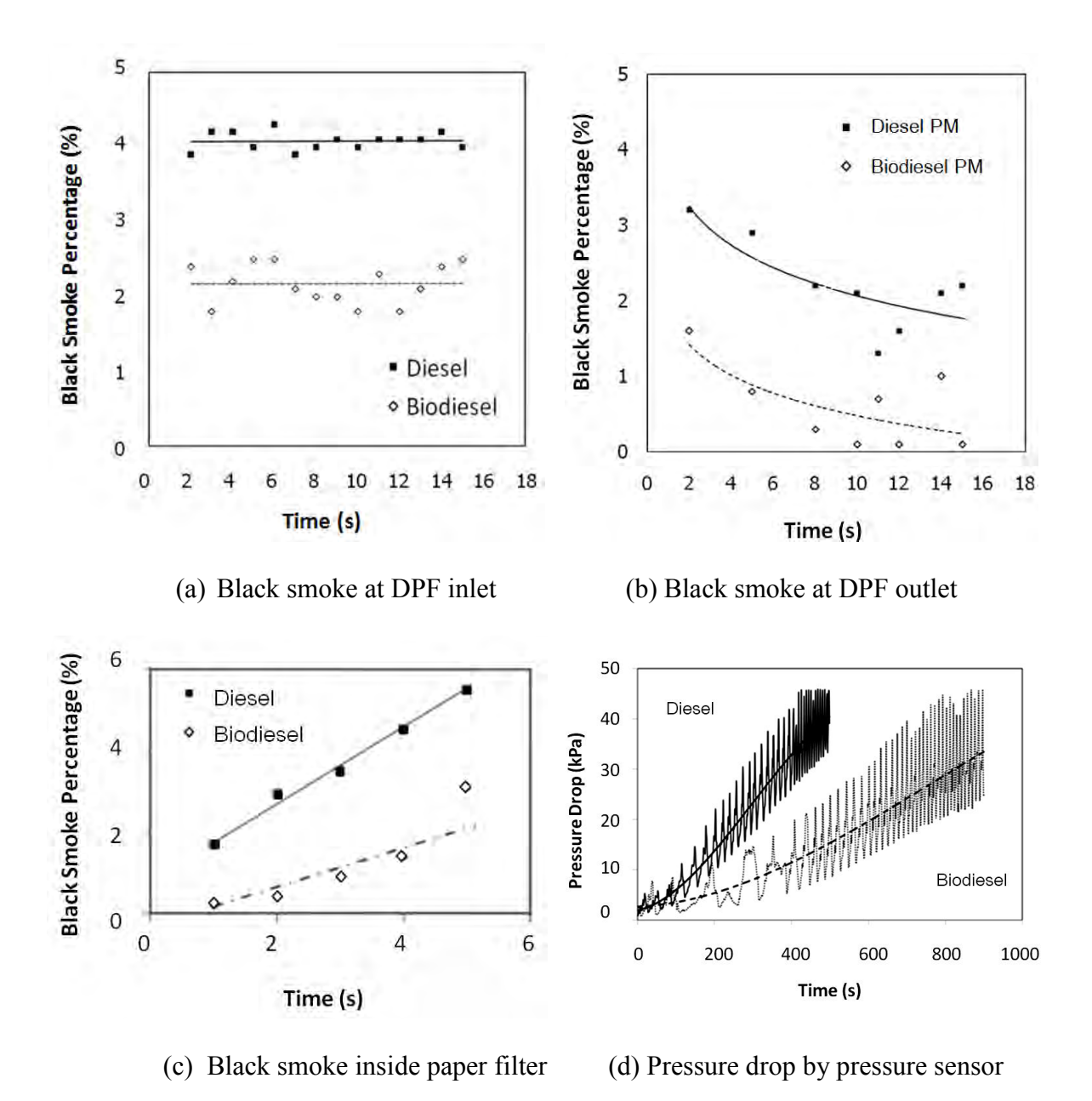


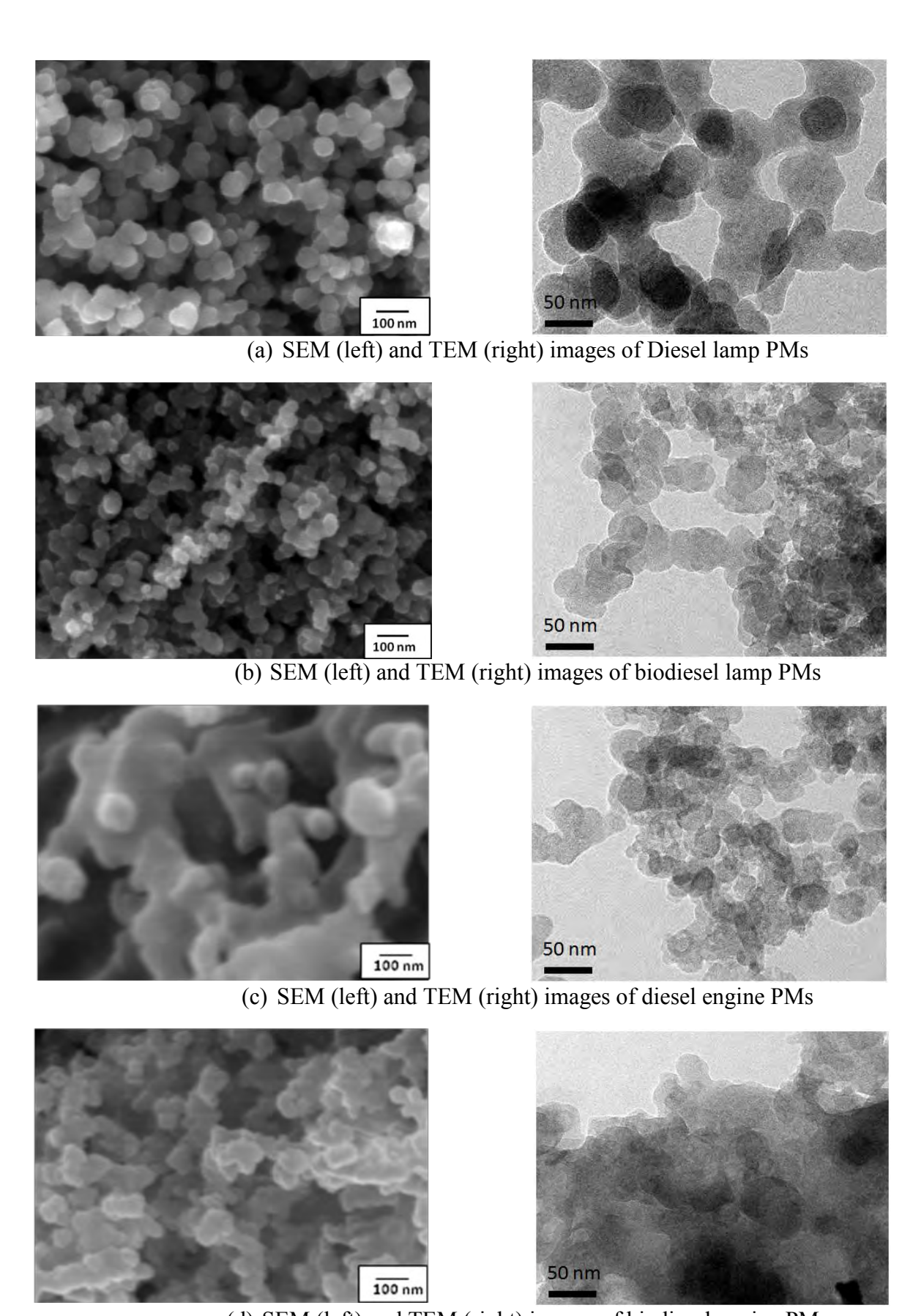
Figure 4. Engine's diesel and biodiesel particulate matters concentrations by smoke meter at (a) DPF inlet, (b) DPF outlet, (c) Inside paper filter [19,20] and by (d) Pressure sensor

In the same method, the remaining soot particle is emitted in the CI engine exhaust pipe. The paper filter was used to trap the emitted diesel and biodiesel soot particle at any time. Subsequently, smoke meter was applied to measure the concentration of trapped particulate on the paper filter by light emitting method. Figure 4 (a) and (b) show the percentage of black smoke of diesel and biodiesel at the inlet and outlet of DPF, respectively. The concentration of diesel black smoke is approximately two times higher than that of biodiesel. Figure 4 (c) shows the percentage of black smoke of diesel and biodiesel when the trapping period is varied. The result showed that the percentage of black smoke of diesel increased faster than that of biodiesel. In addition, it's also clearly observed that the pressure drop between inlet and outlet of DPF for diesel engine is approximately two times higher than that of biodiesel. Hence, diesel particulate formation was higher than biodiesel. This could be explained that more soot particulate was remained in diesel combustion than those of biodiesel. Because it contains oxygen molecule, biodiesel is readily oxidized with available oxygen in the flame zone. Consequently, particulate filter trapping duration of biodiesel fuel is longer than that of diesel fuel because of particulate concentration emitted from bio-oxygenated fuel combustion flame is lower than that of diesel combustion.

Microstructure of Particulate Matter

In this research, the particle image is taken to verify the diesel and biodiesel particle and carbon platelet sizes by micro- and nano- image. Figure 5 shows SEM images of ultrafine particle sizes from of (a) diesel lamp, (b) biodiesel lamp, (c) diesel engine and (d) biodiesel engine (left hand side). The image showed that the biodiesel particle sizes from both sources are slightly smaller than that of diesel particle. On the other hand, particle emitted from the lamp is a slightly smaller than that particle emitted from engine in both fuels. The single particle sizes from diesel and biodiesel diffusion flame are approximately 50-60 nm and 30-40 nm, respectively. However, it is difficult to measure primary size of engine particle by SEM image because the surface of particulate matter emitted from engine could be covered by much amount of unburned hydrocarbon. The TEM method was used to measure primary particle size from diesel and biodiesel fuel. Figures 5 (a), (b), (c) and (d) show particulate matter emitted from diesel lamp, biodiesel lamp, diesel engine and biodiesel engine (right hand side). The primary particle size is approximately 20-80 nm which is in the range of ultrafine particles (diameter size lower than 100 nm). However, the biodiesel particulate matter is a bit smaller than that of diesel particulate matter for both combustions.

The particulates were trapped from exhaust gas from lamp and engine. The TEM method was used to visualize the particle diameter. The particulate size distribution in primary mode for approximately 100 particles which taken from TEM image, was shown in Fig. 6. Most of diesel lamp particle size is around 50-60 nm while the biodiesel lamp particle size has peaked in the range between 30-40 nm which is slightly smaller than that of diesel lamp particle. The peak of primary particle size from diesel and biodiesel engines are approximately 30-40 nm. The primary size of diesel particles is larger than that of biodiesel. This is due to the lower concentration of biodiesel particle, which is readily oxidized with more available oxygen in combustion flame due to oxygenated biodiesel fuel. On the other hand, the primary particle size from diesel engine is smaller than that of diesel lamp particle possibly because of engine conditions such as homogeneous of air/fuel mixture, high pressure in combustion chamber, exhaust gas temperature, may effect to particulate matter oxidation before exiting to the atmosphere. Moreover, higher oxygen content and homogeneity mixture closed to the stoichiometric condition of bio-oxygenated fuel can produce smaller size of primary particulate particle.



(d) SEM (left) and TEM (right) images of biodiesel engine PMs

Figure 5. SEM (left) and TEM (right) images of (a) Diesel lamp, (b) Biodiesel lamp (c) Diesel engine and (d) Biodiesel engine particulate matters [19-20]

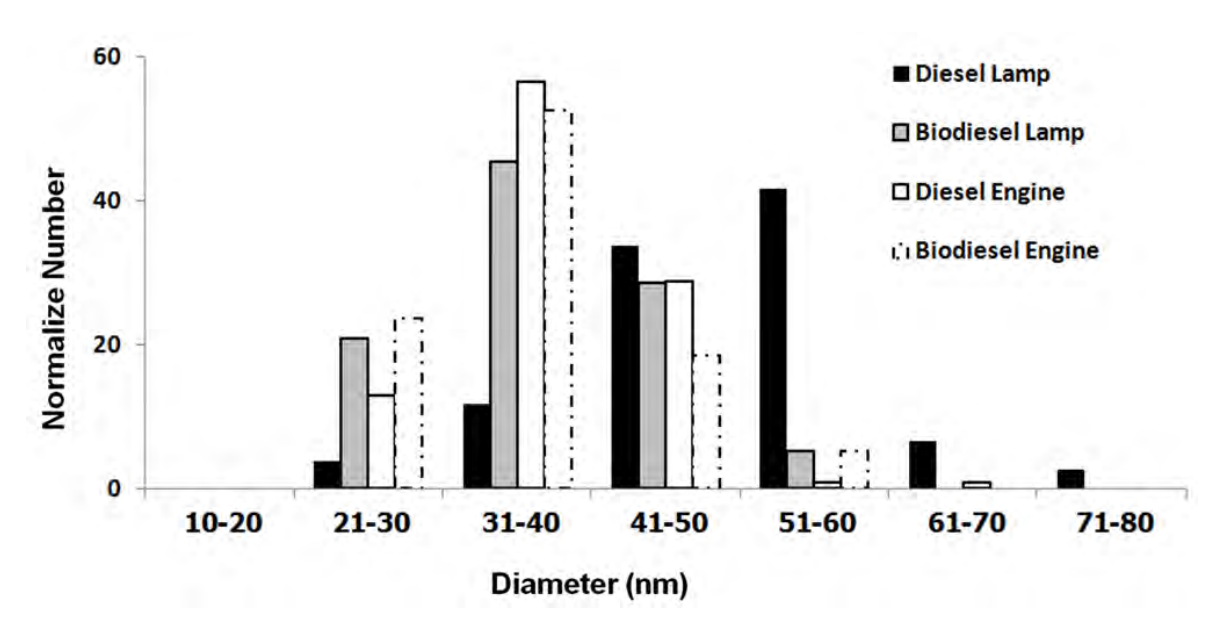


Figure 6. Primary particle size distribution of particulate matter by TEM images which normalized from 38 to 108 particles to be 100 samples of each fuel's particle

Nanostructure of Particulate Matter

Figure 7 shows the nanostructure of diesel particulate matter which emitted from diffusion flame combustion inside a diesel engine. Particulate matter is investigated for number of carbon atom contained in the particle. TEM image is used for numerating platelet number that aggregate layered in the particle. Each of platelets is consisted of proper amount of carbon atom from incomplete combustion product. For each of combustion, lamp and engine, the platelet sizes are shown in Fig. 8. The average of diesel and biodiesel carbon platelets is in the range of 0.5-3.0 nm. However the distance of each platelet for different fuels is not the same.

Another result of carbon atom number per volume is also estimated. The concept of estimation is "the molecule of carbon-6 (C6) is the possible smallest size". Such molecules are agglomerated to be the large ring of carbon then becomes a platelet. The particulate matter from biodiesel lamp and diesel lamp contain 129, 205 atom per nm³ while the particulate matter from biodiesel engine and diesel engine are consisted by carbon atom number of 63 and 72 per nm³, respectively, as shown in Table 1.

The particulate matter from diesel combustion contains carbon atom that is larger than that of biodiesel combustion. The biodiesel combustion which emits lower carbon concentration results in lower carbon atom consisted in particulate matter. In addition, platelet length and atom concentration of particulate matter emitted from the engine are smaller than that of diffusion flame of lamp due to the impact of pressure, temperature and homogeneous mixture of fuel and oxygen.

This is an interesting result of bio-oxygenated fuel combustion behavior and particles emission nanostructure which should be researched in more details to discover the useful information for better understanding and future designs of modern Internal Combustion Engines and DPF configurations.

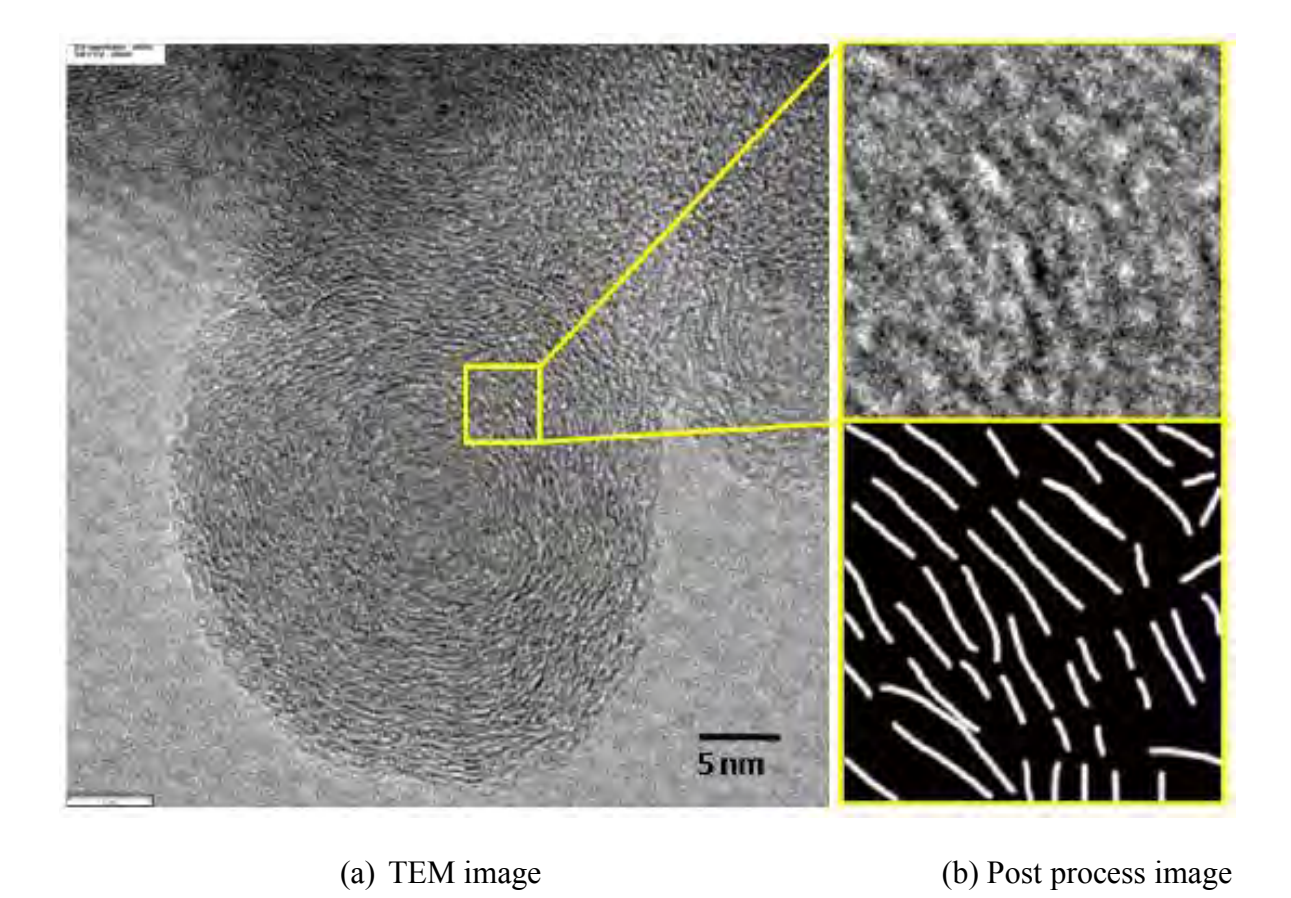


Figure 7. (a) TEM and (b) Post process (by hand draw) images of carbon platelet inside particulate matter

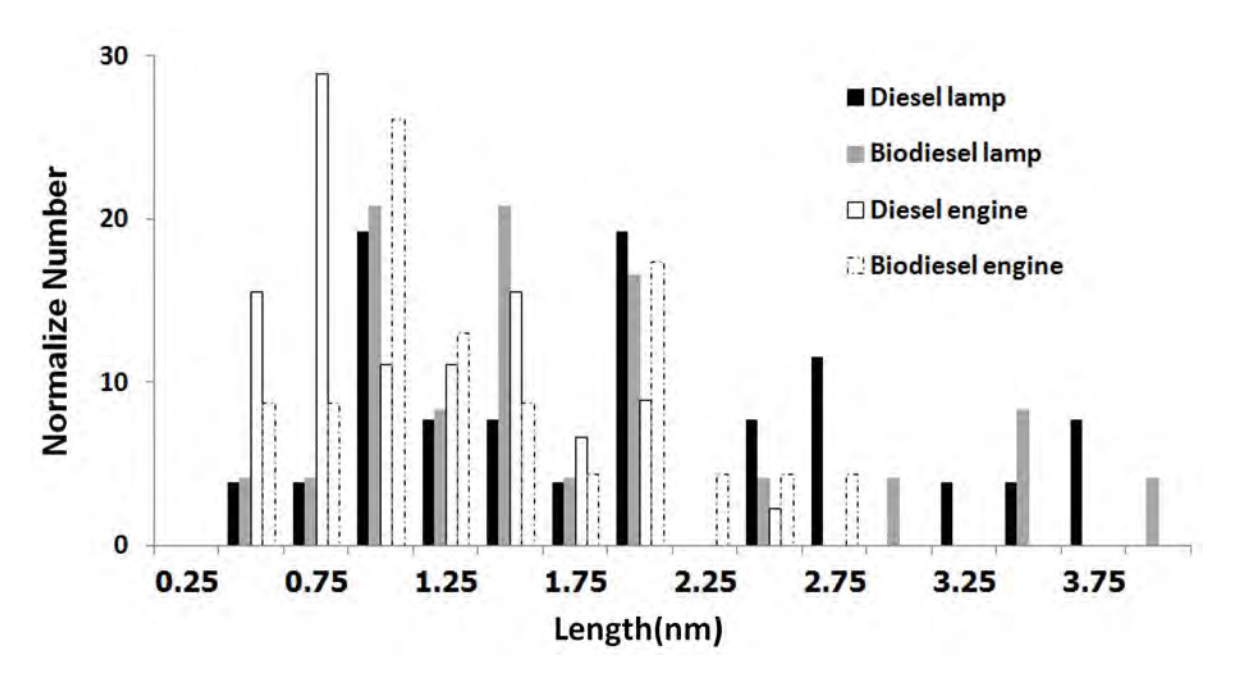


Figure 8. Carbon platelet size distribution of particulate matter by TEM images normalized from 24 to 45 platelets to be 100 samples of each fuel's particle

Table 1. Carbon Atom Include in Particulate Matter

Particulate Matter Type	Density (atom/nm ³)
Biodiesel Lamp PM	129
Diesel Lamp PM	205
Biodiesel Engine PM	63
Diesel Engine PM	72

Oxidation of Particulate Matter

Figure 9 (a) shows Arrhenius plots of diesel and biodiesel particulate matter oxidation by non-isothermal method of TGA at temperature of 400 °C to 480 °C using Eq.1-4. It is assumed that the diesel and oxygenate unburned hydrocarbons oxidation could be oxidized and calculated apparent activation energies are approximately 130 and 91 kJ/mol, respectively. On the other hand, temperature from 490 °C to 520 °C is assumed to be carbon oxidation which has 155-177 kJ/mol of apparent activation energy.

Figure 9 (b) shows Arrhenius plots of remaining pure carbon inside diesel and biodiesel particulate matter oxidation by TGA isothermal method at the temperature from 450 °C to 600 °C. Unburned hydrocarbons were assumed to be successfully oxidized before holding the constant temperature. Apparent activation energy of pure carbon is approximately 155 kJ/mol for both of diesel and biodiesel carbon.

Table 2 summarizes the apparent activation energy of each particulate matter oxidation by non-isothermal and isothermal methods. It is clearly observed that unburned bio-oxygenated hydrocarbon oxidized at the lower temperature and requires lower apparent activation energies than that of fossil fuel even the remaining carbon are oxidized in the same range of apparent activation energies.

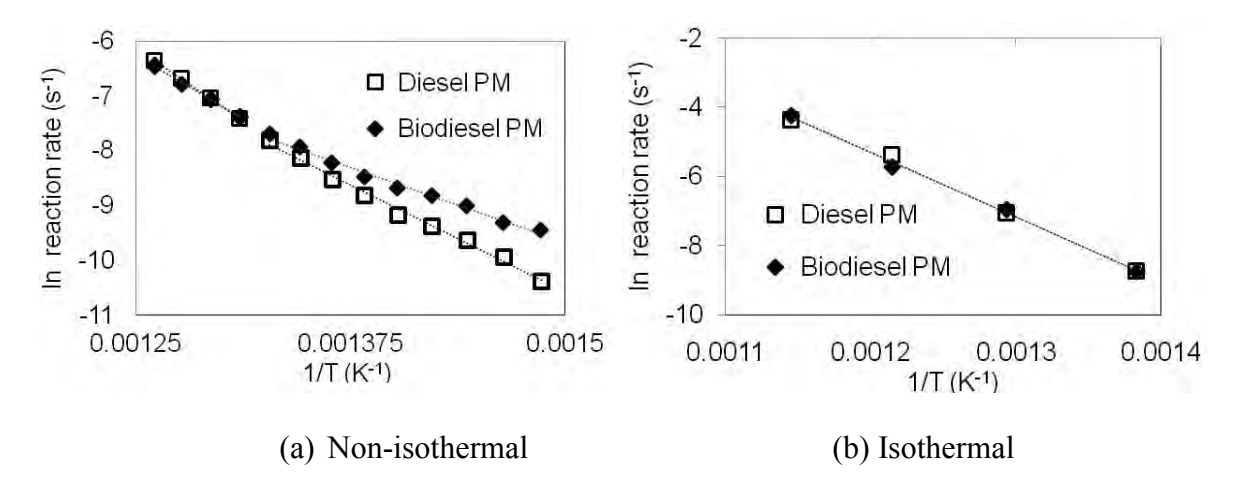


Figure. 9 Arrhenius plots of PM oxidation by (a) Non-isothermal and (b) Isothermal methods

Table 2. Apparent Activation Energy (Ea) of Particulate Matter Oxidation

Particulate Matter Type	Ea (kJ/mol)		
	Non-is e 400-480 °C	othermal 490-520 °C	Isothermal 450-600 °C
Biodiesel Lamp PM	91.3	155.4	155.6
Diesel Lamp PM	129.6	176.7	155.9

Conclusions

- Biodiesel combustion produces particulate matter two times lower than that of diesel combustion. Therefore, the conventional DPF can be used for two times of trapping duration. This means the energy consumption of engine for both the effect of pressure drop while driving and DPF regeneration process can be reduced approximately by two times.
- The primary size of diesel particles is larger than that of biodiesel. This is due to the lower concentration of biodiesel particles, which is readily oxidized with more available oxygen in combustion flame due to oxygenated biodiesel fuel. On the other hand, the primary particle size from diesel engine is smaller than that of diesel lamp particle due to homogeneous air/fuel mixture effect for complete combustion. However the impact is not strong for DPF trapping process because of the pore size of DPF is very large compared to the size of the particle emission.
- The carbon atom density in diesel particulate matter is higher than that of biodiesel. As a result, the impact of carbon and oxygen atom contents in oxygenated fuel must be researched for more understanding to optimize the internal combustion engine and DPF configurations.
- Unburned hydrocarbon from biodiesel combustion can be oxidized faster than that of
 unburned hydrocarbon from diesel combustion because of oxygen atoms included
 inside oxygenated fuel molecule promote complete combustion. Moreover, it is
 clearly observed that there is the same value of apparent activation energies for
 particulate matter without unburned hydrocarbon due to the condition of pure carbon
 oxidation.

References

- [1] J.B. Heywood, *Internal Combustion Engine Fundamental*, McGraw-Hill series in mechanical engineering, Singapore, 1998.
- [2] O.I. Smith, Fundamentals of soot formation in flames with application to diesel engine particulate emissions, *Progress in Energy and Combustion Science*, Vol. 7, pp.275-291, 1981.
- [3] M.M. Maricq, Review Chemical Characterization of particulate emissions from diesel engine: A review, *Journal of Aerosol Science*, Vol.38, pp.1079-1118, 2007.
- [4] D.B. Kittelson, Engines and nanoparticles: A review, *Journal of Aerosol Science*, Vol.29, pp.575-588, 1998.
- [5] W.A. Majewski, and M.K. Khair, Diesel Emissions and Their Control, *SAE Order No.R-303*, SAE International. Warrendale USA, 2006.

- [6] T. Ishiguro, Y. Takatori, and K. Akihama, Microstructure of Diesel Soot Particles Probed by Electron Microscopy: First Observation of Inner Core and Outer Shell, *Combustion and Flame*, 108, pp.231-234, 1997.
- [7] R.A. Vander Wal, A. Yezerets, N.W. Currier, D.H. Kim, and C.H. Wang, HRTEM Study of diesel soot collected from diesel particulate filters, *Carbon*, 45, pp.70-77, 2007.
- [8] T. Aizawa, H. Nishigai, K. Kondo, T. Yamaguchi, J.G. Nerva, C. Genzale, S. Kook, and L. Pickett, Transmission Electron Microscopy of Soot Particles Directly Sampled in Diesel Spray Flame A Comparison between US#2 and Biodiesel Soot, *SAE International Journal of Fuels and Lubricants*, SAE International, Vol.5 No.2, pp.665-673, 2012.
- [9] N. Miyamoto, H. Ogawa, and M.N. Nabi, Approches to extreamly low emissions and efficient diesel combustion with oxygenated fuels, *International Journal of Engine research*, Professional Engineering Publishing, Vol.1, No.1, pp.71-85, 2000.
- [10] A.G. Konstandopoulos, M. Kostoglou, N. Vlachos, and E. Kladopoulos, Progress in Diesel Particulate Filter Simulation, *SAE Technical paper*, 2005-01-0946, 2005.
- [11] A.G. Konstandopoulos, D. Zarvalis, E. Kladopoulou, and L. Dolios, A multi-reactor assembly for screening of diesel particulate filters, *SAE Technical paper*, 2006-01-0874, 2006.
- [12] S. Tushima, I. Nakamura, S. Sakashita, S. Hirai, and D. Kitayama, Lattice Boltzmann simulation on particle transport and captured behaviors in a 3d-reconstructed micro porous DPF, *SAE Technical paper*, 2010-01-0534, 2010.
- [13] K. Hanamura, P. Karin, L. Cui, P. Rubio, T. Tsuruta, T. Tanaka, and T. Suzuki, Micro- and macroscopic visualization of particulate matter trapping and regeneration processes in wall-flow diesel particulate filters, *International Journal of Engine research*, Professional Engineering Publishing, Vol.10, No.5/2009, pp.305-321, 2009.
- [14] P. Karin, L. Cui, P. Rubio, T. Tsuruta, and K. Hanamura, Microscopic Visualization of PM Trapping and Regeneration in Micro-Structural Pores of a DPF Wall, *SAE International Journal of Fuels and Lubricants*, SAE International, Vol.2 No.1, pp.661-669, 2009.
- [15] P. Karin, and K. Hanamura, Particulate Matter Trapping and Oxidation on Catalyst-Membrane, *SAE International Journal of Fuels and Lubricants*, SAE International, Vol.3 No.1 pp.368-379, 2010.
- [16] H. Oki, P. Karin, and K. Hanamura, Visualization of Oxidation of Soot Nanoparticles Trapped on a Diesel Particulate Membrane Filter, *SAE International Journal of Engines*, SAE International, Vol. 4 no. 1 pp.515-526, 2011.
- [17] K. Nakamura, H. Oki, R. Sanui, and K. Hanamura, Soot Oxidation Characteristics of SiC Nanoparticle Membrane Filters, *SAE Technical Paper*, 2012-01-0848, 2012.
- [18] S. Laosuwan, P. Karin, and C. Charoenpornpanich, "Study on Diesel and Biodiesel Particulate Matter Trapping inside a Diesel Particulate Filter", *The7th International Conference of Automotive Engineer (ICAE-7)*, TSAE, 28-29 March, Bangkok-Thailand, 2011.
- [19] S. Laosuwan, P. Karin, and C. Charoenpornpanich, "Thermo-gravimetric Analysis of Biodiesel Diffusion Flame's Particulate Matter", *The Second TSME International Conference on Mechanical Engineering (The 2nd TSME-ICoME)*, 19-21 October, Krabi-Thailand, 2011.
- [20] Y. Songsaengchan, C. Chareonphonphanich, P. Karin, N. Chollacoop, M. Thongroon, and K. Hanamura, "Physical Characterization of Biodiesel Particulate Matter by STEM", *The Second TSME International Conference on Mechanical Engineering (The 2nd TSME-ICoME)*, 19-21 October, Krabi-Thailand, 2011.



Available online at www.sciencedirect.com

SciVerse ScienceDirect

Procedia

Energy Procedia 34 (2013) 757 - 766

10th Eco-Energy and Materials Science and Engineering (EMSES2012)

Nanostructure Investigation of Particle Emission by Using TEM Image Processing Method

Preechar Karin^a*, Yutthana Songsaengchan^a, Songtam Laosuwan^a, Chinda Charoenphonphanich^a, Nuwong Chollacoop^b, Hanamura Katsunori^c

^aKing Mongkut's Institute of Technology Ladkrabang, Ladkrabang, Bangkok 10520, Thailand ^bNational Science and Technology Development Agency, Klongluang, Pathumthani 12120, Thailand ^cTokyo Institute of Technology, Meguro-ku, Tokyo152-8552, Japan

Abstract

Particulate matters (PMs) must be removed from the exhaust gas emitted from engines to protect the environment and human health. The problem of particulate emissions from diesel engine can be reduced in many ways, for examples: development of modern engine, fuel additives, diesel particulate filter (DPF) and oxygenated fuel. This paper describes a part of an ongoing research project in PM reduction as emitted from combustion. The main part is study of PM nanostructure by using Transmission Electron Microscopy (TEM). The primary size distributions as well as PM structures were presented by TEM images. The average primary sizes of biodiesel and diesel fuels PMs are approximately 30-40 nm and 50-60 nm, respectively. The average carbon platelet sizes of both PMs are in the range of 0.1-7.0 nm. Moreover, approximately 830 carbon atoms per cubic nanometer of PMs also could be estimated and presented in the present report. The results of this research would be used as basic information for design and develop removing process of PM emitted from engine combustion which using in diesel and biodiesel fuels.

© 2013 The Authors. Published by Elsevier B.V. Selection and peer-review under responsibility of COE of Sustainalble Energy System, Rajamangala University of Technology Thanyaburi (RMUTT)

Keywords: Engine, Particulate Matter, Particulate Filter, Transmission Electron Microscopy;

^{*} Corresponding author. Tel.: +66-2-329-8261; fax: +66-2-329-8262 *E-mail address*: kkpreech@kmitl.ac.th.

1. Introduction

Among internal combustion engines (ICE), diesel or compression-ignition (CI) engines have the highest thermal efficiency for a given output power. However, particulate matters (PMs) and NOx must be removed from the exhaust gas emitted from diesel engines to protect the environment and human health. Therefore, regulation of vehicle emissions has become increasingly strict. However, it is very difficult to develop internal combustion engine and after treatment systems for simultaneous removal of PM and NOx.

The problem of particle emissions from diesel engine should be improved by developing the high efficiency modern engine, after-treatment and pre-treatment technologies. Diesel Particulate Filters (DPFs) play an important role in PM trapping and oxidation. A DPF is generally made of ceramic materials, such as cordierite or silicon carbide, consisting of many rectangular channels with alternate channels blocked using cement at each end. The exhaust gas is forced to flow through a channel wall having numerous micron-scale pores that trap the PM. Furthermore, the collected PM must be oxidized to regenerate the DPF and reduce the back pressure on the diesel engine [1-3].

The nanostructures of soot primary particles have been characterized using scanning electron microscope (SEM) and transmission electron microscopy (TEM) to understand them in detail. The mean diameter of the primary and agglomerated particles is usually in the range of ultrafine particle and fine particle, respectively. A primary soot particle has two distinct parts: an inner core and an outer shell. The inner core is located at central region of the primary particle [4-11]. The composition of PMs from a diesel engine may vary widely depending on the operating conditions and fuel composition. Based on analysis performance with a combination of physical and chemical methods, PM is traditionally divided into three main fractions: solid fraction (SOL), soluble organic fraction (SOF), and sulfate particulates (SO₄) that consist of sulfuric acid and water. The SOL of diesel PMs is composed primarily of elemental carbon, sometimes referred to as inorganic carbon. This carbon, not chemically bound with other elements, is the finely dispersed carbon black or soot substance responsible for black smoke emission. HCs adsorbed on the surface of the carbon particles are present in the form of fine droplets from the SOF of diesel particulates. At times, this fraction is also referred to as the volatile organic fraction (VOF). The SOF fraction contains most of the polycyclic aromatic HCs (PAHs) and nitro-PAHs emitted with diesel exhaust gases. PAHs are aromatic HCs with two or more benzene rings joined in various forms that are more or less clustered. These require special attention because of their mutagenic and, in some cases, carcinogenic character. The water, unburned HC, carbon and ash regions are verified for oxidation reaction by Thermogravimatric Analysis (TGA) and Temperature Program Oxidation (TPO) [12–17].

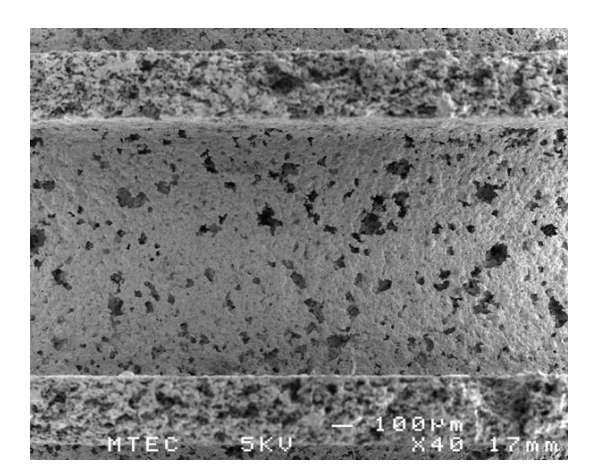
Applications of renewable oxygenated fuels is nowadays a widespread means to reduce amount and particle size of regulated pollutant emissions produced by internal combustion engines because oxygen atoms inside fuel molecules promote more completed combustion, as well as to reduce the green house gas resulting from carbon neutral. The combustion of bio-oxygenated fuel emits carbon dioxide (CO₂) to the atmosphere for the growth of plants, which are produced by biodiesel fuel and released out of the atmosphere as carbon by photosynthesis. More advantages of biodiesel over other fuels are that it contains much lower sulfur and aromatic HC content [18].

The objective of the present research is to study diesel and biodiesel PMs nanostructure by using TEM images. The report would be successfully described as the useful information of diesel and biodiesel PM nanostructures for better understanding and future design of DPF configuration for diesel and biodiesel blends engine application in Thailand and Asian countries.

2. Experimental Setup and Method

2.1. Fuels and PM generators

A conventional diesel fuel (B4-5) was used and compared with the results of biodiesel fuel derived from palm-olein (biodiesel (B100) fuel of TIS 2313-2549). Diesel and biodiesel PMs were emitted from diesel and biodiesel diffusion flame which were generated by lamp and small engine. The lamp energy consumption is 0.01 g/s. On the other hand, the small diesel engine has displacement of 638 cm³ and a rated output of 8.8 kW. The small diesel engine is a single cylinder, four strokes and direct injection. The fuel injection pressure was approximately 19.6 MPa. The engine was operated by constant speed of 2400 rpm on the Eddy current engine dynamometer (Tokyo plant ED-60-LC). The fuel consumption of each fuel was measured by weight loss respect to time for comparison in the view point of energy consumption. PMs were introduced into the micro pores of DPF samples, as shown in Fig.1. The pressure drop between inlet and outlet of the DPF sample were measured in each trapping time in real time by pressure sensor.



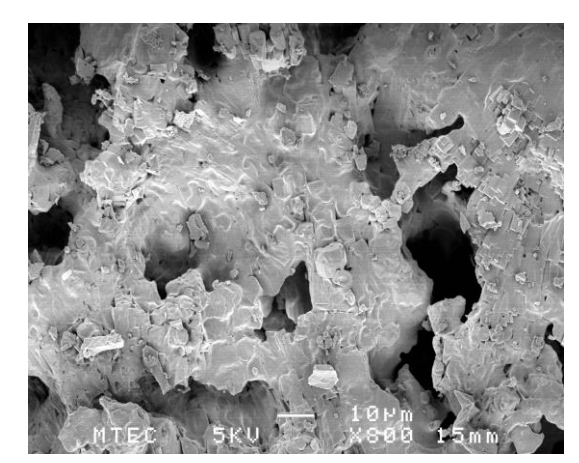


Fig.1. SEM images of cordierite DPF surface pores

2.2. SEM and TEM

The PM emitted from diffusion flame was collected by metal net in exhaust pipe and be removed to be a powder. The nanostructures of PMs and carbon platelet were investigated by using a scanning electron microscopy (FE-SEM: Hitachi S-4700, JEOL JSM-6301F) and a transmission electron microscopy (TEM: JEOL JEM-2010). In addition, carbon platelet length and atom density of PMs were estimated by TEM image using image processing.

3. Results and Discussions

3.1. PMs quantity

Figure 2 (a) and 2 (b) show the results of lamp and engine PMs trapping behaviours. Pressure drop between the inlet and outlet of the filter wall during diesel PM trapping was approximately 2 times higher than that of biodiesel PM. Hence, diesel soot formation was higher than biodiesel. This could be explained that more soot particle was remained in diesel combustion than those of biodiesel. Because it contains oxygen molecule, biodiesel is readily oxidized with available oxygen in the flame zone. Consequently, DPF trapping duration of biodiesel fuel has longer than that of diesel fuel because of PM concentration emitted from bio-oxygenated fuel combustion frame is lower than that of diesel combustion.

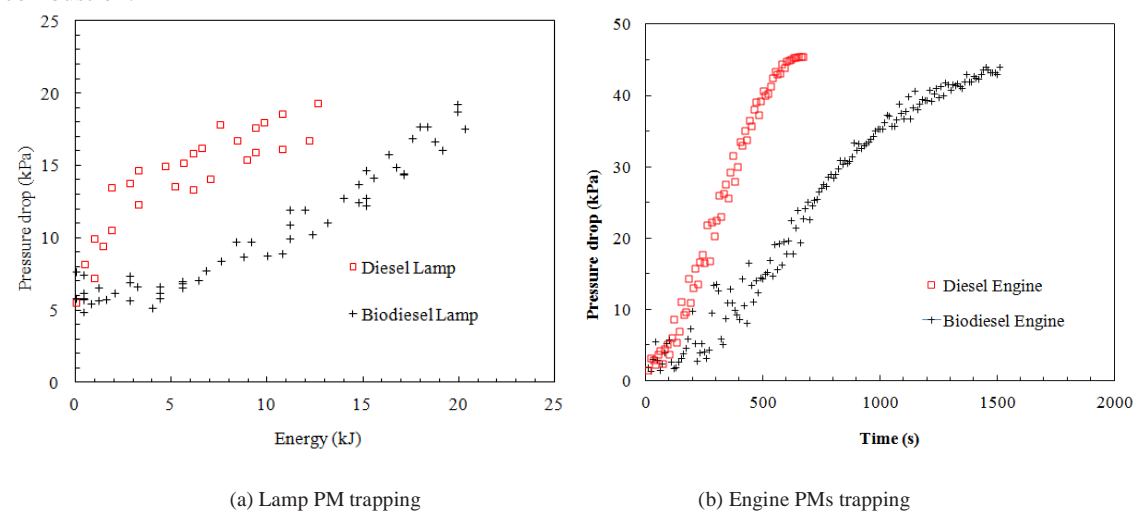


Fig.2. Pressure differential of diesel and biodiesel (a) lamp and (b) engine PMs trapping

3.2. PMs size distribution

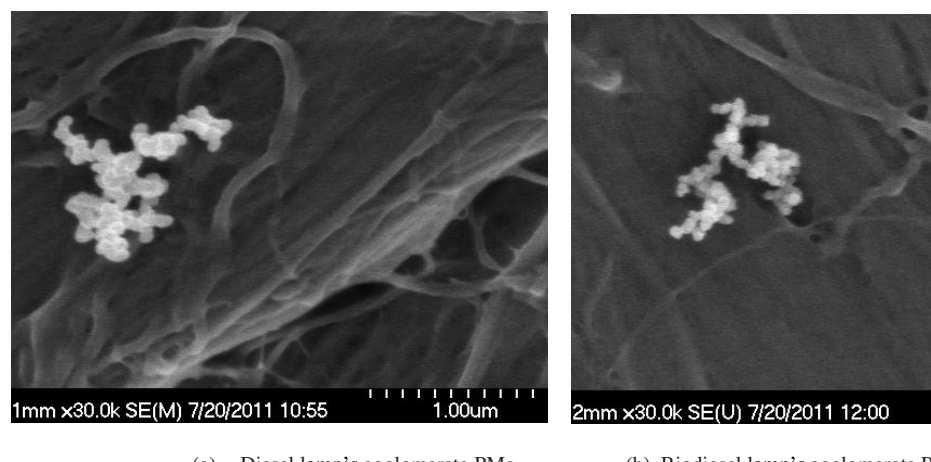
The soot particle is formed in the fuel spray cores, in which the rich fuel is contained, whereas the fuel vapor is heated by mixing with hot burned gases in the flame regions. Simultaneously, the surface of soot particle is also oxidized in the flame zone when it contacts with available oxygen. In this research, the PM image is taken to verify the diesel and biodiesel particle and carbon platelet sizes by micro- and nano-image.

Figure 3 show SEM images of (a) diesel, (b) biodiesel PMs emitted from the lamp and (c) diesel, (d) biodiesel PMs emitted from the engine. Uniform submicron scale agglomeration of PMs is clearly seen. The agglomerate size was about 100 to 600 nm. The normalized of PM size distribution of approximately 100 particles measured by SEM images were shown in Fig. 4 (a) based on particle number. Much amount number of 100 to 300 nm size was observed for both their particles emitted by the engine and lamp. The image showed that the biodiesel agglomerate particle size from both sources is slightly smaller than that of diesel particle.

Figure 4 show TEM images of (a) diesel, (b) biodiesel PMs emitted from the lamp and (c) diesel, (d) biodiesel PMs emitted from the engine. Uniform ultrafine single (primary) particle of soot is clearly seen. The primary size was about 20 to 80 nm. The normalized of PM size distribution of approximately 100 particles measured by TEM images were shown in Fig.4 (b). Much amount number of 30 to 50 nm size

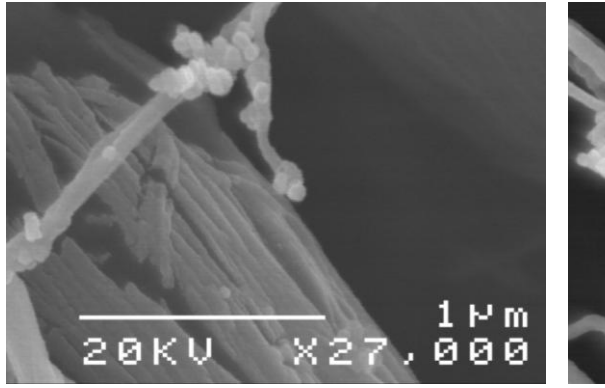
was observed for both their particles emitted by the engine and lamp. Single particle sizes of biodiesel PMs are smaller than that of diesel.

Absolutely, the oxygen content of bio-oxygenated fuel is strongly affected to the more complete combustion resulting in the smaller size of agglomerate and single particle of PMs. Moreover, the remaining oxygen atoms of bio-oxygenated fuel may be also strongly affected to the oxidation of PM surface. Consequently, the different size of a single particle might be depends on not only the accumulation of carbon atom but also the combustion of PM's surface. Therefore, high temperature and high oxygen concentration conditions, such as PM's surface oxidation can be assisted by oxygenated fuel combustion.

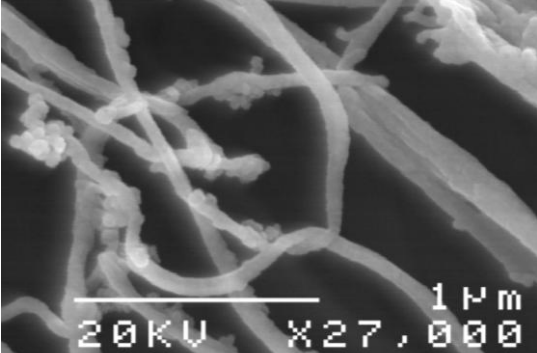


(a) Diesel lamp's agglomerate PMs

(b) Biodiesel lamp's agglomerate PMs

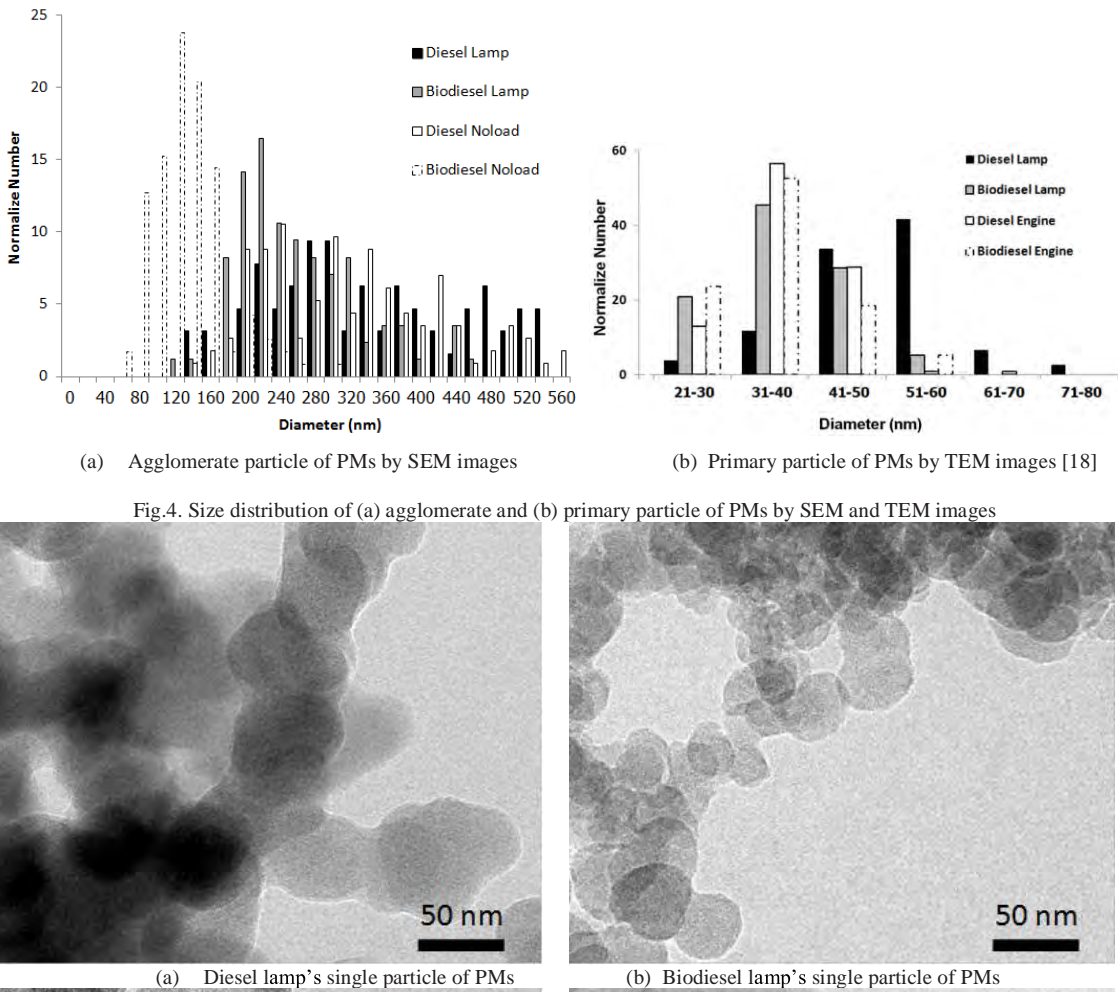


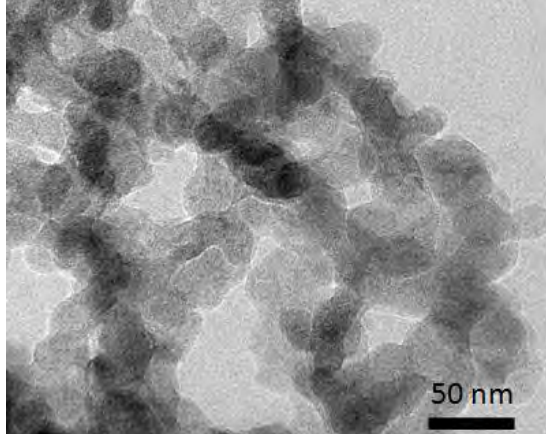
(c) Diesel engine's agglomerate PMs



(d) Biodiesel engine's agglomerate PMs

Fig.3. SEM images of (a) diesel lamp, (b) biodiesel lamp, (c) diesel engine and (d) biodiesel engine PMs





Diesel engine's single particle of PMs

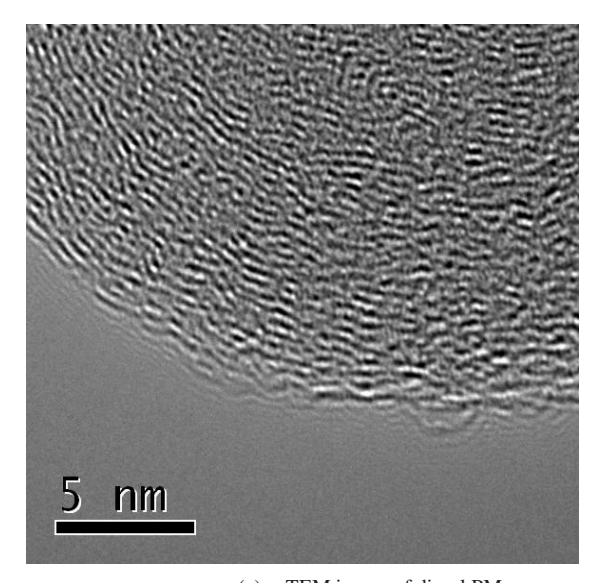
(d) Biodiesel engine's single particle of PMs

50 nm

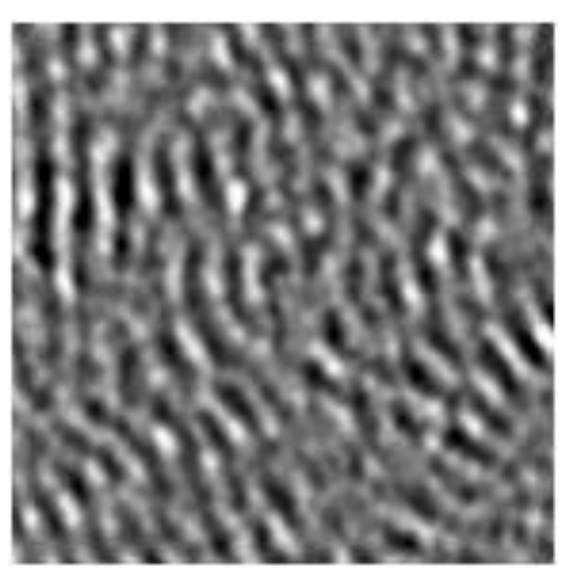
Fig.5. TEM images of (a) diesel lamp, (b) biodiesel lamp, (c) diesel engine and (d) biodiesel engine PMs

3.3. Carbon platelet size distribution

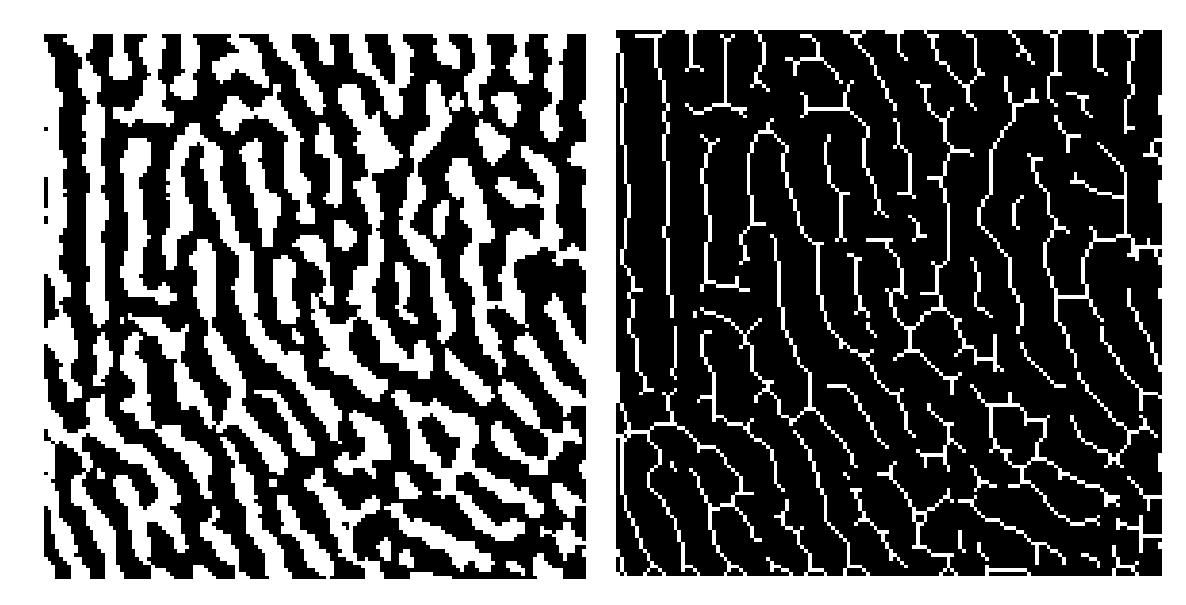
The nanostructures of primary diesel soot particles have been characterized using a TEM to understand them in detail. Figure 6 (a) shows the nanostructure of diesel PM which is emitted from diffusion flame combustion inside a conventional small diesel engine. PM is investigated for number of carbon atom include in the particle. TEM image is used for numerate platelet number that aggregate layered in the particle. Each of platelet is consisted properly by carbon atom from incomplete combustion product. Figures 6 (b), (c), and (d) are the images of focused area before, after post processing of two colors and after post processing of carbon platelet length estimation, respectively. The estimated of platelet sizes are shown in Fig.7. The average of diesel carbon platelets is in the range of 0.1-7.0 nm. Another result of carbon atom number per volume is also estimated. The concept of estimation is "the molecule of carbon-6 (C6) is the possible smallest size". Such molecules are agglomerated to be the large ring of carbon then becomes a platelet. The PM from diesel engine contains approximately 829 atoms per nm³, 9.37 million atoms per a 30 nm diameter of single particle and 2776.46 million atoms per a 200 nm diameter of agglomerate particle, as shown in Table 1. As a result, the estimated of a 30 nm and 200 nm diameter of single and agglomerate particles mass are approximately 0.002 and 0.553 pico-grams, respectively. The atom density and mass of particle emissions is one of useful information for development of automobile after-treatment technology to improve the reduction of particle emission during trapping and oxidation process of the particulate filters.







(b) Focused TEM image of diesel PM



(c) Black and white distribution of carbon platelets

(d) Estimated length of carbon platelets

Fig.6. (a) Original PM's TEM image, (b) focused area and after image processing of (b) two colors and (c) platelet length images

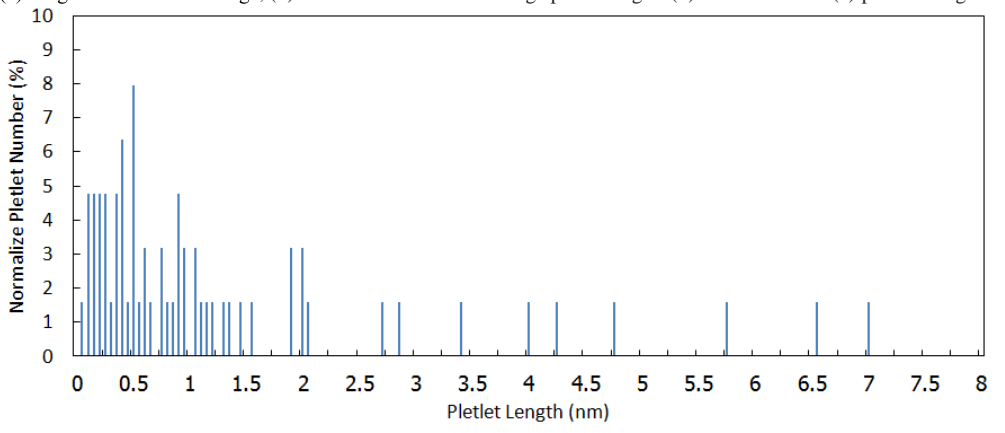


Fig.7. Estimated carbon platelet length of PM by image processing method

Table 1. An example of a table

Carbon inside PM	Atom density	Mass
	(atoms)	(pg)
A cubic nanometer	829	1.65 E-8
Single particle (30 nm diameter)	9.37 E6	0.002
Agglomerate particle (200 nm diameter)	2776.46 E6	0.553

4. Conclusions

Biodiesel combustion produces PM about two times lower than that of diesel combustion. Therefore, the conventional DPF also can be used for about two times of trapping duration. This means the energy consumption of engine for both the effect of pressure drop while driving and DPF regeneration process can be reduced approximately two times.

The single (primary) and agglomerate size of diesel particles is larger than that of biodiesel. This is due to the lower concentration of biodiesel carbon particles, which is readily oxidized with more available oxygen, in combustion flame due to oxygenated biodiesel fuel. Moreover, PM's surface oxidation can be assisted by oxygenated fuel combustion. On the other hand, the primary particle size from diesel engine is smaller than that of diesel lamp particle due to homogeneous air/fuel mixture effect to complete combustion.

The carbon atom density and mass of PM could be estimated by using TEM image processing method. The length and density of carbon platelet might be strongly depended on the fuel properties and soot generation method. The bio-oxygenated fuel plays an important role for agglomerate particle and single particle size due to oxygen atom inside fuel molecule. Moreover, the impact of oxygenated fuel in the length of platelet also needed to investigate for better understanding. This is an interesting result of bio-oxygenated fuel combustion behavior and particles emission nanostructure which should be researched in more details to discover the useful information for better understanding and future designs of modern ICE and DPF configurations.

Acknowledgements

The authors gratefully acknowledge the financial support from Thailand Research Fund (TRF), Ministry of Science and Technology, Thailand.

References

- [1] Konstandopoulos GA, Kostoglou M, Vlachos N, Kladopoulos E. Progress in diesel particulate filter simulation. SAE Technical paper; 2005;01:0946.
- [2] Konstandopoulos AG, Zarvalis D, Kladopoulou E, Dolios L. A multi-reactor assembly for screening of diesel particulate filters. SAE Technical paper; 2006;01:0874.
- [3] Tushima S, Nakamura I, Sakashita S, Hirai S, Kitayama D. Lattice boltzmann simulation on particle transport and captured behaviours in a 3d-reconstructed micro porous DPF. SAE Technical paper; 2010;01:0534.
- [4] Heywood BJ. Internal Combustion Engine Fundamental. McGraw-Hill series in mechanical engineering: Singapore, 1998.
- [5] Smith IO. Fundamentals of soot formation in flames with application to diesel engine particulate emissions. *Progress in Energy and Combustion Science*; 7:275–291.
- [6] Maricq MM. Review chemical characterization of particulate emissions from diesel engine: A review. *Journal of Aerosol Science*; 38:1079–1118.
- [7] Kittelson BD. Engines and nanoparticles: A review. Journal of Aerosol Science; 29:575-588.
- [8] Majewski AW, Khair KM. Diesel emissions and their control. SAE Order No.R-303 SAE International: Warrendale USA.
- [9] Ishiguro T, Takatori T, Akihama K. Microstructure of diesel soot particles probed by electron microscopy: first observation of inner core and outer shell. Combustion and Flame; 108:231–234.
- [10] Vander Wal AR, Yezerets A, Currier WN, Kim HD, Wang HC. HRTEM Study of diesel soot collected from diesel particulate filters. Carbon; 45:70-77.
- [11] Fernundez-Alos V, Watson KJ, Vander Wal AR. Mathew PJ. Soot and char molecular representations generated directly from HRTEM lattice fringe images using fringe3D. *Combustion and Flame*; **158**:1807–1813.
- [12] Neeft PAJ, Nijhuis XT, Smakman E, Makkee M, Moulijn AJ. Kinetics of the oxidation of diesel soot. Fuel; 76-12:1129–1136.

- [13] Darcy P, Costa DP, Mellottee H, Trichard MJ, Mariadassou DG. Kinetics of catalyzed and non-catalyzed oxidation of soot from a diesel engine. *Catalysis Today*; **119**:252–256.
- [14] Yezerets A, Currier WN, Eadler AH. Experimental determination of the kinetics of diesel soot oxidation by O₂ Modeling consequences. SAE Technical paper; 2003-01-0833.
- [15] Lorentzou S, Pagkoura C, Zygogianni A, Kastrinaki G, Konstandopoulos GA. Catalytic nano-structured materials for next generation diesel particulate filters. SAE Technical paper; 2008-01-0417.
- [16] Karin P, Hanamura K. Particulate matter trapping and oxidation on catalyst-membrane. SAE International Journal of Fuels and Lubricants; 3-1:368–379.
- [17] Oki H, Karin P, Hanamura K. Visualization of oxidation of soot nanoparticles trapped on a diesel particulate membrane filter. SAE International Journal of Engine; 2011-01-0602.
- [18] Karin P, Songsaengchan Y, Laosuwan S, Charoenphonphanich C, Chollacoop N, Hanamura K. Nanostructure of Renewable Oxygenated Fuels Particulate Matter. *ASEAN Engineering Journal*; Part A-3.

Physical Characterization of Biodiesel Particle Emission by Electron Microscopy

Preechar Karin, Yutthana Songsaengchan

International College, King Mongkut's Institute of Technology Ladkrabang

Songtam Laosuwan, Chinda Charoenphonphanich

Faculty of Engineering, King Mongkut's Institute of Technology Ladkrabang

Nuwong Chollacoop

National Metal and Materials Technology Center, National Science and Technology Development Agency

Katsunori Hanamura

Department of Mechanical Science and Engineering, Tokyo Institute of Technology

Copyright © 2013 SAE Japan and Copyright © 2013 SAE International

ABSTRACT

Nanostructures of diesel and biodiesel engine particulate matters (PMs) were investigated by using a Transmission Electron Microscopy (TEM). The average single particle sizes of biodiesel and diesel PMs are approximately 30-40 nm and 50-60 nm, respectively. Image processing process was used to estimate each carbon platelet length by using TEM image. The average carbon platelet length of biodiesel and diesel PMs are in the range of 0.1-7.0 nm. Moreover, carbon atoms per cubic volume of PMs are approximately 500-900. The result shows that engine load and fuel property are strongly impact on the size of single particle and carbon atom density of particle. This is one of interesting behaviors need to be investigated for better understanding. The results of this research would be used as basic information for design and develop removing process of PM emitted from engine combustion which using in diesel and biodiesel fuels.

INTRODUCTION

Among internal combustion engines (ICE), diesel engines have the highest thermal efficiency for a given output power. However, particulate matters (PMs) must be removed from the exhaust gas emitted from diesel engines to protect the environment and human health. Therefore, regulation of vehicle emissions has become increasingly strict. Diesel Particulate Filters (DPFs) play an important role in PM trapping and oxidation. A DPF is generally made of ceramic materials, such as cordierite or silicon carbide, consisting of many rectangular channels with alternate channels blocked using cement at each end. The exhaust gas is forced to flow through a channel wall having numerous micron-scale pores that trap the PM. Furthermore, the collected PM must be oxidized to regenerate the DPF and reduce the back pressure on the diesel engine [1-3].

The nanostructures of soot primary particles have been characterized using scanning electron microscope (SEM) and transmission electron microscopy (TEM) to understand them in detail. The mean diameter of the single primary and agglomerated particles is usually in the range of ultrafine particle and fine particle, respectively [4–11].

The composition of PMs from a diesel engine may vary widely depending on the operating conditions and fuel composition. PM is traditionally divided into three main fractions: solid fraction (SOL), soluble organic fraction (SOF), and sulfate particulates (SO4) that consist of sulfuric acid and water. The SOL of diesel PMs is composed primarily of elemental carbon, sometimes referred to as inorganic carbon. This carbon, not chemically bound with other elements, is the finely dispersed carbon black or soot substance responsible for black smoke emission. Hydrocarbons (HCs) adsorbed on the surface of the carbon particles are present in the form of fine droplets from the SOF of diesel particulates. At times, this fraction is also referred to as the volatile organic fraction (VOF). The SOF fraction contains most of the polycyclic aromatic HCs (PAHs) and nitro-PAHs emitted with diesel exhaust gases. PAHs are aromatic HCs with two or more benzene rings joined in various forms that are more or less clustered. These require special attention because of their mutagenic and, in some cases, carcinogenic character. The water, unburned HC, carbon and ash regions are verified for oxidation reaction by Thermogravimatric Analysis (TGA) and Temperature Program Oxidation (TPO) [12–17].

Applications of renewable oxygenated fuels is nowadays a widespread means to reduce amount and particle size of regulated pollutant emissions produced by internal combustion engines because oxygen atoms inside fuel molecules promote more completed combustion, as well as to reduce the greenhouse gas resulting from carbon neutral.

The combustion of bio-oxygenated fuel emits carbon dioxide (CO₂) to the atmosphere for the growth of plants, which are produced by biodiesel fuel and released out of the atmosphere as carbon by photosynthesis. More advantages of biodiesel over other fuels are that it contains much lower sulfur and aromatic HC content [18, 19]. Therefore, the objective of the present research is to study nanostructure of biodiesel PMs by using TEM images and image processing process. The report would be successfully described as the useful information of biodiesel PM nanostructures for better understanding and future design of DPF configuration for diesel and biodiesel blends engine application in Thailand and Asian countries.

METHODOLOGY

A conventional diesel fuel (B4-5) was used and compared with the results of biodiesel fuel derived from palm-olein (biodiesel (B100) fuel of TIS 2313-2549). Diesel and biodiesel PMs were emitted from small engine. The engine has displacement of 638 cm³ and a rated output of 8.8 kW. It is a single cylinder, four strokes and direct injection. The fuel injection pressure was approximately 19.6 MPa. The engine was operated by constant speed of 2400 rpm on the Eddy current engine dynamometer (Tokyo plant ED-60-LC). The PM emitted from engine which fuelled by conventional diesel and palm-olein biodiesel were collected to be a test sample. The metal net was installed at the end of original exhaust pipe, 30 cm after the exhaust valve, of the engine to collect the PM sample in exhaust pipe. The nanostructures of PMs and carbon platelets were investigated by using a transmission electron microscopy (TEM: JEOL JEM-2010).

In addition, carbon platelet length and atom density of PMs were estimated by TEM image using image processing. A high magnification particulate matter image from TEM was investigated in nanostructure by matlab image processing. The 10 nm x 10 nm image was cropped from the TEM image of the particulate matter from each fuel and each load condition as shown. These images were removed a noise and converted to be a black white image. After that, they were changed to be a skeleton to measure the carbon crystallites length which arranged as a layer in a spherical particle. Then, the crystallite lengths were calculated to carbon atom density. For the concept of estimation, the molecule of carbon-6 (C-6) is the possible smallest size. Such molecules are agglomerated to be the large ring of carbon then becomes a platelet. A crystallite length from black white image was valuated a carbon atom by assumed that the crystallite is consisted by 3 layers of platelet.

RESULTS

The nanostructures of primary diesel soot particles have been characterized using a TEM to understand them in detail. Figure 1 shows SEM image of diesel agglomerated PMs. Uniform fine agglomerate particle is clearly seen. The agglomerate size is about 100 to 600 nm and much amount number of 100 to 300 nm diameter was observed for both their particles emitted by the diesel and biodiesel engine. The result showed that the biodiesel agglomerate particle size from both sources is slightly smaller than that of diesel

particle. Figure 2 shows TEM image of diesel PMs emitted from a small diesel engine of the present research. Uniform ultrafine single particle of PM is clearly observed. The PM single particle size was about 20 to 80 nm. The different size of a single particle might be depends on not only amount of carbon atoms accumulation but also the oxidation of PM's surface during fuel combustion process. High temperature and high oxygen concentration conditions would be one of important oxygenated fuel advantage point on PM's surface oxidation.

Figure 3 shows TEM images of engine 50% load (a) diesel and (b) biodiesel, and 80% load (c) diesel and (d) biodiesel single PMs. Single particles are nearly sphere shape even though surface are not so smooth. Carbon platelets in the surface of particle are not so close distance and look like not so strong contact with other platelets. TEM image shows the different structure of inner core zone and outer shell zone of PMs. The inner core diameters are approximately 5 to 10 nm.

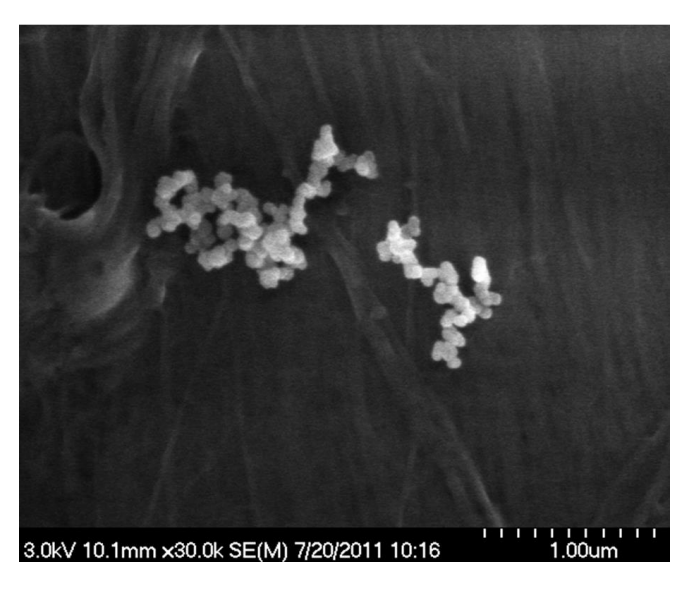


Figure 1. SEM image of fine agglomerated PM emitted from a small diesel engine.

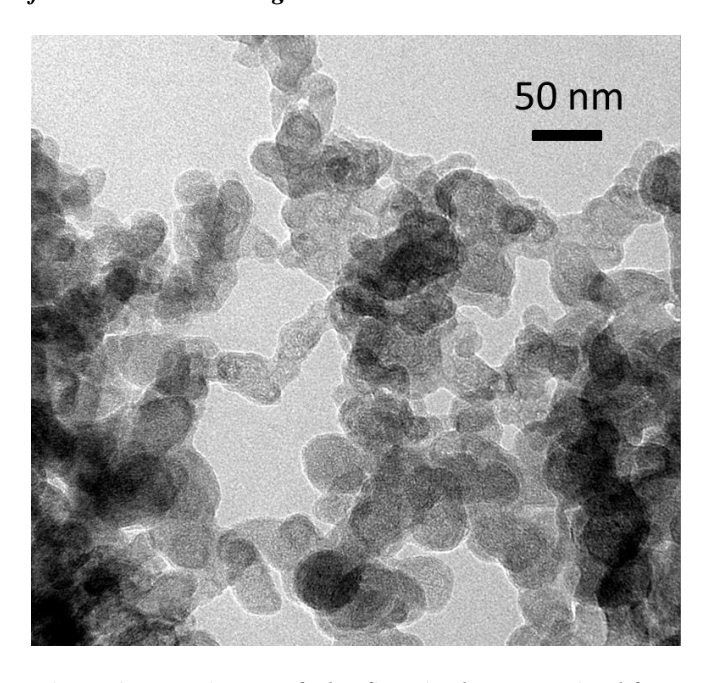


Figure 2. TEM image of ultrafine single PMs emitted from a small diesel engine.

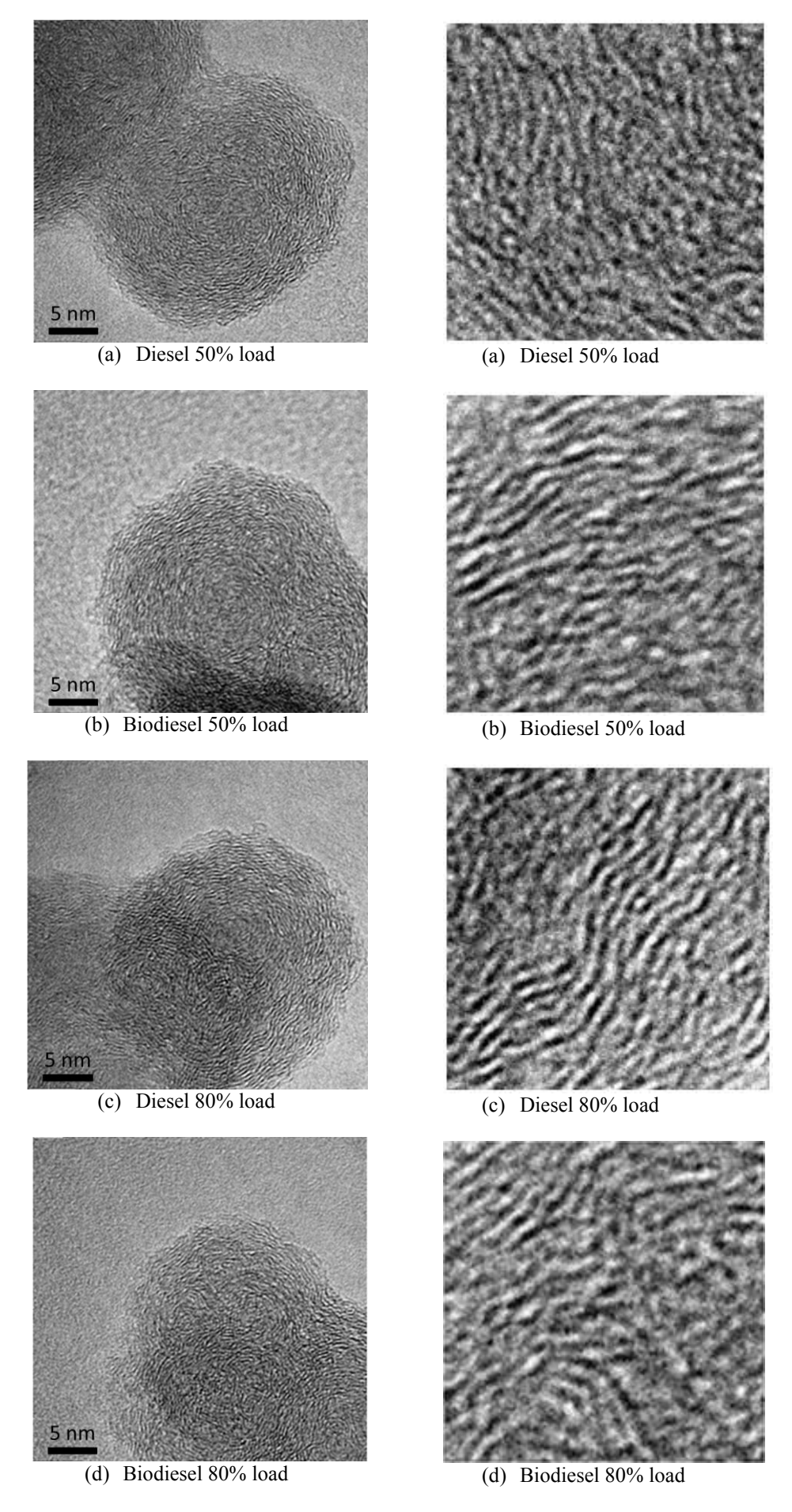


Figure 3. TEM images of engine 50% load (a) diesel and (b) biodiesel, and 80% load (c) diesel and (d) biodiesel single PMs.

Figure 4. TEM images of engine 50% load (a) diesel and (b) biodiesel, and 80% load (c) diesel and (d) biodiesel single PMs 10nm² focused area.

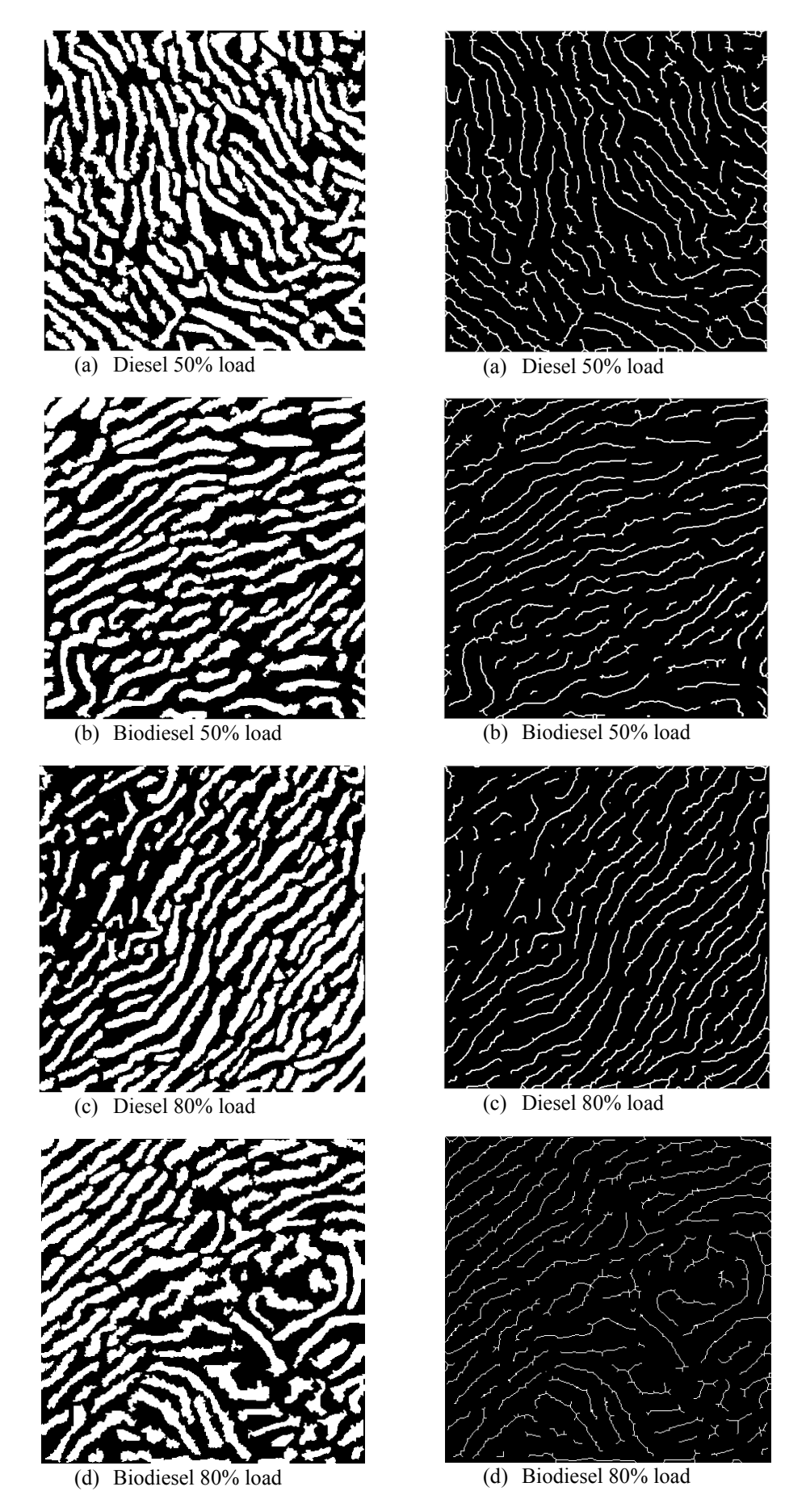


Figure 5. Two colors TEM images post process of engine 50% load (a) diesel and (b) biodiesel, and 80% load (c) diesel and (d) biodiesel single PMs $10nm^2$ focused area.

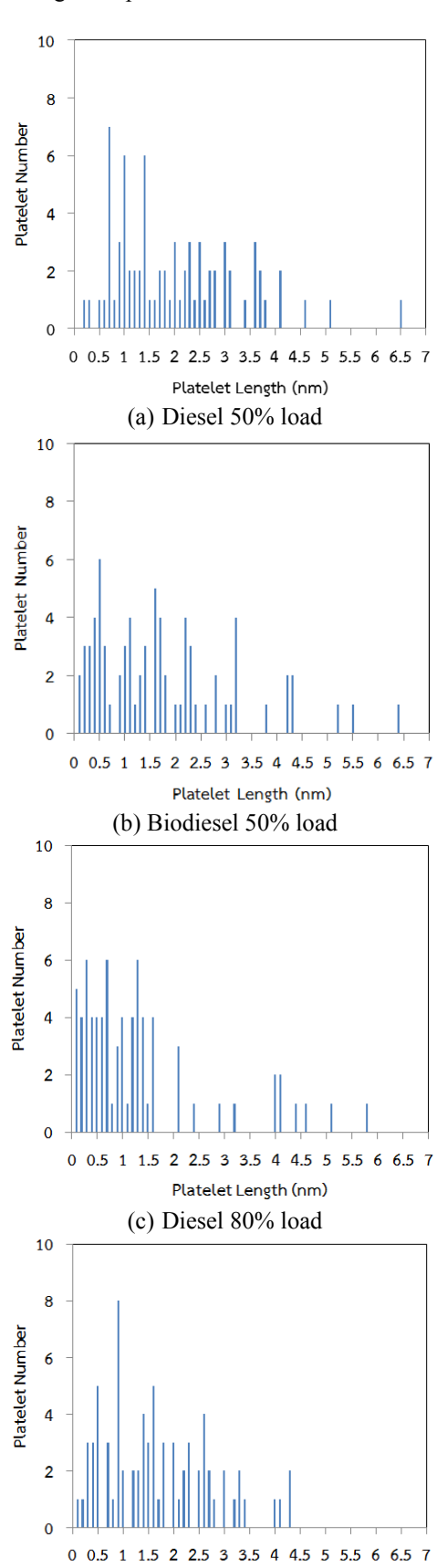
Figure 6. Skeleton TEM images post process of engine 50% load (a) diesel and (b) biodiesel, and 80% load (c) diesel and (d) biodiesel single PMs 10nm² focused area.

Moreover, the structure of carbon platelet inside inner core zone shows short length and non-homogeneous platelets. whereas long length and homogeneous platelets could be clearly observed in outer shell zone. Single particle could be observed two to four inner core portions. In the first process of PM formation, agglomerated inner core portion might be accumulated to be a single primary particle. After that, surface of single primary particle growth up by carbon atom with time until approximately 100 nm of diameter depended on engine operation condition which might be strongly effect on density of carbon atom per volume. In the last process, surface of PM is oxidized by oxygen molecule during combustion process. In addition, images show carbon platelet structures of connection zone between two single primary particles are also quite homogeneous platelet density compare to the inner core zone.

PM is investigated for number of carbon atom include in the particle. TEM image is used for numerate platelet number that aggregate layered in the particle. Each of platelet is consisted properly by carbon atom from incomplete combustion product. Figures 4, 5 and 6 are the images of original 10 nm² focused area, after post processing of two colors and after post processing of skeleton carbon platelet length estimation, respectively. Condition of 50% load diesel, 50% load biodiesel, 80% load diesel and 80 load biodiesel engines are shown in (a), (b), (c), and (d) of each Fig. The focused areas of all images are homogeneous platelet area in each outer shell zone. Original gray color could be successfully changed to two colors images in the first step. The lengths of each platelet in each sample are quite different, whereas the distances of each platelet are also not too different. From the skeleton images, the carbon platelets inside the PM were measured by image processing program. The skeleton carbon platelets, which have 1 unit pixel width for each platelet, were measured for the white area in the image to be a carbon platelet length. The estimated of platelet sizes distribution in each condition are shown in Fig.7. The average of diesel and biodiesel PM carbon platelets is in the range of 0.1-7.0 nm. Another result of carbon atom number per volume is also estimated. Much amount of about 1 nm carbon platelet length is clearly observed in this research.

The concepts of estimation are "the molecule of carbon-6 (C6) is the possible smallest size" and "there are 3 layers arranged to be a platelet". Such molecules are agglomerated to be the large ring of carbon then becomes a platelet. The PM are contains approximately 600 to 900 atoms and 1.1E-8 to 1.7E-8 pico-grams per a cubic nanometer, as shown in Table 1. The particle mass and carbon atom number inside single particle was estimated by base on atom density and average primary size of each condition particle. The million atom number and mass of each particle size and engine operation condition could be successfully calculated and summarized in Fig. 8 (a) and 8 (b), respectively. Atom density and mass per volume of biodiesel is a little bit lower than those of diesel PMs. Moreover, the different result of different load condition was also clearly observed in the present research. The carbon atom density and mass of particle emissions is one of very useful information for development of advanced engine after-treatment technology to improve the reduction of particle emission during trapping and oxidation process of the particulate filters.

Therefore, the different of carbon density inside diesel and biodiesel particle emission would be investigated for better understanding and optimization of after-treatment devices.

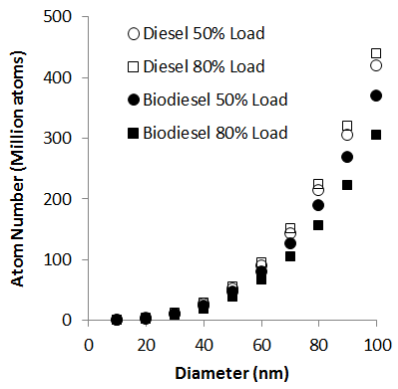


(d) Biodiesel 80% load Figure 7. Platelet length distribution of 50% load (a) diesel and (b) biodiesel, and 80% load (c) diesel and (d) biodiesel single PMs 10nm² focused area.

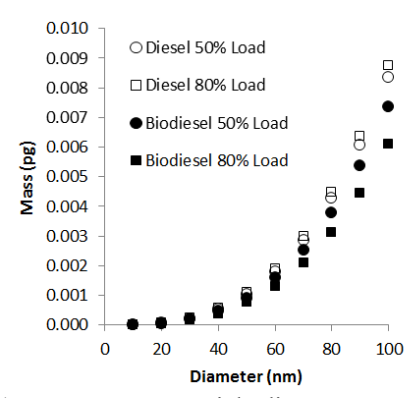
Platelet Length (nm)

Table 1. Result of estimated atom density, mass per volume and atom number of PMs.

	PMs			
	Diesel		Biodiesel	
	50%	80%	50%	80%
	load	load	load	load
Atom Density (atoms/nm3)	800	838	706	584
Mass per Volume	1.594	1.670	1.407	1.164
(pg/nm3)	E-8	E-8	E-8	E-8
Average Single Diameter (nm)	32.13	30.90	31.59	30.31
Average Single Particle	2.767	2.578	2.321	1.696
Mass (pg)	E-4	E-4	E-4	E-4
Average Single Particle Atom (Million atoms)	13.887	12.939	11.647	8.510



(a) Atom number versus particle diameter



(b) Mass versus particle diameter

Figure 8. Calculated total (a) carbon atom number and (b) carbon mass versus diameter of each engine load and fuel PMs.

CONCLUSION

Nanostructure of particulate matters (PMs) emitted from diesel and biodiesel are clearly discussed in the present report. The carbon atom density and mass of PM could be successfully estimated by using TEM image processing method. The length and density of carbon platelet strongly depended on fuel properties and engine operation condition. Estimated atom density and mass per volume of PM are in the range of 600 to 900 atoms and 1.1E-8 to 1.7E-8 picograms per a cubic nanometer. The impact of oxygenated fuel and combustion temperature on the length and distance of platelet needed to investigate for better understanding. This is an interesting result of bio-oxygenated fuel combustion behavior and particles emission nanostructure which should

be researched in more details to discover the useful information for better understanding and future designs of modern Internal Combustion Engines and Diesel Particulate Filter (DPF) configurations.

REFERENCES

- Konstandopoulos GA, Kostoglou M, Vlachos N, Kladopoulos E. Progress in diesel particulate filter simulation. SAE Technical paper; 2005-01-0946.
- [2] Konstandopoulos AG, Zarvalis D, Kladopoulou E, Dolios L. A multi-reactor assembly for screening of diesel particulate filters. SAE Technical paper; 2006-01-0874.
- [3] Tushima S, Nakamura I, Sakashita S, Hirai S, Kitayama D. Lattice boltzmann simulation on particle transport and captured behaviours in a 3d-reconstructed micro porous DPF. SAE Technical paper; 2010-01-0534.
- [4] Heywood BJ. Internal Combustion Engine Fundamental. McGraw-Hill series in mechanical engineering: Singapore, 1998.
- [5] Smith IO. Fundamentals of soot formation in flames with application to diesel engine particulate emissions. Progress in Energy and Combustion Science; 7:275–291.
- [6] Maricq MM. Review chemical characterization of particulate emissions from diesel engine: A review. Journal of Aerosol Science; 38:1079–1118.
- [7] Kittelson BD. Engines and nanoparticles: A review. Journal of Aerosol Science; 29:575–588.
- [8] Majewski AW, Khair KM. Diesel emissions and their control. SAE Order No.R-303 SAE International: Warrendale USA.
- [9] Ishiguro T, Takatori T, Akihama K. Microstructure of diesel soot particles probed by electron microscopy: first observation of inner core and outer shell. Combustion and Flame; 108:231–234.
- [10] Vander Wal AR, Yezerets A, Currier WN, Kim HD, Wang HC. HRTEM Study of diesel soot collected from diesel particulate filters. Carbon; 45:70-77.
- [11] Fernundez-Alos V, Watson KJ, Vander Wal AR. Mathew PJ. Soot and char molecular representations generated directly from HRTEM lattice fringe images using fringe3D. Combustion and Flame; 158:1807–1813.
- [12] Neeft PAJ, Nijhuis XT, Smakman E, Makkee M, Moulijn AJ. Kinetics of the oxidation of diesel soot. Fuel; 76-12:1129–1136.
- [13] Darcy P, Costa DP, Mellottee H, Trichard MJ, Mariadassou DG. Kinetics of catalyzed and non-catalyzed oxidation of soot from a diesel engine. Catalysis Today; 119:252–256.
- [14] Yezerets A, Currier WN, Eadler AH. Experimental determination of the kinetics of diesel soot oxidation by O2 – Modeling consequences. SAE Technical paper; 2003-01-0833.
- [15] Lorentzou S, Pagkoura C, Zygogianni A, Kastrinaki G, Konstandopoulos GA. Catalytic nano-structured materials for next generation diesel particulate filters. SAE Technical paper; 2008-01-0417.
- [16] Karin P, Hanamura K. Particulate matter trapping and oxidation on catalyst-membrane. SAE International Journal of Fuels and Lubricants; 3-1:368-379.
- [17] Oki H, Karin P, Hanamura K. Visualization of oxidation of soot nanoparticles trapped on a diesel particulate membrane filter. SAE International Journal of Engine; 2011-01-0602.
- [18] Karin P, Songsaengchan Y, Laosuwan S, Charoenphonphanich C, Chollacoop N, Hanamura K. Nanostructure of Renewable Oxygenated Fuels Particulate Matter. ASEAN Engineering Journal; 3-1:72-83.
- [19] Karin P, Songsaengchan Y, Laosuwan S, Charoenphonphanich C, Chollacoop N, Hanamura K. Nanostructure Investigation of Particle Emission by Using TEM Image Processing Method. Energy Procedia, Elsevier; 2013 (In Press).

CONTACT INFORMATION

Preechar KARIN (D.Eng. Mechanical Eng.), International College, King Mongkut's Institute of Technology Ladkrabang, Chalongkrung Road, Ladkrabang, Bangkok, Thailand 10520, Tel.: +66-2-329-8261; Fax: +66-2-329-8262, E-mail address: kkpreech@kmitl.ac.th.

ACKNOWLEDGEMENTS

The authors gratefully acknowledge the financial support from Thailand Research Fund (TRF), Ministry of Science and Technology, Thailand.

AEC-1025



Characterization of Engine Particle Emission Size Distribution by SMPS

Preechar Karin 1,* Chinda Charoenphonphanich Katsunori Hanamura and Thomas Vuckovic

International College, ² Faculty of Engineering, King Mongkut's Institute of Technology Ladkrabang, Bangkok, 10520 Thailand
 Department of Mechanical Sciences and Engineering, Tokyo Institute of Technology, Tokyo, 152-8550 Japan
 Institute for Internal Combustion Engines and Thermodynamics, Graz University of Technology, Graz, 8010 Austria
 *Corresponding Author: kkpreech@kmitl.ac.th, Telephone +66-2-329-8261, Fax. +66-2-329-8262

Abstract

Size distribution of particulate matters (PMs) emitted from a diesel vehicle were investigated by using a Scanning Mobility Particle Sizer (SMPS). The single and agglomerated particle sizes of PMs are in the range of 10-60 nm and 60-130 nm, respectively. The maximum single and agglomerated particle numbers are approximately 20-40 nm and 90-110 nm. At the engine warm-up idle condition, the number of single particle is quite high and then gradually decreased with time. Finally, the single particle number is nearly constant after an hour of the engine operates in idle condition. This is an interesting result of particles emission which should be researched in more details to discover the useful information for better understanding and future designs of modern Internal Combustion Engines and Diesel Particulate Filter configurations.

Keywords: Diesel Engine, Particulate Matter, SMPS, Electrostatic Classifier

1. Introduction

Among internal combustion engines (ICE), diesel engines have the highest thermal efficiency for a given output power. However, particulate matters (PMs) must be removed from the exhaust gas emitted from diesel engines to protect the environment and human health. Therefore, regulation of vehicle emissions has become increasingly strict.

The composition of PMs from a diesel engine may vary widely depending on the operating conditions and fuel composition. PM is traditionally divided into three main fractions: solid fraction (SOL) and soluble organic fraction (SOF). The SOL of diesel PMs is composed primarily of

elemental carbon, sometimes referred to as inorganic carbon. This carbon, not chemically bound with other elements, is the finely dispersed carbon black or soot substance responsible for black smoke emission. Hydrocarbons (HCs) adsorbed on the surface of the carbon particles are present in the form of fine droplets from the SOF of diesel particulates. At times, this fraction is also referred to as the volatile organic fraction (VOF). The SOF fraction contains most of the polycyclic aromatic HCs (PAHs). PAHs are aromatic HCs with two or more benzene rings joined in various forms that are more or less clustered. The water, unburned HC, carbon and

AEC-1025

TSME-ICOME 2013

ash regions are verified for oxidation reaction by Thermogravimatric Analysis (TGA) [1–11].

Particle emissions size and structure is very complicate and difficult to measure the exact value because of very small size. Size distribution and nanostructures of soot primary particles have been characterized using scanning electron microscope (SEM) and transmission electron microscopy (TEM) to understand them in detail. The mean diameter of the single primary and agglomerated particles is usually in the range of ultrafine particle (30-60 nm) and fine particle (100-300 nm), respectively [12-16].

The present research objective is to characterize diesel vehicle PM size distribution by using a Scanning Mobility Particle Sizer (SMPS). The results could be compared to the previous research which successfully report PM size distribution by using SEM and TEM images. The result would be successfully described as the useful information of biodiesel PM nanostructures for better understanding and future design of DPF configuration for diesel engines.

2. Methodology

A conventional diesel fuel in Graz, Austria as shown in Table 1 was used in the present research. The lower heating value (LHV) of diesel fuel is 42,482 J/g. Carbon, hydrogen and oxygen contents are 85.6, 13.4 and 0.5 percent, respectively. Diesel PM was emitted from a diesel van as shown in Table 2. The vehicle engine has displacement of 2,461 cm³ and a rated output of 75 kW. It is a four cylinders, four strokes and direct injection. The engine was operated by idle condition at neutral position. The PM emitted from engine was characterized by "Particle Emission"

Test Laboratory", Institute for Internal Combustion Engines and Thermodynamics, Graz University of Technology, Graz as shown in Fig. 1.

Table 1 Diesel Fuel Properties

	Method	Value	Unit
LHV	DIN 51 900-2 mod.	42,482	J/g
Carbon	DIN 51 732	85.6	% (m/m)
Hydrogen	DIN 51 732	13.4	% (m/m)
Oxygen	DIN 51 732 mod.	0.5	% (m/m)

Table 2 Vehicle and Engine Specification

	Method	Unit
Maker	VOLKSWAGEN	-
Trade Name	KASTENWAGEN TDI	-
Vehicle Type	70 T - KASTEN	-
Fuel	Diesel	-
Engine Displacement	2,461	СС
Rated Output	75	kW
After Treatment	Non-DPF	-



Fig. 1 A diesel van particle emissions test laboratory in "Institute for Internal Combustion Engines and Thermodynamics, Graz University of Technology.



Fig. 2 Particle size distribution measurement device "Series 3080 Electrostatic Classifiers (Courtesy of www.tsi.com)".



Fig. 3 A Scanning Mobility Particle Sizer (SMPS) for particle size distribution at "Institute for Internal Combustion Engines and Thermodynamics, Graz University of Technology.

Exhaust gas emitted from the exhaust pipe of vehicle was introduced into the dilution system and then gas sample was sucked from the dilution system to a Scanning Mobility Particle Sizer (SMPS) for size distribution characterization in the range of 10 nm to 400 nm diameter as shown in Fig.2 and Fig.3. Gas sample was characterized for both during engine warm-up approximately one hour and also after engine warm-up. The sample was characterized every 10 to 20 minutes.

3. Results and Discussion

Figure 4 shows the particle size distribution during engine warm-up condition. The first peak of particle size distribution is approximately 20 nm to 30 nm. This first region is the single particle of PMs. The second peak of particle size distribution is approximately 90 nm to 100 nm. This second region is the agglomerated particle of PMs. It was clearly observed that during engine warm-up, particle number decreased with time for both and agglomerated zones. It means combustion efficiency of the engine increased with the temperature of engine during warm-up condition. Moreover, much amount number of single particle could be observed at the beginning of warm-up condition and decreased with time. The number of single and agglomerated particle number are in the same range after 40 minutes engine warm-up in idle condition.

Figure 5 shows the particle size distribution during the second hour of testing. It was clearly seen that amount of single and agglomerated particles are nearly constant in 300 and 400 particles per cubic centimeter, respectively.

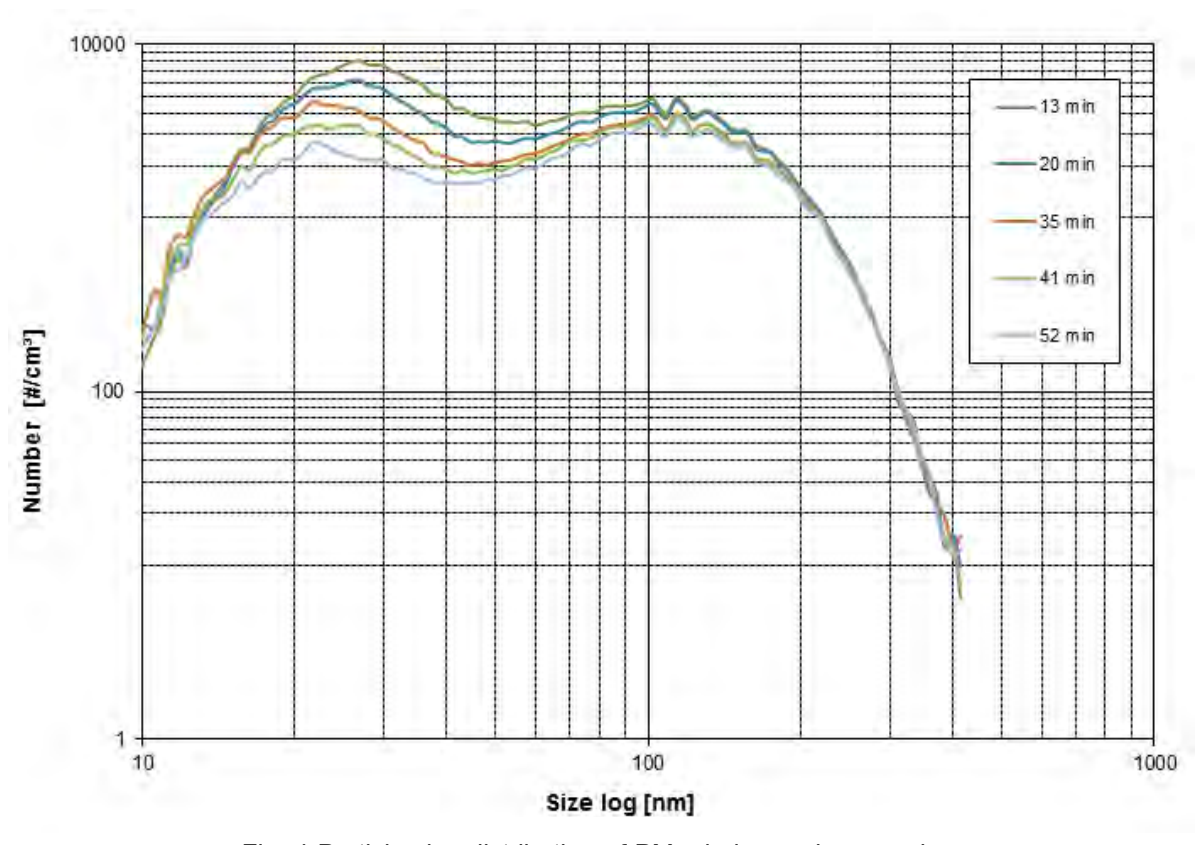


Fig. 4 Particle size distribution of PMs during an hour engine warm-up.

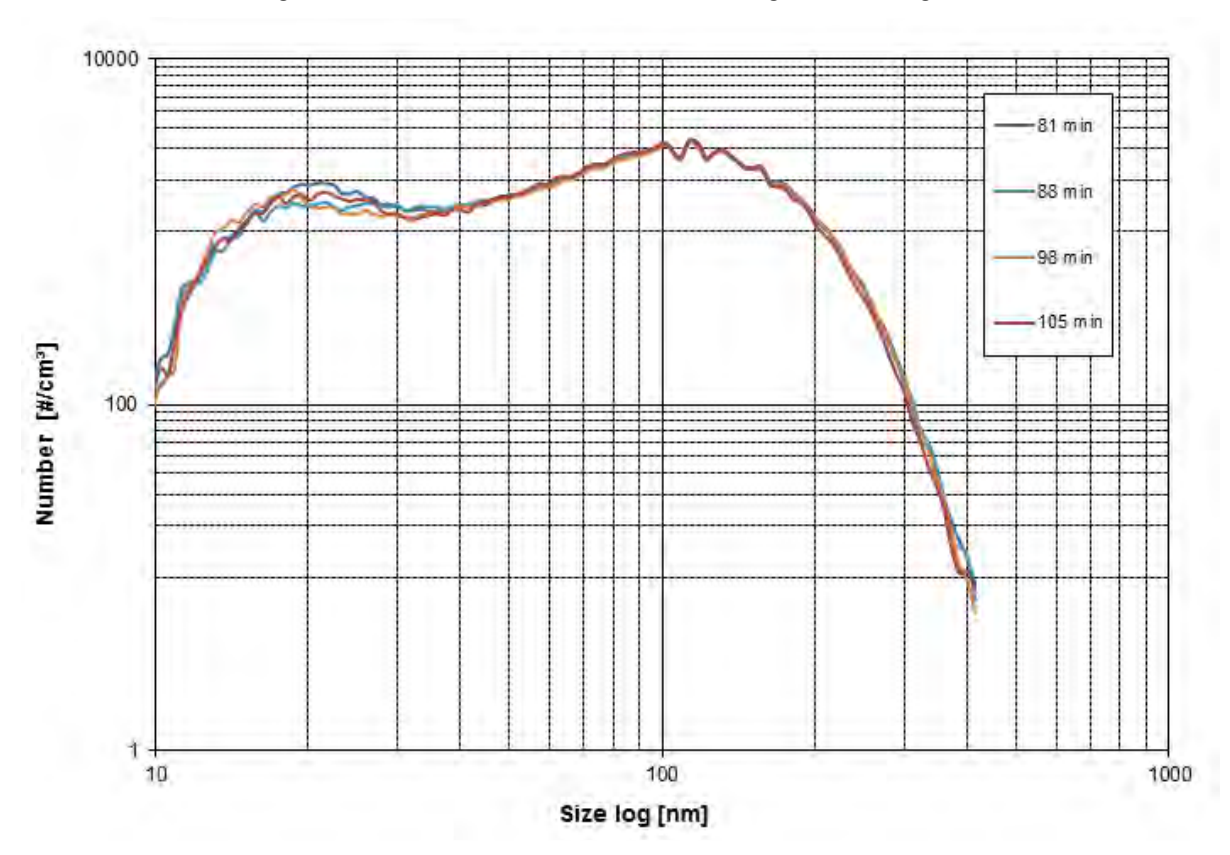


Fig. 5 Particle size distribution of PMs after an hour engine warm-up.

Figure 6 and 7 show Scanning Electron Microscope (SEM) and model images of PMs. Single and agglomerated particle model could be imaged based on the result of SEM images. The particle size range is also acceptable value when compare to the result from Scanning Mobility Particle Sizer (SMPS). However, the small different of size from both type of measurement is depend on the definition of each diameter which should be clearly clarify for high performance DPF design and development.

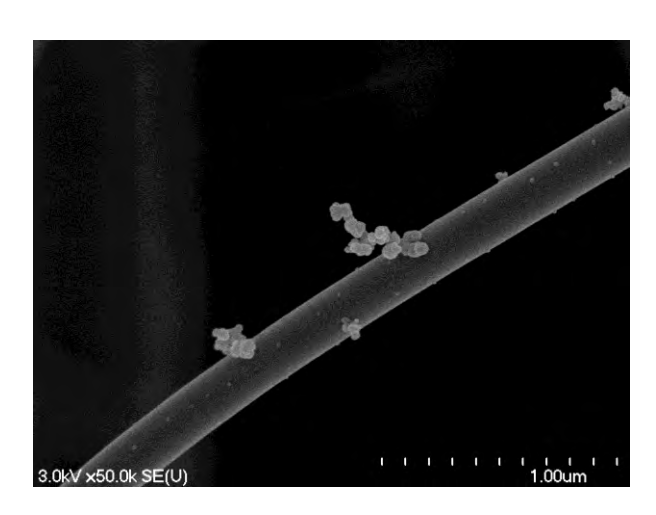


Fig. 6 Scanning Electron Microscope (SEM) images of PMs (Courtesy of Doctoral Thesis, P.Karin Tokyo Institute of Technology).

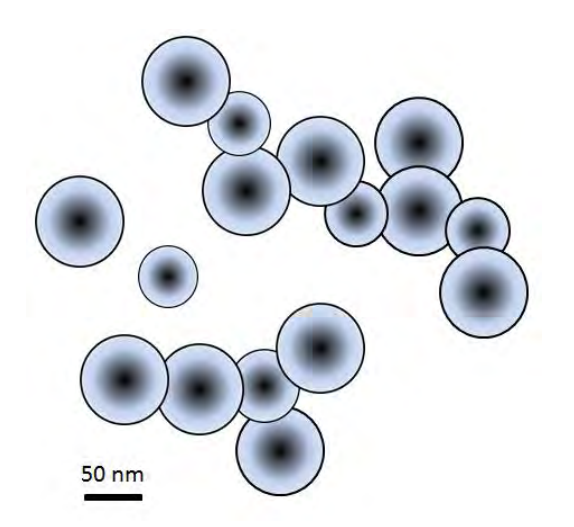


Fig. 7 Model of PMs which consisted of single and agglomerated size.

5. Conclusions

Size distribution of particulate matters (PMs) emitted from a diesel vehicle were successfully investigated by using a Scanning Mobility Particle Sizer (SMPS). The single and agglomerated particle sizes of PMs are in the range of 10-60 nm and 60-130 nm, respectively. Much amount of single and agglomerated particle diameter are in the range of approximately 20-40 nm and 90-110 nm. At the engine warm-up idle condition, the number of single particle is quite high and then gradually decreased with time.

Particle size and structure are agreed with SEM image result from previous research. This is an interesting result of particles emission which should be researched in more details to discover the useful information such as particle weight and charge for future designs of modern Internal Combustion Engines and Particulate Filter configurations.

6. Acknowledgement

The authors gratefully acknowledge the research financial support from "Thailand Research Fund (TRF)", Ministry of Science and Technology, Thailand. The authors are grateful to "ASEA-UNINET Staff Exchange Scholarship" from Thai-Austrian Governments for staffs exchange financial support.

7. References

- [1] Heywood BJ. Internal Combustion Engine Fundamental. McGraw-Hill series in mechanical engineering: Singapore, 1998.
- [2] Smith IO. Fundamentals of soot formation in flames with application to diesel engine

AEC-1025



particulate emissions. Progress in Energy and Combustion Science; 7:275–291.

- [3] Maricq MM. Review chemical characterization of particulate emissions from diesel engine: A review. Journal of Aerosol Science; 38:1079–1118.
- [4] Kittelson BD. Engines and nanoparticles: A review. Journal of Aerosol Science; 29:575–588.
- [5] Majewski AW, Khair KM. Diesel emissions and their control. SAE Order No.R-303 SAE International: Warrendale USA.
- [6] Fernundez-Alos V, Watson KJ, Vander Wal AR. Mathew PJ. Soot and char molecular representations generated directly from HRTEM lattice fringe images using fringe3D. Combustion and Flame; 158:1807–1813.
- [7] Neeft PAJ, Nijhuis XT, Smakman E, Makkee M, Moulijn AJ. Kinetics of the oxidation of diesel soot. Fuel; 76-12:1129–1136.
- [8] Darcy P, Costa DP, Mellottee H, Trichard MJ, Mariadassou DG. Kinetics of catalyzed and non-catalyzed oxidation of soot from a diesel engine. Catalysis Today; 119:252–256.
- [9] Yezerets A, Currier WN, Eadler AH. Experimental determination of the kinetics of diesel soot oxidation by O2 Modeling consequences. SAE Technical paper; 2003-01-0833.
- [10] Karin P, Hanamura K. Particulate matter trapping and oxidation on catalyst-membrane. SAE International Journal of Fuels and Lubricants; 3-1:368–379.
- [11] Oki H, Karin P, Hanamura K. Visualization of oxidation of soot nanoparticles trapped on a diesel particulate membrane filter.

SAE International Journal of Engine; 2011-01-0602.

- [12] Ishiguro T, Takatori T, Akihama K. Microstructure of diesel soot particles probed by electron microscopy: first observation of inner core and outer shell. Combustion and Flame; 108:231–234.
- [13] Vander Wal AR, Yezerets A, Currier WN, Kim HD, Wang HC. HRTEM Study of diesel soot collected from diesel particulate filters. Carbon; 45:70-77.
- [14] Karin P, Songsaengchan Y, Laosuwan S, Charoenphonphanich C, Chollacoop N, Hanamura K. Nanostructure of Renewable Oxygenated Fuels Particulate Matter. ASEAN Engineering Journal; 3-1:72-83.
- [15] Karin P, Songsaengchan Y, Laosuwan S, Charoenphonphanich C, Chollacoop N, Hanamura K. Nanostructure Investigation of Particle Emission by Using TEM Image Processing Method. Energy Procedia, Elsevier; 2013 (In Press).
- [16] Karin P, Songsaengchan Y, Laosuwan S, Charoenphonphanich C, Chollacoop N, Hanamura K. Physical Characterization of Biodiesel Particle Emission by Electron Microscopy. SETC2013, SAE International; 2013-32-9150 (In Press).





Jul. 20, 2014

[IJAT] Paper No. 220140181

■ Certificate of Acceptance ■

The Editorial Board of the IJAT hereby certifies that the following paper has been accepted for publication in the IJAT.

Paper No. 220140181

Paper Title OXIDATION KINETICS OF SMALL CI ENGINE'S BIODIESEL PARTICULATE MATTER

Category Engine, Emission Technology

Author(s) Dr. Preechar Karin (King Mongkut's Institute of Technology Ladkrabang)*

The Korean Society of Automotive Engineers

Editor-in-Chief

Int. J. Automotive Technology

- IJAT Web Site: http://www.ijat.net

13th Fl. Paradise Venture Tower, 21 52-gil Teheran-ro, Gangnam-gu, Seoul 135-919, Korea TEL +82-2-564-3971/2 FAX +82-2-564-3973 E-mail paper@ksae.org

Oxidation Kinetics of Small CI Engine's Biodiesel Particulate Matter

P. KARIN $^{1)*}$, M. BORHANIPOUR 1 , Y. SONGSAENGCHAN 1 , S. LAOSUWAN 2 , C. CHAROENPHONPHANICH 2 , N. CHOLLACOOP 3 and K. HANAMURA 4

¹⁾ International College, ²⁾ Department of Engineering,
 King Mongkut's Institute of Technology Ladkrabang, Bangkok, 10520, Thailand
 ³⁾ National Science and Technology Development Agency, Pathumthani 12120, Thailand
 ⁴⁾ Tokyo Institute of Technology, Meguro-ku, Tokyo152-8552, Japan

(Received date ; Revised date ; Accepted date)* Please leave blank

ABSTRACT— Particulate matters (PMs) oxidation kinetics by Thermo-gravimetric analysis (TGA) was successfully studied. The chemical content percentage of PM can be divided by oxidation temperature zoning in three main regions which are moisture, unburned hydrocarbon (HC) and carbon. It is clearly observed that the amount of each region is strongly depending on engine operating condition, the amount of unburned HC in low load condition of the engine load are larger than that of high load condition. The calculated apparent activation energies of biodiesel PM oxidation are lower than that of diesel PM and carbon black because of unburned oxygenated molecule. The calculated apparent activation energy of biodiesel and diesel PMs oxidize with air is in the range of 147–157 kJ/mole and 153–165 kJ/mole, respectively. The results of this research would be used as basic information for design and develop removing process of particulate matter emitted from engine combustion which using in diesel and biodiesel fuels.

KEY WORDS: Diesel engine, Particulate matter, Biodiesel, Activation Energy, Oxidation Kinetics.

1. INTRODUCTION

Among conventional internal combustion engines (ICE), diesel or compression-ignition (CI) engines have the highest thermal efficiency for a given output power. However, diesel engines are an important source of particulate matters (PMs); between about 0.2 and 0.5 percent of the fuel mass in emitted as small particles which consist primary of soot with some additional absorbed hydrocarbon material (Heywood, 1998). PMs must be removed from the exhaust gas emitted from diesel engines to protect the environment and human health. Therefore, regulation of vehicle emissions has become increasingly strict.

Recent research trends are reviewed for physical and chemical PM characterization methods for gasoline and diesel fueled engines under various vehicle certification cycles and real-world driving conditions (Myung et al., 2014). Physical properties of engine PMs have been published by several researchers. The formation of PMs is through to take place via a number of elemental steps: pyrolysis, nucleation, surface growth

and coagulation, aggregation and oxidation. These processes take place on different time scales, ranging from a few microseconds to some milliseconds (Neeft et al., 1996). Surface growth is the process in which the precursor molecules grow from nanoparticles. Simultaneously, another process coagulation. Small particulates collide and coalesce, forming larger spherical particles. Aggregation or chain-forming coagulation accounts for the formation of the well-known "fractal" structure of soot (Eastwood, 2008). The carbon atoms are bonded together in hexagonal face-centered arrays in planes commonly referred to as platelets. Platelets are arranged in layers to form crystallites (Smith, 1981). Diesel PM consists of two particles: i) fractal-like agglomerates of primary particles, consisting of carbon and traces of metallic ash, and coated with condensed heavier and organic compounds and sulfate, and ii) nucleation particles composed of condensed HCs and sulfate (Maricq, 2007).

Chemical composition of diesel PMs have been also clearly reported by researchers in all regions. The composition of PMs from diesel engines may vary widely, depending on the operating conditions and fuel composition. PM is traditionally divided into three main

^{*} Corresponding author. e-mail: kkpreech@kmitl.ac.th

fractions: i) solid fraction (SOL) that consists of elemental carbon and metallic ash, ii) soluble organic fraction (SOF) that consists of organic material derived from engine lubricating oil and fuel, and iii) sulfate particulates (SO4) that consist of sulfuric acid and water (Kittelson, 1998; Majewski et al., 2006). The element carbon, not chemically bound with other elements, is the finely dispersed carbon black or soot substance responsible for black smoke emission. Ash consists of a mixture of: i) sulfates, phosphates, or oxides of calcium, zinc, magnesium, and other metals that are formed in the combustion chamber from burning additives in the engine lubricating oil, ii) metal oxide (iron, copper, chromium, and aluminum) impurities resulting from engine wear, which are carried into the combustion chamber by the lube oil, and iii) iron oxides resulting from corrosion of the engine exhaust manifold and exhaust system components (Merkel, 2001).

Scanning Electron Microscopic (SEM) and Transmission Electron Microscope (TEM) observation of PMs have been conducted by several researchers. A primary soot particle has two distinct parts: an inner core and an outer shell. The inner core, with a diameter of 10 nm, exists at the center of the primary particle and consists of several fine particles, 3-4 nm in diameter. The outer shell is composed of microcrystallites with periodic orientation of carbon sheets, also called a graphitic structure. Almost all the crystallites are planar, 1 nm thick and 3-5 nm wide, and are oriented perpendicular to the radius of the primary particle (Ishiguro, et al., 1997). Some primary particles were found to have a hollow interior and the outer shell exhibiting evidence of graphitization, with a higher crystalline than the non-hollowed particles (Vander Wal, et al., 2007).

Size distribution of diesel PMs have been reported by several researchers. Most of the particle mass exists in the accumulation mode in the diameter range of few hundred nanometers. The nuclei mode typically consists of particles in the few nanometers diameter range. This mode usually consists of volatile organic and solid carbon compounds. The nuclei mode typically contains lower than 20% of the particle mass, and more than 90% of the particle number. The coarse mode contains up to 20% of the particle mass; it consists of accumulation mode particles that deposit on cylinder and exhaust system surfaces, and are later reentrained. Size definitions for atmospheric particles are PM10, diameter (D) < 10 μ m; fine particles, D < 2.5 μ m; ultrafine particles, D < 0.10 μ m; and nanoparticles, $D < 0.05 \mu m$ or 50 nm (Kittelson, 1998). The particles in the size range from 20 to 200 nm are very sensitive to sudden changes of the engine power (Soylu, 2014).

The oxidation behavior of PMs has been investigated using thermogravimetric analysis (TGA) and temperature program oxidation (TPO) to evaluate

reaction activity. The fit curve results of reaction order for both oxygen and carbon, and the activation energies, were defined and reported. The order in carbon is close to the order of 2/3 (0.67), making it applicable for the shrinking-core model. The order of reaction rate in oxygen is close to 1. The activation energy (E_a) of carbon oxidation is around 150–170 kJ/mole (Neeft *et al.*, 1997; Darcy *et al.*, 2007; Fino *et al.*, 2008).

A diesel after-treatment technology that substantially reduces diesel engine particle emissions is a Diesel Particulate Filter (DPF). The DPF plays an important role in particulate trapping and oxidation. These processes involve the most complex behavior of PMs and reaction phenomena. Mechanisms of engine PMs trapping and oxidation on DPF wall surface were successfully clarified via real-time macro-microscopic visualization method (Hanamura *et al.*, 2009; Karin *et al.*, 2010; Oki *et al.*, 2011).

Moreover, PMs from biodiesel fuel also investigated and compared with the conventional diesel fuel. Since, the biodiesel fuel is the alternative fuel which is a possible choice for usage instead of diesel fuels. Thai government promote biodiesel using to Thai people because of Thailand can produce the biodiesel in the country by palm oil. The PM diameter size and quantity from biodiesel engine emission is smaller than that of diesel. It might be the effect of oxygenated fuel promotes more completely combustion and makes smaller size exiting (Karin et al., 2013). In the case of biofuel, especially, measured particle parameters such as primary particle size and the radius of gyration were decreased compared to those of conventional diesel (Lee et al., 2013). The objective of the present research is to study diesel and biodiesel blends PMs oxidation kinetics by TGA method. The oxidation kinetics and apparent activation energies would be calculated by using chemical composition, micro-nanostructures and oxidation temperature for better understanding and future design of DPF configuration for diesel and biodiesel blends engine application.

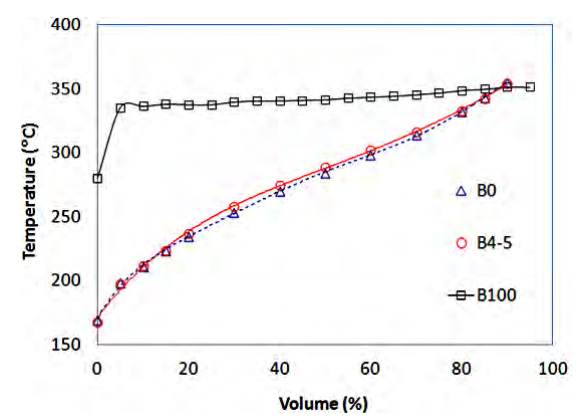


Figure 1. Distillation curves of palm-olein biodiesel (B100) and conventional diesel (B4-5) in Thailand.

2. METHODOLOGY

2.1. Fuels

A conventional diesel fuel (B4-5) was used and compared with the results of biodiesel fuel derived from palm-olein (B100: TIS 2313-2549). Distillation curves (Temperature-Vaporization) of both fuels are shown in Figure 1. It was clearly observed that diesel fuel could be distilled in wide range of temperature due to fossil fuel consisted of much kind of molecules whereas biodiesel is quite pure molecule resulting in vaporized at the constant temperature. The vaporize temperature of biodiesel is higher than that of diesel. Therefore, the high temperature inside the biodiesel engine combustion chamber will be reduced.

2.2. Engine

Diesel and biodiesel PMs were emitted by diesel and biodiesel small engine. The small diesel engine has displacement of 638 cm³ and a rated output of 8.8 kW. The small diesel engine is a single cylinder, four strokes and direct injection. The fuel injection pressure was approximately 19.6 MPa. The engine was operated by constant speed of 2400 rpm on the Eddy current engine dynamometer (Tokyo plant ED-60-LC).

2.3. Thermo-gravimetric Analysis (TGA)

The oxidation kinetics of carbon black (N-330), PMs emitted from diesel and biodiesel engine were investigated by using TGA method with 0.1 mg sensitivity, 0.1% accuracy of balance mass and C of temperature error. Non-isothermal method was also used to investigate oxidation kinetics of each unburned HC and carbon under the condition of temperature increasing rate of 10 C per minute from 5 C to C with 100% oxygen atmosphere.

Isothermal TGA test was also done for all PM samples. Diesel and biodiesel PM samples were collected at 80% load from the single cylinder engine. Each sample was tested at four different temperature including 450, 500, 550 and 600 C. Nitrogen was used to heat up the sample to desired temperature then pure oxygen is introduced for soot oxidation for one hour. The same process is done with air as oxidizer. Chemical kinetics of PM oxidation is studied by using mass conversion behavior from TGA. The chemical reaction rate in Eq.1 can be calculated from the TGA mass conversion curve based on the chemical kinetic in Eq.2. Where PM is PM mass, t is time, n, m are the reaction order of PM and oxygen, respectively. The reaction order n is assumed to be 2/3 as shrinking core model because PM is like spherical shape. In order to calculate the apparent activation energy (E_a) of PM oxidation, the chemical reaction rate constant k at each temperature in Eq.2 is expressed by Eq.3. Where A is the frequency

factor, E_a is the activation energy, R is the gas constant. Finally, the apparent activation energy can be calculated by Eq.4 using the Arrhenius plot.

$$PM + O_2 \rightarrow CO_2$$
 (1)

$$-\frac{d[PM]}{dt} = k[PM]^n [O_2]^m \tag{2}$$

$$k = Ae^{-\frac{E_a}{RT}} \tag{3}$$

$$\ln \left[\frac{-1}{[PM]^n} \frac{d[PM]}{dt} \right] = -\frac{E_a}{RT} + (\ln A + m \ln[O_2])$$
 (4)

3. RESULTS AND DISCUSSION

3.1 SEM and TEM images

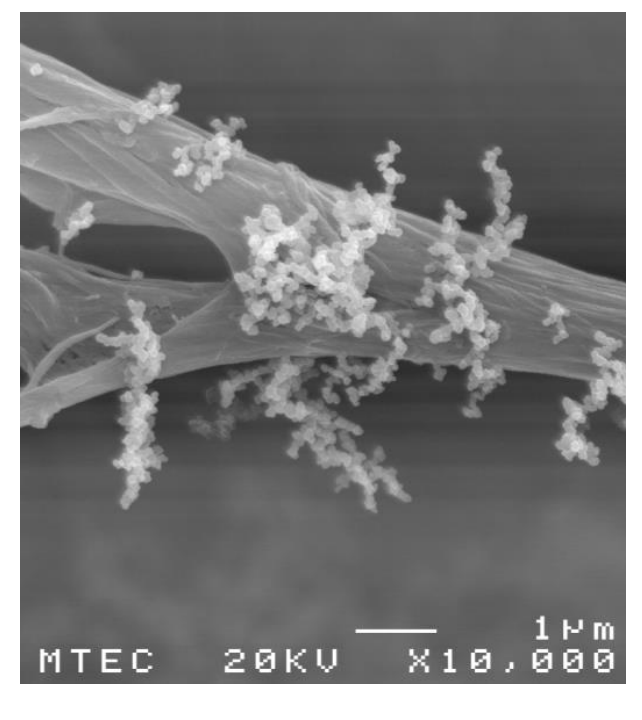
Figure 2 (a) and (b) show SEM and TEM images of engine diesel PMs. Uniform submicron scale agglomeration and single of PM is clearly seen. The agglomerate and single size were micron (fine particle) and submicron (ultrafine particle) scale, respectively. Smaller size of biodiesel agglomerated and single particle PMs are clearly seen. Size distribution of PMs was clearly observed by SEM and TEM images (Karin *et al.*, 2013).

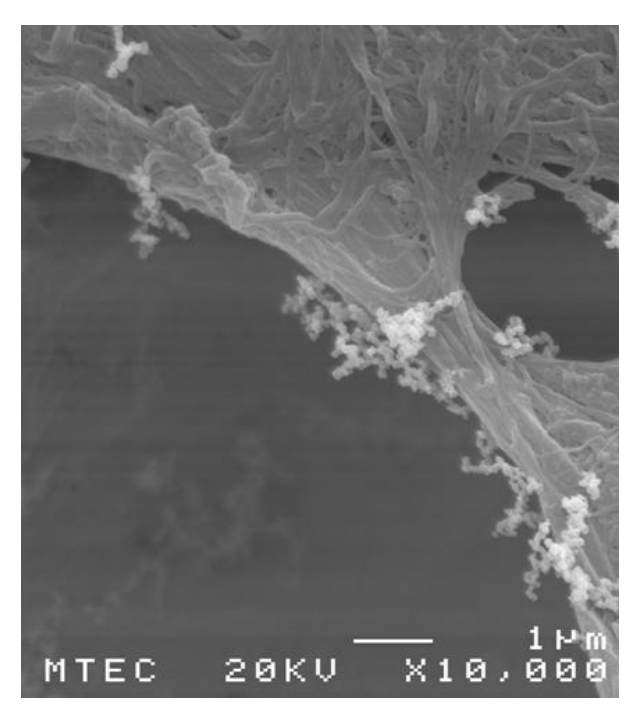
Figure 3 (a) and (b) show SEM and TEM images of engine biodiesel PMs. Uniform submicron and micron scale of agglomeration and single of PM is also clearly observed. The average agglomerate and single sizes of both diesel and biodiesel PMs are approximately 100-300 nm and 30-60 nm, respectively. PMs are collected by the metal net from the exhaust gas during engine running for PMs oxidation kinetics investigation by TGA method. Chemical composition and morphology of PMs surface will strongly impact on the oxidation behavior of each PMs.

3.2 Non Isothermal PMs Oxidation Kinetics

Figure 4 (a) shows the mass conversion of PM emitted from diesel and biodiesel engine. It's clearly observed that carbon black was start of oxidation around 5 while diesel and biodiesel Ms were start of oxidation around 3 -4 . Ms emitted from biodiesel engine were oxidized faster than that of PMs emitted from diesel engine. Moreover, PMs emitted from the low load operation condition of the engine were oxidized faster than that of the high load operation condition of the engine.

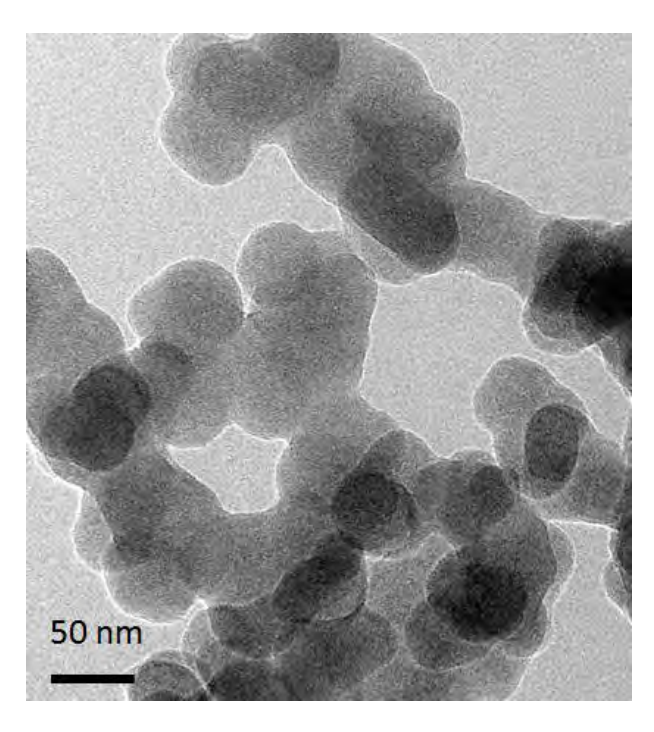
P.KARIN





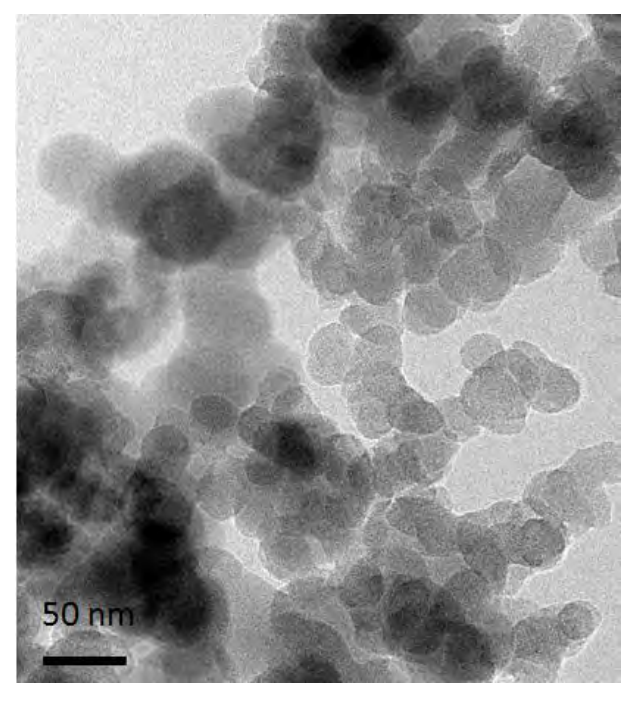
(a) SEM image of diesel PMs

(a) SEM image of biodiesel PMs



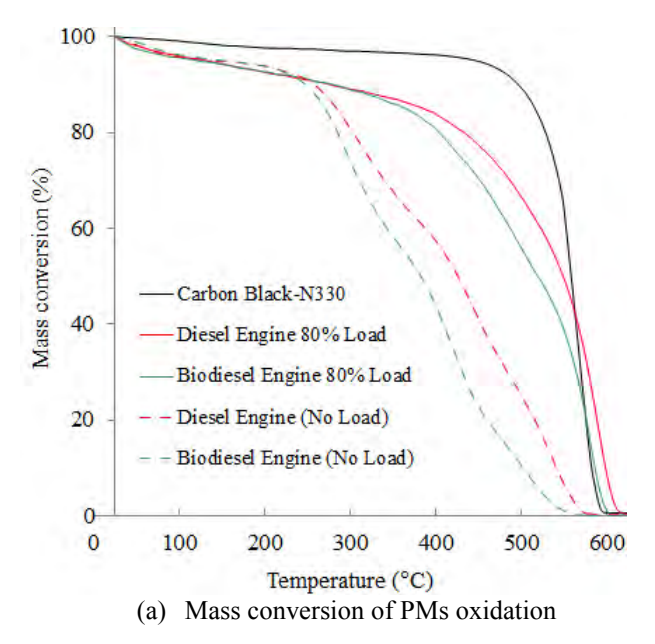
(b) TEM image of diesel PMs

Figure 2. (a) SEM and (b) TEM images of uniform submicron scale diesel PMs.



(b) TEM image of biodiesel PMs

Figure 3. (a) SEM and (b) TEM images of uniform submicron scale of biodiesel PMs.



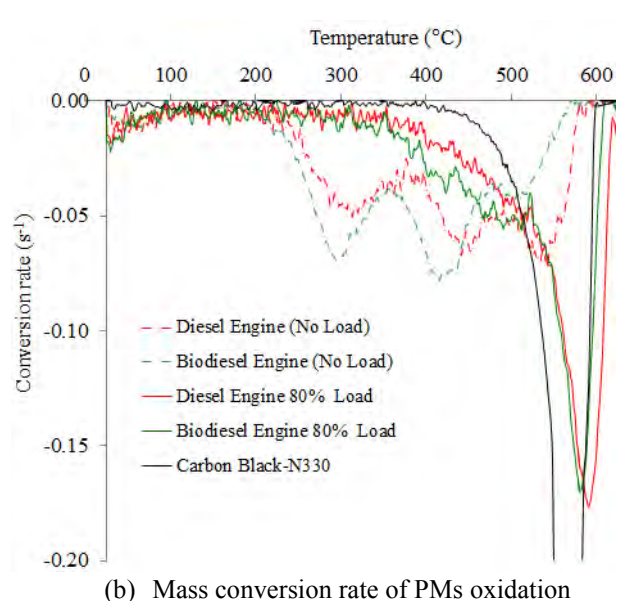


Figure 4. Mass (a) conversion and (b) conversion rate of PMs emitted from diesel and biodiesel engine in the operation condition of no-load and 80% load compared with carbon black by TGA.

Figure 4 (b) shows the mass conversion rate of PMs oxidation. It can be described that the different oxidation rate at each temperature range are caused by the difference of incomplete combustion product inside each PM. PMs can be clearly divided the chemical consistent by consider the oxidation temperature zone. Moisture is vaporized in the first peak at low temperature 5— . n burned is oxidized in second and third peaks at temperature of —4 and

3 -5 . in ally, carbon inside PM is oxidized in last peak at temperature 5 -6 same as carbon black oxidation.

Consequently, the unburned hydrocarbon of engine combustion strongly impact on the oxidation temperature and oxidation rate of PMs. Oxygenated unburned hydrocarbon of biodiesel engine also reduce the oxidation temperature and increase oxidation rate of PMs. Much amount of unburned hydrocarbon at low load condition of the engine operation is play important role in lower oxidation temperature of PMs.

3.3 Chemical Consistent of PMS

Figure 5 shows the estimation results of chemical consistent inside diesel and biodiesel PM in each operation condition of the engine by TGA method. PM of the diesel engine is consisted approximately of 4% moisture, 68% unburned HC and 28% carbon of no-load condition while medium load condition has 6% moisture, 54% unburned HC and 40% carbon and high load condition has 4% moisture, 38% unburned HC and 58% carbon, as shown in Figure 5 (a). Figure 5 (b) shows the results of PMs emitted from the biodiesel engine. PM of biodiesel combustion is consisted approximately of 4% moisture, 83% unburned HC and 13% carbon of no-load condition while medium load condition has 9% moisture, 77% unburned HC and 14% carbon and high load condition has 4% moisture, 49% unburned HC and 47% carbon.

PM in the high load condition has lower unburned HC fraction than that of the lower load condition. It might be expected that the combustion temperature, the temperature of gas in high load condition is higher than from low load condition, are strongly impact to unburned HC fraction. Some of unburned HC might be oxidized with remain oxygen in high temperature inside the combustion chamber and exhaust gas in exhaust manifold. PM from biodiesel engine combustion has more unburned HC fraction than that of diesel engine combustion. According to that biodiesel fuel has lower heating value than that of diesel fuel. In the same load condition, biodiesel must be used more for fuel injection to combustion chamber in combustion duration. More of fuel remaining in combustion duration is burned to be more HC in PM. The estimated carbon and hydrocarbon content inside PMs are agree with the results of CHN analysis, as shown in Figure 6. Carbon fraction inside carbon black is higher than that of diesel and biodiesel engine PMs. respectively due to unburned oxygenated hydrocarbon of biodiesel PMs. It was clearly observed that carbon

fraction inside low load engine PMs are lower that of

high load engine operation condition due to unburned

fuels.

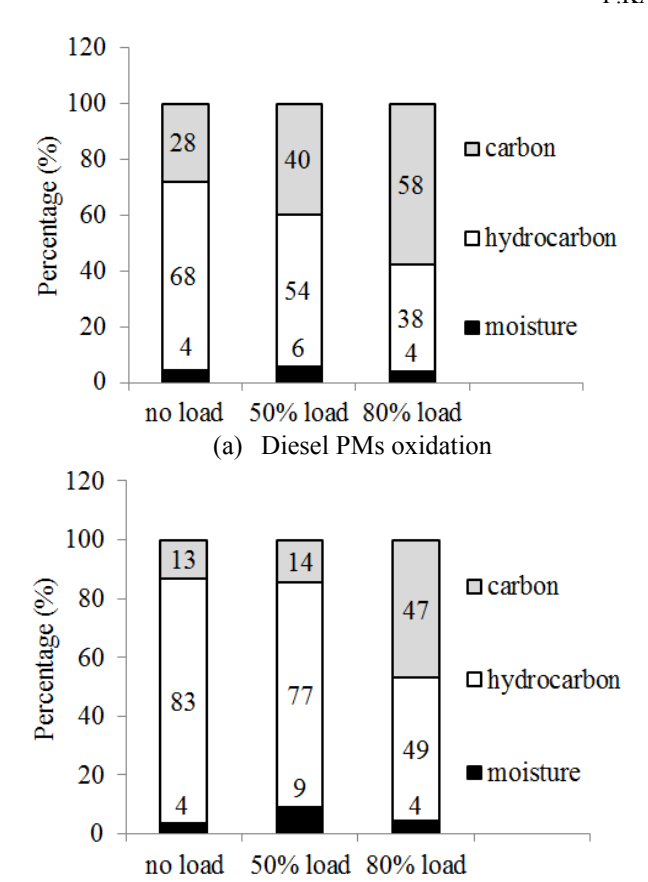


Figure 5. Chemical consistent of (a) diesel PMs oxidation and (b) biodiesel PMs oxidation using PMs mass conversion by TGA.

Biodiesel PMs oxidation

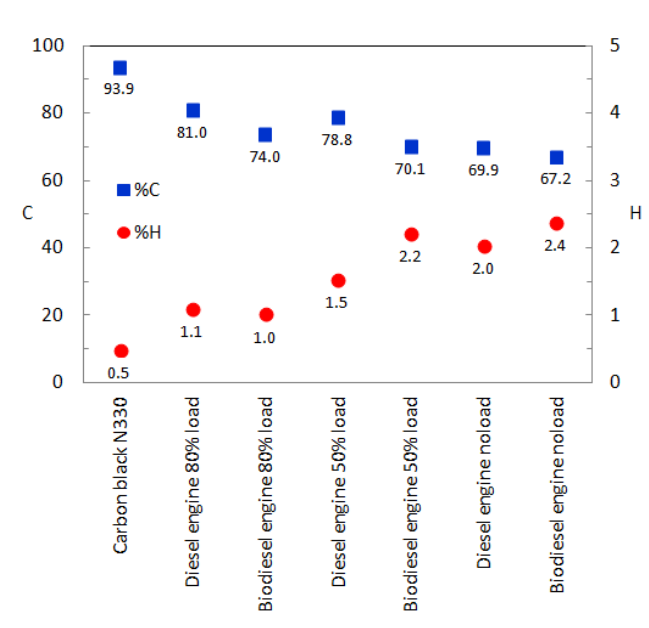


Figure 6. Chemical (carbon and hydrogen) consistent of diesel and biodiesel PMs using CHN analyzer.

3.4 Isothermal PMs Oxidation Kinetics of PMS

The result of isothermal TGA at higher temperatures including 450, 5 , 55 and 6 C is plotted at Figure 7 and Figure 8 for oxygen and air, respectively. The conversion rate of all 80% engine load PM samples including diesel and biodiesel increases by increase of temperature. The conversion rate of biodiesel and diesel PMs is almost the same while after introduction of oxygen at desired temperature the PM sample from biodiesel shows a relatively faster conversion rate in comparison with the diesel. The main reason for all these behaviors is due to difference in composition of PM from diesel and biodiesel.

The PM from biodiesel consists of unburned oxygenated hydrocarbon (HC) in comparison with unburned non-oxygen hydrocarbon from diesel fossil fuel. As biofuels are oxygenated fuels, they may have more oxygen content in the PM and this can boost oxidation and thus biodiesel shows faster oxidation rate in comparison with diesel. The increase in temperature is also responsible for increase in rate of conversion.

The difference of composition of PM will result in difference of apparent activation energy. In comparison between oxygen and air, the conversion results of air shows slower graph in all temperatures for both diesel and biodiesel PMs. This can be due to lower abundance of oxygen in the air (about 21%) in comparison with pure oxygen and thus more oxygen molecules can be present to start the oxidation reaction with PMs, therefore faster conversion and oxidation can be seen in presence of pure oxygen and slopes of the graphs are sharper in comparison with air.

Figure 9 and 10 show samples of Arrhenius plots of the 80% engine load PM oxidation with pure oxygen and air respectively, by using Eq.4. The slope of diesel and biodiesel PM oxidation with air are not much different even some different results in the case of pure oxygen are observed. Moreover, the calculated apparent activation energies, E_a which was calculated from the results of the present research, of different PM oxidation fraction are also showed that it's not much different. It might be expected that high engine load condition emitted low concentration of unburned hydrocarbon and much amount of carbon fraction which is same apparent activation energy of soot oxidation.

Table 1 shows the comparison of calculated apparent activation energies of the 80% engine load diesel and biodiesel PMs oxidized with pure oxygen and air in different PM burned fraction. The apparent activation energy of biodiesel and diesel PMs with air are in the range of 147–157 kJ/mole (with error of 3%, 152±5) and 153–165 kJ/mole (with error of 4%, 159±6), respectively. However, the apparent activation energies in the case of pure oxygen are very wide range. It might be expected that very high concentration of oxygen

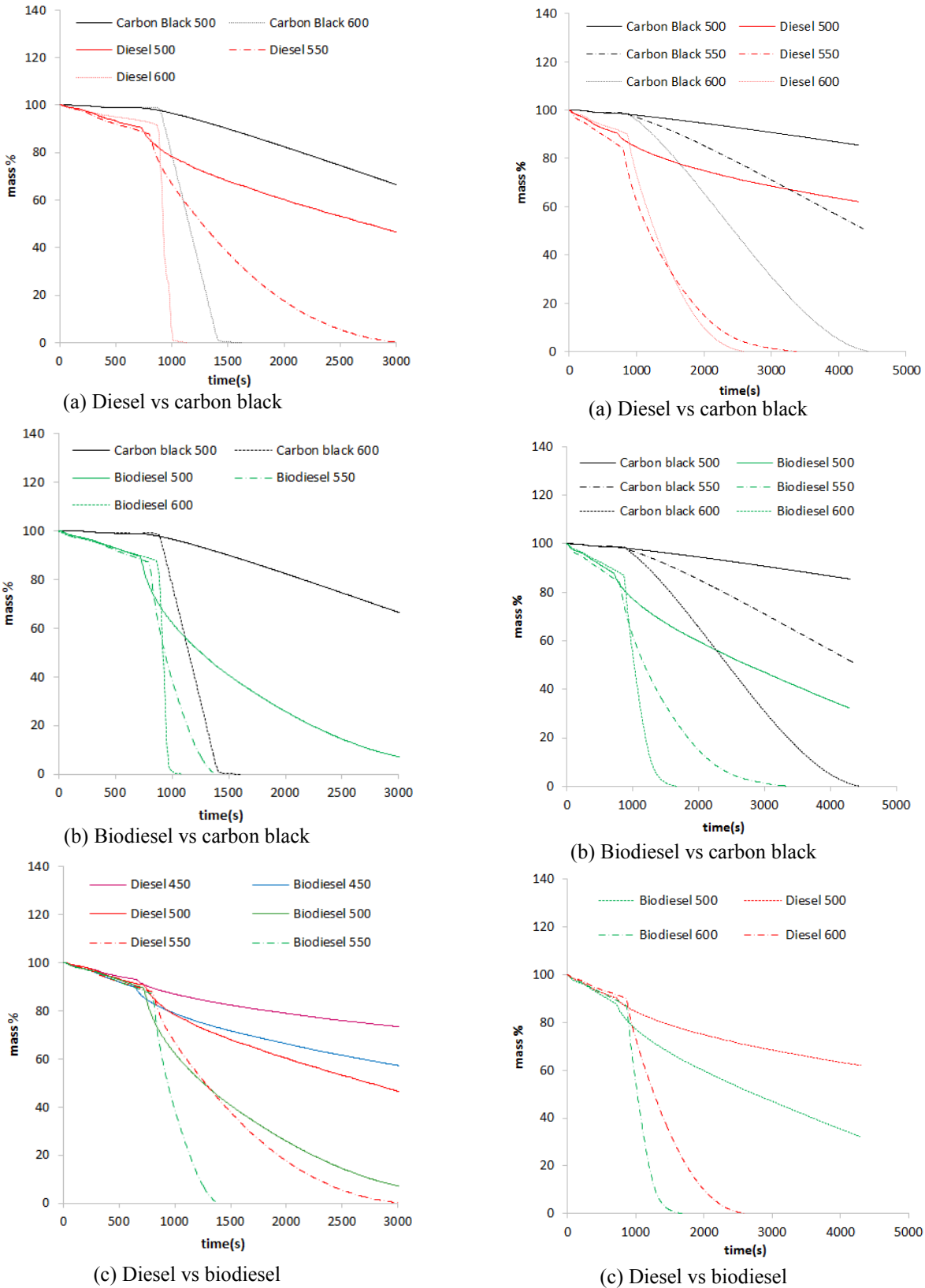
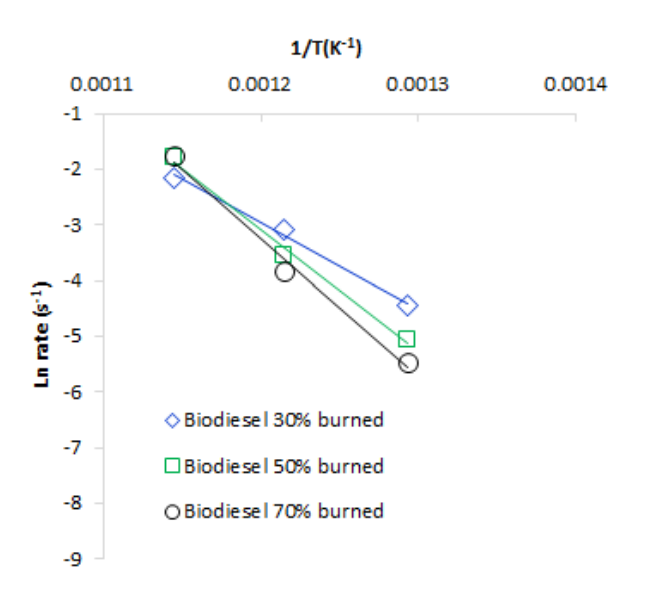
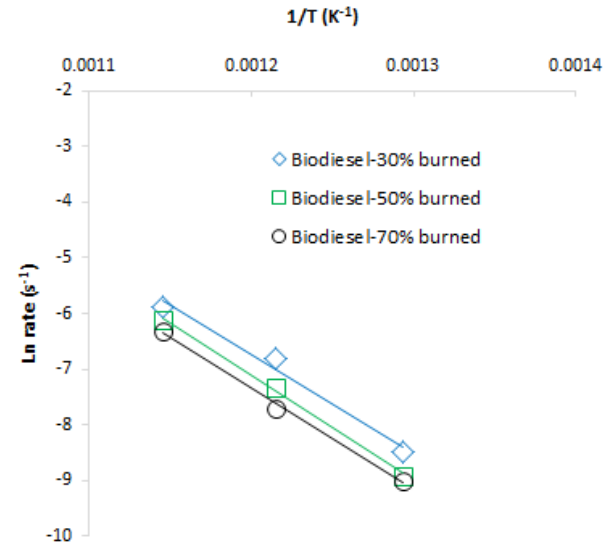


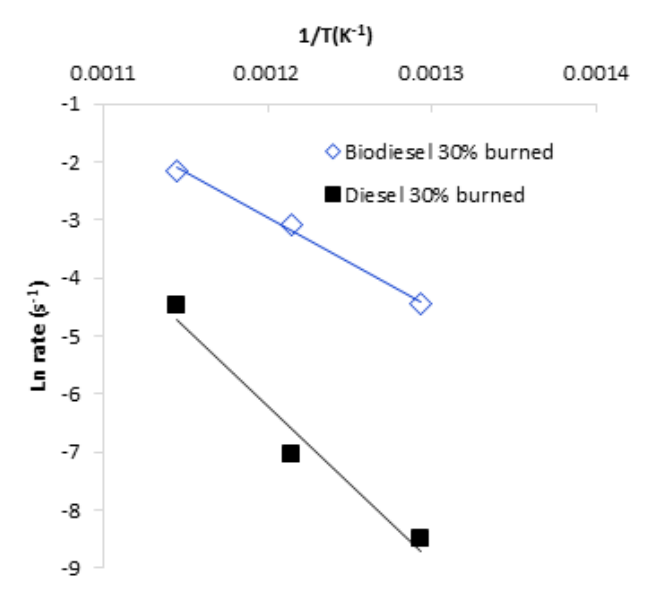
Figure 7. Conversion (a) diesel vs carbon black (b) biodiesel vs carbon black and (c) diesel vs biodiesel PMs oxidation with pure oxygen.

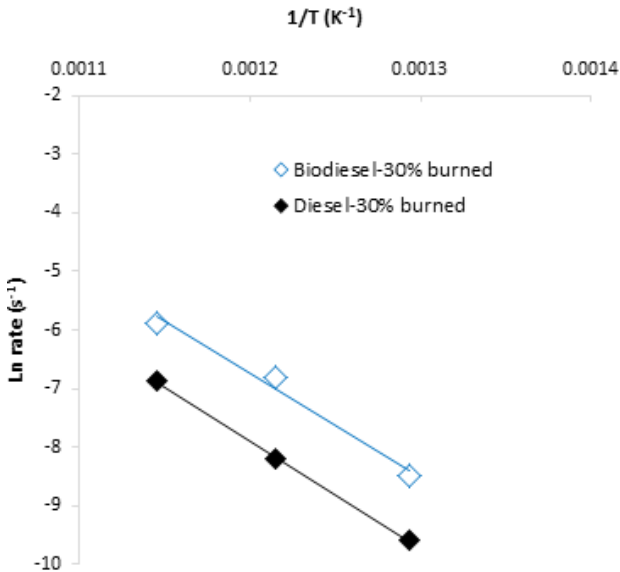
Figure 8. Conversion (a) diesel vs carbon black (b) biodiesel vs carbon black and (c) diesel vs biodiesel PMs oxidation with pure air.





- (a) Arrhenius plots of diesel vs biodiesel PMS oxidize with pure oxygen in 30% PM burned
- (a) Arrhenius plots of diesel vs biodiesel PMS oxidize with air in 30% PM burned





- (b) Arrhenius plots of biodiesel PM oxidation with pure oxygen in different PM burned fraction of 30%, 50% and 70%
- (b) Arrhenius plots of biodiesel PM oxidation with air in different PM burned fraction of 30%, 50% and 70%

Figure 9. Sample of Arrhenius plots of PM oxidation with pure oxygen (a) diesel vs biodiesel in 30% burned fraction and (b) biodiesel in different burned fraction of 30%, 50% and 70%.

Figure 10. Sample of Arrhenius plots of PM oxidation with air (a) diesel vs biodiesel in 30% burned fraction and (b) biodiesel in different burned fraction of 30%, 50% and 70%.

cause very high oxidation rate of PMS and resulting in more error of estimation. Consequently, PMs emitted from biodiesel can be oxidized at the lower apparent activation energy when compared to that of diesel because the impact of some unburned oxygenated fuel of biodiesel plays an important role in PM combustion even though the oxidation behavior of carbon zone for both fuel are not too different.

Table 1. The apparent activation energies of diesel and biodiesel PMs oxidize with pure oxygen and air.

PM burned fraction	Apparent Ea (kJ/mole)	
	Pure oxygen	Air
Biodiesel		152±5
Biodiesel 30% burned	147	147
Biodiesel 50% burned	181	157
Biodiesel 70% burned	206	151
Diesel		159±6
Diesel 30% burned	182	153
Diesel 50% burned	245	165
Diesel 70% burned	236	159

4. CONCLUSIONS

Diesel and biodiesel PMs oxidation kinetics was clearly observed in this research. PM in high load condition of the engine has lower unburned hydrocarbons (HCs) fraction than that lower load condition. The amount of unburned HC in PM might effect in faster oxidation because oxidation temperature at lower than 5 C of unburned HC can oxidization. Biodiesel PM is easier to oxidize than diesel PM and carbon black because of unburned oxygenated hydrocarbon.

The calculated apparent activation energy (non-isothermal method as practical use in the actual vehicle) of biodiesel PM oxidation is also lower than that of diesel PM and carbon black. The apparent activation energy of PMs emitted from the biodiesel and diesel high load engine is 152±5 kJ/mole and 159±6 kJ/mole, respectively. Because of oxygen atom included inside oxygenated fuel molecule promotes low PM oxidation activation energy. However, oxidation rate of PMs is strongly related to not only apparent activation energy but also physical impact of reaction order and frequency factor would be investigated.

ACKNOWLEDGEMENT

The authors gratefully acknowledge the financial support from Thailand Research Fund (TRF), Ministry of Science and Technology, Thailand.

REFERENCES

- Heywood, J. B. (1988). *Internal Combustion Engine Fundamentals*. McGraw-Hill. Singapore.
- Myung, C. L. Choi, S. and Park, S. (2014). Review on Characterization of Nano-particle Emissions and Morphology from Internal Combustion Engines: Part 2. *International Journal of Automotive Technology*, **15**, **2**, 219-227.
- Neeft, J. A., Makkee, M., and Moulijn, J. (1996). Diesel Particulate Emission Control. *Fuel Processing Technology*, **47**, 1-69.
- Eastwood, P. (2008). *Particulate Emissions from Vehicles*. SAE International and John Wiley & Sons, Ltd. Pennsylvania.
- Smith, O. I. (1981). Fundamentals of Soot Formation in Flames with Application to Diesel Engine Particulate Emissions. *Progress in Energy and Combustion Science*, **7**, 275-291.
- Maricq, M. M. (2007). Review Chemical Characterization of Particulate Emissions from Diesel Engine: A Review. *Journal of Aerosol Science*, **38**, 1079-1118.
- Kittelson, D. B. (1998). Engines and Nanoparticles: A Review. *Journal of Aerosol Science*, 29, 575-588.
- Majewski, W. A. and Khair, M. K. (2006). *Diesel Emissions and Their Control*. SAE International and John Wiley & Sons, Ltd. Pennsylvania.
- Merkel, G. A., Cutler W. A. and Warren, C. J. (2001). Thermal Durability of Wall Flow Ceramic Diesel Particulate Filters. *SAE Technical Paper*, 2001-01-0190.
- Ishiguro, T., Takatori Y., Akihama, K. (1997). Cutler W. A. and Warren, C. J. (2001). Microstructure of Diesel Soot Particles Probed by Electron Microscopy: First Observation of Inner Core and Outer Shell. Combustion and Flame, 108, 231-234.
- Vander Wal, R. L., Yezerets, A. Currier, N. W., Kim, D. H. and Wang, C. H. (2007). HRTEM Study of Diesel Soot Collected from Diesel Particulate Filters. *Carbon*, **45**, 70-77.
- Soylu, S. (2014). Examination of PN Emissions and Size Distributions of a Hybrid City Bus under Real World Urban Driving Conditions. *International Journal of Automotive Technology*, **15**, **3**, 369-376.
- Neeft, J. A., Nijhuis, T. X., Smakman, E., Makkee, M. and Moulijn, J. A. (1997). Kinetics of the Oxidation of Diesel Soot. *Fuel*, **76**, **12**, 1129-1136.
- Dacy, P., Costa, P. D., Mellottee, H., Trichard, J. M. and Mariadassou, G. D. (2007). Kinetics of Catalyzed and Non-catalyzed Oxidation of Soot from a Diesel Engine. *Catalysis Today*, **119**, 252-256.
- Fino, D. and Specchai, V. (2008). Review Open Issues in Oxidative Catalysis for Diesel Particulate Abatement. *Powder Technology*, **180**, 64-73.

- Hanamura, K., Karin, P., Cui, L., Rubio, P., Tsuruta, T.,
 Tanaka, T. and Suzuki, T. (2009). Micro- and
 Macroscopic Visualization of Particulate Matter
 Trapping and Regeneration Processes in Wall-flow
 Diesel Particulate Filters. *International Journal of Engine Research*, 10, 305-321.
- Karin, P., Cui, L., Rubio, P., Tsuruta, T. and Hanamura, K. (2009). Microscopic Visualization of PM Trapping and Regeneration in Micro-Structural Pores of a DPF Wall. SAE International Journal of Fuels and Lubricants, 2, 1, 661-669.
- Karin, P. and Hanamura, K. (2010). Particulate Matter Trapping and Oxidation on Catalyst-Membrane. *SAE International Journal of Fuels and Lubricants*, **3**, **1**, 368-379.
- Oki, H., Karin, P. and Hanamura, K. (2011). Visualization of Oxidation of Soot Nanoparticles Trapped on a Diesel Particulate Membrane Filter. *SAE International Journal of Engines*, **4**, **1**, 515-526.
- Karin, P., Songsaengchan, Y., Laosuwan, S.,
 Charoenphonphanich, C., Chollacoop, N., Hanamura,
 K. (2013). Nanostructure Investigation of Particle
 Emission by Using TEM Image Processing Method.
 Energy Procedia, 34, 757-766.
- Karin, P., Songsaengchan, Y., Laosuwan, S.,
 Charoenphonphanich, C., Chollacoop, N., Hanamura,
 K. (2013). Physical Characterization of Biodiesel
 Particle Emission by Electron Microscopy. SAE Technical Paper, 2013-32-9150.
- Lee, S., Lee, D., Choi, S. C. (2013). Impact of SME Blended Fuel Combustion on Soot Morphological Characteristics in a Diesel Engine. *International Journal of Automotive Technology*, **14**, **5**, 757-762.